WAVE INDUCED OSCILLATIONS IN HARBORS OF ARBITRARY SHAPE

Thesis by

Jiin-Jen Lee

In Partial Fulfillment of the Requirements

For the Degree of

Doctor of Philosophy

California Institute of Technology

Pasadena, California

1970

(Submitted November 11, 1969)

ACKNOWLEDGMENTS

The writer wishes to express his deepest gratitude to his thesis advisor, Professor Fredric Raichlen, who suggested this research problem and offered the most valuable guidance and encouragement throughout every phase of this investigation. The advice and encouragement of Professors Vito A. Vanoni and Norman H. Brooks are also deeply appreciated.

The writer also wishes to express his appreciation to Professors Theodore Y. T. Wu, Thomas K. Caughey, Herbert B. Keller, and Donald S. Cohen for the helpful discussions during the development of the theoretical analysis of this problem. The help from Professor James J. Morgan and Mr. Soloukid Pourian in developing the technique for controlling corrosion of the wave energy dissipators is very much appreciated.

The writer is deeply indebted to Mr. Elton F. Daly, supervisor of the shop and laboratory, for his assistance and patient instruction in both designing and building the experimental set up. Appreciation is also due Robert L. Greenway who assisted with the construction of the experimental apparatus; Mr. Albert F. W. Chang who assisted in the computer programming; Mr. Joseph L. Hammack who assisted in performing experiments and reducing data; Messrs. George Chan, Yoshiaki Daimon, and Claude Vidal who assisted in data reduction; Mr. Carl Green who prepared the drawings; Mr. Carl Eastvedt who did the photographic work; Mrs. Arvilla F. Krugh who typed the

manuscript; and Mrs. Patricia Rankin who offered many valuable suggestions in preparing the manuscript. The writer also wishes to express his sincere appreciation to his officemate, Mr. Edmund A. Prych, for friendly and helpful advice during the last three years.

This research was supported by the U. S. Army Corps of Engineers under Contract DA-22-079-CIVENG-64-11. The experiments were conducted in the W. M. Keck Laboratory of Hydraulics and Water Resources at the California Institute of Technology.

The writer wishes to express his deep appreciation to his wife, Sage, for her understanding, patience and encouragement during the period of his graduate study.

ABSTRACT

Theoretical and experimental studies were conducted to investigate the wave induced oscillations in an arbitrary shaped harbor with constant depth which is connected to the open-sea.

A theory termed the "arbitrary shaped harbor" theory is developed. The solution of the Helmholtz equation, $\nabla^2 f + k^2 f = 0$, is formulated as an integral equation; an approximate method is employed to solve the integral equation by converting it to a matrix equation. The final solution is obtained by equating, at the harbor entrance, the wave amplitude and its normal derivative obtained from the solutions for the regions outside and inside the harbor.

Two special theories called the circular harbor theory and the rectangular harbor theory are also developed. The coordinates inside a circular and a rectangular harbor are separable; therefore, the solution for the region inside these harbors is obtained by the method of separation of variables. For the solution in the open-sea region, the same method is used as that employed for the arbitrary shaped harbor theory. The final solution is also obtained by a matching procedure similar to that used for the arbitrary shaped harbor theory. These two special theories provide a useful analytical check on the arbitrary shaped harbor theory.

Experiments were conducted to verify the theories in a wave basin 15 ft wide by 31 ft long with an effective system of wave energy dissipators mounted along the boundary to simulate the open-sea condition.

Four harbors were investigated theoretically and experimentally: circular harbors with a 10° opening and a 60° opening, a rectangular harbor, and a model of the East and West Basins of Long Beach Harbor located in Long Beach, California.

Theoretical solutions for these four harbors using the arbitrary shaped harbor theory were obtained. In addition, the theoretical solutions for the circular harbors and the rectangular harbor using the two special theories were also obtained. In each case, the theories have proven to agree well with the experimental data.

It is found that: (1) the resonant frequencies for a specific harbor are predicted correctly by the theory, although the amplification factors at resonance are somewhat larger than those found experimentally, (2) for the circular harbors, as the width of the harbor entrance increases, the amplification at resonance decreases, but the wave number bandwidth at resonance increases, (3) each peak in the curve of entrance velocity vs incident wave period corresponds to a distinct mode of resonant oscillation inside the harbor, thus the velocity at the harbor entrance appears to be a good indicator for resonance in harbors of complicated shape, (4) the results show that the present theory can be applied with confidence to prototype harbors with relatively uniform depth and reflective interior boundaries.

TABLE OF CONTENTS

TABLE OF CONTENTS (Cont'd)

TABLE OF CONTENTS (Cont'd)

TABLE OF CONTENTS (Cont'd)

LIST OF FIGURES

LIST OF FIGURES (Cont'd)

LIST OF FIGURES (Cont'd)

LIST OF FIGURES (Cont'd)

LIST OF FIGURES (Cont'd)

LIST OF FIGURES (Cont'd)

LIST OF TABLES

CHAPTER 1

INTRODUCTION

1.1 BACKGROUND

A natural or an artificial harbor can exhibit frequency- (or period-) dependent water surface oscillations when exposed to incident water waves in a way which is similar to the response of mechanical and acoustical systems which are exposed to exterior forces, pressures or displacements. For a particular harbor, it is possible that for certain wave periods the wave amplitude at a particular location inside the harbor may be much larger than the amplitude of the incident wave, whereas for other wave periods significant attenuation may occur at the same location. This phenomenon of harbor resonance has generally been thought to be caused by waves from the open-sea incident upon the harbor entrance, although other possible excitations may be earthquakes, local winds, and local atmospheric pressure anomalies, etc.

These resonant oscillations (also termed seiche and harbor surging) can cause significant damage to moored ships and adjacent structures. The ship and its mooring lines also constitute a dynamic system; therefore, if the period of resonant oscillation of the harbor is close to that of the ship-mooring system, an extremely serious problem could result. In addition, the currents induced by this oscillation can cause navigation hazards.

There have been natural and artificial harbors in various locations around the world where resonant oscillations have occurred and have caused damage to ships and dockside facilities, e.g. Table Bay Harbor, Cape Town, South Africa; Monterey Bay, California and Marina del Rey, Los Angeles, California. In order to correct an existing resonance problem one must first be able to predict the response of that particular harbor to incident waves, i.e. the expected wave amplitude at various locations within the harbor for various wave periods, so that the effect of any change of the interior can be investigated. Until quite recently such a study was done using a hydraulic model alone. If an acceptable analytical solution of the problem could be developed it could be used in conjunction with a hydraulic model to provide a guide for the most effective and efficient use of the laboratory model.

1.2 OBJECTIVE AND SCOPE OF PRESENT STUDY

The major objective of this study is to investigate, both theoretically and experimentally, the response of an arbitrary shaped harbor of constant depth to periodic incident waves. The harbors are considered to be directly connected to the open-sea with no artificial boundary condition imposed at the harbor entrance. The laboratory experiments are conducted in order to verify the theoretical solution for different harbors.

In Chapter 2 previous studies of the harbor resonance problem are surveyed. A theoretical analysis is presented in Chapter 3 by which one may predict the response of an arbitrary shaped harbor of constant depth to incident wave system. In Chapter 4 a theoretical analysis is presented for two harbors with special shapes: a circular harbor and a rectangular harbor. These analyses provide theoretical results which can be compared to those of the general theory developed in Chapter 3. In Chapter 5 the experimental equipment and procedures are described. The experimental and theoretical results are presented and discussed in Chapter 6. Conclusions are stated in Chapter 7.

CHAPTER 2

LITERATURE SURVEY

2.1 WAVE OSCILLATIONS IN HARBORS OF SIMPLE SHAPE

A significant amount of work has been done on resonant oscillations in harbors of idealized planform such as a circular harbor or a rectangular harbor. The methods of approach used for solving these problems ranged from imposing a prescribed boundary condition at the harbor entrance to matching, at the harbor entrance, the solution obtained for the regions inside and outside the harbor.

McNown (1952) studied both theoretically and experimentally some of the response characteristics of a circular harbor of constant depth excited by waves incident upon a small entrance gap. The analysis was to solve Laplace's equation:

$$\frac{\partial^2 \bar{\Phi}}{\partial x^2} + \frac{\partial^2 \bar{\Phi}}{\partial y^2} + \frac{\partial^2 \bar{\Phi}}{\partial z^2} = 0 \qquad (2.1)$$

with certain prescribed boundary conditions. The boundary conditions used included the linearized free surface condition at the water surface and the condition that the velocity normal to all solid boundaries was zero. However, the assumption was made at the harbor entrance that the crest of a standing wave occurred at the entrance when the harbor was in resonance and the water surface remained essentially horizontal across the small entrance. Thus, for resonant motion, this hypotheses

led to a boundary condition identical to that for a completely closed circular basin. Therefore, the wave frequencies associated with resonant oscillations would be those eigenvalues for the free oscillation of a circular basin. Based on this assumption, McNown computed the amplitude variation inside the harbor for various modes of oscillation and found the theoretical results compared reasonably well with the experiments. This imposed condition at the harbor entrance is not satisfactory in the sense that the slope of the water surface at the harbor entrance should be part of the solution of the problem and should not be imposed initially. However, it can be shown that the resonant frequencies (or the wave numbers) associated with the circular harbor are indeed close to that for the free oscillation in the closed basin if the entrance is very small.

Using the same idea of assuming an antinode at the harbor entrance for resonant oscillation, Kravtchenko and McNown (1955) have studied seiche (wave oscillations) in a rectangular harbor. In that study the definition of resonance was similar to that used by McNown (1952), i.e. the modes of oscillation corresponding to the closed basin configuration were termed resonant all others termed non-resonant. For non-resonant oscillations the boundary condition, at the harbor entrance would have to be determined from observations in the laboratory.

Extending McNown's work for circular harbors, Apté (1954, 1957) investigated, both experimentally and theoretically, the problem of the rectangular harbor with a wide entrance. Both the experimental

and mathematical models consisted of a rectangular harbor with an asymmetric entrance to which a relatively long wave channel was connected. A theoretical solution was obtained for the amplitude distribution within the partially closed harbor by matching up the entrance velocities between the two domains: the harbor and the attendant wave channel. Good agreement was found between the theoretical solution and the experimental data. However, the solution obtained was not for the more realistic problem of a harbor connected directly to the open-sea.

Biesel and LeMehaute (1955, 1956) and LeMehaute (1960, 1961) studied the resonant oscillations in rectangular harbors with various types of entrances: fully open, partially open, change in depth at the entrance and combinations of these as well as a sloping beach inside the harbor. The harbor was connected to a wave basin having a width less than half of a wave length and an infinite length in the direction of wave propagation. The method which was used was based on complex number calculus with a direct application of the superposition of the various incident, reflected, and transmitted waves. An expression was developed for the amplification factor (defined as the wave amplitude at the rear of the harbor to the incident wave amplitude). However, in order to use that result an empirical reflection coefficient and attenuation parameter are needed, in general the values of these parameters are not obvious.

The problem of a rectangular harbor connected directly to the open-sea has been ably treated, theoretically, by Miles and Munk (1961). Their work was an important contribution since it included the effect of

the wave radiation from the harbor mouth to the open-sea. This effect limits the maximum wave amplitude within the harbor for the invicid case to a finite value even at resonance. They considered an arbitrary shaped harbor and formulated the problem as an integral equation in terms of a Green's function. This Green's function , $g(x, y, \xi)$, must satisfy the Helmholtz equation inside the harbor:

$$\frac{\partial^2 g}{\partial x^2} + \frac{\partial^2 g}{\partial y^2} + k^2 g = 0 \quad , \tag{2.2}$$

and have a vanishing normal derivative on the boundary of the harbor except at the entrance where the normal derivative of the Green's function is a delta function. Unfortunately, as they have noted, the Green's function for an arbitrary shaped harbor is beyond reach. Thus, they have applied this general formulation to a harbor of simple shape: a rectangular harbor, and found most interestingly that a narrowing of the harbor entrance leads not to a reduction in harbor surging (oscillation), but to an enhancement. This result was termed by them the "harbor paradox". At that time, there were considerable differences in opinion as to the existance of the paradox. LeMehaute (1962) suggested that if it had been possible to introduce the effect of viscous dissipation into the anlysis the paradox would become invalid. (However, the present study on circular harbors, both theoretically and experimentally, has supported the "harbor paradox", although the experimental data also show that viscous dissipation of energy is most important for harbors with small openings. (see Subsection 6.2.2).)

Ippen and Raichlen (1962) and Raichlen and Ippen (1965) have studied, both theoretically and experimentally, the wave induced oscillations in a smaller rectangular harbor connected to a larger highly reflective rectangular wave basin. The solution was obtained by solving the boundary value problem in both regions, i. e. the region inside the harbor and the region in the wave basin, using the matching condition that the water surface is continuous at the harbor entrance. Because of the high degree of coupling between the small rectangular harbor and its attendant wave basin the response characteristics of the harbor as a function of incident wave period were radically different from a similar prototype harbor connected to the open-sea. The former was characterized by a large number of closely spaced spikes as opposed to the latter that would have discrete resonant modes of oscillation. Those results most emphatically demonstrated the importance of adequate energy dissipators in the model system when investigating resonance of a harbor connected to the open-sea. It was pointed out that in order to reduce the coupling effect of the reflections of the wave energy which is radiated from the harbor entrance, efficient wave absorbers and wave filters in the main wave basin are necessary. A subsequent study by Ippen, Raichlen and Sullivan (1962) showed that the coupling effect is indeed significantly reduced by the use of artificial energy dissipators in the main wave basin.

Ippen and Goda (1963) also studied, both theoretically and experimentally, the problem of a rectangular harbor connected to the open-sea. In that analysis the waves radiated from the harbor entrance to

the open-sea were evaluated using the Fourier transformation method which was different from the point source method employed by Miles and Munk (1961). The solution inside the rectangular harbor was obtained by the method of separation of variables and expressed in terms of the slope of water surface at the harbor entrance. The solution in the open-sea region was obtained by superimposing the standing wave and the radiated wave (also expressed in terms of the slope of the water surface at the harbor entrance). Thus by matching the wave amplitude, at the entrance, from the solutions in both regions the final solution was obtained. Fairly good agreement was found between the theory and the experiments conducted in a wave basin (9 ft wide and 11 ft long) where satisfactory wave energy dissipators were installed around the boundary to simulate the "open-sea".

These previous studies of the wave induced oscillations in a harbor with a special shape have helped to understand some of the characteristics of the harbor resonance problem. However, the practical application of these studies is limited simply because it is not probable that the shape of an actual harbor will be as simple as those studied.

In the following section previous studies on harbors of more complex shape will be surveyed.

2.2 WAVE OSCILLATIONS IN HARBORS OF COMPLEX SHAPE

Knapp and Vanoni (1945) conducted a hydraulic model study in connection with the harbor improvements at the Naval Operating Base, Terminal Island, California (The present East and West Basins of Long Beach Harbor). The initial phase of that study helped to choose the "optimum" mole alignment and an extensive series of experiments was then conducted to completely determine the water motions in the basin so defined. A harbor response in which the maximum vertical water motion anywhere within the basin was plotted against incident wave period was obtained for a range of prototype wave periods from 10 sec to 15 min. Contours of water surface elevation throughout the basin were determined for various wave and surge periods. These measurements have delineated the characteristic modes of oscillation of the basin and established the regions of maximum and minimum motion in the basin. That study demonstrated the need and the merit of a model study to determine the location and the magnitude of the amplification in a harbor of complex shape when exposed to incident periodic waves.

Research and model studies on the surging problem in Table Bay Harbor, Cape Town, South Africa were conducted by Wilson between 1942-1951. (That work was made known in two papers: Wilson, 1959, 1960.) In that study Table Bay Harbor was shown to be affected by two forms of surging, one of which was responsible for the ranging of moored ships, the other for a pumping action of the basin and attendant navigational hazard. These model studies helped to reduce the surging inside the harbor.

Although model studies can provide many answers and are by far still the most reliable way of obtaining information concerning the wave induced oscillations in harbors, they are generally very expensive and, most importantly, require a considerable amount of time. Therefore, many researchers have searched for methods of theoretically analyzing the wave induced oscillations in a harbor of arbitrary shape which although perhaps not replacing the model tests at least provide a useful guide for the experimental program.

Wilson, Hendrickson and Kilmer (1965) have studied the two-dimensional and three-dimensional oscillations in an open basin of variable depth. For the two-dimensional oscillation the method is similar to one used earlier by Raichlen (1965b) in which attention is directed to free oscillations in a closed basin. In the analysis they have assumed that the wave lengths are large compared to the water depths; the equation of continuity combined with the linearized dynamic free surface condition was written in the form of a difference equation. The periods of oscillation and the variation of the water surface elevation within the harbor were obtained by solving for the eigenvalues and eigenvectors of the resultant system of difference equations. However, in this approach, an artificial boundary condition was assumed at the entrance to the harbor or bay. The boundary condition which was used results either from an assumed nodal line at the entrance or using certain observed amplitudes. Although this method of approach gives some useful answers, it is not a complete solution to the problem.

An ideal solution would automatically take care of the entrance condition by matching the wave amplitudes and velocities at the harbor entrance derived from solutions for the domain of the harbor and of the open-sea.

Leendertse (1967) has developed a numerical model for the propagation of long-period waves in an arbitrary shaped basin. In that study, the partial differential equations for shallow water waves (continuity and linearized momentum equations) were replaced by a difference equation to operate in spatial- and time-coordinates on definite points of a grid system. The results agreed well with certain field measurement; however, the water surface elevations at the open boundary still must be given.

Most recently a study conducted by Hwang and Tuck (1969) developed an analytical method to solve the harbor resonance problem for harbors of arbitrary shape and constant depth connected to the open-sea. Their method of approach is to superimpose scattered waves which are caused by the presence of the boundary on the standing wave system. The scattered waves are computed by a distribution of sources (chosen as the Hankel function $H_o^{(1)}(kr)$) with an unknown strength to be determined along the coastline and the boundary of the harbor. Thus the potential function $\varphi_t(\vec{x})$ at any point $\vec{x}(x, y)$ in space can be expressed as:

$$\varphi_t(\vec{x}) = \varphi_o(\vec{x}) + \int_s q(\vec{x}_o)\, H_o^{(1)}(k\,|\,\vec{x} - \vec{x}_o\,|)\,ds\,(\vec{x}_o) \quad , \qquad (2.3)$$

where $\varphi_o(\vec{x})$ represents the standing wave system and $q(\vec{x}_o)$ is the source strength along the entire coastline which includes the boundary of the harbor. The strength $q(\vec{x}_o)$ was determined numerically such that the boundary condition $\frac{\partial \varphi_t}{\partial n} = 0$ was satisfied along the entire reflecting boundary. This method did not require a matching condition at the harbor entrance; the calculation of the source strength $q(\vec{x}_o)$ along the entire reflecting boundary must be terminated at some distance from the harbor entrance ($q(\vec{x}_o) = 0$ between that location and $\pm\infty$). Physically, this implies that the influence of the source distribution at some distance away from the entrance is negligible; however, for an arbitrary shaped harbor the position at which the source strength becomes zero is not obvious unless trial calculations are made.

Although the theoretical solutions for wave induced oscillations in harbors, especially for an arbitrary shaped harbor, are limited, there is a considerable amount of literature in other fields such as optics, acoustics, electromagnetics, and mechanical vibrations which deal with similar physical problems. Some of these studies which are pertinent are concerned with the scattering of acoustic waves by surfaces of arbitrary shape (Friedman and Shaw (1962), Banaugh and Goldsmith (1963 a, b), Shaw (1967), etc.), sound radiation from an arbitrary body or vibrating surfaces (Chen and Schweikert (1963), Chertock (1964), Copley (1967), Kuo (1968), etc.), and the scattering of electromagnetic waves by cylinders of arbitrary cross section (Mullin, Sandburg, and Velline (1965), Richmond (1965), etc.).

Mathematical equations which describe these problems are nearly identical to those for the water wave problem. Thus, similar analytical techniques may be used for the harbor resonance problem. In fact, the investigation of Hwang and Tuck (1969) as well as this independent study are closely related to some of the literature just cited.

CHAPTER 3

THEORETICAL ANALYSIS FOR AN ARBITRARY SHAPED HARBOR

The theoretical solution for the wave induced oscillations in an arbitrary shaped harbor with a constant depth is presented in this chapter. The solution to the boundary value problem is formulated as an integral equation, and an approximate method is presented to solve this integral equation by converting it to a matrix equation which can be solved using a high-speed digital computer. The final solution is obtained using a matching condition at the harbor entrance, i.e. equating, at the harbor entrance, the wave amplitude and its normal derivative obtained from the solutions in the regions outside and inside the harbor. The numerical analysis is described in this chapter and examples are presented which confirm the numerical techniques used; a comparison of the theoretical and experimental results dealing with the full problem of the response of a harbor to incident waves will be presented in Chapter 6.

3.1 DEVELOPMENT OF THE HELMHOLTZ EQUATION

In order to solve the problem mathematically, the flow is assumed irrotational so that a velocity potential Φ may be defined, such that the fluid particle velocity vector can be expressed as the gradient of the velocity potential, i.e. $\vec{u} = \nabla\Phi$, where $\vec{u}$ is the velocity

vector with components u, v, and w in the x, y, and z directions respectively, and ∇ is the gradient operator defined as $\frac{\partial}{\partial x}\vec{i} + \frac{\partial}{\partial y}\vec{j} + \frac{\partial}{\partial z}\vec{k}$, in which $\vec{i}$, $\vec{j}$, and $\vec{k}$ are the unit vectors respectively in the directions x, y, and z. A definition sketch for the coordinates is presented in Fig. 3.1. From the continuity equation for an

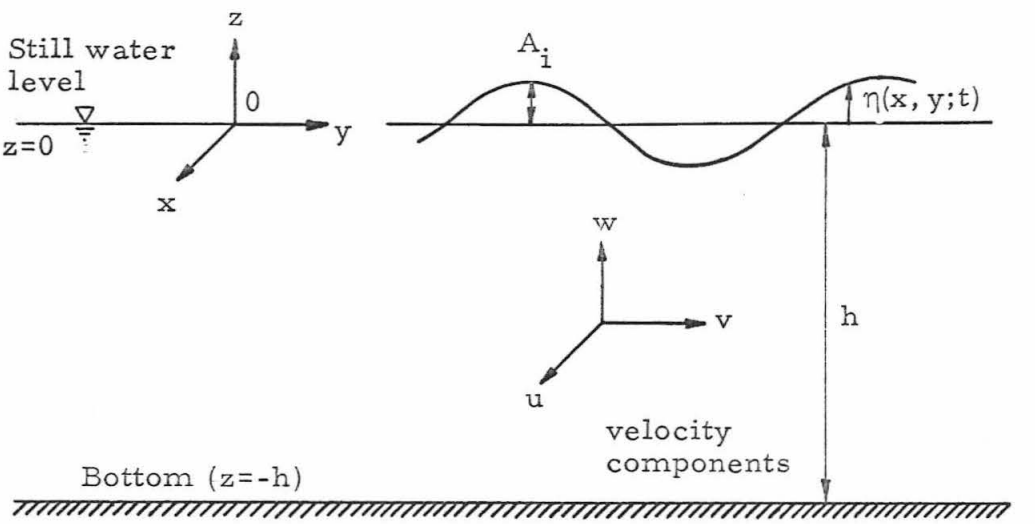

Fig. 3.1 Definition sketch of the coordinate system

incompressible fluid, $\nabla \cdot \vec{u} = 0$, and the definition of the velocity potential, Laplace's equation is obtained:

$$\nabla \cdot \vec{u} = \nabla^2 \bar{\Phi} = 0 \qquad . \qquad (3.1)$$

Therefore, the problem is to find the velocity potential $\bar{\Phi}$, which satisfies Laplace's equation, Eq. 3.1, subject to a number of prescribed boundary conditions; one of these is that the fluid does not penetrate the solid boundaries which define the limits of the domain of interest. Therefore, the outward normal velocities at the boundary of the harbor, at the coastline, and at the bottom are zero, i.e. $\frac{\partial \bar{\Phi}}{\partial n} = 0$ on solid boundaries.

The form of the solution of the velocity potential Φ which is sought is:

$$\Phi(x, y, z; t) = \frac{1}{-\lambda\sigma} f(x, y)\ Z(z)\ e^{-\lambda\sigma t} \quad , \tag{3.2}$$

where σ is the angular frequency, defined as $\frac{2\pi}{T}$ (T is the wave period), λ is the imaginary number $\sqrt{-1}$, and f(x, y) is defined as the wave function which describes the variation of Φ in the x and y - directions.

Substituting Eq. 3.2 into Laplace's equation (Eq. 3.1) the following expression results:

$$\frac{1}{f}\left(\frac{\partial^2 f}{\partial x^2} + \frac{\partial^2 f}{\partial y^2}\right) = -\frac{1}{Z}\frac{\partial^2 Z}{\partial z^2} \quad . \tag{3.3}$$

It is expected from consideration of small amplitude water wave theory that the function Z(z) will be in an exponential form rather than in a sinusoidal form. Therefore, since the left-hand-side of Eq. 3.3 is independent of z and the right-hand-side is independent of x and y, each side can be set equal to the same constant chosen here as $-k^2$ to insure Z(z) varying exponentially. Thus the following set of equations is obtained:

$$\text{(i)} \qquad \frac{d^2 Z}{dz^2} = k^2 Z, \quad \text{i.e.} \quad \frac{d^2 Z}{dz^2} - k^2 Z = 0 \tag{3.4}$$

$$\text{(ii)} \qquad \frac{\partial^2 f}{\partial x^2} + \frac{\partial^2 f}{\partial y^2} + k^2 f = 0 \tag{3.5}$$

The boundary condition at the bottom is $\frac{d\Phi}{dz}(x, y, -h; t) = 0$, in which the depth is assumed constant. Eq. 3.4 and the boundary condition at the bottom suggest the solution: $Z(z) = A_o \cosh k(h+z)$, where A_o is a constant to be determined. The dynamic free surface

condition from small amplitude wave theory, neglecting surface tension, can be combined with this expression and Eq. 3.2 to give:

$$\eta = -\frac{1}{g}\left(\frac{\partial \bar{\Phi}}{\partial t}\right)_{z=0} = -\frac{1}{g} A_o \cosh(kh)\left[f(x,y)\, e^{-i\sigma t}\right]$$

$$= A_i f(x,y)\, e^{-i\sigma t} \quad , \tag{3.6}$$

where η is the wave amplitude at the position (x, y) and at the time t, A_i is the wave amplitude at the crest of the incident wave (see Fig. 3.1), and g is the acceleration of gravity.

From Eq. 3.6 the constant A_o is:

$$A_o = -\frac{A_i g}{\cosh kh} \quad .$$

Therefore, the function $Z(z)$ in the velocity potential, Eq. 3.2, can be expressed as:

$$Z(z) = -\frac{A_i g \cosh k(z+h)}{\cosh kh} \quad . \tag{3.7}$$

Thus the velocity potential $\bar{\Phi}$ becomes:

$$\bar{\Phi}(x, y, z; t) = \frac{1}{i\sigma} \frac{A_i g \cosh k(z+h)}{\cosh kh} f(x,y)\, e^{-i\sigma t} \quad . \tag{3.8}$$

Substituting Eqs. 3.6 and 3.8 into the linearized kinematic free surface condition obtained from the small amplitude wave theory:

$$\frac{\partial \eta}{\partial t} = \left(\frac{\partial \bar{\Phi}}{\partial z}\right)_{z=0} \quad , \tag{3.9}$$

the well known "dispersion relation" for water waves is obtained:

$$\sigma^2 = gk \tanh(kh) \quad . \tag{3.10}$$

The dispersion relation relates the wave frequency to the wave number and the depth of the water; therefore, the arbitrary constant, k, used in Eqs. 3.4 and 3.5 is the wave number, k, which appears in the dispersion relation, where k is defined as $\frac{2\pi}{L}$, (L is the wave length).

In order to complete the expression for the velocity potential Φ, i.e. Eq. 3.2, the main problem which remains is to determine the wave function f(x, y), which satisfies Eq. 3.5, commonly known as the Helmholtz equation (Eq. 3.5 is repeated here for clarity.):

$$\frac{\partial^2 f}{\partial x^2} + \frac{\partial^2 f}{\partial y^2} + k^2 f = 0 \quad , \tag{3.5}$$

subject to the following boundary conditions:

(i) $\frac{\partial f}{\partial n} = 0$ along all fixed boundaries such as the coastline and the boundary of the harbor (where n denotes the outward normal from the boundary).

(ii) as $\sqrt{x^2 + y^2} \to \infty$, there is no effect of the harbor on the wave system; this is defined as the radiation condition. Physically, the radiation condition means that the outgoing radiated wave emanating from the harbor entrance will decay at an infinite distance from the harbor. Mathematically, the radiation condition is needed in order to ensure a unique solution of wave function f(x, y) in the unbounded domain.

In the following section (Section 3.2) the method for solving the Helmholtz equation, Eq. 3.5, for an arbitrary shaped harbor will be presented, thereby allowing one to determine the wave induced oscillations in such a harbor.

3.2 SOLUTION OF THE HELMHOLTZ EQUATION FOR AN ARBITRARY SHAPED HARBOR

The procedure in the development of the theory of the response of an arbitrary shaped harbor to incident wave systems is as follows:

(i) The domain of interest shown in Fig. 3.2 is divided into two regions: the infinite ocean region (Region I), and the region bounded by the limits of the harbor (Region II). The coastline which in part forms the shoreward limit of Region I is located along the x-axis and is considered to be perfectly reflecting and perpendicular to the bottom.

(ii) The wave function f_1 is determined in Region I in terms of the unknown normal derivative $\frac{\partial f_1}{\partial n}$ at the harbor entrance. Likewise, the wave function f_2 is evaluated in Region II in terms of the unknown normal derivative $\frac{\partial f_2}{\partial n}$ at the harbor entrance.

(iii) The condition is used that at the entrance the wave amplitude and the slope of the water surface obtained from the solution in Region I must equal to these quantities obtained from the solution in Region II, i.e. with reference to Fig. 3.2, at y=0 in the region between A and B, $f_1 = f_2$ and $\frac{\partial f_1}{\partial n} = -\frac{\partial f_2}{\partial n}$. This "continuity condition" is used to solve for the unknown normal derivatives of the wave function f, at the harbor entrance: $\frac{\partial f}{\partial n}$. (Note that the

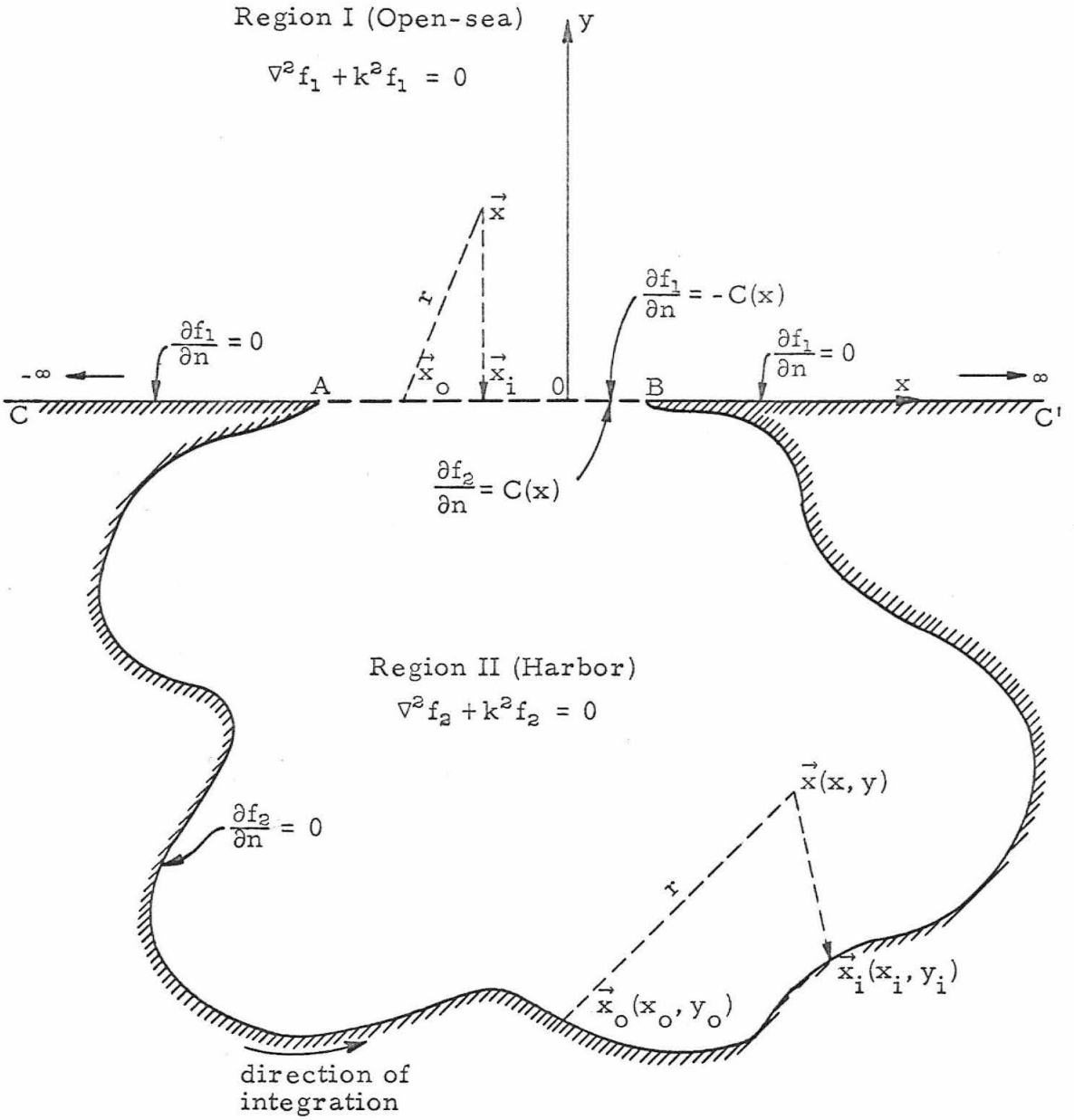

Fig. 3.2 Definition sketch of an arbitrary shaped harbor

negative sign results from the sign convention that the outward normal to the domain of interest is considered to be positive.)

(iv) Once the normal derivative of the wave function $\frac{\partial f_2}{\partial n}$ at the harbor entrance is obtained, the wave function f_2 in Region II, i.e. inside the harbor, can then be evaluated.

In the Subsection 3.2.1, the solution of the wave function f_2 inside the harbor is presented, followed by the solution of wave function f_1 in the infinite ocean region presented in Subsection 3.2.2. In Subsection 3.2.3 the procedure for matching the solutions at the harbor entrance is shown, leading to the desired result of the response of an arbitrary shaped harbor to incident wave systems.

3.2.1 Wave Function Inside the Harbor (Region II)

In Region II Green's identity formula (see Appendix I, Eq. A.1.1) is applied and the Hankel function of the 1st kind and zero order, $H_o^{(1)}(kr)$, is chosen to be the fundamental solution of the two-dimensional Helmholtz equation, Eq. 3.5. The function $H_o^{(1)}(kr)$ is chosen because it satisfies the Helmholtz equation, and possesses the proper type of singularity at the origin, which will be discussed. Therefore, the wave function f_2 at any position in the domain of interest can be expressed in integral form as a function of the value of f_2 and the value of $\frac{\partial f_2}{\partial n}$ at the boundary. (This derivation has been discussed by Baker and Copson (1950) and is referred to as Weber's solution of the Helmholtz equation; it is presented in Appendix I.)

$$f_2(\vec{x}) = -\frac{\lambda}{4}\int_s \left[f_2(\vec{x}_o)\frac{\partial}{\partial n}\left(H_o^{(1)}(kr)\right) - H_o^{(1)}(kr)\frac{\partial}{\partial n}\left(f_2(\vec{x}_o)\right)\right] ds(\vec{x}_o) \qquad (3.11)$$

where: $f_2(\vec{x})$ is the wave function f_2 at the position $\vec{x}$ shown in Fig Fig. 3.2,

$\vec{x}$ is the position vector of the field point (x, y) inside the harbor,

$f_2(\vec{x}_o)$ is the wave function f_2 on the boundary at the position $\vec{x}_o$,

$\vec{x}_o$ is the position vector of the source point (x_o, y_o) on the boundary (the significance of the source point will be discussed presently),

$\frac{\partial f_2(\vec{x}_o)}{\partial n}$ is the outward normal derivative of f_2 at the boundary source point $\vec{x}_o$,

r is the distance between the field and source points, $|\vec{x} - \vec{x}_o|$, and

λ is the imaginary number of $\sqrt{-1}$.

The integration indicated by Eq. 3.11 is to be performed along the boundary of the harbor traveling in a counterclockwise direction as indicated in Fig. 3.2.

It is worthwhile to point out that similar to the arguments used in potential theory, Eq. 3.11 represents the potential at the position $\vec{x}$ as a combination of the contributions from the two different kinds of singularities (or source points). Looking first at the second part in the integrand of Eq. 3.11, it is seen that this represents a simple source or a sink located on the boundary with strength $\frac{\partial}{\partial n} f_2(\vec{x}_o)$. On

the other hand, the first part in the integrand of Eq. 3.11 represents the contribution of the distribution of doublets located on the boundary with a strength $f_2(\vec{x}_o)$. These singularities are evidently represented by Eq. 3.11 because the asymptotic behavior of the imaginary part of the Hankel function $H_o^{(1)}(kr)$ for very small kr is a logarithmic singularity:

$$\text{Imaginary}\left(H_o^{(1)}(kr)\right) \sim \frac{2}{\pi}\log(kr)$$

From Eq. 3.11, it is clear that in order to be able to determine the wave function, f_2, at any interior point of Region II, either the value f_2 or the value $\frac{\partial f_2}{\partial n}$ on the boundary of the region must be known. The boundary conditions set previously stated that the normal derivative of the wave function on the solid boundary is zero, i.e. $\frac{\partial f_2}{\partial n} = 0$, but its value at the harbor entrance is unknown. At this point in the derivation the value of the wave function f_2 everywhere on the boundary is also unknown. In order to determine the wave function f_2 on the boundary, Eq. 3.11 is modified by allowing the field point $\vec{x}$ to approach a boundary point $\vec{x}_i(x_i, y_i)$ from the interior of the harbor (see Fig. 3.2). If the boundary is sectionally smooth, the following expression can be obtained: (This derivation is presented in Appendix II.)

$$f_2(\vec{x}_i) = -\frac{\lambda}{4}\int_S \left\{ f_2(\vec{x}_o)\frac{\partial}{\partial n}\left[H_o^{(1)}(k|\vec{x}_i - \vec{x}_o|)\right] - H_o^{(1)}(k|\vec{x}_i - \vec{x}_o|)\frac{\partial}{\partial n}\left[f_2(x_o)\right]\right\} ds(\vec{x}_o)$$

$$+\tfrac{1}{2} f_2(\vec{x}_i) \qquad (3.12)$$

Rearranging Eq. 3.12 one obtains:

$$f_2(\vec{x}_i) = -\frac{i}{2}\int_s \left\{ f_2(\vec{x}_o)\frac{\partial}{\partial n}\left[H_o^{(1)}(k|x_i - x_o|)\right] - H_o^{(1)}(k|\vec{x}_i - \vec{x}_o|)\frac{\partial}{\partial n}\left[f_2(\vec{x}_o)\right]\right\} ds(\vec{x}_o). \tag{3.13}$$

To solve Eq. 3.13 for the value of f_2 on the boundary for an arbitrary shaped harbor, an approximate method is proposed. In the approximate method the integral equation is converted to a matrix equation. (Similar approaches used in solving an integral equation have been employed by others, e.g., Banaugh and Goldsmith (1963), Chertock (1964), Copley (1967), Mikhlin and Smolitskiy (1967).) This is accomplished by dividing the boundary into a sufficiently large number of segments where along each segment the average value on that segment of $f_2(\vec{x}_o)$, $\frac{\partial}{\partial n} f_2(\vec{x}_o)$, $H_o^{(1)}(kr)$, $\frac{\partial}{\partial n}(H_o^{(1)}(kr))$, is used. The line integral of Eq. 3.13, which represents the wave function f_2, is approximated by a finite summation of the contributions of the singularities from each segment, where the singularities are the average values just mentioned and are considered to be located at the center of each segment.

Writing the integral equation Eq. 3.13 as a summation one obtains:

$$f_2(\vec{x}_i) = -\frac{i}{2}\sum_{j=1}^{N}\left[f_2(\vec{x}_j)\frac{\partial}{\partial n}\left(H_o^{(1)}(kr_{ij})\right) - H_o^{(1)}(kr_{ij})\frac{\partial}{\partial n} f_2(\vec{x}_j)\right]\Delta s_j \tag{3.14}$$

where the boundary is divided into N segments, and:

r_{ij} is the distance between the points $\vec{x}_j$ and $\vec{x}_i$ and is defined as $r_{ij} = |\vec{x}_j - \vec{x}_i| = r_{ji}$,

$\vec{x}_i$ is the position vector for the field point on the boundary,

$\vec{x}_j$ is the position vector for the source point on the boundary,

and

Δs_j is the length of the j^{th} segment of the boundary.

The segments of the boundary will be numbered counterclockwise starting from the right-hand-side of the harbor opening; with reference to Fig. 3.3 the starting point is point B. It should be noted that because of this approximate representation of the boundary, the original curved boundary is replaced by a boundary approximating it and composed of straight-line segments.

Eq. 3.14 can be written in a matrix form as:

$$\underline{X} = b_o\left[G_n\underline{X} - G\underline{P}\right] \quad , \tag{3.15}$$

or rearranging this expression:

$$\left(b_o G_n - I\right)\underline{X} = b_o G\underline{P} \tag{3.16}$$

where $b_o = -\frac{i}{2}$ and the following notation is used:

$$\underline{X} = f_2(\vec{x}_i) \qquad i = 1,2,.....N \tag{3.17a}$$

$$(G_n)_{ij} = \frac{\partial}{\partial n}\left(H_o^{(1)}(kr_{ij})\right)\Delta s_j \qquad \begin{matrix} i = 1,2,.....N \\ j = 1,2,.....N \end{matrix} \tag{3.17b}$$

$$\underline{P} = \frac{\partial}{\partial n}\left[f_2(\vec{x}_j)\right] \qquad j = 1,2,.....N \tag{3.17c}$$

$$(G)_{ij} = H_o^{(1)}(kr_{ij})\Delta s_j \qquad \begin{matrix} i = 1,2,.....N \\ j = 1,2,.....N \end{matrix} \tag{3.17d}$$

$$I = \delta_{ij}\begin{cases} 0 & \text{if } i \neq j \\ 1 & \text{if } i = j \end{cases} \qquad \begin{matrix} i = 1,2,.....N \\ j = 1,2,.....N \end{matrix} \tag{3.17e}$$

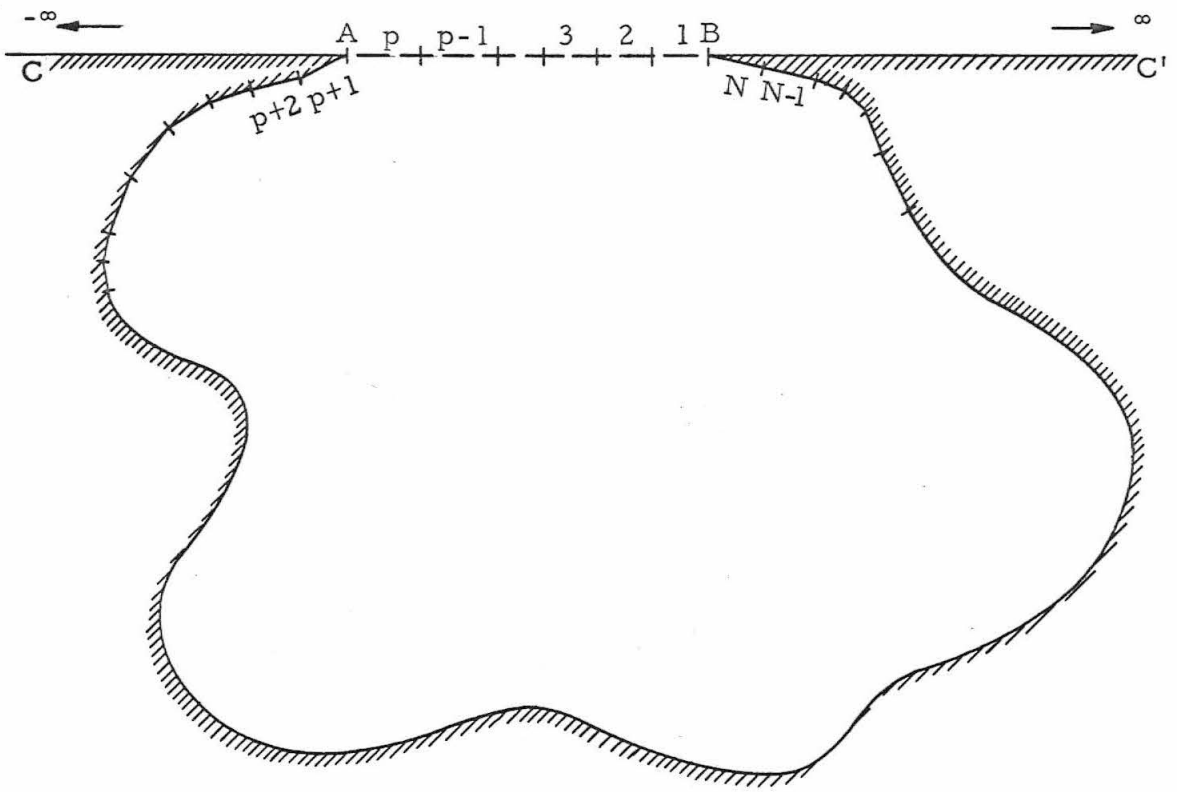

p = Total number of segments at the harbor entrance

N = Total number of segments on the harbor boundary (including entrance)

Fig. 3.3 Definition sketch of the harbor boundary approximated by straight-line segments

The evaluation of these matrix elements will be discussed in Section 3.3 which deals with the numerical analysis. It should be noted that special care must be taken in evaluating the matrices, especially the elements when i=j.

If the inverse of the matrix $(b_o G_n - I)$ exists, where I is the identity matrix, the vector $\underline{X}$ can be expressed as:

$$\underline{X} = (b_o G_n - I)^{-1} (b_o G \underline{P}) \quad , \tag{3.18}$$

in which $(b_o G_n - I)^{-1}$ is defined as the inverse of the matrix $(bG_n - I)$.

The vector $\underline{P}$ in Eqs. 3.16 and 3.18 involve the unknown normal derivatives of the wave function at the harbor entrance as well as the normal derivatives of the wave function on the boundary. These latter values are zero, i.e. the values of the normal derivative of the wave function f_2 for the segment i=p+1,.....N are zero. The vector $\underline{P}$ can be represented in the following way:

$$\underline{P} = \begin{bmatrix} \frac{\partial f_2}{\partial n}(\vec{x}_1) \\ \cdot \\ \cdot \\ \cdot \\ \frac{\partial f_2}{\partial n}(\vec{x}_p) \\ \frac{\partial f_2}{\partial n}(\vec{x}_{p+1}) \\ \cdot \\ \cdot \\ \cdot \\ \frac{\partial f_2}{\partial n}(\vec{x}_N) \end{bmatrix} = \begin{bmatrix} C_1 \\ \cdot \\ \cdot \\ \cdot \\ C_p \\ 0 \\ \cdot \\ \cdot \\ \cdot \\ 0 \end{bmatrix} = \begin{bmatrix} 1 & 0 & 0 & . & 0 \\ 0 & 1 & 0 & . & 0 \\ 0 & 0 & 1 & . & 0 \\ . & . & . & . & . \\ 0 & 0 & . & . & 1 \\ 0 & 0 & . & . & 0 \\ 0 & 0 & . & . & 0 \\ . & . & . & . & . \\ . & . & . & . & . \\ 0 & 0 & . & . & 0 \end{bmatrix} \cdot \begin{bmatrix} C_1 \\ \cdot \\ \cdot \\ \cdot \\ C_p \end{bmatrix} = U_m \underline{C} = \sum_{j=1}^{p} \delta_{ij} C_j \tag{3.19}$$

in which, $U_m = \delta_{ij} = \begin{cases} 0 & \text{for } i \neq j \\ 1 & \text{for } i = j \end{cases}$ (the index i = 1, 2, ... N, and the index j=1, 2, ... p). Since the total number of segment into which the harbor entrance is divided is defined as p, the values of C_j for j=1, 2, ... p are the unknown normal derivatives of wave function f_2 at the harbor entrance, which is represented by the unknown vector $\underline{C}$.

Substituting Eq. 3.19 into Eq. 3.16 and Eq. 3.18 the following matrix equation results:

$$(b_o G_n - I)\underline{X} = (b_o G U_m) \cdot \underline{C} \quad , \tag{3.20}$$

or rearranging:

$$\underline{X} = (b_o G_n - I)^{-1} (b_o G U_m)\underline{C} = M\underline{C} \quad , \tag{3.21}$$

where $M = (b_o G_n - I)^{-1} \cdot b_o G U_m$ is a N x p matrix and can be computed directly.

Eq. 3.21 shows that the wave function on the boundary, $f_2(\vec{x}_i)$, can be expressed as a function of the unknown normal derivative of f_2 at the harbor entrance, i.e.:

$$f_2(\vec{x}_i) = \sum_{j=1}^{p} M_{ij} C_j \quad , \tag{3.22}$$

where i=1, 2, 3..... N.

If the normal derivatives of the wave function C_1, C_2, C_3, ... C_p at the entrance of the harbor (which at this point are unknown) can be obtained, then the wave function f_2 on the boundary of the harbor can be computed directly from Eq. 3.22. (It should be noted that Eq. 3.22 can also be interpreted as the contribution to the

wave function on the boundary at a particular point from the superposition of the effect of p small harbor openings). Once the wave function f_2 on the boundary is known, the wave function in the interior of the harbor can be evaluated from Eq. 3.11 expressed in discrete form as:

$$f_2(\vec{x}) = -\frac{i}{4}\sum_{j=1}^{N}\left[f_2(\vec{x}_j)\left[\frac{\partial}{\partial n}H_o^{(1)}(kr)\right] - H_o^{(1)}(kr)\frac{\partial}{\partial n}\left[f_2(\vec{x}_j)\right]\right]\Delta s_j \quad , \quad (3.23)$$

where $\vec{x}$ is the field point inside the harbor, r is the distance between the field point and the source point. Eq. 3.23 will be discussed in more detail in Subsection 3.2.3.

In order to evaluate the normal derivatives at the harbor entrance: $C_1, C_2, \ldots . C_p$ in Eq. 3.22, the wave function f_1 in Region I at the entrance of the harbor must be expressed as a function of the same normal derivatives: $C_1, C_2, \ldots . C_p$. By matching these wave functions f_1 and f_2 at the harbor entrance, the normal derivatives $C_1, C_2, \ldots . C_p$ can be evaluated from the resulting expression and the complete solution to the response problem can be obtained.

3.2.2 Wave Function Outside the Harbor (Region I)

In Eq. 3.6, the wave amplitude η is expressed as a product of the incident wave amplitude at the crest A_i, the wave function $f(x, y)$, and the time varying function $e^{-i\sigma t}$. Because the analytical treatment is linear, the wave amplitude in Region I can be considered as composed of three separate parts: an incident wave, a reflected wave, (from the "coastline" with the harbor entrance closed), and a radiated wave emanating from the harbor entrance. Thus, the wave function

in Region I can be separated into three parts:

$$f_1 = f_i + f_r + f_3 \tag{3.24}$$

where: f_i represents an incident wave function,

f_r represents a reflected wave function considered to occur as if the harbor entrance were closed,

f_3 represents the radiated wave function due to the presence of the harbor.

It should be noted that Eq. 3.24 implies that the wave amplitude in Region I, $\eta_1 = A_i f_1 e^{-i\sigma t}$, is equivalent to $\eta_1 = A_i(f_i + f_r + f_3) e^{-i\sigma t}$. This implies that any differences among the wave amplitudes for the three portions: η_i, η_r, and η_3, compared to the amplitude of η_1 are incorporated in constants contained in the wave functions: f_i, f_r, and f_3.

The incident wave function, f_i, can be specified in an arbitrary fashion; for example, a periodic incident wave with the wave ray at an angle α to the x-axis (the coastline in Fig. 3.2) can be represented as $f_i(x, y) = \cos(ky \sin \alpha) e^{ikx \cos \alpha}$. The reflected wave function f_r, can be represented by $f_r(x, y) = f_i(x, -y)$. For the case of a periodic incident wave with the wave ray perpendicular to the coastline ($\alpha = 90^\circ$), the function which represents the x and y variation of the incident wave, $f_i(x, y)$, can be represented by $\frac{1}{2} \cos ky$. This is the case which was treated experimentally in this study and therefore the following discussion will be concerned with periodic waves normally incident to the coastline.

The wave function f_1 in Eq. 3.24 must satisfy the Helmholtz equation in Region I (Eq. 3.5):

$$\frac{\partial^2 f_1}{\partial x^2} + \frac{\partial^2 f_1}{\partial y^2} + k^2 f_1 = 0 \qquad (3.25)$$

with the following boundary conditions:

(i) $\frac{\partial f_1}{\partial n} = 0$ on boundary $\overline{AC}$ and $\overline{BC}'$ (as shown in Fig. 3.2),

(ii) $\frac{\partial f_1}{\partial n} = -\frac{\partial f_2}{\partial n}$ on boundary $\overline{AB}$ (harbor entrance) ,

(iii) $\lim_{r^2 \to \infty} f_1 = f_i + f_r$, and the radiation condition (where $r^2 = x^2 + y^2$) .

Boundary condition (i) states that the normal velocity is zero at the coastline. The second boundary condition (ii) states that the slope of the water surface is continuous at the harbor entrance and the value from Region I is equal in magnitude to that obtained at the entrance from Region II. The negative sign is specified for the adapted sign convention that the outward normal to the domain of interest is considered positive. For the case of normal wave incidence in Fig. 3.2 it is noted that the normal to the boundary in Region I is in the direction of the y-axis. The last boundary condition (iii) specifies that the radiated wave in Region I emanating from the harbor entrance will decay to zero at infinity, hence at infinity only the standing wave resulting from the incident and reflected waves remains.

As mentioned earlier, the reflected wave function f_r is known once the incident wave function f_1 is specified. Therefore, to complete the evaluation of the wave function f_1, the main problem is to evaluate the radiated wave function f_3. Since the analytical treatment is linear,

the functions f_i, f_r, and f_3 all must satisfy the same differential equation, Eq. 3.25. In addition the boundary conditions in Region I can be simplified since the normal derivative of the wave function is zero on the impermeable boundaries being considered. With reference to Fig. 3.2, on the boundary $\overline{CABC'}$ $\frac{\partial}{\partial n}(f_i + f_r) = \frac{\partial}{\partial y}(f_i + f_r) = 0$, and hence boundary condition (ii) can be replaced by $\frac{\partial f_3}{\partial n} = -\frac{\partial f_2}{\partial n}$ at harbor entrance (boundary $\overline{AB}$). Thus, the radiation function f_3 in Region I can be formulated as satisfying the Helmholtz equation:

$$\frac{\partial^2 f_3}{\partial x^2} + \frac{\partial^2 f_3}{\partial y^2} + k^2 f_3 = 0 \quad , \tag{3.26}$$

with the following boundary conditions:

(i) $\frac{\partial f_3}{\partial n} = 0$ on boundary $\overline{AC}$ and $\overline{BC'}$ (as shown in Fig. 3.2),

(ii) $\frac{\partial f_3}{\partial n} = -\frac{\partial f_2}{\partial n}$ on boundary $\overline{AB}$ (harbor entrance),

(iii) $\lim_{r^2 \to \infty} f_3 = 0$ and the radiation condition (where $r^2 = x^2 + y^2$).

It is noted the these boundary conditions are reduced from those associated with Eq. 3.25.

To construct a solution for the radiated wave function f_3 in Eq. 3.26, Green's identity formula (Appendix I, Eq. A. 1. 1) will be used again and the fundamental solution $H_o^{(1)}(kr)$ used in previous section will be used here also. The fundamental solution $H_o^{(1)}(kr)$ also satisfies the radiation condition at infinity, i. e. boundary condition (iii), since as $kr \to \infty$ it asymptotically goes to zero:

$$H_o^{(1)}(kr) \sim \sqrt{\frac{2}{\pi(kr)}}\, e^{i\left(kr - \frac{\pi}{4}\right)} \quad . \tag{3.27}$$

If the fundamental solution is multiplied by the time dependent function $e^{-i\sigma t}$, the resultant expression represents an outgoing radiated wave satisfying boundary condition (iii) (see Appendix I):

$$H_o^{(1)}(kr)e^{-i\sigma t} \sim \sqrt{\frac{2}{\pi(kr)}}\, e^{i\left(kr-\sigma t-\frac{\pi}{4}\right)} \quad , \tag{3.28}$$

The radiated wave function f_3 in Region I can be expressed using Weber's formula in a similar fashion as Eq. 3.11 was used for the expression of the wave function f_2 in Region II:

$$f_3(\vec{x}) = -\frac{i}{4}\int_s \left[f_3(\vec{x}_o)\frac{\partial}{\partial n}\left(H_o^{(1)}(kr)\right) - H_o^{(1)}(kr)\frac{\partial}{\partial n}\left(f_3(\vec{x}_o)\right)\right] ds(\vec{x}_o) \quad , \tag{3.29}$$

where $\vec{x}_o$ is the source point $(x_o, 0)$ along the x-axis, $\vec{x}$ is the field point (x, y) in Region I, and r is the distance between the field point and the source point, i.e. $r = \sqrt{(x-x_o)^2 + y^2}$ (see Fig. 3.2).

In order to find the radiated wave function f_3 on the x-axis, the field point (x, y) is allowed to approach the x-axis at the point $(x_i, 0)$. (This approach is the same as in the treatment of Region II.) Thus, the following equation can be obtained (see Appendix II):

$$f_3(x_i, 0) = -\frac{i}{2}\int_s \left[f_3(x_o, 0)\frac{\partial}{\partial n}\left(H_o^{(1)}(kr)\right) - H_o^{(1)}(kr)\frac{\partial}{\partial n}\left(f_3(x_o, 0)\right)\right] ds(x_o, 0) \quad . \tag{3.30}$$

The term $\frac{\partial}{\partial n}\left[H_o^{(1)}(kr)\right]$ in the integral can be expanded to become $-kH_1^{(1)}(kr) \cdot \frac{\partial r}{\partial n}$. However, because the field point $\vec{x}_i(x_i, 0)$ and the source point $\vec{x}_o(x_o, 0)$ are all on the x-axis, the term $\frac{\partial r}{\partial n}$ is equal to zero. Therefore, the first term inside the integral in Eq. 3.30 is equal to zero and can be eliminated. In the second term, $\frac{\partial f_3}{\partial n}(x_o, 0)$, the normal derivative of the radiated wave function f_3, is equal to zero

everywhere except across the harbor entrance. The integral unit $ds(x_o, 0)$ becomes dx_o because the integration is to be performed along x-axis. Thus, Eq. 3.30 can be simplified to:

$$f_3(x_i, 0) = \frac{i}{2} \int_{\overline{AB}} H_o^{(1)}(kr) \frac{\partial}{\partial n}\left[f_3(x_o, 0)\right] dx_o \quad . \tag{3.31}$$

Using boundary condition (ii) of Eq. 3.26, Eq. 3.31 can be rewritten as:

$$f_3(x_i, 0) = -\frac{i}{2} \int_{\overline{AB}} H_o^{(1)}(kr) \frac{\partial}{\partial n}\left[f_2(x_o, 0)\right] dx_o \quad . \tag{3.32}$$

Eq. 3.32 shows that the radiation wave function f_3 at the harbor entrance can be expressed as a function of the unknown normal derivative of the wave function at the harbor entrance computed from Region II, i.e. in terms of $\frac{\partial}{\partial n} f_2(x_o, 0)$.

Eq. 3.32 can be expressed in summation form similar to Eq. 3.22:

$$f_3(x_i, 0) = -\frac{i}{2} \sum_{j=1}^{p} H_{ij} C_j \quad , \tag{3.33}$$

where the matrix $H_{ij} = H_o^{(1)}(kr_{ij})\Delta s_j$, is a p x p matrix (the evaluation of the elements of this matrix especially for i=j will be discussed in Subsection 3.3.3), r_{ij} is the distance $|x_i - x_j|$ wherein x_i, x_j are the midpoints of the i^{th} and j^{th} segments of the harbor entrance respectively. The term C_j in Eq. 3.33 is the normal derivative of the wave function f_2 at the j^{th} segment of the harbor entrance, Δs_j is the length of the j^{th} segment of the harbor entrance, and p is the total number of segments into which the harbor entrance has been divided.

Because the incident wave function plus the reflected wave function at the harbor entrance, $f_i + f_r$, is a constant, by substituting Eq. 3.33 into Eq. 3.24 the wave function f_1 at the harbor entrance can be represented as:

$$f_1(\vec{x}_i) = 1 + (-\frac{i}{2}) \sum_{j=1}^{p} H_{ij} C_j \quad , \tag{3.34}$$

where i=1, 2, ... p. The first term at the right hand side of Eq. 3.34 represents the incident wave plus the reflected wave if the entrance is closed and for convenience it is chosen as unity; the second term represents the contribution of the radiated wave to the total wave system.

3.2.3 Matching the Solution for Each Region at the Harbor Entrance

Eq. 3.22 shows that from the solution in Region II, the wave function at the boundary of the harbor can be expressed in terms of the normal derivatives of the wave function f_2 at the entrance of the harbor, C_j. The corresponding equation in Region I, Eq. 3.34 shows that the wave function at the harbor entrance can also be expressed as a function of C_j. Since the water surface must be continuous at the harbor entrance, the wave functions from Regions I and II must be equal at the entrance, i.e. $f_1 = f_2$. Thus, by matching the two solutions at the harbor entrance, one is able to determine the unknown function C_j. This is done in the following fashion:

Take the first p equations from Eq. 3.22 for the wave function f_2 at the harbor entrance:

$$f_2(\vec{x}_i) = \sum_{j=1}^{p} M_{ij} C_j = M_p \cdot \underline{C} \quad , \tag{3.35}$$

in which the index $i=1,2,\ldots..p$, (p is the number of segments into which the harbor entrance is divided). The matrix M_p in Eq. 3.35 is a p x p matrix obtained from the first p rows of the matrix M.

Equating Eqs. 3.34 and 3.35, i.e. $f_1(\vec{x}_i) = f_2(\vec{x}_i)$, for $i=1,2,\ldots.p$ the following matrix equation is obtained:

$$M_p \underline{C} = \underline{1} + b_o H \underline{C} \quad , \tag{3.36a}$$

$$\underline{C} = (M_p - b_o H)^{-1} \cdot \underline{1} \quad , \tag{3.36b}$$

where M_p and H are each p x p matrices, $(M_p - b_o H)^{-1}$ is the inverse of the matrix $(M_p - b_o H)$, the term b_o is equal to $-\frac{i}{2}$ as defined earlier, and $\underline{1}$ is the vector with each p element equal to unity. Therefore, the value of the normal derivative of the wave function at the harbor entrance for each of the p-segments, $\underline{C}$, can be obtained from Eq. 3.36b.

With the normal derivatives of the wave function f_2 at the harbor entrance obtained by this matching procedure, the wave function on the boundary can now be calculated from Eq. 3.22 and the wave function at any position inside the harbor can be determined from Eq. 3.23 or the equivalent expression:

$$f_2(\vec{x}) = -\frac{i}{4} \sum_{j=1}^{N} \left[f_2(\vec{x}_j) \left[-kH_1^{(1)}(kr) \frac{\partial r}{\partial n} \right] - H_o^{(1)}(kr) \frac{\partial}{\partial n} \left[f_2(\vec{x}_j) \right] \right] \Delta s_j$$

$$= -\frac{i}{4} \left\{ \sum_{j=1}^{N} \left[f_2(\vec{x}_j) \left[-kH_1^{(1)}(kr) \frac{\partial r}{\partial n} \right] \right] \Delta s_j - \sum_{j=1}^{p} H_o^{(1)}(kr) \cdot C_j \cdot \Delta s_j \right\} \quad , \tag{3.37}$$

where $\vec{x}_j$ is at the mid-point of the j^{th} segment of the boundary, $\vec{x}$ is the position of the interior point and r is the distance between $\vec{x}_j$ and x, i.e. $r=|\vec{x}_j-\vec{x}|$. It should be noted that Eq. 3.23 is written in the form of Eq. 3.37 because the normal derivative of the wave function at the boundary is zero except at the harbor entrance.

In order to determine the response of the harbor to incident waves, the wave amplitude inside the harbor is usually compared to the incident plus the reflected wave amplitude which exists in the "open-sea" in the absence of the harbor, i.e. the harbor entrance is closed. A parameter called the "amplification factor" is defined as the ratio of the wave amplitude at any position (x, y) inside the harbor to the incident plus reflected wave amplitude at the coastline (with the entrance closed).

$$R = \frac{|\eta_2(x,y;t)|}{|A_i(f_i+f_r)e^{-i\sigma t}|} = \frac{|A_i f_2(x,y)e^{-i\sigma t}|}{|A_i \cdot 1 \cdot e^{-i\sigma t}|} = |f_2(x,y)| \quad . \tag{3.38}$$

In Eq. 3.38, R is defined as the amplification factor. The wave function $f_2(x,y)$ is a complex number; therefore, in computing the wave amplitude the absolute value is taken.

3.2.4 Velocity at the Harbor Entrance

With the wave function $f_2(x,y)$ determined in Subsection 3.2.3, the calculation of the velocity potential $\Phi(x,y,z;t)$ for the region inside the harbor is now complete:

$$\Phi(x,y,z;t) = \frac{1}{i\sigma} \frac{A_i g \cosh k(z+h)}{\cosh kh} f_2(x,y)\, e^{-i\sigma t} \quad . \tag{3.39}$$

In accordance with the definition sketch presented in Fig. 3.1, the velocities at the position (x, y, z) in the directions of x, y, z are defined as follows:

$$u(x,y,z;t) = \text{Real}\left(\frac{\partial\Phi}{\partial x}\right) = \text{Real}\left[\frac{1}{\lambda\sigma}\frac{A_i g \cosh k(z+h)}{\cosh kh}\frac{\partial f_2}{\partial x}(x,y)e^{-\lambda\sigma t}\right], \quad (3.40a)$$

$$v(x,y,z;t) = \text{Real}\left(\frac{\partial\Phi}{\partial y}\right) = \text{Real}\left[\frac{1}{\lambda\sigma}\frac{A_i g \cosh k(z+h)}{\cosh kh}\frac{\partial f_2}{\partial y}(x,y)e^{-\lambda\sigma t}\right], \quad (3.40b)$$

$$w(x,y,z;t) = \text{Real}\left(\frac{\partial\Phi}{\partial z}\right) = \text{Real}\left[\frac{1}{\lambda\sigma}\frac{kA_i g \sinh k(z+h)}{\cosh kh} f_2(x,y)e^{-\lambda\sigma t}\right], \quad (3.40c)$$

and the total velocity at any position (x, y, z) and time t, can be expressed as:

$$V^*(x,y,z;t) = \sqrt{u^2 + v^2 + w^2} \quad . \quad (3.40d)$$

The velocity at the harbor entrance is of interest because it is directly related to the kinetic energy transmitted into the harbor. This total velocity V^* is a periodic function of time. In order to find the maximum total velocity for all time, the function $V^*(x,y,z;t)$ is differentiated with respect to time and the derivative is set equal to zero; from this condition one can determine the time for which the velocity is a maximum. Thus, the maximum total velocity, which is denoted as V_o^*, at a particular position (x, o, z) at the harbor entrance can be calculated as follows:

$$V_o^*(x,o,z) = \frac{A_i g}{\sigma}\left[\frac{A_1^2+A_2^2+A_3^2}{2} + \frac{1}{2}\left(A_1^4+A_2^4+A_3^4+2A_1^2A_2^2\cos 2(\alpha_1-\alpha_2)\right.\right.$$
$$\left.\left. + 2A_2^2A_3^2\cos 2(\alpha_2-\alpha_3) + 2A_1^2A_3^2\cos 2(\alpha_1-\alpha_3)\right)^{\frac{1}{2}}\right]^{\frac{1}{2}} \quad (3.41)$$

where:

$$A_1 = \left|\frac{\partial f_2}{\partial x}\right| \frac{\cosh k(z+h)}{\cosh kh}$$

$$A_2 = \left|\frac{\partial f_2}{\partial y}\right| \frac{\cosh k(z+h)}{\cosh kh}$$

$$A_3 = \left|f_2\right| \frac{k \sinh k(z+h)}{\cosh kh}$$

$$\alpha_1 = \tan^{-1}\left[-\frac{\left(\frac{\partial f_2}{\partial x}\right)_R}{\left(\frac{\partial f_2}{\partial x}\right)_I}\right]$$

$$\alpha_2 = \tan^{-1}\left[-\frac{\left(\frac{\partial f_2}{\partial y}\right)_R}{\left(\frac{\partial f_2}{\partial y}\right)_I}\right]$$

$$\alpha_3 = \tan^{-1}\left[-\frac{(f_2)_R}{(f_2)_I}\right]$$

wherein the subscripts R and I which appear in the expressions for α_1, α_2, α_3 denote the real part and imaginary part respectively.

As will be discussed in Subsection 6.2.5, experiments were conducted to measure the velocity at the harbor entrance using a hot-film anemometer. The hot-film sensor was oriented with its longitudinal axis parallel both to the "coastline" and the bottom, and, hence, it was primarily sensitive to the velocities in the y and z directions (the v and w components respectively). For comparison with the experimental data the theoretical value of the maximum resultant velocity of the v and w components, which is denoted as V_o, can be determined by setting u^2 equal to zero in Eq. 3.40d (or $A_1 = 0$ in Eq. 3.41):

$$V_o(x,o,z) = \frac{A_i g}{\sigma}\left[\frac{A_2^2 + A_3^2}{2} + \frac{1}{2}\left(A_2^4 + A_3^4 + 2A_2^2 A_3^2 \cos 2(\alpha_2 - \alpha_3)\right)^{\frac{1}{2}}\right]^{\frac{1}{2}} \tag{3.42}$$

where A_2, A_3, α_2, and α_3 are defined in Eq. 3.41.

3.3 THE NUMERICAL ANALYSIS

Section 3.2 was concerned only with the transformation of the Weber's solution of the Helmholtz equation (Eq. 3.11) into an integral equation (Eq. 3.13) and the formulation of an approximate solution to this integral equation. In this section the methods for evaluating the elements of the matrices defined in Eqs. 3.15 and 3.33 will be discussed as well as the numerical method for solving the wave function f_2 in Region II and the matching procedure.

3.3.1 Region II: Evaluation of Matrices Defined in Eq. 3.15

i) Off-diagonal elements of the matrix G_n

As defined in Eq. 3.14 the notation $\vec{x}_i(x_i, y_i)$ is used for $i=1,2,.....N$, to refer to the field points, and the notation $\vec{x}_j(x_j, y_j)$ for $j=1,2,.....N$ is used to refer to the source points. The elements $(G_n)_{ij}$ for $i \neq j$ can be evaluated as follows:

$$(G_n)_{ij} = \frac{\partial}{\partial n}\left[H_o^{(1)}(kr_{ij})\right]\Delta s_j$$

$$= -kH_1^{(1)}(kr_{ij})\frac{\partial r_{ij}}{\partial n}\Delta s_j \quad , \tag{3.43}$$

in which $r_{ij} = \sqrt{(x_i - x_j)^2 + (y_i - y_j)^2}$ is the distance between the mid-points of the i^{th} segment and the j^{th} segment of the boundary. The Hankel function $H_1^{(1)}(kr_{ij})$ in Eq. 3.43 can be expressed in terms of the Bessel functions by the equations:

$$H_1^{(1)}(kr_{ij}) = J_1(kr_{ij}) + iY_1(kr_{ij}) \quad . \tag{3.44}$$

Hence, Eq. 3.44 is known once the argument kr_{ij} is known.

The term $\frac{\partial r_{ij}}{\partial n}$ in Eq. 3.43 can be evaluated as follows:

$$\left(\frac{\partial r_{ij}}{\partial n}\right)_j = \frac{\partial r_{ij}}{\partial x_j}\left(\frac{\partial x}{\partial n}\right)_j + \frac{\partial r_{ij}}{\partial y_j}\left(\frac{\partial y}{\partial n}\right)_j \quad . \tag{3.45}$$

In the right-hand side of Eq. 3.45 the differentiation with respect to the outward normal direction of the boundary, n, i.e. $\left(\frac{\partial x}{\partial n}\right)_j$ and $\left(\frac{\partial y}{\partial n}\right)_j$, can be changed into differentiation with respect to the tangential direction along the boundary, $\frac{\partial}{\partial s}$. Therefore, according to the definition sketch of Fig. 3.4, Eq. 3.45 can be rewritten as:

$$\left(\frac{\partial r_{ij}}{\partial n}\right)_j = \frac{\partial r_{ij}}{\partial x_j}\left(\frac{\partial y}{\partial s}\right)_j - \frac{\partial r_{ij}}{\partial y_j}\left(\frac{\partial x}{\partial s}\right)_j \quad . \tag{3.46}$$

Referring to the definition of r_{ij} and performing the differentiation of $\frac{\partial r_{ij}}{\partial x_j}$ and $\frac{\partial r_{ij}}{\partial y_j}$ Eq. 3.46 becomes:

$$\left(\frac{\partial r_{ij}}{\partial n}\right)_j = -\frac{x_i - x_j}{r_{ij}}\left(\frac{\partial y}{\partial s}\right)_j + \frac{y_i - y_j}{r_{ij}}\left(\frac{\partial x}{\partial s}\right)_j \quad . \tag{3.47}$$

Writing the terms $\left(\frac{\partial y}{\partial s}\right)_j$ and $\left(\frac{\partial x}{\partial s}\right)_j$ in difference form Eq. 3.47 becomes:

$$\left(\frac{\partial r_{ij}}{\partial n}\right)_j \approx -\frac{x_i - x_j}{r_{ij}}\left(\frac{\Delta y}{\Delta s}\right)_j + \frac{y_i - y_j}{r_{ij}}\left(\frac{\Delta x}{\Delta s}\right)_j \quad . \tag{3.48}$$

Therefore, the off-diagonal elements of the matrix G_n can be evaluated by substituting Eqs. 3.44 and 3.48 into Eq. 3.43.

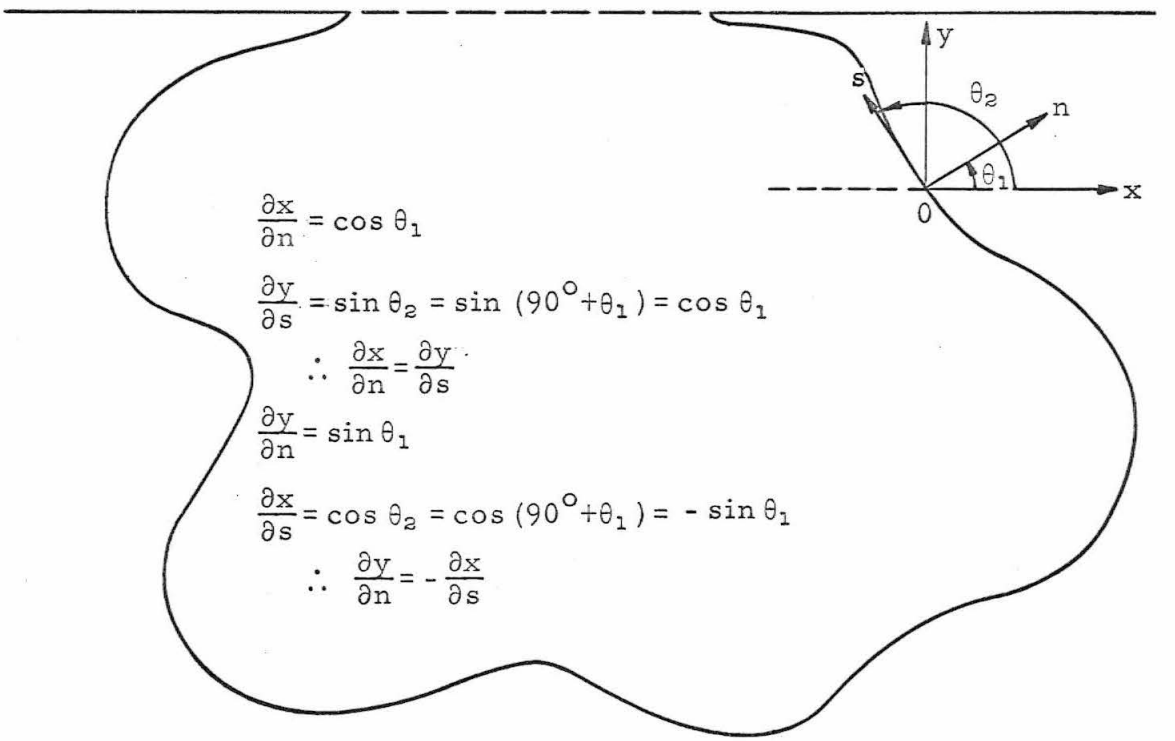

Fig. 3.4 Change of derivatives from normal to tangential direction

ii) Diagonal elements of the Matrix G_n

For matrix G_n, since the source and field points are located at the mid-point of the straight-line segments which have been used to approximate the boundary, the diagonal elements of the matrix G_n correspond to the condition of the coincidence of a particular field point and source point. Due to the singular behavior of the Hankel function $H_1^{(1)}(kr)$ as $kr \to 0$, special attention must be given in evaluating these diagonal elements.

The function $Y_1(x)$ in Eq. 3.44 can be expressed as a series as (see Hildebrand (1962) p. 147):

$$Y_1(x) = \frac{2}{\pi}\left[(\log \frac{x}{2} + \gamma) J_1(x) - \frac{1}{x} - \frac{x}{4} + \left\{\frac{1 + (1 + \frac{1}{2})}{2}\right\} \frac{x^3}{2^3 2!} - \ldots\ldots\right], \quad (3.49)$$

in which $\gamma = 0.577216\ldots$ is termed Euler's constant, and the logarithm is to the Naperian base e (= 2.7128), (all logarithms will be to this base unless indicated otherwise). The real part of Hankel function $H_1^{(1)}(kr)$ presented in Eq. 3.44 is $J_1(kr)$ which is approximately equal to $\frac{kr}{2}$ when kr becomes very small; therfore, $J_1(kr) \to 0$ as $kr \to 0$. Thus, from Eq. 3.49 as $kr \to 0$ the function $Y_1(kr)$ can be approximated as:

$$Y_1(kr) \sim -\frac{2}{\pi}\left(\frac{1}{kr}\right) \qquad \text{for } kr \to 0 \quad . \quad (3.50)$$

Thus, the diagonal elements of the matrix G_n can be evaluated as the limiting value as r approaches zero (Eq. 3.43 for i=j):

$$(G_n)_{ii} = \lim_{r \to 0}\left(-kH_1^{(1)}(kr)\frac{\partial r}{\partial n}\right)\Delta s_i = \lim_{r \to 0} -k\left[J_1(kr) + \lambda Y_1(kr)\right]\frac{\partial r}{\partial n}\Delta s_i$$

$$= 0 + \lambda \frac{2}{\pi}\Delta s_i \left[\lim_{r \to 0} \frac{\frac{\partial r}{\partial n}}{r}\right] \quad . \quad (3.51)$$

Therefore, in evaluating the diagonal elements of the matrix G_n, the most important step is to evaluate the term $\lim_{r\to 0} \frac{\frac{\partial r}{\partial n}}{r}$ in Eq. 3.51.

The definition of r is:

$$r = \sqrt{(x-x_i)^2 + (y-y_i)^2}$$

where (x_i, y_i) are the coordinates of the mid-point of the i^{th} segment on the boundary thus the term $\frac{\partial r}{\partial n}$ can be expressed in a form similar to Eq. 3.47:

$$\frac{\partial r}{\partial n} = \frac{\partial r}{\partial x}\frac{\partial x}{\partial n} + \frac{\partial r}{\partial y}\frac{\partial y}{\partial n} = \frac{x-x_i}{r}\left(\frac{\partial y}{\partial s}\right) + \frac{y-y_i}{r}\left(-\frac{\partial x}{\partial s}\right) . \qquad (3.52)$$

The terms $(x-x_i)$, $(y-y_i)$, $\frac{\partial x}{\partial s}$, and $\frac{\partial y}{\partial s}$ in Eq. 3.52 can be expanded in a Taylor's series in the neighborhood of (x_i, y_i):

$$x-x_i \approx (x_s)_i \Delta s + (x_{ss})_i \frac{(\Delta s)^2}{2!} + (x_{sss})_i \frac{(\Delta s)^3}{2!} + \ldots . \qquad (3.53)$$

$$\frac{\partial x}{\partial s} \approx (x_s)_i + (x_{ss})_i \Delta s + (x_{sss})_i \frac{(\Delta s)^2}{2!} + \ldots . \qquad (3.54)$$

where the subscript s refers to differentiation with respect to s. (The index i means that the values of interest are evaluated at the mid-point of the i^{th} segment.) The expansion $(y-y_i)$ and $\frac{\partial y}{\partial s}$ can be done in exactly the same way by changing x to y in Eqs. 3.53 and 3.54.

Thus the term $\lim_{r\to 0} \frac{\frac{\partial r}{\partial n}}{r}$ in Eq. 3.51 can be evaluated using the definition of r, Eq. 3.52, and Eqs. 3.53 and 3.54 to give:

$$\lim_{r\to 0} \frac{\frac{\partial r}{\partial n}}{r} = \lim_{\Delta s\to 0} \frac{\frac{\partial r}{\partial n}}{r}$$

$$\approx \frac{\left((y_s)_i + (y_{ss})_i \Delta s + \ldots\right)\left((x_s)_i \Delta s + (x_{ss})_i \frac{(\Delta s)^2}{2!} + \ldots\right) - \left((x_s)_i + (x_{ss})_i \Delta s \ldots\right)\left((y_s)_i \Delta s + (y_{ss})_i \frac{(\Delta s)^2}{2!} + \ldots\right)}{\left((x_s)_i \Delta s + (x_{ss})_i \frac{(\Delta s)^2}{2!} + \ldots\right)^2 + \left((y_s)_i \Delta s + (y_{ss})_i \frac{(\Delta s)^2}{2!} + \ldots\right)^2}$$

(3.55)

The numerator of Eq. 3.55 can be arranged as:

$$\left(-x_{ss}y_s + x_s y_{ss}\right)_i \frac{(\Delta s)^2}{2!} + o(\Delta s^3)$$

where $o(\Delta s^3)$ means terms of order Δs^3.

The denominator of Eq. 3.55 can be arranged as:

$$\left(x_s^2 + y_s^2\right)_i (\Delta s)^2 + o(\Delta s^3)$$

this expression can be simplified farther to become $(\Delta s)^2 + o(\Delta s^3)$ because in reference to Fig. 3.4 the term $x_s^2 + y_s^2$ is equal to unity.

Thus, neglecting the higher order terms in Eq. 3.55, this expression can be approximated as:

$$\lim_{\Delta s \to 0} \frac{\frac{\partial r}{\partial n}}{r} \approx \frac{\left(-x_{ss}y_s + x_s y_{ss}\right)_i}{2} \quad . \tag{3.56}$$

Therefore, the diagonal elements of the matrix G_n can be found from Eq. 3.51 and the approximation described in Eq. 3.56:

$$(G_n)_{ii} = \frac{\lambda}{\pi}\left(x_s y_{ss} - x_{ss} y_s\right)_i \Delta s_i \quad . \tag{3.57}$$

In Eq. 3.57, the first and second derivatives of x_s, y_s, x_{ss}, y_{ss} are evaluated at the mid-point of the i^{th} segment of the boundary.

For a boundary which is originally composed of straight lines the value of $x_s y_{ss}$ and $y_s x_{ss}$ in Eq. 3.57 are both equal to zero (because the second derivatives x_{ss} and y_{ss} are both zero); therefore the diagonal elements of the matrix G_n are equal to zero. For a curved boundary which has been approximated by straight-line segments the expression of the first and second derivatives, x_s and x_{ss}, can be written in a difference form as:

$$x_s = \frac{\Delta x}{\Delta s} = \frac{x_{i+\frac{1}{2}} - x_{i-\frac{1}{2}}}{\Delta s_i} \tag{3.58a}$$

$$x_{ss} = \frac{6}{\Delta s_{i+1} + \Delta s_i + \Delta s_{i-1}} \left[\frac{x_{i+1} - x_i}{\Delta s_{i+1} + \Delta s_i} - \frac{x_i - x_{i-1}}{\Delta s_i + \Delta s_{i-1}} \right] \tag{3.58b}$$

where x_i is the x coordinate at the mid-point of the i^{th} segment of the boundary, $x_{i-\frac{1}{2}}$ is the x coordinate at the beginning of the i^{th} segment of the boundary, and $x_{i+\frac{1}{2}}$ is the x coordinate at the end of the i^{th} segment of the boundary, $\Delta s_{i-1}, \Delta s_i$, and Δs_{i+1} are the length of the $(i-1)^{th}$ i^{th}, and $(i+1)^{th}$ segments of the boundary. The derivatives y_s, y_{ss} can be evaluated in exactly the same way by changing x to y in Eqs. 3.58.

iii) Off-diagonal elements of the matrix G

The elements $(G)_{ij}$ for $i \neq j$ can be evaluated directly by the following expression:

$$(G)_{ij} = H_o^{(1)}(kr_{ij})\Delta s_j = \left[J_o(kr_{ij}) + \lambda Y_o(kr_{ij}) \right] \Delta s_j \quad . \tag{3.59}$$

For a given value of kr_{ij}, in Eq. 3.59, the function $J_o(kr_{ij})$ and $Y_o(kr_{ij})$ are known functions.

iv) Diagonal elements of the matrix G

The diagonal elements of the matrix G correspond to the case of $i=j$ in Eq. 3.59. As before, due to the singular behavior of the function $Y_o(kr)$, special attention must be given in evaluating the diagonal elements of matrix G. Using the asymptotic formula of $J_o(kr)$ and $Y_o(kr)$ as the argument for kr approach zero, the following approximations are obtained (see Hildebrand (1962)):

$$J_o(kr) \approx 1 \quad ,$$

$$Y_o(kr) \approx \frac{2}{\pi}\left(\log\frac{kr}{2} + \gamma\right) \quad .$$

Therefore, as $kr \to 0$ the Hankel function $H_o^{(1)}(kr)$ can be expressed as:

$$H_o^{(1)}(kr) = J_o(kr) + \lambda Y_o(kr) \approx 1 + \lambda\left[\frac{2}{\pi}\left(\log\frac{kr}{2} + \gamma\right)\right] \quad (\text{for } kr \to 0)$$

where γ is the Euler's constant as mentioned earlier.

Using this asymptotic formula for the Hankel function $H_o^{(1)}(kr)$, the diagonal elements of the matrix G can be evaluated by performing the following integration to determine the average of this function over the length of the segment of interest:

$$(G)_{ii} = \left[\frac{1}{\frac{1}{2}\Delta s_i}\int_0^{\frac{1}{2}\Delta s_i}\left[1 + \lambda\frac{2}{\pi}\left(\log\left(\frac{kr}{2}\right) + \gamma\right)\right]dr\right] \cdot \Delta s_i$$

$$= \left[1 + \lambda\frac{2}{\pi}\left[\log\left(\frac{k\Delta s_i}{4}\right) - 1 + \gamma\right]\right]\Delta s_i \qquad (3.60)$$

$$= \left[1 + \lambda\frac{2}{\pi}\left[\log\left(\frac{k\Delta s_i}{4}\right) - 0.42278\right]\right]\Delta s_i$$

where $i = 1, 2, \ldots\ldots N$.

3.3.2 Region II: Method of Solution for Wave Function f_2

In Subsection 3.3.1 the methods for evaluating the elements of the matrices G and G_n have been discussed; thus, the next step is to evaluate the matrix M, as defined in Eq. 3.21, in order to determine the variation of the wave function f_2 along the boundary of the harbor. As shown in Eq. 3.22 the wave function f_2 along the boundary of the harbor can be expressed as a function of the unknown normal derivative of the wave function f_2 at the harbor entrance, i.e. $C_1, C_2, \ldots\ldots C_p$; Eq. 3.22 is repeated here for clarity:

$$f_2(\vec{x}_i) = \sum_{j=1}^{p} M_{ij} C_j \quad , \tag{3.22}$$

wherein M_{ij} is a N x p matrix which is the solution of the following matrix equation, rearranged from that shown in Eq. 3.21:

$$(b_o G_n - I) M = b_o G U_m \quad . \tag{3.61}$$

The matrix $(b_o G_n - I)$ is a N x N matrix, its elements can be determined as described in Subsection 3.3.1 using the definitions of b_o and I given in Subsection 3.2.1. The right-hand-side of Eq. 3.61, matrix $b_o G U_m$, is a N x p matrix, where U_m is defined by Eq. 3.19. (It should be noted that the matrices G, G_n and M shown in Eq. 3.61 are all complex numbered matrices.)

To solve Eq. 3.61 for the complex numbered matrix M, a subroutine for the IBM 360/75 digital computer: "CSLECD/Complex System of Linear Equations and Complex Determinant" was used which is available at the Booth Computing Center of the California Institute of Technology. The subroutine is based on the Gaussian elimination method where rows are interchanged leading to the conversion of the left-hand side matrix in Eq. 3.61 to an upper triangular matrix. The solution of M is then obtained by backward substitution.

3.3.3 Region I: Evaluation of Matrix H Defined in Eq. 3.33

The matrix H defined in Eq. 3.33 can be evaluated in the same way as was matrix G. The matrix H will be called the "radiation matrix" because it is the main part of the radiated wave function $f_3(\vec{x})$ described in Eq. 3.33; it is a p x p matrix and its off-diagonal elements can be evaluated in a manner similar to that shown in Eq. 3.59:

$$(H)_{ij} = H_o^{(1)}(kr_{ij})\Delta s_j = \left[J_o(kr_{ij}) + \lambda Y_o(kr_{ij})\right]\Delta s_j \qquad (3.62)$$

(for $i \neq j$ and $i, j = 1, 2, \ldots . p$) .

The diagonal elements can be evaluated in a manner similar to that shown in Eq. 3.60:

$$(H)_{ii} = \left[1 + \lambda \frac{2}{\pi}\left(\log\left(\frac{k\Delta s_i}{4}\right) - 0.42278\right)\right]\Delta s_i \qquad (3.63)$$

(for $i = 1, 2, \ldots . p$) .

3.3.4 Harbor Entrance: Matching Procedure

After solving Eq. 3.61 for the N x p matrix M and evaluating the elements of the matrix H as outlined in Subsection 3.3.3, the next important step is the matching of the two solutions from Region I and Region II at the harbor entrance. Eq. 3.36a is the result of this matching procedure and the object of this section is to describe how the vector $\underline{C}$ (the normal derivative of the wave function at the harbor entrance) is obtained.

Eq. 3.36a is first rewritten as:

$$(M_p - b_o H)\ \underline{C} = \underline{1} \qquad (3.64)$$

in which M_p is a p x p matrix as explained in Subsection 3.2.3. To sólve Eq. 3.64 for the vector $\underline{C}$ again involves the subroutine "CSLECD/ Complex System of Linear Equations and Complex Determinant", but this time the matrix size is only p x p and the solution $\underline{C}$ is a p x 1 vector.

After evaluating the vector $\underline{C}$, the procedure for determining the quantities of interest such as the response of the harbor, the amplitude distribution, etc. are described in Subsection 3.2.3.

3.4 CONFIRMATION OF THE NUMERICAL ANALYSIS

The theory for an arbitrary shaped harbor has been presented in Sections 3.2 and 3.3. However, prior to evaluating the wave induced oscillations of an actual harbor, it is necessary to make sure that the method presented in Subsection 3.2.1 and the numerical procedure presented in Subsections 3.3.1 and 3.3.2 are correct. Therefore, the approximate solution obtained using the method developed will be tested by comparing it with the exact solution of the Helmholtz equation for two different shapes. These two shapes are a circle and a square. They are chosen for several reasons: (1) the theoretical solution for both shapes can be obtained easily, (2) the boundary of a circle represents an extreme case for which the tangent to the boundary is continuously changing direction, and (3) the boundary of a square (or a rectangular) represents another extreme case that is composed of four straight lines; along each line the direction of the tangent to the boundary remains the same.

The procedure for this test program can be outlined as follows:

1) A theoretical solution is selected for the wave function, f, that satisfies the Helmholtz equation, $\nabla^2 f + k^2 f = 0$, in the domain of interest (either a circle or a square).
2) Based on this theoretical solution the value of the wave function, f, at the boundary of the domain, the value of its normal derivative at the boundary of the domain, $\frac{\partial f}{\partial n}$, and the value of f at any position inside the domain are

calculated. (It should be noted that the boundaries for these two test examples do not necessarily represent solid boundaries.)

3) The boundary of the domain is divided into N segments; the average of the theoretical values of f and $\frac{\partial f}{\partial n}$ on each segment are calculated.

4) These averaged theoretical values of the normal derivative $\frac{\partial f}{\partial n}$ for each segment on the boundary are used to calculate the value of f for each corresponding segment by the method described in Subsection 3.2.1. One test of this approximate method is the comparison of this computed value with the theoretical value of f on the boundary of the domain. Any difference between these two results which is found can be attributed to the approximations resulting from converting the integral equation (Eq. 3.13) to the matrix equation (Eq. 3.15).

5) The computed value of f (Step 4) and the theoretical value of $\frac{\partial f}{\partial n}$ on the boundary of the domain are used to compute the value of f at various locations inside the domain using Eq. 3.37. The values of f so obtained are compared with the theoretical values. The difference is the error admitted in Step 4 plus the error due to using Eq. 3.37 which has been used as an approximation to the exact solution, Eq. 3.11.

6) The theoretical values of f and $\frac{\partial f}{\partial n}$ at the boundary of the domain are used to caluclate the value of f at some points inside the domain by using Eq. 3.37; the values of f so obtained are compared with the theoretical values. The difference is solely due to the use of Eq. 3.37 which approximates the exact equation, Eq. 3.11.

It should be noted that these two examples (circle and square) are not directly connected with the actual problem of wave induced oscillations in harbors, since the boundary conditions imposed by this test program (steps 2 and 3) do not correspond to the boundary conditions prescribed for the harbor oscillation problem (as described in Section 3.1). Rather, these examples are employed in a mathematical sense serving as an analytical check for the approximate method that will be used in solving the problem which is of major concern: wave induced oscillations in an arbitrary shaped harbor.

3.4.1 The First Example: A Circle

The first example that will be investigated is a circular domain, a definition sketch of which is presented in Fig. 3.5. The Helmholtz equation is written in polar coordinates as:

$$\frac{1}{r}\frac{\partial}{\partial r}\left(r\frac{\partial f}{\partial r}\right) + \frac{1}{r^2}\frac{\partial^2 f}{\partial \theta^2} + k^2 f = 0 \quad . \tag{3.65}$$

The steps outlined previously are followed; the following particular solution which satisfies the Helmholtz equation, Eq. 3.65, is selected:

$$f(r,\theta) = J_1(kr)\cos\theta \tag{3.66}$$

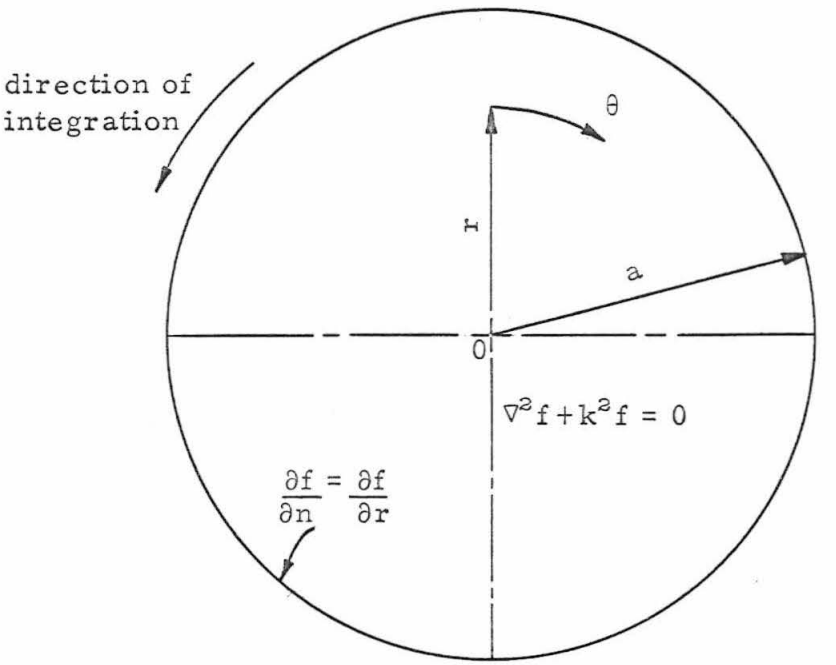

Fig. 3.5 Definition sketch of a circular domain

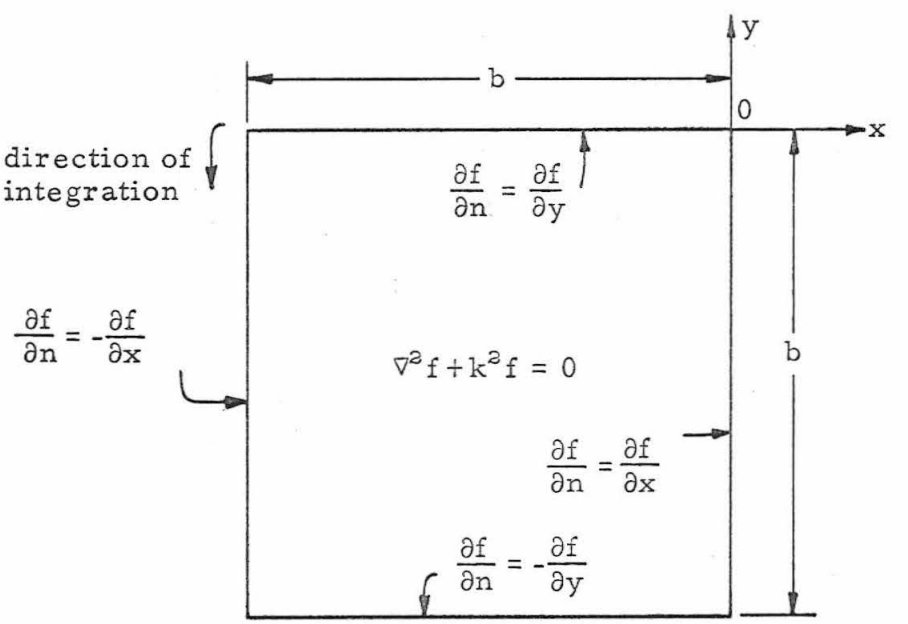

Fig. 3.6 Definition sketch of a square domain

thus, differentiating Eq. 3.66 with respect to r one obtains:

$$\frac{\partial}{\partial r}\left[f(r,\theta)\right] = \left[kJ_o(kr) - \frac{1}{r}J_1(kr)\right]\cos\theta \quad . \tag{3.67}$$

Suppose a boundary of the domain is located at r=a, then the value of f and $\frac{\partial f}{\partial n}$ on the boundary can be expressed as:

$$f(a,\theta) = J_1(ka)\cos\theta \quad , \tag{3.68a}$$

$$\frac{\partial f}{\partial n}(a,\theta) = \frac{\partial f}{\partial r}(a,\theta) = \left[kJ_o(ka) - \frac{1}{a}J_1(ka)\right]\cos\theta \quad . \tag{3.68b}$$

The boundary is then divided into 36 segments (each segment includes 10^o of the central angle). On each segment the average theoretical value of the functions $f(a,\theta)$ and $\frac{\partial f}{\partial n}(a,\theta)$ can be evaluated as follows:

$$\begin{aligned}(\overline{f})_i &= \frac{J_1(ka)}{\theta_{i+\frac{1}{2}} - \theta_{i-\frac{1}{2}}}\int_{\theta_{i-\frac{1}{2}}}^{\theta_{i+\frac{1}{2}}}\cos\theta\, d\theta \\ &= J_1(ka)\,\frac{\sin\theta_{i+\frac{1}{2}} - \sin\theta_{i-\frac{1}{2}}}{\theta_{i+\frac{1}{2}} - \theta_{i-\frac{1}{2}}} \quad ,\end{aligned} \tag{3.69a}$$

$$\begin{aligned}\left(\overline{\frac{\partial f}{\partial n}}\right)_i &= \frac{kJ_o(ka) - \frac{1}{a}J_1(ka)}{\theta_{i+\frac{1}{2}} - \theta_{i-\frac{1}{2}}}\int_{\theta_{i-\frac{1}{2}}}^{\theta_{i+\frac{1}{2}}}\cos\theta\, d\theta \\ &= \left[kJ_o(ka) - \frac{1}{a}J_1(ka)\right]\frac{\sin\theta_{i+\frac{1}{2}} - \sin\theta_{i-\frac{1}{2}}}{\theta_{i+\frac{1}{2}} - \theta_{i-\frac{1}{2}}} \quad ,\end{aligned} \tag{3.69b}$$

where $(\overline{f})_i$ and $\left(\overline{\frac{\partial f}{\partial n}}\right)_i$ are the average theoretical values on the boundary of the domain of f and $\frac{\partial f}{\partial n}$ for the i^{th} segment, $(a, \theta_{i-\frac{1}{2}})$ are the coordinates of the beginning of the i^{th} segment of the boundary, and $(a, \theta_{i+\frac{1}{2}})$ are the coordinates of the end of the i^{th} segment of the boundary.

In Step 4, the value of $\left(\overline{\frac{\partial f}{\partial n}}\right)_i$, presented in Eq. 3.69 b for each segment is used to calculate the value of f of each segment on the boundary by the approximate method of Subsection 3.2.1. These computed values will be denoted as $\overline{f}_c$. The value of $\overline{f}_c$ and $\overline{f}$ should be very close if the approximate method is to be useful. Three different values of ka, i.e. ka=0.30, 2.25, 3.75 have been tested (where k is the wave number in ft^{-1} and a is the radius of the circular domain and chosen as 0.75 ft for this case). The approximate result ($\overline{f}_c$) agreed with the theoretical values ($\overline{f}$) within 0.1% to 3% for ka=0.3 and 3.75 respectively. The effect of the magnitude of ka on the solution will be discussed more fully in Chapter 6.

After the values of f on the boundary, i.e. $\overline{f}_c$, have been obtained, the value of f at any interior point can be computed using Eq. 3.37 (Step 5). The results for ka=0.30, 2.25 and 3.75 are presented in Table 3.1. For each value of ka, the value of f at five interior points are computed. The theoretical value of f at each interior point is calculated using Eq. 3.66 and presented in Col. 3. The results of Step 5, i.e. the computed approximate values of f at each interior point, are presented in Col. 4. The difference between the value in Cols. 3 and 4 can be attributed to: (i) the error admitted in the approximate solution, Eq. 3.15, which is used to approximate the integral equation (Eq. 3.13) in evaluating the value of f on the boundary (Step 4), and (ii) the error admitted in the use of Eq. 3.37 to approximate the exact solution, Eq. 3.11, in evaluating the value of f for the interior points.

Table 3.1 Comparison of the approximate solution with the theoretical solution of the Helmholtz equation in a circular domain

k & ka (1)	Position of Interior Point (r, θ) (2)		Theoretical Value of f (Step 2) (3)		N = 36				N = 45			
					Computed Value of f (Step 5) (4)		Computed Value of f (Step 6) (5)		Computed Value of f (Step 5) (6)		Computed Value of f (Step 6) (7)	
	r (ft)	θ (deg.)	Real Part	Imaginary Part	Real Part	Imaginary Part	Real Part	Imaginary Part	Real Part	Imaginary Part	Real Part	Imaginary Part
$k=0.40\ ft^{-1}$	0.50	30	0.08617	0	0.08604	0.00003	0.08642	-0.00001	0.08604	0.00003	0.08633	-0.00001
	0.50	60	0.04975	0	0.04967	0.00002	0.04989	-0.00001	0.04967	0.00002	0.04984	-0.00000
ka = 0.30	0.50	150	-0.08617	0	-0.08604	-0.00003	-0.08642	0.00001	-0.08604	-0.00003	-0.08633	0.00001
	0.20	0	0.03997	0	0.03991	0.00001	0.04008	-0.00001	0.03991	0.00001	0.04004	-0.00000
	0.20	180	-0.03997	0	-0.03991	-0.00001	-0.04008	0.00001	-0.03991	-0.00001	-0.04004	0.00000
	0.50	240	-0.04975	0	-0.04967	-0.00002	-0.04989	0.00001	-0.04967	-0.00001	-0.04984	0.00000
	0.50	30	0.48319	0	0.49190	0.00592	0.48273	-0.00333	0.48854	0.00446	0.48290	-0.00213
$k=3.0\ ft^{-1}$	0.50	60	0.27897	0	0.28400	0.00342	0.27871	-0.00192	0.28206	0.00257	0.27880	-0.00123
	0.50	150	-0.48319	0	-0.49191	-0.00592	-0.48274	0.00333	-0.48854	-0.00446	-0.48290	0.00213
ka = 2.25	0.20	0	0.28670	0	0 29188	0.00351	0.28643	-0.00198	0.28988	0.00264	0.28653	-0.00127
	0.20	180	-0.28670	0	-0.29187	-0.00351	-0.28643	0.00198	-0.28988	-0.00264	-0.28653	0.00127
	0.50	240	-0.27897	0	-0.28400	-0.00342	-0.27871	0.00192	-0.28206	-0.00257	-0.27880	0.00123
	0.50	30	0.43050	0	0.42902	0.00613	0.43020	-0.00599	0.42939	0.00496	0.43031	-0.00384
$k=5.0\ ft^{-1}$	0.50	60	0.24855	0	0.24770	0.00354	0.24837	-0.00346	0.24791	0.00287	0.24844	-0.00222
	0.50	150	-0.43050	0	-0.42902	-0.00613	-0.43020	0.00599	-0.42939	-0.00496	-0.43031	0.00384
ka = 3.75	0.20	0	0.44005	0	0.43854	0.00626	0.43974	-0.00613	0.43892	0.00508	0.43986	-0.00392
	0.20	180	-0.44005	0	-0.43854	-0.00626	-0.43974	0.00613	-0.43892	-0.00508	-0.43986	0.00392
	0.50	240	-0.24854	0	-0.24770	-0.00354	-0.24838	0.00346	-0.24791	-0.00287	-0.24844	0.00222

The results of Step 6 are shown in Col. 5; they are obtained by using the theoretical values of f and $\frac{\partial f}{\partial n}$ at the boundary (Eqs. 3.69) to compute the value of f at the interior point by applying Eq. 3.37. The difference between the theoretical results of Col. 3 and the approximate results in Col. 5 is solely due to the use of Eq. 3.37 which approximates the exact solution of Eq. 3.11.

It should be noted that Step 6 applied to a given domain does not correspond to a mathematically realistic boundary value problem, simply because both the value of f and $\frac{\partial f}{\partial n}$ on the boundary are usually not given in advance; usually one or the other is given. However, it does give an indication of how good the approximation of Eq. 3.37 is, if the correct boundary values f and $\frac{\partial f}{\partial n}$ are provided. Step 5 does correspond to a mathematically realistic boundary value problem and in fact it is basically the procedure used for solving the harbor resonance problem, that is: given a particular value of $\frac{\partial f}{\partial n}$ at the boundary, calculate the value of f at the boundary and finally calculate the value of f at any interior point (r, θ).

It is expected that if the number of segments into which the boundary of the domain is divided is increased, the results of the approximate method will agree better with the theoretical results. The results for N=45 (each segment includes 8^{o} of the central angle) are presented in Cols. 6 and 7 of Table 3.1. By comparing Cols. 3, 4, and 6 (also comparing Cols. 3, 5, and 7) it is seen that as the number of boundary segment is increased the results of the approximate method compared to the theoretical results are improved only slightly.

3.4.2 The Second Example: A Square

Suppose the square has sides of length b as shown in Fig. 3.6, then a simple particular solution of the function f that satisfies the Helmholtz equation, Eq. 3.5, can be chosen as:

$$f(x,y) = \cos\left(\frac{\pi}{2b}x\right)\cosh\left(\sqrt{\left(\frac{\pi}{2b}\right)^2 - k^2}\, y\right) \quad \left(\text{for } k < \frac{\pi}{2b}\right) \tag{3.70a}$$

$$f(x,y) = \cos\left(\frac{\pi}{2b}x\right)\cos\left(\sqrt{k^2 - \left(\frac{\pi}{2b}\right)^2}\, y\right) \quad \left(\text{for } k > \frac{\pi}{2b}\right) \tag{3.70b}$$

thus, the outward normal derivative of the function f at the boundary of the domain can be evaluated as following:

$$\frac{\partial f}{\partial n} = \frac{\partial f}{\partial y}, \quad \text{for } y=0, \quad -b \le x \le 0$$

$$\frac{\partial f}{\partial n} = -\frac{\partial f}{\partial y}, \quad \text{for } y=-b, \quad -b \le x \le 0$$

$$\frac{\partial f}{\partial n} = \frac{\partial f}{\partial x}, \quad \text{for } x=0 \quad -b \le y \le 0$$

$$\frac{\partial f}{\partial n} = -\frac{\partial f}{\partial x}, \quad \text{for } x=-b, \quad -b \le y \le 0$$

The steps outlined previously are followed. The boundary of the square domain is divided equally into 40 segments. The theoretical value of f at any interior point (x, y) can be calculated by Eqs. 3.70 once the value of wave number k is fixed. The results for two different values of kb, i.e. kb = 0.50 and 2.0 (where k is the wave number and the length of sides of the square domain is b = 0.50 ft) are presented in Table 3.2. For each value of kb the value of f at nine interior points are computed. The theoretical values of f at each point for kb = 0.50 are computed using Eq. 3.70a; the theoretical values of f for kb = 2.0 are computed using Eq. 3.70b. These theoretical values are presented in Col. 3 of Table 3.2. The approximate results of the value of f in

Table 3.2 Comparison of the approximate solution with the theoretical solution of the Helmholtz equation in a square domain

k & kb (1)	Position of Interior Point (x, y) (2)		Theoretical Value of f (Step 2) (3)		N = 40				N = 48			
					Computed Value of f (Step 5) (4)		Computed Value of f (Step 6) (5)		Computed Value of f (Step 5) (6)		Computed Value of f (Step 6) (7)	
	x (ft)	y (ft)	Real Part	Imaginary Part	Real Part	Imaginary Part	Real Part	Imaginary Part	Real Part	Imaginary Part	Real Part	Imaginary Part
$k = 1.00\ ft^{-1}$	-0.25	-0.25	0.91232	0	0.94304	-0.05257	0.91394	0.00100	0.93601	-0.04071	0.91410	0.00086
	-0.40	-0.25	0.39870	0	0.43391	-0.05293	0.40008	0.00101	0.42617	-0.04102	0.40012	0.00087
kb = 0.50	-0.10	-0.25	1.22707	0	1.25409	-0.05166	1.22863	0.00097	1.24747	-0.03998	1.22860	0.00084
	-0.25	-0.10	0.73870	0	0.77000	-0.05290	0.73985	0.00097	0.76273	-0.04074	0.73994	0.00084
	-0.25	-0.40	1.27106	0	1.30042	-0.05200	1.27284	0.00101	1.29354	-0.04026	1.27311	0.00087
	-0.40	-0.10	0.32282	0	0.35710	-0.05290	0.32378	0.00099	0.34948	-0.04106	0.32402	0.00085
	-0.40	-0.40	0.55547	0	0.59341	-0.05225	0.55713	0.00102	0.58578	-0.04052	0.55790	0.00088
	-0.10	-0.10	0.99355	0	1.02083	-0.05149	0.99579	0.00095	1.01499	-0.03989	0.99618	0.00082
	-0.10	-0.40	1.70957	0	1.72833	-0.05082	1.71415	0.00098	1.72460	-0.03934	1.71455	0.00085
	-0.25	-0.25	0.57591	0	0.57861	-0.00170	0.57660	-0.00010	0.57821	-0.00107	0.57666	-0.00011
$k = 4.00\ ft^{-1}$	-0.40	-0.25	0.25168	0	0.25607	-0.00510	0.25208	-0.00012	0.25526	-0.00391	0.25203	-0.00013
	-0.10	-0.25	0.77460	0	0.77538	0.00196	0.77535	-0.00006	0.77531	0.00193	0.77540	-0.00007
kb = 2.00	-0.25	-0.10	0.68554	0	0.68740	0.00032	0.68623	-0.00003	0.68714	0.00058	0.68631	-0.00004
	-0.25	-0.40	0.38775	0	0.39099	-0.00340	0.38820	-0.00015	0.39038	-0.00250	0.38818	-0.00015
	-0.40	-0.10	0.29959	0	0.30421	-0.00363	0.29998	-0.00006	0.30363	-0.00273	0.30025	-0.00006
	-0.40	-0.40	0.16946	0	0.17310	-0.00672	0.16957	-0.00017	0.17223	-0.00530	0.16955	-0.00017
	-0.10	-0.10	0.92205	0	0.91932	0.00488	0.92410	0.00000	0.92062	0.00432	0.92443	-0.00000
	-0.10	-0.40	0.52153	0	0.52320	-0.00003	0.52244	-0.00011	0.52335	0.00025	0.52275	-0.00011

Step 5 are shown in Col. 4, while the results of Step 6 are shown in Col. 5. Comparing the results in Cols. 3 and 4, it is seen that dependent upon the position of the interior point the results agree within 1% to 3%, and, as expected, the results in Col. 5 are closer to the theoretical results (Col. 3).

The results for N=48 (each side of the boundary contains 12 boundary segments) are presented in Cols. 6 and 7. Comparing the results in Cols. 3, 4, and 6 (also Cols. 3, 5, and 7) it is seen that the results for N=48 agree better with the theoretical value than when the boundary is divided into 40 segments.

From the results of these two examples, a circle and a square, which were used it is seen that this numerical method and the approximations it entails can be used to solve the Helmholtz equation with reasonable accuracy. Thus, the real problem of determining wave induced oscillations in an arbitrary shaped harbor which may have both curved and/or straight lined boundaries can be approached with confidence.

CHAPTER 4

THEORETICAL ANALYSIS FOR TWO HARBORS WITH SPECIAL SHAPES

Two theories which deal with the wave induced oscillations in a circular and a rectangular harbor are presented in this chapter. A circular harbor represents one extreme case for which the tangent to the boundary of the harbor is continuously changing direction; a rectangular harbor represents another extreme case whose boundary is composed of four straight lines and along each line the tangent to the boundary remains in the same direction. Thus, these two special theoretical solutions provide a useful analytical check for the approximate theory developed in Chapter 3 for an arbitrary shaped harbor as well as being used to compare to the results of experiments conducted in the laboratory. The results for these particular cases and their comparison with the theory developed for arbitrary shapes discussed in Chapter 3 applied to these two harbors will be presented in Chapter 6.

4.1 THEORETICAL ANALYSIS FOR A CIRCULAR HARBOR

The theory developed in Chapter 3 can be used for any arbitrary shaped harbor. However, if the harbor is a special shape such as circular, the coordinates inside the harbor are separable and a different method can be used to obtain a solution in Region II. (For a list of separable coordinate systems see Morse and Feshback (1953) pp. 656-666.) The theoretical analysis for a circular harbor based on this approach will be presented in this section.

In the analysis, the wave function f_2 which satisfies the Helmholtz equation, Eq. 3.5, in Region II is found by the method of separation of variables. The solution for the open-sea, Region I, which is used for this development is the same as that presented in Chapter 3. By matching the solutions in both regions at the harbor entrance, the complete solution of the wave induced oscillation in a circular harbor can be obtained.

4.1.1 Wave Function Inside the Circular Harbor

For the wave function f_2 inside the circular harbor, the Helmholtz equation, Eq. 3.5, is written in cylindrical coordinates:

$$\frac{1}{r}\frac{\partial}{\partial r}\left(r\frac{\partial f_2}{\partial r}\right)+\frac{1}{r^2}\frac{\partial^2 f_2}{\partial \theta^2}+k^2 f_2 = 0. \tag{4.1}$$

The boundary conditions that the function f_2 must satisfy are:

$$\frac{\partial f_2}{\partial r}(a,\theta)=\begin{cases} C(\theta) & \text{for } |\theta| \le \theta_o \\ 0 & \text{for } |\theta| > \theta_o \end{cases} \tag{4.2}$$

where a is the radius of the circular harbor, $2\theta_o$ is the central angle of the harbor opening, and $C(\theta)$ is the initially unknown normal derivative of the wave function f_2 at the harbor entrance. A definition sketch of the circular harbor showing both regions: Region I (the "open-sea") and Region II (inside the harbor), is presented in Fig. 4.1.

The solution of Eq. 4.1 will be constructed by Fourier series, by first seeking the solution of $f_2(r,\theta)$ in the form of:

$$f_2(r,\theta) = \sum_{m=-\infty}^{\infty} f_m(r) e^{im\theta} \quad . \tag{4.3}$$

Substituting Eq. 4.3 into Eq. 4.1, it is found that the function $f_m(r,\theta)$ must satisfy the following differential equation:

$$f_m''(r) + \frac{1}{r} f_m'(r) + \left(k^2 - \frac{m^2}{r^2}\right) f_m(r) = 0 \, . \tag{4.4}$$

This equation is a form of the Bessel equation; hence, its solution can be expressed as:

$$f_m(r) = \alpha_m J_m(kr) + \beta_m Y_m(kr) \, , \tag{4.5}$$

wherein the function $J_m(kr)$ is the Bessel function of the first kind, and $Y_m(kr)$ is the Bessel function of the second kind; α_m and β_m are arbitrary constants to be determined.

The function $Y_m(kr)$ possesses a singular behavior at r=0, but since the solution of the wave function $f_2(r,\theta)$ must be smooth and finite at r=0, the constant β_m must be zero. Thus, from Eq. 4.3, the solution of Eq. 4.1 can be expressed as:

$$f_2(r,\theta) = \sum_{m=-\infty}^{\infty} \alpha_m J_m(kr) e^{im\theta} \, . \tag{4.6}$$

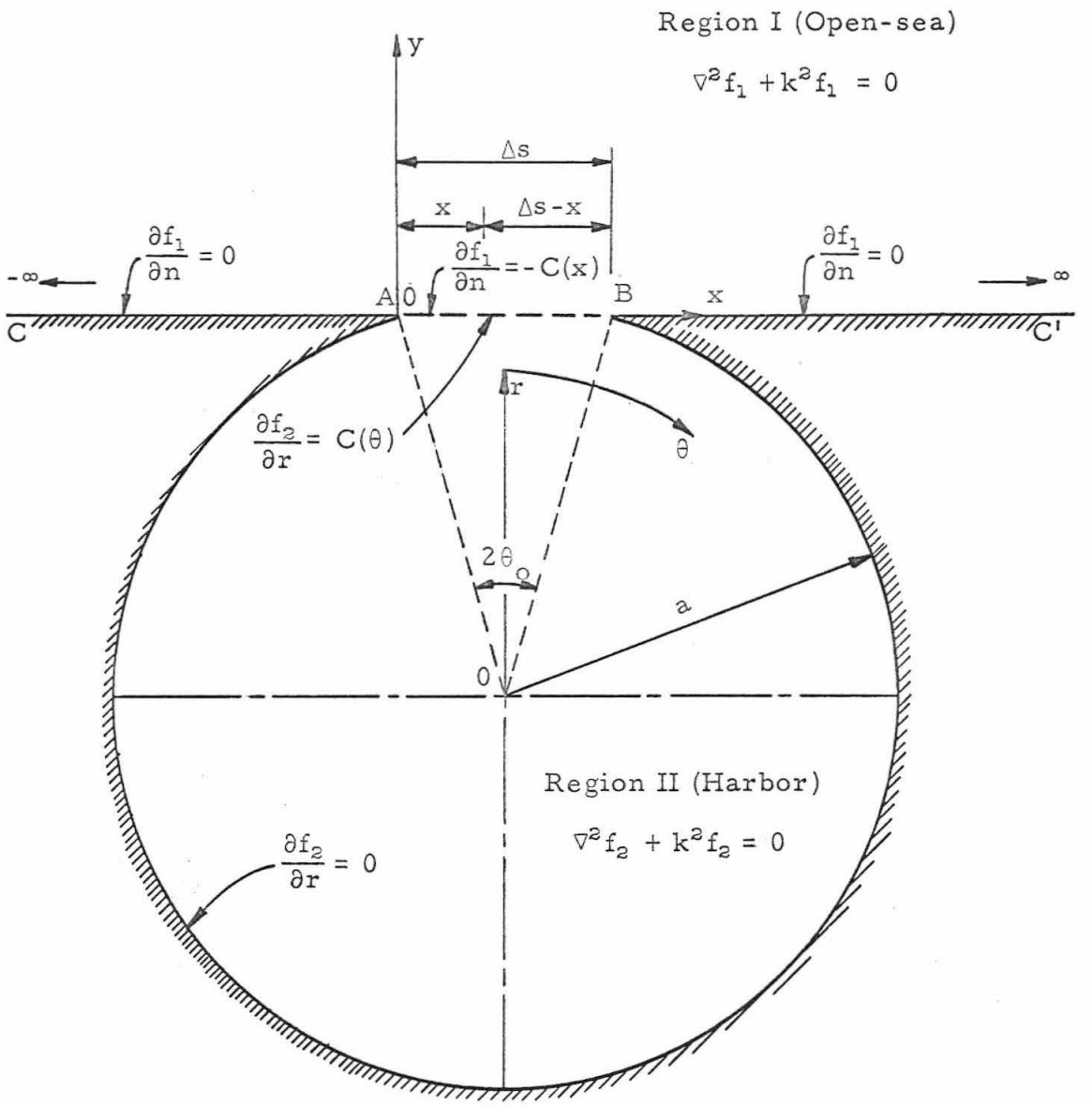

Fig. 4.1 Definition sketch of a circular harbor

Because $J_{-m}(kr)$ is equivalent to $(-1)^m J_m(kr)$, Eq. 4.6 is equivalent to:

$$f_2(r,\theta) = \sum_{m=0}^{\infty} \left(A_m \cos m\theta + B_m \sin m\theta \right) J_m(kr) \ , \qquad (4.7)$$

where A_m and B_m are constants with real and imaginary parts to be determined. For this particular case where the incident wave propagates in the direction of $\theta=0$ the wave function $f_2(r,\theta)$ is an even function of θ, i.e. the wave amplitude is symmetrical with respect to the center line $\theta=0$. Therefore, the constant B_m in Eq. 4.7 is set equal to zero. Hence, the general solution to Eq. 4.1 reduces to:

$$f_2(r,\theta) = \sum_{m=0}^{\infty} A_m J_m(kr) \cos m\theta \ . \qquad (4.8)$$

Differentiating Eq. 4.8 with respect to r, and evaluating the resulting expression at the boundary, r=a one obtains:

$$\frac{\partial f_2}{\partial r}(a,\theta) = \sum_{m=0}^{\infty} \left[A_m \cos m\theta \cdot kJ_m'(ka) \right] \ , \qquad (4.9)$$

where: $kJ_m'(ka) = kJ_{m-1}(ka) - \frac{m}{a} J_m(ka)$. The coefficients A_m must be determined such that Eq. 4.9 will satisfy the prescribed boundary conditions, Eq. 4.2. To evaluate the coefficients A_m, the method of Fourier cosine transformation will be used, by first multiplying both sides of Eq. 4.9 by $\cos n\theta$ and integrating the resulting expression with respect to θ from zero to 2π:

$$\int_0^{2\pi} \frac{\partial f_2}{\partial r}(a,\theta)\cos n\theta d\theta = \int_0^{2\pi} \sum_{m=0}^{\infty} \left[A_m \cos m\theta \cdot kJ_m'(ka) \right] \cos n\theta d\theta$$

$$= \sum_{m=0}^{\infty} \int_0^{2\pi} kJ_m'(ka) A_m \cos m\theta \cos n\theta d\theta$$

$$= \sum_{m=0}^{\infty} \int_0^{2\pi} kJ_m'(ka) A_m \cdot \tfrac{1}{2}\Big(\cos(m+n)\theta + \cos(m-n)\theta\Big) d\theta. \tag{4.10}$$

If $m \neq n$, upon integration Eq. 4.10 is equal to zero, and if $m=n=0$, Eq. 4.10 is equal to:

$$\int_0^{2\pi} \frac{\partial f_2}{\partial r}(a,\theta) d\theta = \int_0^{2\pi} kJ_o'(ka) A_o d\theta \ . \tag{4.11}$$

Therefore, the constant A_o can be evaluated as:

$$A_o = \frac{\int_0^{2\pi} \frac{\partial f_2}{\partial r}(a,\theta) d\theta}{2\pi k J_o'(ka)} \tag{4.12}$$

on the other hand, if $m=n \neq 0$, Eq. 4.10 becomes:

$$\int_0^{2\pi} \frac{\partial f_2}{\partial r}(a,\theta)\cos m\theta d\theta = \tfrac{1}{2}\int_0^{2\pi} kJ_m'(ka) A_m d\theta \ . \tag{4.13}$$

Thus, the constant A_m can be evaluated as:

$$A_m = \frac{\int_0^{2\pi} \frac{\partial f_2}{\partial r}(a,\theta)\cos m\theta d\theta}{\pi k J_m'(ka)} \ . \tag{4.14}$$

Because the normal derivative of the wave function on the boundary, $\frac{\partial f_2}{\partial r}(a,\theta)$, is zero everywhere except at the harbor entrance, as shown in Eq. 4.2, Eqs. 4.12 and 4.14 can be simplified further.

Using the relations:

$$J_o'(ka) = -J_1(ka);$$

$$kJ_m'(ka) = kJ_{m-1}(ka) - \frac{m}{a} J_m(ka)$$

the constants A_o, A_m in Eqs. 4.12 and 4.14 can be written in the following forms:

$$A_o = \frac{\int_{-\theta_o}^{\theta_o} C(\tilde{\theta}) d\tilde{\theta}}{2\pi k\left(-J_1(ka)\right)} \quad , \tag{4.15a}$$

$$A_m = \frac{\int_{-\theta_o}^{\theta_o} C(\tilde{\theta}) \cos m\tilde{\theta} d\tilde{\theta}}{\pi\left[kJ_{m-1}(ka) - \frac{m}{a} J_m(ka)\right]} \quad , \tag{4.15b}$$

where $\tilde{\theta}$ is a dummy variable of integration and $C(\tilde{\theta})$ represents the normal derivative of the wave function evaluated at the entrance.

Therefore, the solution to Eq. 4.1 and the boundary conditions, Eq. 4.2, can be obtained by the substitution of Eqs. 4.15 into Eq. 4.8:

$$f_2(r,\theta) = \frac{J_o(kr) \int_{-\theta_o}^{\theta_o} C(\tilde{\theta}) d\tilde{\theta}}{2\pi k\left(-J_1(ka)\right)} + \sum_{m=1}^{\infty} \frac{J_m(kr)\left[\int_{-\theta_o}^{\theta_o} C(\tilde{\theta}) \cos m\tilde{\theta} d\tilde{\theta}\right] \cos m\theta}{\pi\left[kJ_{m-1}(ka) - \frac{m}{a} J_m(ka)\right]} \quad . \tag{4.16}$$

If the harbor entrance is small, it is assumed that $C(\theta)$ can be approximated by a constant $\bar{C}$, and hence, Eq. 4.16 can be expressed as:

$$f_2(r,\theta) = \frac{J_o(kr)\cdot\bar{C}\cdot\theta_o}{-\pi k J_1(ka)} + \sum_{m=1}^{\infty} \frac{2\cdot J_m(kr)\cdot\bar{C}\cdot\sin m\theta_o\cdot\cos m\theta}{\pi m\left[kJ_{m-1}(ka) - \frac{m}{a}J_m(ka)\right]} \quad . \qquad (4.17)$$

In order to determine the coefficient $\bar{C}$, i.e. the average of the normal derivative of the wave function across the harbor entrance, the wave function f_2 evaluated at the harbor entrance has to be set equal to the wave function in Region I evaluated at the entrance. This means that at the entrance the average of the wave amplitude across the entrance must be the same when determined either in Region I or Region II. For this purpose, the average of the wave function f_2 across the harbor entrance (designated as $\bar{f}_2$) is determined as:

$$\bar{f}_2 = \frac{1}{2\theta_o}\int_{-\theta_o}^{\theta_o} f_2(a,\theta)d\theta$$

$$= \bar{C}\left[\frac{J_o(ka)\theta_o}{-\pi k J_1(ka)} + \sum_{m=1}^{\infty} \frac{2J_m(ka)\left[\sin m\theta_o\right]^2}{\pi\theta_o m^2\left[kJ_{m-1}(ka) - \frac{m}{a}J_m(ka)\right]}\right]. \qquad (4.18)$$

Eq. 4.18 is written in abbreviated form defining the bracketed term on the right-hand-side as M_c; therefore:

$$\bar{f}_2 = \bar{C}\cdot M_c \quad . \qquad (4.19)$$

The series M_c can be calculated once the radius a, the central angle of the entrance $2\theta_o$, and the wave number k are fixed. It is noted that Eq. 4.19 is similar to Eq. 3.35; in both of these equations the wave function at the harbor entrance is expressed in terms of its normal derivative at the harbor entrance. (It should be recalled

that the normal derivative of the wave function is proportional to the horizontal velocity.) The next step in the solution is to express the average value of f_1 (for Region I) at the harbor entrance also as a function of the average normal derivative of the wave function, $\overline{C}$, so that by equating the solutions at the harbor entrance in both regions the value of $\overline{C}$ can be determined.

4.1.2 Wave Function Outside the Harbor

As mentioned in Subsection 4.1.1, the harbor entrance is considered small. Thus, even though the harbor entrance is an arc in Region II and a chord in Region I, the difference between the length of the arc and that of the chord is assumed to be negligible. As developed in Subsection 3.2.2. the wave function at the harbor entrance obtained from the solution in Region I can be expressed as:

$$f_1(x,0) = 1 + \left(\frac{i}{2}\right) \int_{\overline{AB}} \frac{\partial f_3}{\partial n}(x_o, 0)\, H_o^{(1)}(k|x-x_o|)dx_o$$

$$= 1 + \left(-\frac{i}{2}\right) \int_{\overline{AB}} C(x_o, 0)\, H_o^{(1)}(k|x-x_o|)dx_o \quad , \qquad (4.20)$$

where $\overline{AB}$ is the chord at the harbor entrance, the function $C(x_o, 0)$ is the normal derivative specified in Eq. 4.2, the negative sign is specified for the adapted sign convention that the outward normal derivative to the domain of interest is considered positive. (Eq. 4.20 is an integral form of the Eq. 3.34 that was developed previously.) The first term on the right-hand-side of Eq. 4.20 represents the

incident wave and reflected wave at the harbor entrance if the entrance is closed; the second term represents the radiated wave from the entrance.

In order to facilitate performing the integration in Eq. 4.20, the origin of the coordinate system is shifted to the left corner of the harbor entrance (point A in reference to Fig. 4.1). To keep the same approximation as mentioned in Section 4.1.1, the function $C(x_o, 0)$ is approximated by a constant $\overline{C}$. Thus, Eq. 4.20 can be simplified by taking the constant $\overline{C}$ outside the integral sign:

$$f_1(x, 0) = 1 - \frac{\lambda}{2}\overline{C} \int_{\overline{AB}} H_o^{(1)}(k|x-x_o|)dx_o \quad . \tag{4.21}$$

The Hankel function $H_o^{(1)}(k|x-x_o|)$ in Eq. 4.21 can be separated into its real and imaginary parts:

$$H_o^{(1)}(k|x-x_o|) = H_o^{(1)}(kr) = J_o(kr) + \lambda Y_o(kr) \quad , \tag{4.22}$$

where $r=|x-x_o|$ is the distance between the field point $(x, 0)$ and the source point $(x_o, 0)$. Substituting Eq. 4.22 into Eq. 4.21 and performing the integration across the harbor entrance, it becomes:

$$f_1(x, 0) = 1 - \frac{\lambda}{2}\overline{C}\left[f_{jo}(x, 0) + \lambda\frac{2}{\pi}f_{yo}(x, 0)\right] \quad , \tag{4.23}$$

where the terms $f_{jo}(x, 0)$ and $\frac{2}{\pi}f_{yo}(x, 0)$ are the results of the integration of the real part and imaginary part of the Hankel function $H_o^{(1)}(kr)$ in Eq. 4.21. The interested reader is referred to Appendix III for the detailed derivation of $f_{jo}(x, 0)$ and $f_{yo}(x, 0)$, (see Eqs. A.3.3

and A. 3. 6). In order to determine the value of $\overline{C}$ by the matching procedure, the average of the wave function, $\overline{f}_1$, across the harbor entrance can be found as:

$$\overline{f}_1 = \frac{1}{\Delta s}\int_0^{\Delta s} f_1(x, 0)dx \quad , \tag{4.24}$$

where Δs is the length of the chord across the harbor entrance. Substituting Eq. 4.23 into Eq. 4.24 one obtains:

$$\overline{f}_1 = 1 - \frac{i}{2}\overline{C}\left(J_c + i\frac{2}{\pi}Y_c\right)\Delta s \tag{4.25}$$

where:

$$J_c = \sum_{n=0}^{\infty} \frac{(-1)^n\left(\frac{k\Delta s}{2}\right)^{2n}}{(n!)^2(n+1)(2n+1)}$$

$$= 1 - \frac{\left(\frac{k\Delta s}{2}\right)^2}{6} + \frac{\left(\frac{k\Delta s}{2}\right)^4}{60} - \frac{\left(\frac{k\Delta s}{2}\right)^6}{1008} + \frac{\left(\frac{k\Delta s}{2}\right)^8}{25920} + \cdots\cdots \tag{4.26a}$$

$$Y_c = \sum_{n=0}^{\infty} \frac{(-1)^n\left(\frac{k\Delta s}{2}\right)^{2n}}{(n!)^2(2n+1)(n+1)}\left[\log\left(\frac{k\Delta s}{2}\right) + \gamma - \frac{1}{2(n+1)} - \frac{1}{2n+1}\right]$$

$$+ \sum_{n=1}^{\infty} \frac{(-1)^{n+1}\rho(n)\left(\frac{k\Delta s}{2}\right)^{2n}}{(n!)^2(2n+1)(n+1)}$$

$$= \left[\log\left(\frac{k\Delta s}{2}\right) + \gamma - \frac{3}{2}\right] - \frac{\left(\frac{k\Delta s}{2}\right)^2}{6}\left[\log\left(\frac{k\Delta s}{2}\right) + \gamma - \frac{19}{12}\right]$$

$$+ \frac{\left(\frac{k\Delta s}{2}\right)^4}{60}\left[\log\left(\frac{k\Delta s}{2}\right) + \gamma - \frac{55}{30}\right] - \frac{\left(\frac{k\Delta s}{2}\right)^6}{1008}\left[\log\left(\frac{k\Delta s}{2}\right) + \gamma - \frac{353}{168}\right]$$

$$+ \frac{\left(\frac{k\Delta s}{2}\right)^8}{25920}\left[\log\left(\frac{k\Delta s}{2}\right) + \gamma - \frac{826}{360}\right] + \cdots\cdots \tag{4.26b}$$

The development of the series for J_c and Y_c are also presented in Appendix III. (see Sections III. 3 and III. 4).

4. 1. 3 Matching the Solution for Each Region at the Harbor Entrance

With the average wave function f_2 at the harbor entrance ($\overline{f_2}$) for Region II obtained from Eq. 4. 19 and the average wave function f_1 at the harbor entrance ($\overline{f_1}$) for Region I obtained from Eq. 4. 25, the two solutions can now be matched to solve for the average normal derivative of the wave function, $\overline{C}$. Eq. 4. 25 is simplified as:

$$\overline{f_1} = 1 + B_o \overline{C} \quad , \tag{4.27}$$

where $B_o = -\frac{\lambda}{2}\left(J_c + \lambda\frac{2}{\pi}Y_c\right)\Delta s$, in which J_c and Y_c are defined by Eqs. 4. 26a and 4. 26b.

Equating Eq. 4. 19 to Eq. 4. 27, one obtains:

$$\overline{C}M_c = 1 + B_o \cdot \overline{C} \quad ; \tag{4.28}$$

thus, the average value of the normal derivative of the wave function at the harbor entrance, $\overline{C}$, can be determined from Eq. 4. 28 as:

$$\overline{C} = \frac{1}{M_c - B_o} \quad , \tag{4.29}$$

where M_c and B_o are defined by Eqs. 4. 19 and 4. 27 respectively.

After the value of the average normal derivative of the wave function at the harbor entrance, $\overline{C}$, has been determined from Eq. 4. 29, the wave function f_2 at any position (r, θ) inside the harbor can be calculated from Eq. 4. 17. It should be noted that the functions $\overline{C}$ and $f_2(r, \theta)$ are both complex numbers.

Once the value of the complex number $\bar{C}$ has been determined by Eq. 4.29, the amplification factor, R, at any position (r, θ) for a particular wave number k can be evaluated in exactly the same way as discussed in Subsection 3.2.3 (as shown in Eq. 3.38):

$$R(r,\theta;k) = \frac{|\eta_2(r,\theta;t)|}{|A_i(f_i+f_r)e^{-i\sigma t}|} = \frac{|A_i f_2(r,\theta)e^{-i\sigma t}|}{|A_i \cdot 1 \cdot e^{-i\sigma t}|} = |f_2(r,\theta)|$$

$$= |\bar{C}| \cdot \left| \frac{J_o(kr)\theta_o}{-\pi k J_1(ka)} + \sum_{m=1}^{\infty} \frac{2J_m(kr)\sin m\theta_o \cos m\theta}{\pi m\left[kJ_{m-1}(ka) - \frac{m}{a}J_m(ka)\right]} \right| \quad (4.30)$$

It should be mentioned that the analysis presented in this section so far is concerned only with one complex constant $\bar{C}$ which is determined through the matching procedure. This means that the quantities of interest are averaged over the full entrance; however, if a better approximation is intended, the harbor entrance can be divided into p segments. Thus, there are p complex constants C_1, $C_2, \ldots . C_p$, i.e. the average normal derivative of the wave function for each segment, to be determined by the matching procedure. The average value of the wave function for each entrance segment is expressed as a function of C_1, $C_2, \ldots . C_p$; thus, a set of equations similar to those used in the approximate method and shown in Eq. 3.35 can be developed. As for the solution in Region I, Eq. 3.34 developed in Chapter 3 represents the wave function f_1 for each entrance segment and can be used in the solution instead of Eq. 4.25. Therefore, by matching the average value of f_1 and f_2 at each entrance segment, a set of p simultaneous linear equations can be obtained; the value of the normal derivative of wave function for each segment, i.e. C_1,

$C_2, \ldots . C_p$, can be determined by solving this set of simultaneous equations similar to what was discussed in Subsection 3.2.3. After evaluating the value of C_1, $C_2, \ldots . C_p$, the wave function $f_2(r, \theta)$ at any position inside the harbor can be calculated.

It should also be noted that even though there is no limitation on the number of segments into which the harbor entrance can be divided the entrance still cannot be very large. This is because to use the theoretical analysis presented in this section the arc and the chord at the entrance must be approximately the same length. In addition if the harbor entrance is very large, the harbor geometry can no longer be considered as circular and the method of separation of variables cannot be applied. For such cases it is necessary to resort to the approximate methods described in Chapter 3.

4.2 THEORETICAL ANALYSIS FOR A RECTANGULAR HARBOR

Another example for which the coordinates inside the harbor are separable is a harbor with a rectangular shape. Similar to the circular harbor, for a rectangular harbor the solution inside the harbor (Region II) can be obtained in an eigen function expansion with the coefficients to be determined by the boundary conditions. The solution in Region II that will be presented below is the same as the work of Ippen and Goda (1963), since it involves the standard separation of variable method. For the solution in Region I, the method discussed in the previous section, i.e. Subsection 4.1.2, will be used. This method is different from the Fourier transformation method that Ippen and Goda (1963) used in their work. This theoretical

analysis can be used as a check both of the theory developed by Ippen and Goda (1963) as well as the theory developed in Chapter 3 for an arbitrary shaped harbor.

4.2.1 Wave Function Inside the Rectangular Harbor

For the wave function $f_2(x, y)$ inside the rectangular harbor, the Helmholtz equation, Eq. 3.5, is written in rectangular coordinates:

$$\frac{\partial^2 f_2}{\partial x^2} + \frac{\partial^2 f_2}{\partial y^2} + k^2 f_2 = 0 \quad , \tag{4.31}$$

the wave function f_2 must satisfy the following boundary conditions:

$$\begin{aligned}
&\text{(i)} \quad \frac{\partial f_2}{\partial x}(0, y) = 0, \text{ and } \frac{\partial f_2}{\partial x}(b, y) = 0 \qquad \text{for } -\ell < y < 0 \\
&\text{(ii)} \quad \frac{\partial f_2}{\partial y}(x, -\ell) = 0 \qquad \text{for } 0 < x < b \\
&\text{(iii)} \quad \frac{\partial f_2}{\partial y}(x, 0) = \begin{cases} 0 & \text{for } 0 < x < d_o \text{ or } d_o + d < x < b \\ C(x) & \text{for } d_o \le x \le d_o + d \end{cases}
\end{aligned} \tag{4.32}$$

A definition sketch of the rectangular harbor showing both regions: Region I and Region II, is presented in Fig. 4.2.

Using the method of separation of variables and considering the boundary conditions (i) and (ii), the solution of the Helmholtz equation, Eq. 4.31, can be represented by the following infinite series:

$$f_2(x, y) = \sum_{m=0}^{\infty} A_m \cos \frac{m\pi}{b} x \cosh \beta_m (y + \ell) \quad , \tag{4.33}$$

where $\beta_m = \sqrt{\left(\frac{m\pi}{b}\right)^2 - k^2}$, and A_m is an arbitrary constant to be

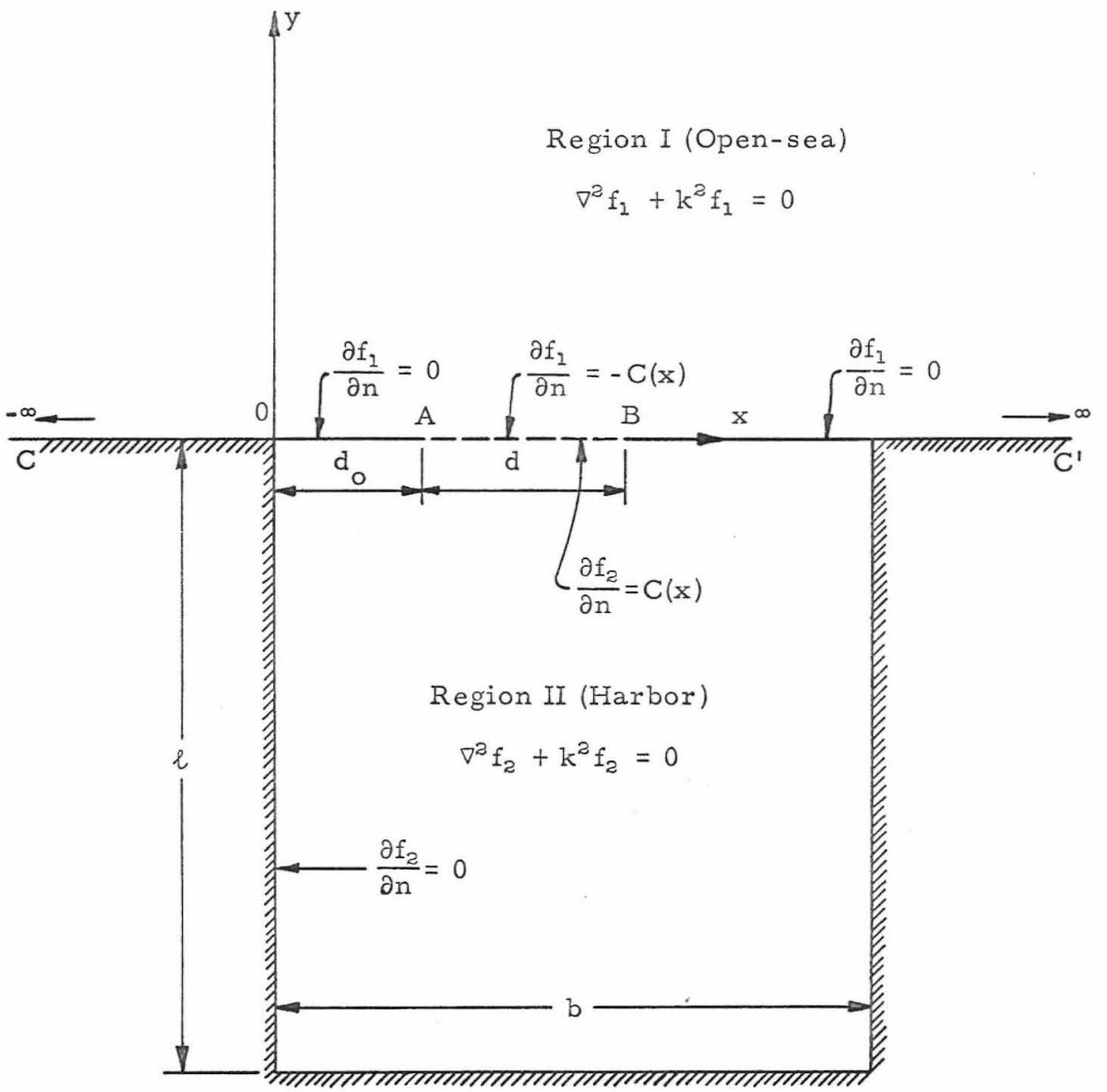

Fig. 4.2 Definition sketch of a rectangular harbor

determined. It is obvious that Eq. 4.33 satisfies the Helmholtz equation, Eq. 4.31, and also satisfies the boundary conditions (i) and (ii) in Eq. 4.32. Thus, the constants A_m have to be determined so that the solution $f_2(x, y)$ will satisfy the boundary condition (iii) in Eq. 4.32.

Differentiating Eq. 4.33 with respect to y, one obtains:

$$\frac{\partial f_2}{\partial y}(x, y) = \sum_{m=0}^{\infty} A_m \cdot \beta_m \left[\cos \frac{m\pi}{b} x \sinh \beta_m (y+\ell)\right] \quad . \quad (4.34)$$

Evaluating Eq. 4.34 at y=0 and expanding, one obtains:

$$\frac{\partial f_2}{\partial y}(x, 0) = A_o k(-\sin k\ell) + \sum_{m=1}^{\infty} A_m \beta_m (\sinh \beta_m \ell) \cos \frac{m\pi}{b} x \quad . \quad (4.35)$$

The coefficients A_o and A_m can be determined by the Fourier cosine transformation method which was used in Subsection 4.1.1. Using this method the following expressions are obtained for A_o and A_m:

$$A_o = \frac{\frac{2}{b}\int_0^b \frac{\partial f_2}{\partial y}(x, 0)\, dx}{2k\,(-\sin k\ell)} = -\frac{\int_{d_o}^{d+d_o} C(x)\, dx}{bk \sin k\ell} \quad , \quad (4.36a)$$

$$A_m = \frac{\frac{2}{b}\int_0^b \frac{\partial f_2}{\partial y}(x, 0) \cos \frac{m\pi}{b} x dx}{\beta_m \sinh \beta_m \ell} = \frac{\int_{d_o}^{d+d_o} C(x) \cos \frac{m\pi}{b} x dx}{b\beta_m \sinh \beta_m \ell} \quad . \quad (4.36b)$$

If C(x) can be approximated by a constant $\overline{C}$, as has been done in Subsection 4.1.1, the coefficients A_o and A_m in Eqs. 4.36a and 4.36b can be evaluated as:

$$A_o = -\frac{\bar{C}d}{bk \sin k\ell} \quad , \tag{4.37a}$$

$$A_m = \frac{2\bar{C}\left[\sin\frac{m\pi}{b}(d+d_o) - \sin\frac{m\pi}{b}d_o\right]}{m\pi\beta_m \sinh \beta_m \ell} \quad . \tag{4.37b}$$

Substituting Eqs. 4.37 into Eq. 4.33, the solution of the wave function f_2 inside the harbor can be written as:

$$f_2(x,y) = \bar{C}\left[S_o(x,y) + S_m(x,y)\right] \quad , \tag{4.38}$$

wherein:

$$S_o = -\frac{d \cos k\,(y+\ell)}{bk \sin k\ell} \quad ,$$

$$S_m = \sum_{m=1}^{\infty} \frac{2\left(\sin\frac{m\pi}{b}(d+d_o) - \sin\frac{m\pi}{b}d_o\right)}{m\pi\beta_m \sinh \beta_m \ell} \cos\frac{m\pi}{b}x \cosh\beta_m(y+\ell) \quad .$$

The complex constant $\bar{C}$, i.e. the average normal derivative of the wave function across the harbor entrance, in Eq. 4.38 has to be determined by a matching procedure similar to that used previously. The matching procedure used for the rectangular harbor is to equate the average wave function f_2 evaluated at the harbor entrance $(\bar{f}_2)$ to the average wave function f_1 evaluated at the harbor entrance $(\bar{f}_1)$.

The average wave function f_2 across the harbor entrance $(\bar{f}_2)$ can be evaluated as:

$$\bar{f}_2 = \frac{1}{d}\int_{d_o}^{d_o+d} f_2(x,0)\,dx$$

$$= \bar{C}\,(\bar{S}_o + \bar{S}_m) \quad , \tag{4.39}$$

where:

$$\overline{S}_o = -\frac{d}{bk}\cot k\ell \quad ,$$

$$\overline{S}_m = \sum_{m=1}^{\infty} \frac{2b\left[\sin\frac{m\pi}{b}(d+d_0) - \sin\frac{m\pi}{b}d_o\right]^2}{(m\pi)^2 \beta_m \tanh \beta_m \ell} \quad .$$

4.2.2 Matching of the Solution for Each Region at the Harbor Entrance

The average wave function, f_2, determined in Region II at the harbor entrance can be obtained from Eq. 4.39. For the solution in Region I, the relation developed in Subsection 4.1.2, i.e. Eq. 4.27, can be used for the average wave function, $\overline{f}_1$. Thus by matching these two solutions at the harbor entrance, the average normal derivative of the wave function across the harbor entrance, $\overline{C}$, can be determined. Equating Eq. 4.39 to Eq. 4.27 one obtains:

$$\overline{C}\,(\overline{S}_o + \overline{S}_m) = 1 + B_o \overline{C} \quad ; \tag{4.40}$$

thus, the value of $\overline{C}$ can be determined as:

$$\overline{C} = \frac{1}{\overline{S}_o + \overline{S}_m - B_o} \quad . \tag{4.41}$$

After the value of $\overline{C}$ has been determined from Eq. 4.41, the wave function f_2 at any position (x, y) inside the rectangular harbor can be determined using Eq. 4.38. The absolute value of the wave function $f_2(x, y)$ is equal to the amplification factor at the position (x, y) as was shown in Eq. 3.38 and Eq. 4.30.

It is noted that in the circular harbor theory developed in Section 4. 1, the harbor entrance is limited by the requirement that the arc is approximately equal to the chord at the harbor entrance. This type of limitation does not exist in the rectangular harbor theory developed in this section, since no matter how large the harbor entrance is, the geometry in Region II is still rectangular and the separation of variable method can be used. For the case of a wide harbor entrance compared to the length of the harbor the entrance can be divided into a number of segments using the matching procedure to equate the average value of f_1 and the average value of f_2 at each segment at the entrance. Therefore, a set of simultaneous equations can be obtained; the value of the normal derivative of the wave function C for each segment can be determined by solving these simultaneous equations. After the normal derivative of the wave function for each entrance segment has been determined, the wave function $f_2(x, y)$ at any position inside the harbor can be calculated.

CHAPTER 5

EXPERIMENTAL EQUIPMENT AND PROCEDURES

5.1 WAVE BASIN

A wave basin 1 ft 9 in. deep, 15 ft 5 in wide, and 31 ft 5 in. long shown in Figs. 5.1 and 5.2 was used for the experiments. The vertical walls of the basin were constructed of 3/4 in. marine plywood with the floor constructed of 1 in. marine plywood. The basin floor was located 10 in. above the laboratory floor. This can be seen in Figs. 5.1 and 5.2 where a substructure supporting the basin floor was built to allow for proper leveling of the basin floor and to raise the basin to a more comfortable working level. This substructure consisted of wood sills and joists; seven wood sills (1-5/8 in. x 3-5/8 in. with the short dimension vertical) were fastened to the laboratory floor, 2 ft 8 in. on center running the length of the basin. Perpendicular to these sills, a system of joists (1-5/8 in. x 7-5/8 in. with the long dimension vertical) was fastened on 1 ft 4 in. centers. The upper face of the joists was leveled to within $\pm$ 1/32 in. by placing shim material between the sill and the joist at each intersection. The 1 in. plywood was then glued and screwed to the joists to become the basin floor and the 3/4 in. vertical walls and their supporting structure were fastened in place. (For additional details of the construction of the basin, see

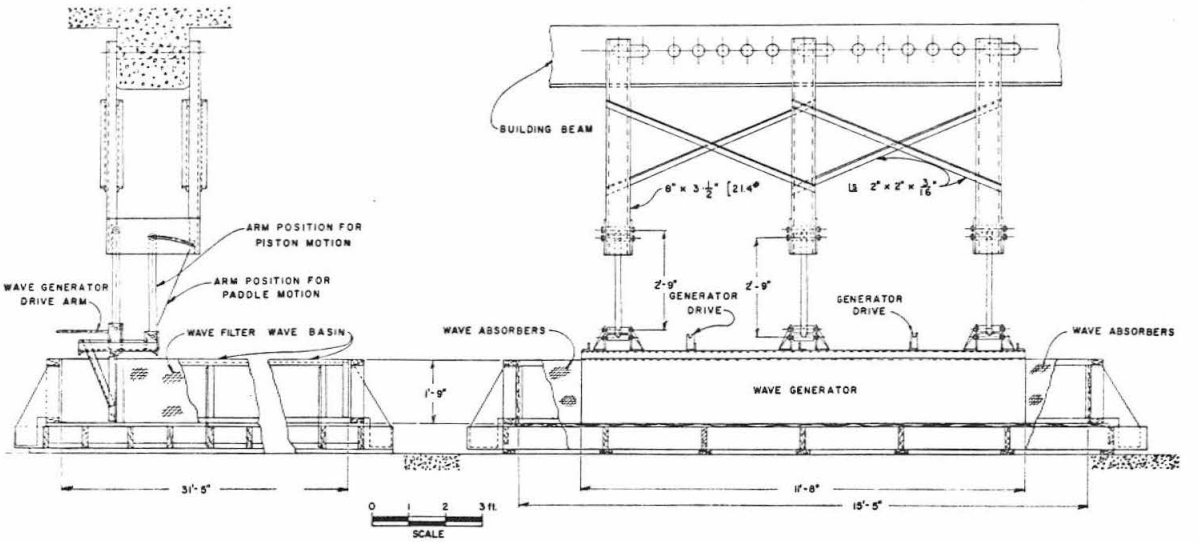

Fig. 5.1 Drawing of the wave basin and wave generator (modified from Raichlen (1965))

9331

Fig. 5.2 Over-all view of the wave basin and wave generator with wave filter and absorbers in place

Raichlen (1965).) In order to ensure watertightness and to provide a level bottom, before this study was initiated, a layer of polyester resin ("CYBOND 2501 Part 1" manufactured by American Cyanamid Company) approximately 1/4 in. thick was poured into the basin. The resin sought its own level before it solidified; therefore, a bottom which was horizontal to within at least $\pm$0.02 in. was obtained by this treatment. All the joints were sealed by fiber glass cloth and resin and the interior of the basin was then painted with an epoxy base paint. After this treatment the wave basin remained free of leaks throughout the course of the experiments.

Also shown in Figs. 5.1 and 5.2 are wave energy dissipators: a wave filter located in front of the wave machine and wave absorbers located along two sides of the basin. The details of the construction and the characteristics of these units will be presented in Sections 5.6 and 6.1 respectively.

5.2 WAVE GENERATOR

The wave generator used for this study was a pendulum type designed to operate either as a paddle- or piston-type wave machine; its detailed description and design consideration were given by Raichlen (1965). A photograph of the wave generator and the overhead support is shown in Fig. 5.3. It is seen that the plate of the generator is obscured by the wave filter; however, this shows the arrangement of the filter relative to the generating surface. The generating surface was an aluminum plate 11 ft 8 in. long, 2 ft high,

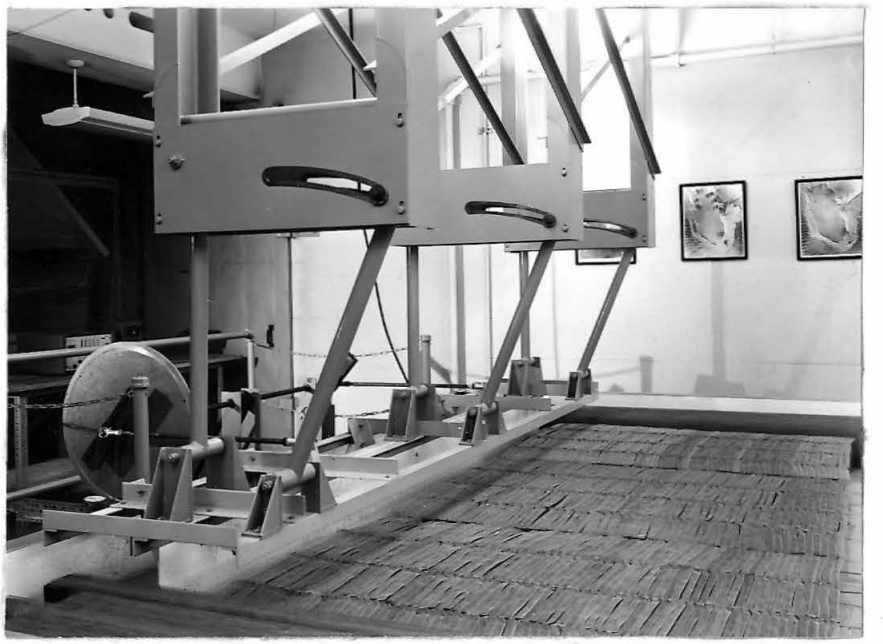

9322

Fig. 5.3 Wave generator and overhead support with wave filter and wave absorber in place

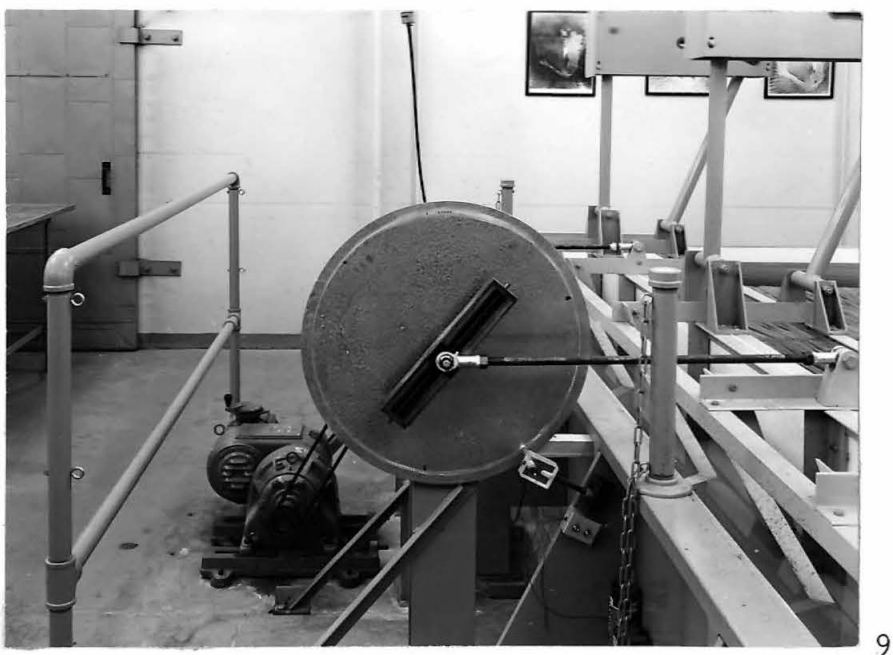

9333

Fig. 5.4 Motor drive, eccentric, and light source and perforated disc for wave period measurement

and 1/4 in. thick attached to a structural aluminum angle frame which provided rigidity. As can be seen in Fig. 5.3, this assembly was suspended from three pairs of arms connected to an overhead structure which in turn was fastened to the reinforced concrete ceiling beam. Each supporting arm was 2 ft 9 in. long with the upper end of each forward arm able to be moved along a slot which was an arc of radius 2 ft 9 in. Hence, when the forward arm at each support was parallel to the rear arm the wave machine operated as a piston-type generator; when the upper end of the forward supporting arm was moved to the furthermost forward position, the wave machine operated as a paddle-type wave generator with the bottom of the generating plate acting as an imaginary hinge point. This arrangement facilitated the generation of shallow water and deep water waves. The wave generator was driven by two arms connected to independent eccentrics which in turn were connected through a pulley system to a 1-1/2 hp variable speed motor. This arrangement can be seen in Fig. 5.4. The eccentrics allowed for a maximum wave machine stroke of 12 in., but careful adjustment was necessary to insure that both eccentrics had identical settings. This was accomplished by measuring the stroke of the generator at two locations using dial gages, and it was possible to adjust the eccentrics to within 0.001 in. of each other. The motor was a 1-1/2 hp U.S. Varidrive Motor with a 10:1 speed range and a continuous variation over this range. Wave periods ranging from 0.34 sec to 3.8 sec could be obtained with this system.

5.3 MEASUREMENT OF WAVE PERIOD

A pulse counting technique was used for the determination of the wave period. As can also be seen in Fig. 5.4, the pulse was generated by interrupting a light beam, which was directed at a photocell, by a disc with 360 evenly spaced holes arranged in a circle near its outer edge. The disc was directly connected to one eccentric of the wave drive mechanism. A schematic diagram and circuit of the photocell device is presented in Fig. 5.5. The voltage pulses so generated by the photocell circuit were counted over an interval of 10 seconds by a Beckman/Berkeley Division Industrial Counter Model 7351. The wave period in seconds was obtained simply by dividing the product of the number of holes times the counting interval (3600) by the number of counts registered by the counter in 10 seconds. Hence, the period measured was an average over a 10 second interval; throughout an experiment this period varied at most by $\pm$0.03%.

5.4 MEASUREMENT OF WAVE AMPLITUDE

5.4.1 Wave Gage

Resistance wave gages were used in conjunction with the Sanborn (150 series) recorder for the measurement of wave amplitude. A drawing of a typical wave gage is shown in Fig. 5.6. The wave gage consisted of two 0.010 in. diameter stainless steel wires 3-1/2 in. long, spaced 1/8 in. apart. The wires were stretched taut and parallel in a frame constructed of 1/8 in. diameter stainless steel.

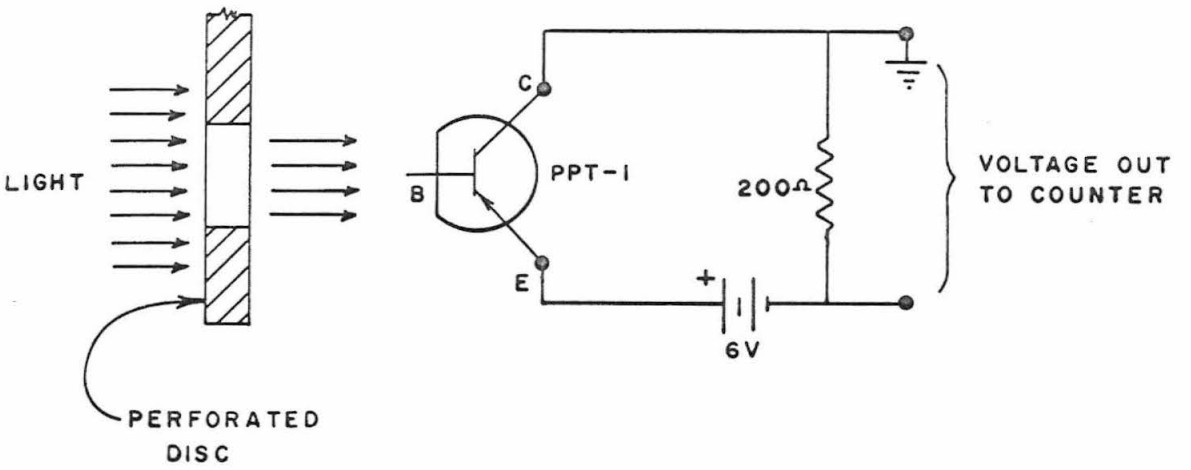

Fig. 5.5 Schematic diagram and circuit of photo-cell device (from Raichlen (1965))

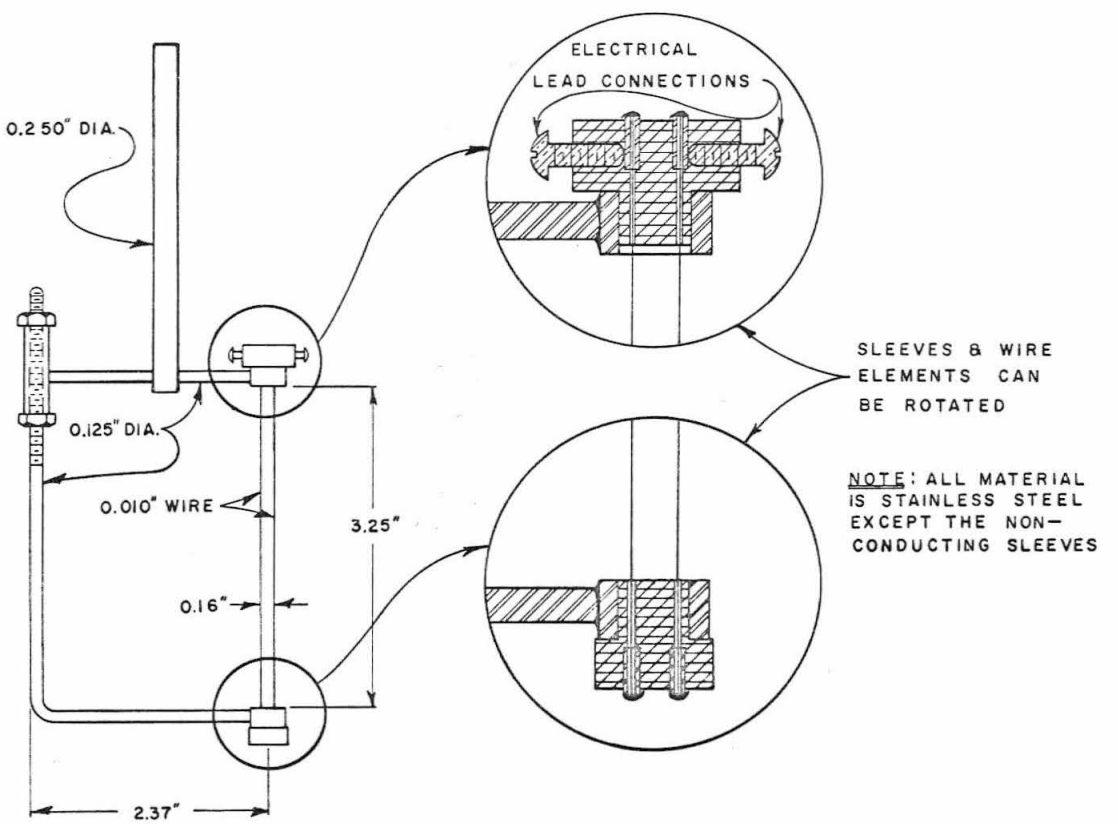

Fig. 5.6 Drawing of a typical wave gage (from Raichlen (1965))

The wires were insulated electrically from each other, except that current could pass from one wire to the other through the water in which the gage was immersed.

A circuit diagram for the wave gage is shown in Fig. 5.7. A Sanborn Carrier Preamplifier (Model 150 - 1100 AS) supplied the 2400 cps - 4.5 volt excitation for the gages and in turn received the output from the wave gages which after demodulation and amplification were displayed on the recording unit. The displacement of the stylus of the recorder was proportional to the probe resistance, which in turn was proportional to the depth of immersion of wires.

The wave gage was calibrated before and after an experiment (approximately one hour apart). Three typical calibration curves are presented in Fig. 5.8 for a wave gage with three different attenuation settings of the amplifier, i.e. x50, x20, x10. The ordinate shows the immersion plus withdrawal in centimeters while the abscissa shows the stylus deflection of the recorder in millimeters. The calibration of wave gage was performed manually by first increasing its immersion 0.05 cm, then returning to the original position and withdrawing it 0.05 cm. The same procedure was then repeated with a larger increment of immersion and withdrawal. A calibration curve representing an average over the duration of an experiment was used in the data reduction procedure. Most calibration curves were essentially linear and showed very little change during an experiment as can be seen in Fig. 5.8.

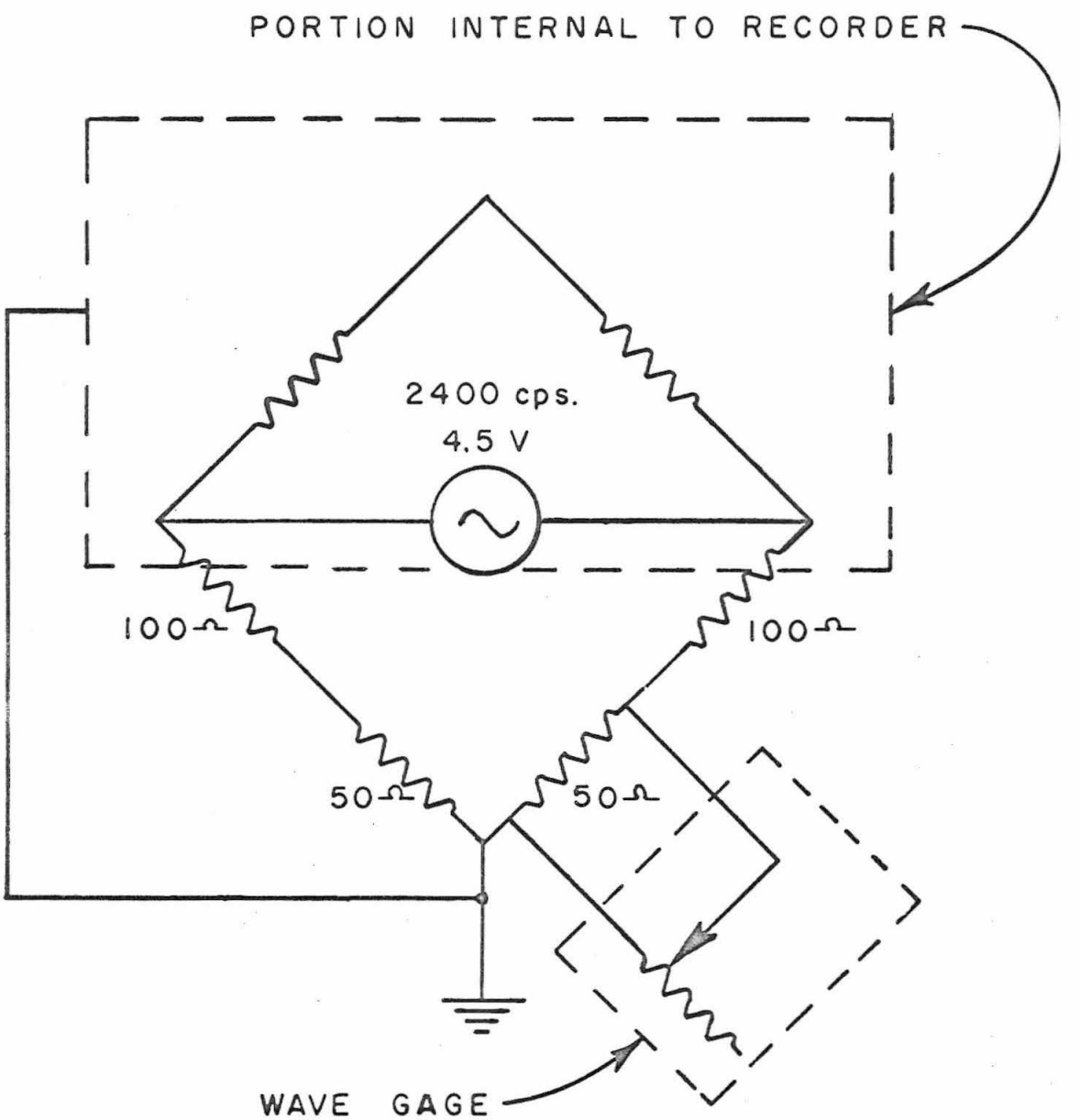

Fig. 5.7 Circuit diagram for wave gages (from Raichlen (1965))

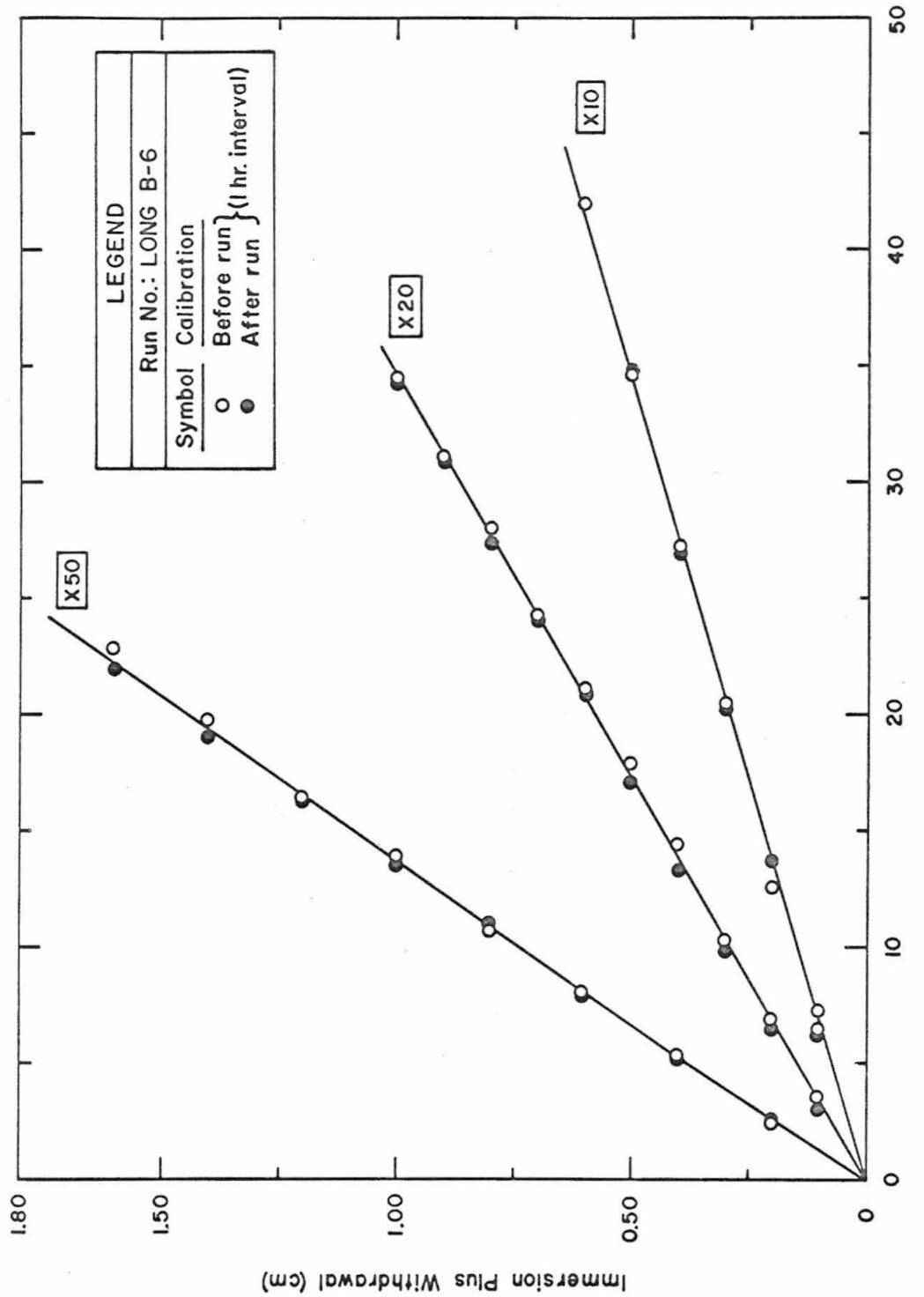

Fig. 5.8 Typical calibration curves of a wave gage

5.4.2 Measurement of Standing Wave Amplitude for the Closed Harbor

As mentioned in Subsection 3.2.3, the amplification factor is defined as the wave amplitude at a particular location inside the harbor divided by the sum of the amplitude of the incident and the reflected wave when the harbor entrance is closed; this latter is the standing wave amplitude. Therefore, in order to determine the amplification factor experimentally, both the wave amplitude inside the harbor and the standing wave amplitude when the entrance is closed must be measured.

The amplitude inside the harbor is measured in a straightforward manner using the resistance wave gages just described. Due to the variation in the standing wave amplitude along a crest, caused by the diffraction of waves off the edges of the wave machine and by the wave absorbers (see also Ippen and Goda (1963)), it was necessary to use an average amplitude of the standing wave across the entrance in defining the amplification factor.

This average standing wave amplitude along the "coastline" was obtained as follows. With the harbor entrance closed, three wave gages were placed 1/4 in. from the false wall (which represents the "coastline") with the wires in a plane parallel to the wall. One wave gage was located on the center line of the harbor entrance, and the other two gages were located 2 ft to either side. After the wave amplitude at these three locations had been determined, the wave

amplitude at the two limits of the harbor entrance were determined by interpolation after fitting a second order polynomial to the measured values. The subroutine "AITKEN/Polynomial Interpolation Function" available at the Booth Computing Center of the California Institute of Technology was used to accomplish this. The average of the wave amplitude measured by the center gage and those interpolated as just described was used to represent the standing wave amplitude. Therefore, the amplification factor was determined by dividing the measured wave amplitude at a given location inside the harbor by the standing wave amplitude so determined.

5.5 MEASUREMENT OF VELOCITY

The velocity at the harbor entrance was measured using a hot-film anemometer manufactured by Thermo-Systems, Inc. (Heat Flux System Model 1020A). The system minimized the effect of the thermal inertia of the probe by keeping the sensitive element at a constant temperature (constant resistance) and using the heating current as the measure of the heat transfer and hence the velocity of the flow. The sensor was a glass cylinder (with a diameter of 0.001 in. or 0.006 in.) coated with a platinum film which in turn was covered with a sputtered quartz layer; the platinum and quartz coatings were each approximately 10^{-5} in. thick. The sensor was supported by two insulated needles, and for the experiments, the sensor was aligned with its longitudinal axis parallel to the bottom of the basin and perpendicular to the incoming wave ray. A photograph of one sensor is shown in Fig. 5.9 with the associated electronics shown in Fig. 5.10.

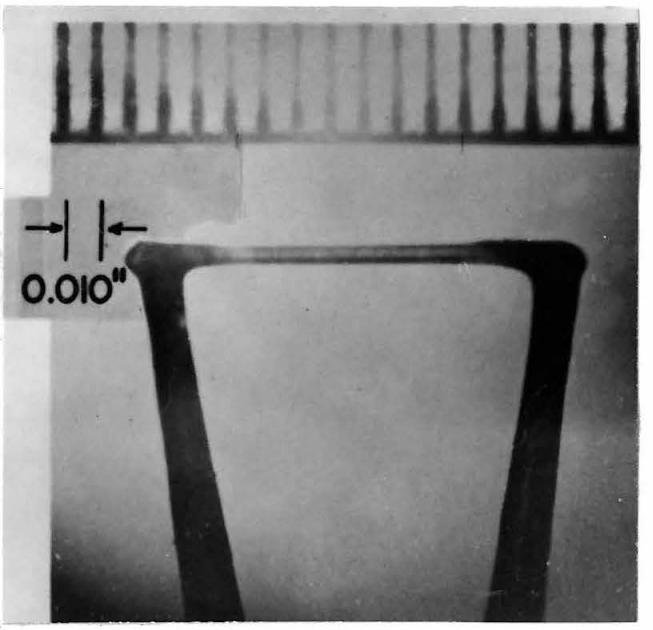

Fig. 5.9 Photograph of a hot-film sensor (from Raichlen (1967))

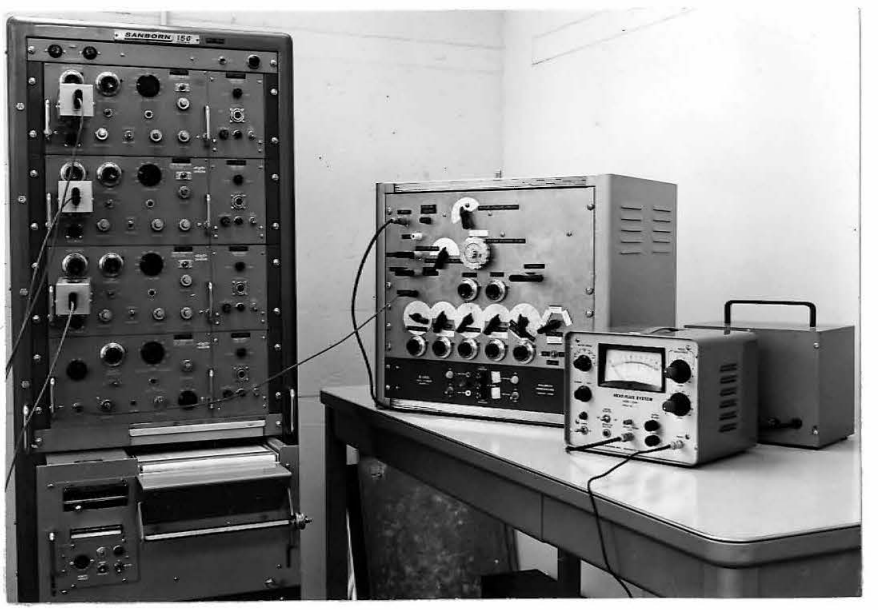

9334

Fig. 5.10 Hot-film anemometer, linearizer, and recording unit

The output of the hot-film sensor is not linearly proportional to the flow velocity; instead, it has the following general relation (see Hinze((1959)):

$$E = I_a \cdot R_w = (c_1 + c_2 V^{c_3})^{\frac{1}{2}} \quad , \tag{5.1}$$

where E is the output voltage of the anemometer, I_a is the current to the sensor, R_w is the operating resistance, V is the fluid velocity normal to the axis of the hot-film sensor, and c_1 and c_2 are constants which depend upon the properties of the hot-film and the temperature difference between it and the fluid. In steady flow, the exponent c_3 in Eq. 5.1 is usually taken as 1/2; such a relationship is referred to as King's law (see Hinze (1959)).

For a constant temperature system, the operating resistance of the sensor, R_w, is kept constant by electronic feedback. The value $(R_w - R_g)/R_g$ (wherein R_g is the cold resistance of the hot-film sensor) is usually called the "over-heat ratio". For present experiments, an over-heat ratio of 2% to 3% was used.

Assuming King's law applies for the present experiments (see Subsection 6.2.5 for a discussion of the shortcomings of this assumption), Eq. 5.1 can be written as:

$$E = (c_1 + c_2 \sqrt{V})^{\frac{1}{2}} \quad ; \tag{5.2}$$

providing a simple relationship which can be linearized so that the output voltage is directly proportional to the fluid velocity. In order to accomplish this, a linearizing circuit built by Townes (1965) was used.

The sequence of operation of the linearizer is as follows. The output of the anemometer was first amplified to the best operating level for the linearizer (approximately 10 volts) and used as the input to the first squaring circuit of the linearizer; the output from the first squaring circuit, S_1, can be expressed as:

$$S_1 = (c_a E)^2 = c_a{}^2 (c_1 + c_2 \sqrt{V}) \quad , \tag{5.3}$$

where c_a is the amplification by the preamplifier.

It can be seen from Eq. 5.3 that the output of the first squaring circuit S_1 is not equal to zero when the fluid velocity is zero. Therefore, a mean voltage was subtracted from that shown in Eq. 5.3, when the velocity was equal to zero. Hence, the signal can then be expressed as:

$$S_b = S_1 - c_a{}^2 c_1 = c_a^2 c_2 \sqrt{V} \quad . \tag{5.4}$$

This voltage was then amplified again to the best operating level for the linearizer, and introduced to the second squaring circuit. The final output voltage from that stage, S_2, can be expressed as:

$$S_2 = (c_b S_b)^2 = (c_b c_a^2 c_2 \sqrt{V})^2 = \alpha_v V \quad . \tag{5.5}$$

Thus, after the linearizing operation, the output voltage from the second squaring circuit, S_2, is linearly proportional to the fluid velocity, V. It should be noted that the relationship shown in Eq. 5.5 implies that King's law (Eq. 5.2) applies. A calibration is required if one is to determine the constant α_v in Eq. 5.5 and thus the absolute velocity; for the present experiments no attempt was made to calibrate

the sensor. If the applicability of Eq. 5.5 is assumed, the relative velocity at two positions can be obtained as the ratio of the final output voltage S_2 at those two positions. For example, for the experiments dealing with the velocity distribution across the harbor entrance the output voltage at various positions can be normalized with respect to either the value at the center or the average value across the entrance; both normalizations yield information regarding the shape of the velocity distribution across the entrance.

5.6 WAVE ENERGY DISSIPATION SYSTEM

Two types of wave energy dissipators were employed in the present experiments: a wave filter placed in front of the wave generator, and wave absorbers located along the side-walls of the wave basin. This system was designed to simulate open-sea conditions in the restricted laboratory basin, and the design criterion and characteristics of the system will be discussed in Section 6.1.

An overall view of the wave energy dissipators is shown in the photograph, Fig. 5.11. The wave filter, shown in front of the wave generator in Fig. 5.11, was 11 ft 9 in. long, 1 ft 4 in. high and 5 ft deep in the direction of wave propagation and was constructed of 70 sheets of galvanized iron wire screen in three sections each 3 ft 11 in. long. The wire diameter of the screens was 0.011 in with 18 wires per inch in one direction and 14 wires per inch in the other. As seen in Fig. 5.12 each section of the filter had three vertical stiffening pleats located approximately 1 ft apart on each sheet; in addition, right angle bends each 0.8 in. long were made at the top and bottom

9320

Fig. 5.11 Wave energy dissipators placed in the basin

(a) Front view

9311

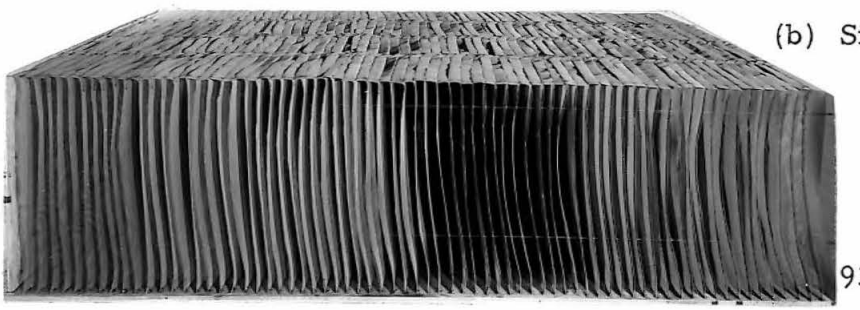

(b) Side view

9314

Fig. 5.12 Section of wave filter

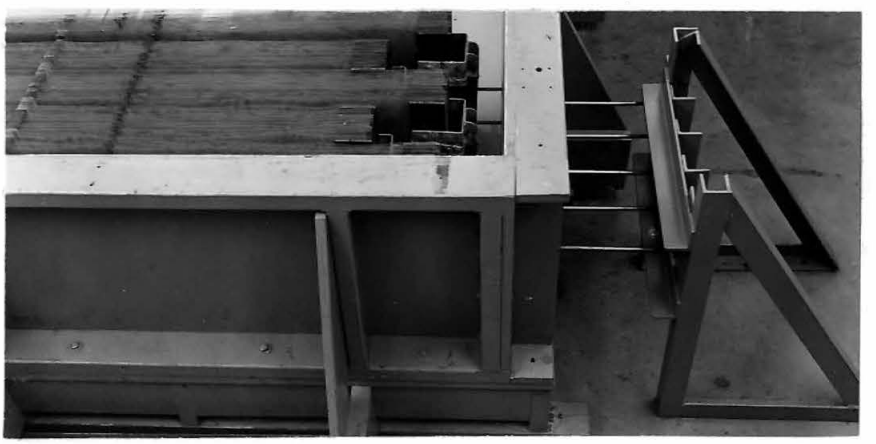

9337

Fig. 5.13 Bracket and structural frame for supporting wave absorbers

of each sheet to further stiffen them. Seventy identical sheets were then fastened together with 6 stainless steel rods of 1/8 in. diameter. Spacers consisting of 1/8 in. I. D. lucite tubing 0. 8 in. long were placed on each rod to maintain a uniform spacing. These lucite spacers can be seen from the side view of the filter in Fig. 5. 12. The right angle bends at the top and the bottom of each screen also served as spacers. The 70 sheets were then tacked together by soldering to become a relatively stiff unit that could stand by its own rigidity in the wave basin, resisting the waves without fixed supports.

While the wave filter was built to stand in the wave basin by its own rigidity without additional support, the wave absorbers, shown in Fig. 5. 11, were supported by structural frames outside the wave basin. (One of these structural frames is shown in Fig. 5. 13.) The wave absorbers, placed along the side-walls of the basin, were each 1 ft 6 in. high, 1 ft 10 in. thick, and 30 ft long and consisted of 50 layers of the same galvanized iron screen as used in the wave filter. To construct these wave absorbers, a unit of 10 screens, each 30 ft long, 1 ft 6 in. wide spaced 3/8 in. apart was held together by brackets at each end of the screens. The spacers were composed of pieces of pressed fiberboard called Benelex (3/8 in. thick, 2 in. wide, 1 ft 6 in. long) placed between each screen. Benelex was used since it absorbed only a small amount of water compared to some other materials. A bracket was fastened over the screens and spacers clamping the 10 screens together firmly as a unit. The screens in a unit of 10 layers were then stretched taut by 3/8 in. diameter stainless

steel rods which connected from the brackets at the ends of the units to the structural frames located outside the basin. Holes were drilled into the wall of the basin for the rods; fittings with "O"-ring seals were mounted in the wall to prevent the leakage around the rods. Therefore, the rods transmitted all the tension required to hold the screens taut to the structural frames at each end; hence no significant forces were applied to the basin walls. Five identical units (a total of 50 layers of screens) were built in this manner along each side of the basin as shown in Fig. 5.11.

The wave energy dissipating system provided a large area of galvanized iron in the wave basin, 9.0 ft^2 of wire screen per ft^3 of basin water. Because of the chemical reaction between the wire screens and the water when the screens were initially installed the zinc in the galvanized screens deposited in the basin. This not only decreased the amount of zinc that protected the wires of the screens but the reaction also produced a coating of undissolved zinc on the water surface. The latter effect led to undesirable operating characteristics of the wave gages. For this reason, it was necessary to introduce additives to the water to reduce and even prevent this reaction. A series of experiments were conducted in order to find a proper additive. It was found that a technical grade of sodium dichromate ($Na_2 Cr_2 O_7$)added to the water in a concentration of 500 ppm (by weight) could accomplish this. The concentration of the sodium dichromate was checked periodically by a light absorption technique and if the concentration was found to be less than desired, more was

added. In order that this additive could function properly as a corrosion inhibitor, it was necessary to keep the pH of the water less than 6.5; usually the pH was maintained in the range of 6.2 to 6.5 by periodically adding hydrochloric acid (HCl). This treatment of the basin water proved to be successful in both preserving the wire screens and eliminating the precipitate on the water surface, and it had no observable effect on the wave gages.

5.7 HARBOR MODELS

Four different harbors with constant depth were investigated experimentally: a rectangular harbor, a circular harbor with a 10° opening, a circular harbor with a 60° opening, and a model of the East and West Basins of the Long Beach Harbor (Long Beach, California). The harbor models were designed so that each would fit into a false-wall simulating a perfectly reflecting "coastline" and it was installed 27 ft 6 in. from and parallel to the wave paddle, i.e. 2 ft. 6 in. from the back-wall of the basin. The false-wall was made of lucite 3/8 in. thick and 1 ft 3 in. high mounted to a frame composed of galvanized iron angles constructed in two identical pieces: the east-wing and the west-wing. Each wing extended 4 ft 9 in. from 1 ft off the center of the wave basin to the inner most screen of the wave absorbers. A photograph of the supporting frames and the walls is presented in Fig. 5.14. The walls were weighted to hold them in place without direct connections to the basin floor. In line with the false-wall, lucite spacers 3/8 in. thick, 1 in. wide and 1 ft 6 in. high were placed between each screen of the absorbers. These spacers

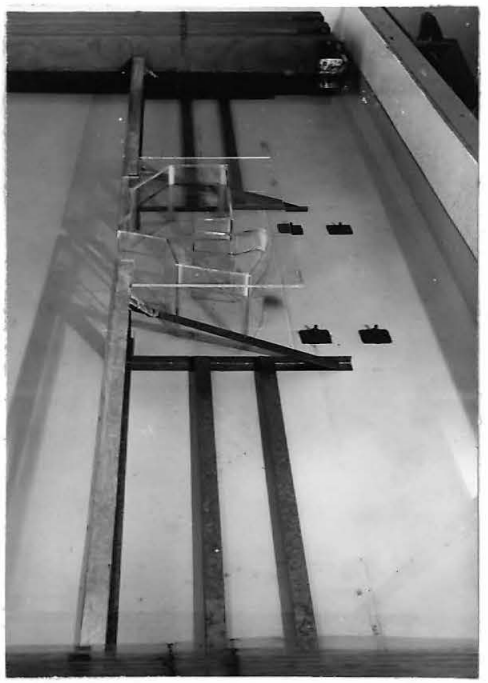

9335

Fig. 5.14 False-walls and supporting frames representing "coastline"

9318

Fig. 5.15 Rectangular harbor in place in the basin

which can be seen in upper left-hand-portion of Fig. 5.13 were placed to prevent waves penetrating through the absorbers to the still water region behind the false wall thereby creating undesirable oscillations in the basin.

In the following, a brief description of the harbor models is presented:

(i) Rectangular harbor: The rectangular harbor was 12-1/4 in. long, 2-3/8 in. wide with a fully open entrance and it was constructed of 1/4 in. thick lucite. Fig. 5.15 shows how the rectangular harbor was placed in relation to the false-wall inside the wave basin. It should be mentioned that the false-wall, "coastline", shown in Fig. 5.15 was different from the false-wall described in the previous paragraph. This wall was constructed from plywood (3/4 in. thick) and painted with an epoxy based paint. However, it was found that this wall expanded due to water absorption; therefore, after the experiments with the rectangular harbor were finished this false-wall was replaced by the one constructed of lucite just described which was used for all subsequent experiments.

(ii) Circular harbors: The two circular harbors (a 10° opening and a 60° opening), shown in Figs. 5.16 and 5.17, were each 1 ft 6 in. diameter and 1 ft 3 in. high, and they were constructed of 1/4 in. lucite plate which was heated and bent to shape. The cylinders were each connected on the top and the bottom to two 1/2 in. lucite reinforcing plates with holes cut to an inside diameter of 1 ft 6-1/2 in.; this is clearly shown in Figs. 5.16 and 5.17. These two reinforcing

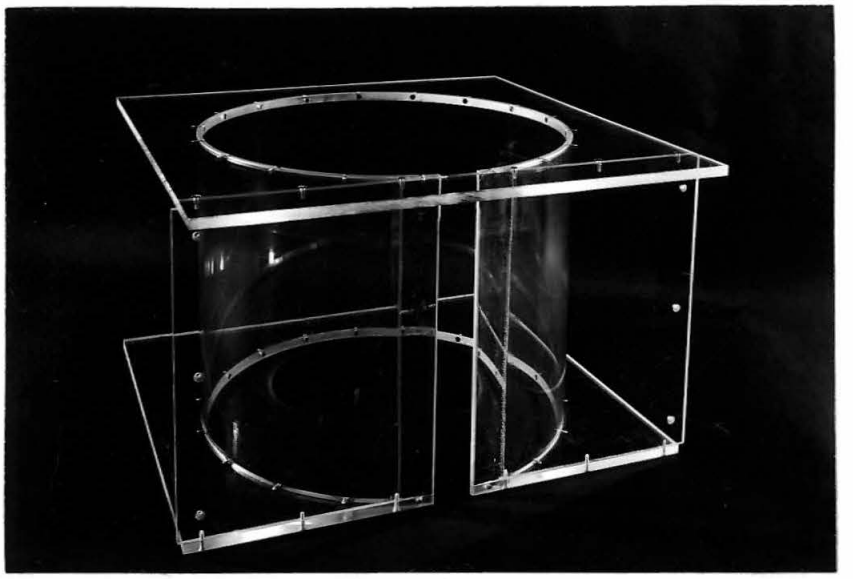

9323

Fig. 5.16 Circular harbor with a 10° opening

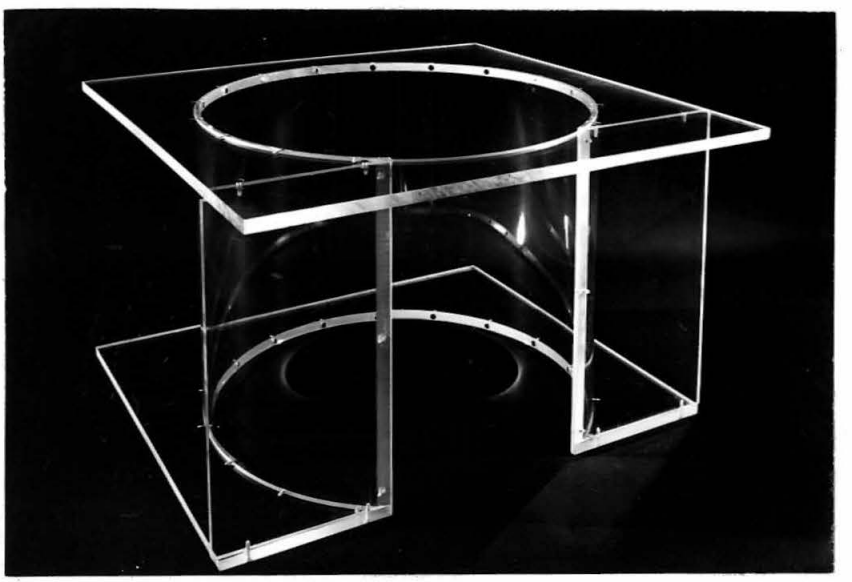

9325

Fig. 5.17 Circular harbor with a 60° opening

plates were necessary to keep the planform of the harbors circular. The two vertical plates shown near the harbor entrance in both Figs. 5.16 and 5.17 connected to the harbor fitted into the two foot space which had been left in the false-walls just described; thereby resulting in a smooth "coastline" extending from the wave absorbers to the limits of the harbor entrance.

(iii) Model of Long Beach Harbor: The model of Long Beach Harbor shown in Fig. 5.18 was also constructed from 1/4 in. thick lucite plate. The shape of the planform of the harbor was cut from two lucite sheets using dimensions such that when the vertical boundary walls were cemented in place the inside dimension of the harbor would be as desired. These supporting plates can be seen at the top and bottom of the harbor model in Fig. 5.18. This model was composed of 15 pieces of lucite cemented to the supporting plates and rubber cement was used as filets in the corners. The planform of the model was simplified from the existing harbor and can be compared to the prototype in the map (Fig. 5.19) which was extracted from the U.S.C. & G.S. map No. 5147.

5.8 INSTRUMENT CARRIAGE AND TRAVERSING BEAM

A photograph of the instrument carriage and traversing beam is presented in Fig. 5.20; also seen in this photograph is the frame which was placed outside the model of the harbor to support the instrument carriage. This frame, constructed of galvanized steel angles, was bolted to four pads that were cemented to the basin floor. An aluminum plate 3/8 in. thick, 2 ft 4 in. square with a

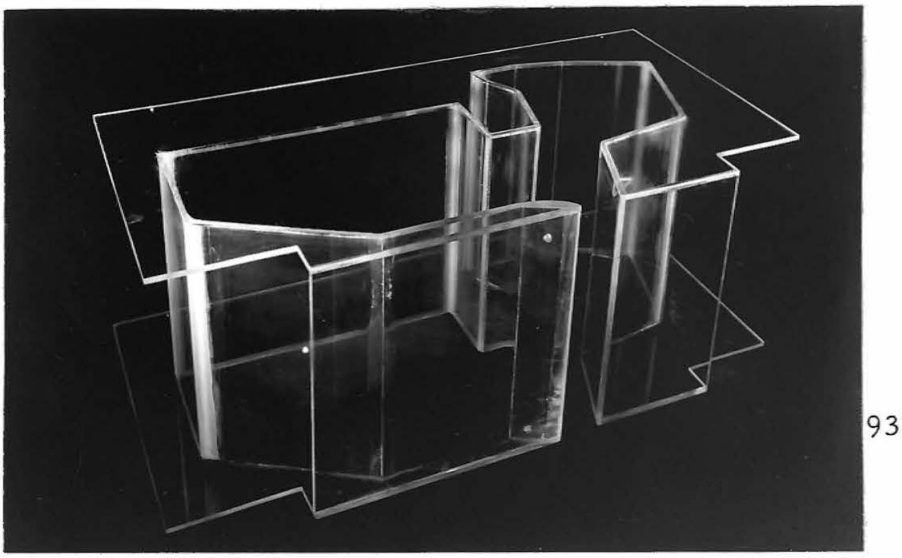

Fig. 5.18 Model of the East and West Basins of Long Beach Harbor (Long Beach, California)

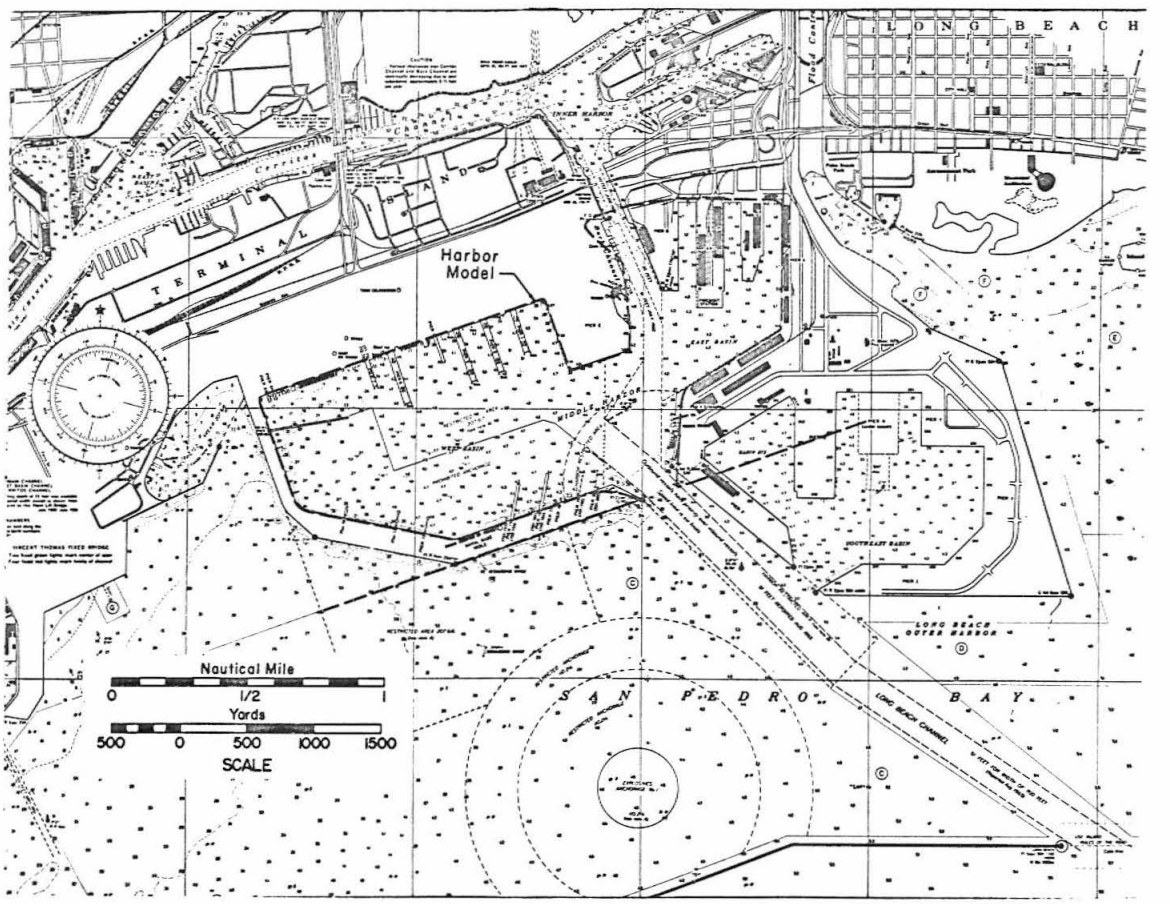

Fig. 5.19 Map showing the position of the East and West Basins of Long Beach Harbor and the model planform. (The harbor model is shown with dashed lines.)

circular hole of 2 ft inside diameter was mounted to the top of the structural frame. The carriage which was supported at three points with ball bearings was free to rotate with the hole in the plate as its guide and coupled with the traversing beam the wave gage could therefore be moved to any position inside the harbor. The complete frame could be moved toward or away from the false-wall so that the center of the circular hole on the aluminum plate coincided with the center of the circular harbor. In addition, the frame could be leveled by adjusting the bolts on the supporting pads so that the wave gages remained at the same immersion if moved to other positions within the harbor.

The traversing beam shown in Fig. 5.20 consisted of an aluminum channel to which two lead screws (16 threads per inch) were mounted. These screws were connected to a gear arrangement at one end so that they could be rotated either alone or simultaneously. The screws passed through two threaded blocks to which the wave gages were attached. As the lead screws were rotated these blocks moved in slots cut in the channel thus positioning the wave gages.

9336

Fig. 5.20 Instrument carriage and traversing beam shown mounted above 10^{o} opening circular harbor

CHAPTER 6

PRESENTATION AND DISCUSSION OF RESULTS

Experimental and theoretical results are presented in this chapter which deal with the wave induced oscillations of three harbors with specific shapes: circular harbors with 10^{o} and 60^{o} openings, a rectangular harbor, and a model of the East and West Basins of Long Beach Harbor located in Long Beach, California. All the harbors investigated were of constant depth and were connected to the open-sea; thus, an effective wave energy dissipating system was necessary to simulate these open-sea conditions in the laboratory. The characteristics of the wave energy dissipators chosen for this system will be discussed first, followed by the presentation and discussion of the results for the three harbors mentioned. All numerical computations were accomplished using an IBM 360/75 high speed digital computer.

6.1 CHARACTERISTICS OF THE WAVE ENERGY DISSIPATION SYSTEM

The theories developed in Chapter 3 and 4 treat the case of a harbor connected to the open-sea which lead to the existence of the "radiation condition", i.e. the radiated waves which emanate from the harbor entrance decay to zero at an infinite distance from the harbor. However, in the laboratory, experiments must be conducted in a wave basin of finite size; thus, the radiated waves from the harbor will be

reflected from the wave paddle and the sidewalls of the basin unless effective energy dissipators are provided. Indeed in the absence of dissipators Ippen and Raichlen (1962) (also Raichlen and Ippen (1965)) have shown that the response curve of a rectangular harbor connected to a highly reflective basin is characterized by numerous closely spaced resonant spikes. This result is strikingly different from the response curve for a rectangular harbor connected to the open-sea which was subsequently studied by Ippen and Goda (1963) where fewer modes of resonant oscillation were observed over similar ranges of wave period. In this section the design considerations and characteristics of the wave energy dissipating system (described in Section 5.6) which was used in these experiments to alleviate this problem will be presented and discussed.

A theoretical and experimental investigation of wave energy dissipators composed of wire mesh screens aligned normal to the direction of wave propagation was conducted by Goda and Ippen (1963). In their analysis each screen was considered to be composed of numerous equally spaced circular cylinders aligned vertically and horizontally; it was assumed that there was no wave reflection from the energy dissipator, and the energy dissipated by each cylinder was assumed to be independent of its proximity to the other cylinders. Therefore, the total energy dissipation was taken to be equal to the sum of that from each of the cylinders in the unit. Based on these assumptions, Goda and Ippen (1963) developed the following semi-empirical equation for the transmission coefficient of such a dissipator:

$$K_t = \left[1 + 13.4\, m \frac{D}{S} \left(\frac{\sigma D L}{\nu}\right)^{-0.5} \left(\frac{H_i}{L}\right)^{0.5} \varphi(h/L)\right]^{-2} \qquad (6.1)$$

where: K_t = transmission coefficient, defined as the ratio of the transmitted wave height to the incident wave height, H_t/H_i,

m = number of layers of screens,

D = diameter of the screen wire,

S = center to center distance between wires,

σ = circular wave frequency ($2\pi/T$),

ν = kinematic viscosity of the fluid,

L = wave length, and

$\varphi(h/L)$ = depth effect factor which is a function of the ratio of depth to wave length. (The interested reader is referred to Goda and Ippen (1963) Eq. 2.29 for this expression; for deep water waves it is equal to 1.81.)

Based on the experimentally determined values of the transmission coefficient, K_t, and the reflection coefficient, K_r, for various dissipators, an empirical relation was obtained to correlate these quantities:

$$K_r \approx K_t^{2.5} \qquad (6.2)$$

wherein K_r is defined as the ratio of the reflected wave height to the incident wave height, H_r/H_i.

To confirm the validity of Eqs. 6.1 and 6.2 so that they could be used with confidence in designing the wave energy dissipators for this study (described in Section 5.6) a series of experiments using model dissipators was conducted. These experiments were carried out in a wave tank 1 ft 6 in. wide, 1 ft 9 in. deep, and 31 ft long using a paddle type wave generator and using the procedures employed by

Goda and Ippen (1963). Two model dissipators were tested, denoted here as Dissipator A and Dissipator B; their characteristics are presented in Table 6.1.

Table 6.1 Model wave energy dissipators

Dissipator	Mesh (S)* Averaged Center to Center Spacing of Wires (in.)	Screen Wire Diameter (D) (in.)	Distance Between Layers of Screens (in.)	Number of Layers of Screens (m)
A	0.0625	0.011	0.5	38
B	0.0625	0.011	0.375	50

*For this study the horizontal and vertical spacing of the wires were not equal and the value denoted as S is the average spacing (see Section 5.6).

A dissipator is called a wave filter if it is placed between the wave generator and the back-wall of the wave tank; it is called wave absorber if placed against a reflecting surface of the tank. In order to determine the transmission and reflection coefficients of the wave filter, two wave gages were used to measure the wave envelope in the region ahead and behind the wave filter. To determine the reflection coefficient of the wave absorber one wave gage was used to measure the wave envelope in the region in front of the wave absorber. It can be shown that the incident and reflected waves can be determined simply from such wave envelopes (see Ippen, 1966, pp. 46-49).

The experimental and theoretical variation of the reflection coefficient, K_r, with the incident wave steepness, H_i/L, for Dissipators A and B are presented in Figs. 6.1 and 6.2 respectively. In both Figs. 6.1 and 6.2, the experimentally determined reflection

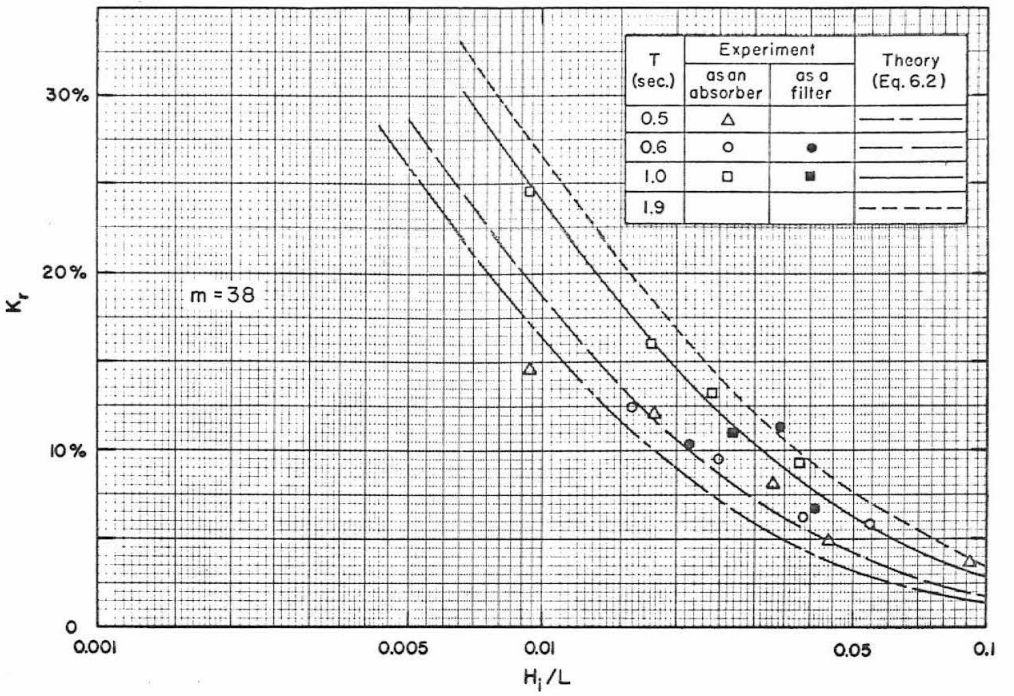

Fig. 6.1 Reflection coef., K_r, as a function of the incident wave steepness, H_i/L, for Dissipator A (m=38)

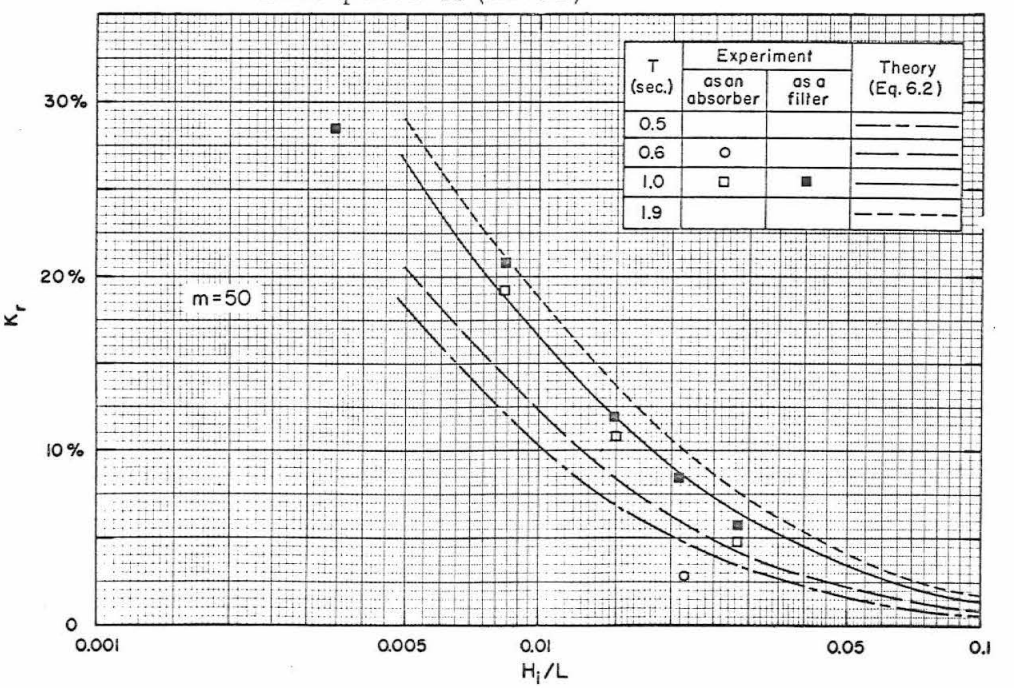

Fig. 6.2 Reflection coef., K_r, as a function of the incident wave steepness, H_i/L, for Dissipator B (m=50)

coefficients are presented for each dissipator used both as an absorber and as a filter. The former refers to the case where the dissipator was placed against the back-wall of the wave tank, while the latter refers to the case where the dissipator was located between the wave machine and the back-wall. The theoretical curves presented in Figs. 6.1 and 6.2 are computed in the following way: first, the transmission coefficient, K_t, is computed from Eq. 6.1, and the reflection coefficient, K_r, is then determined from the empirical relation, Eq. 6.2. The experimental data presented in Fig. 6.1 show considerable scatter; however, the data follow the trend predicted by Eqs. 6.1 and 6.2, i.e. for a constant wave period the reflection coefficient, K_r, decreases as the wave steepness, H_i/L, increases, and for a constant wave steepness, the reflection coefficient, K_r, increases as the wave period, T, increases.

Similar data are presented in Fig. 6.2 for Dissipator B where the number of screens has been increased from 38 to 50 and the spacing of the screens reduced from 0.5 in. to 0.375 in. By comparing Figs. 6.1 and 6.2, as expected, it is seen that Dissipator B is more efficient than Dissipator A.

In Fig. 6.3 the experimentally determined reflection and transmission coefficients for these two dissipators are shown. The experimental data obtained by Goda and Ippen (1963) which were the basis for their empirical relation, Eq. 6.2, are also included in Fig. 6.3. Three relations: $K_r = K_t^2$, $K_r = K_t^{2.5}$ and $K_r = K_t^3$, are shown in Fig. 6.3 for reference. It is seen that the experimental data show considerable scatter; nevertheless, the results for Dissipator A agree

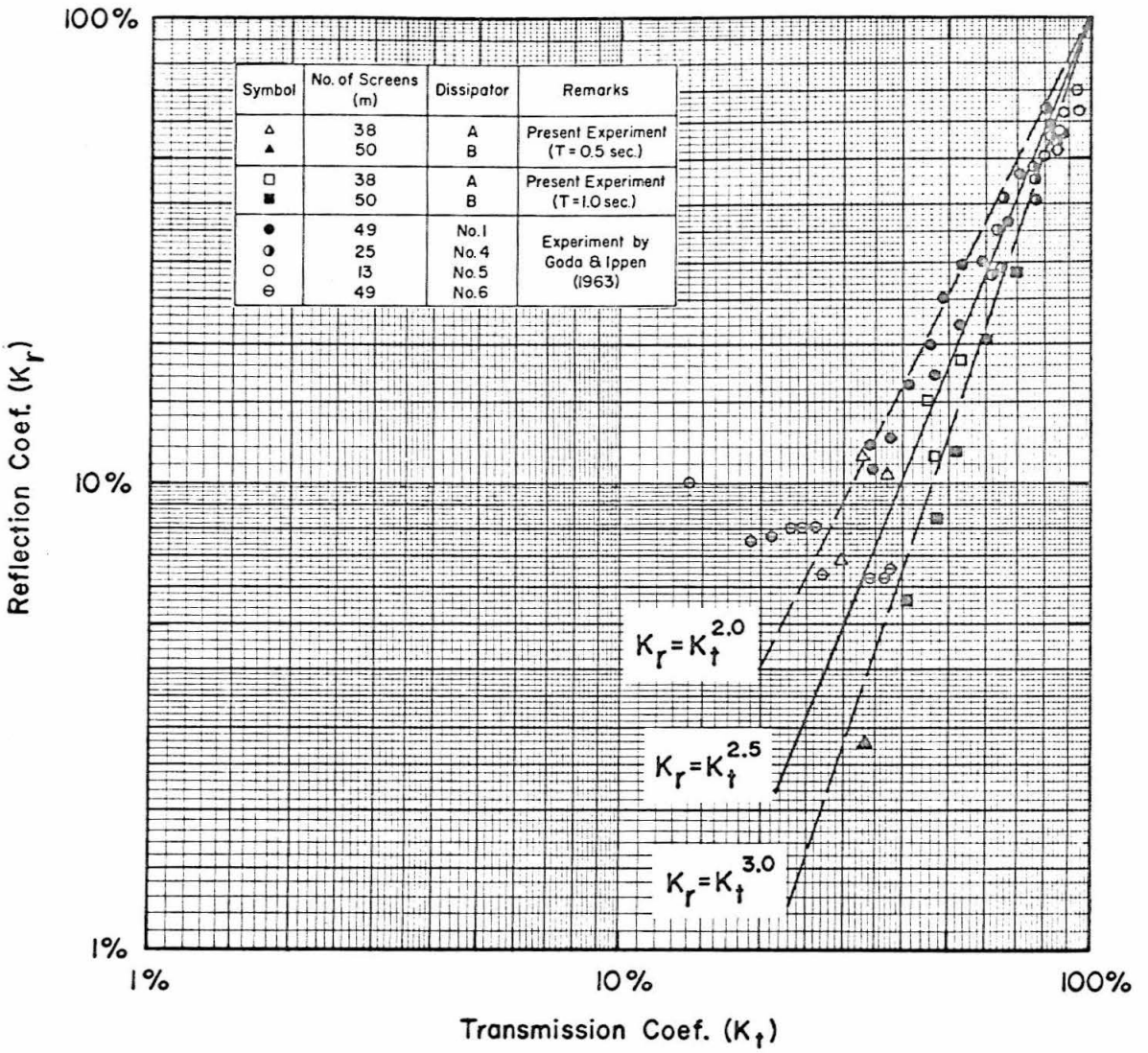

Fig. 6.3 The variation of the measured reflection coef. K_r, with the measured transmission coef. K_t, for various wave dissipators.

best with the expression: $K_r = K_t^{2.5}$, and the results for Dissipator B with: $K_r = K_t^{3.0}$. This difference for the two dissipators suggests that the wave energy dissipation characteristics might be affected by the spacing between the screens which was neglected in the analysis by Goda and Ippen (1963). The results also show that for a constant reflection coefficient, K_r, the transmission coefficients, K_t, obtained from the present experiments are somewhat larger than those obtained by Goda and Ippen (1963).

The most important characteristic of the wave energy dissipators in simulating the unbounded open-sea is the reflection coefficient, K_r. It was suggested by Ippen and Goda (1963) that the reflection coefficient, K_r, of wave filters and absorbers should be less than 20% for proper simulation of open-sea conditions in a restricted wave basin. The wave absorbers finally chosen for this investigation consisted of 50 layers of screens with a spacing of 0.375 in. between screens (as described in Section 5.6). Therefore, the wave energy dissipation characteristics of the wave absorbers used are identical to those of Dissipator B used in these preliminary experiments and shown in Fig. 6.2. With reference to Fig. 6.2, except for very small incident wave steepnesses the reflection coefficient of the absorbers is estimated to be less than 20% for the majority of the harbor resonance experiments which were conducted.

The wave filter used, which has been described in Section 5.6, consisted of 70 layers of screens with a spacing of 0.8 in. between layers of screens. The reflection coefficient of the wave filter is expected to be less than that of the wave absorbers for comparable

incident wave steepnesses due to the smaller number of screens and spacing in the latter. Therefore, it is expected that except again for the case of an extremely small wave steepnesses, the reflection coefficient of the wave filter used is less than 20%.

In order to ensure that the open-sea condition was properly modeled in the wave basin using the wave energy dissipators described, in initial phases of this study the response to periodic incident waves of a fully open rectangular harbor (2-3/8 in. wide and 1 ft 1/4 in. long and identical to that studied by Ippen and Goda (1963)) was studied experimentally. The results obtained agreed well with both the theoretical "open-sea solution" and the experimental results obtained by Ippen and Goda (1963). Thus, the open-sea condition for the radiated wave was considered to have been simulated properly in these experiments. The results of these experiments will be presented and discussed in detail later in Section 6.3.

6.2 CIRCULAR HARBOR WITH A 10° OPENING AND A 60° OPENING

6.2.1 Introduction

As discussed previously, the wave induced oscillations in a circular harbor connected to the open-sea can be evaluated by using either the special theory developed in Section 4.1 (if the chord which represents the harbor entrance can be approximated by an arc of the circle) or using the general theory developed in Chapter 3 for an arbritrary shaped harbor. In this section, the theoretical results obtained from these two theories are compared to the experimental

results for harbors with a 10^{o} and a 60^{o} opening. In order to verify the theory the following results will be presented and discussed:

(i) the variation of the amplification factor at a fixed position inside the harbor as a function of incident wave number (or wave period),

(ii) the variation of the wave amplitude inside the harbor for various resonant modes,

(iii) the variation of the total velocity at the harbor entrance as a function of incident wave number, and

(iv) the distribution of velocity across the harbor entrance for various wave numbers.

6.2.2 Response of Harbor to Incident Waves

The response of a harbor is defined, for this study, as the variation of the amplification factor, R, with the wave number parameter ka (wherein k is the wave number and a is a characteristic planform dimension of the harbor, the radius for the circular harbor). The function ka is of course dependent upon wave period and depth whereas the amplification factor R is also a function of position. The amplification factor R is defined as the wave amplitude at the position (r, θ) divided by the standing wave amplitude which exists in the wave basin with the harbor entrance closed for the wave number (or period) of interest. Over some range of wave number the wave amplitude inside the harbor may be amplified while over another range it may be attenuated. Physically, for such a harbor this resonance results from the trapping of incident wave energy inside the harbor at

particular wave numbers (or wave periods) which depend on the geometry of the harbor as well as the depth.

Two response curves for a circular harbor with a 10^{o} opening are presented in Figs. 6.4 and 6.5, where the two theories described in Chapters 3 and 4 are compared to experiments. The experiments were conducted in a circular harbor of 1.5 ft diameter with the depth of water constant and equal to 1 ft in both the harbor and the "open-sea". In both figures, the solid line represents the theoretical curve computed from the theory for an arbitrary shaped harbor (Chapter 3); the theory for the circular harbor (Section 4.1) is shown with dashed lines. The theoretical amplification factor was calculated using Eq. Eq. 3.38 and Eq. 4.30 for the arbitrary shaped harbor theory and the circular harbor theory respectively. The experimental amplification factor was obtained by dividing the wave amplitude at the point investigated inside the harbor (center of the harbor or the position: $r=0.7$ ft, $\theta=45^{o}$) by the average wave amplitude of the standing wave system at the harbor entrance. The standing wave system was measured at the "coastline" when the entrance was closed; the procedure for obtaining the average wave amplitude of the standing wave system was described in Section 5.4.

Fig. 6.4 shows the response at the center of the harbor while Fig. 6.5 shows the response at the postion $r=0.7$ ft, $\theta=45^{o}$. The center of the harbor is a unique position to investigate because it is the location having an equal distance to any point on the boundary. The position: $r=0.7$ ft, $\theta=45^{o}$ is near the harbor entrance and was chosen because it was of interest to know whether the harbor entrance had any

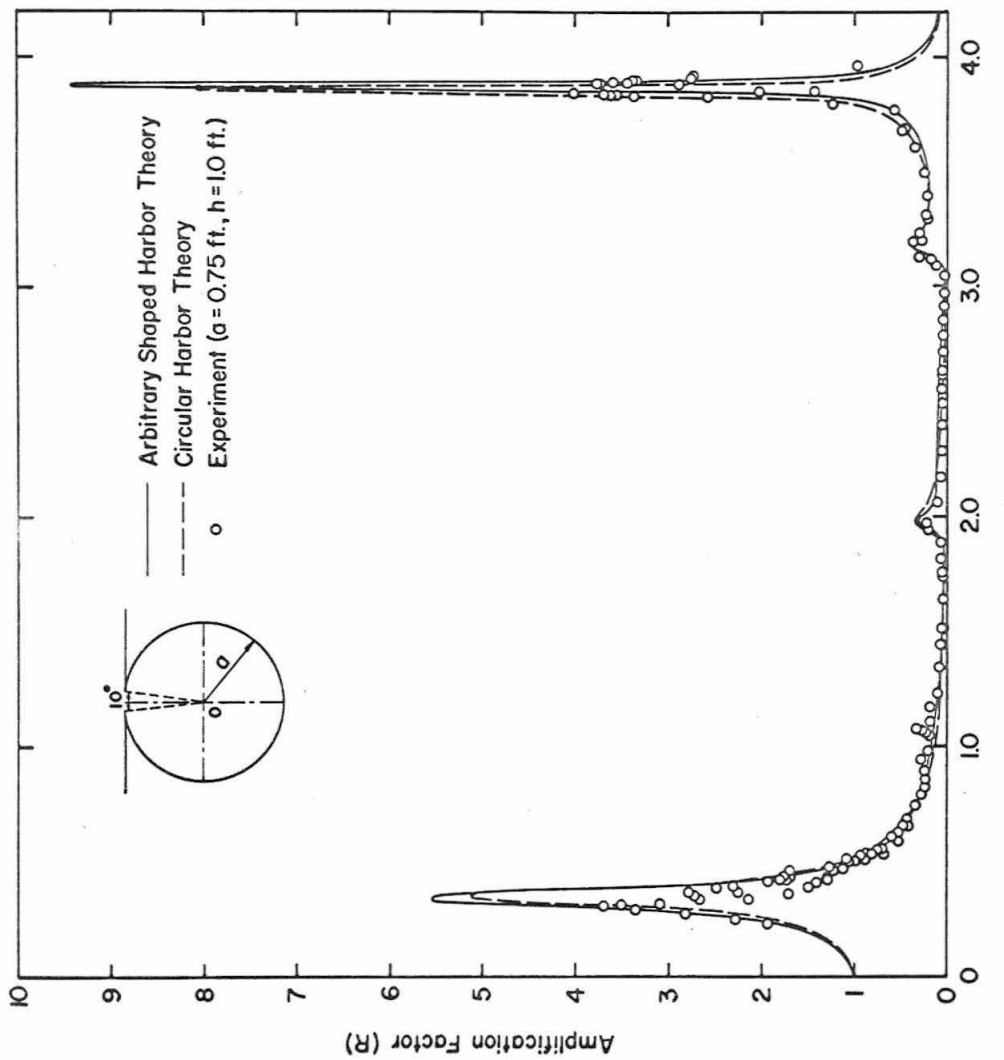

Fig. 6.4 Response curve of the circular harbor with a 10^{o} opening at the center.

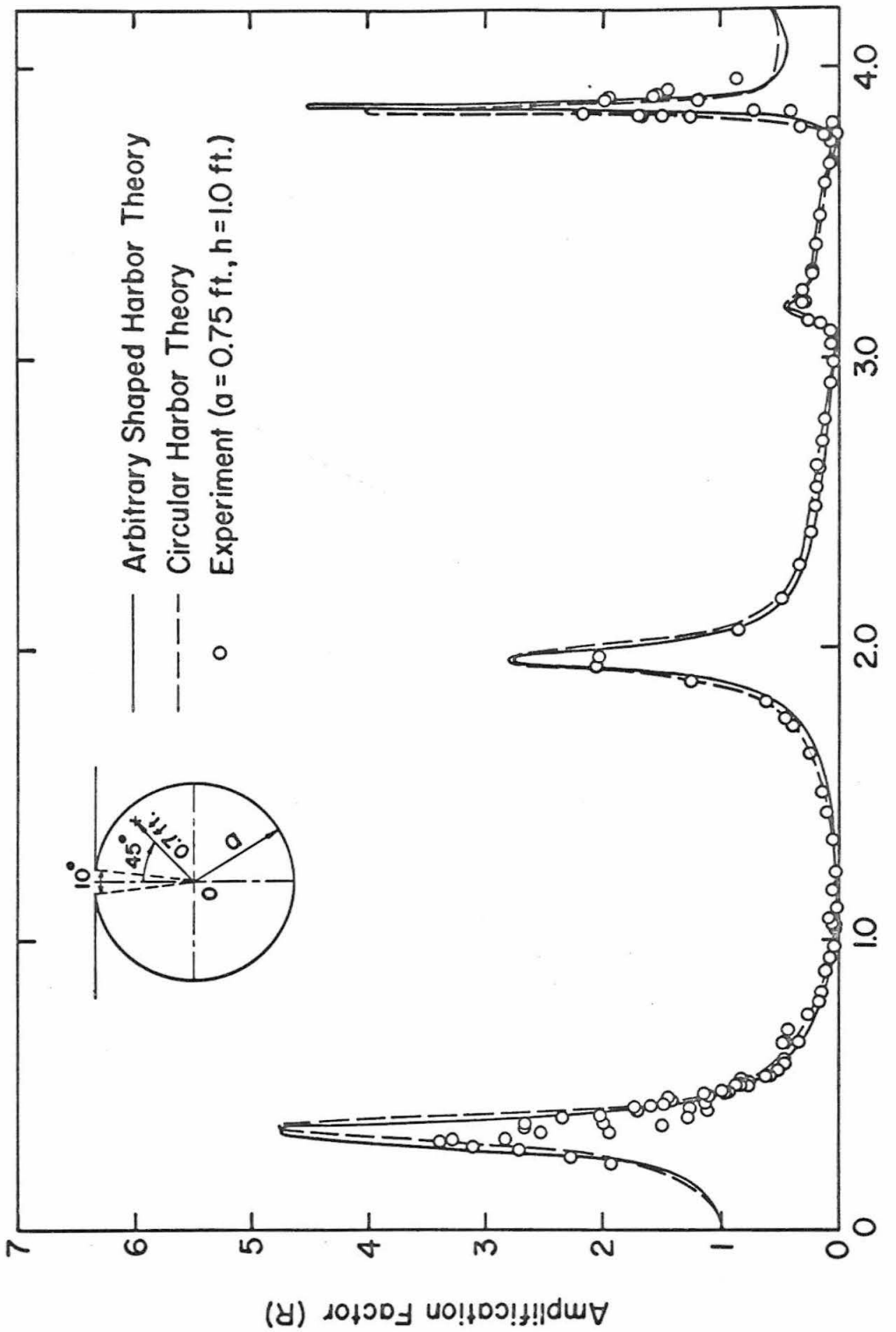

Fig. 6.5 Response curve of the circular harbor with a 10^{o} opening at r=0.7 ft, $\theta=45^{o}$

special influence on the response that might not be predicted by the two theories. In the experiments the wave amplitude at these two positions was measured simultaneously; however, the gages were separated by about one radius, thus any disturbance caused by one of the wave gages would not be expected to seriously affect the other.

For the case of a circular harbor with a 10^{o} opening the arc and the chord at the harbor entrance are almost the same length, therefore the theory for the circular shaped harbor developed in Section 4.1 can be considered to be applicable. In using the theory for an arbitrary shaped harbor, the boundary of the circular harbor was divided into 36 segments with each segment containing 10^{o} of the central angle. Since the harbor entrance was represented by one of these segments, only one unknown complex constant of the normal derivative of the wave function $\left(\frac{\partial f_2}{\partial n}\right)$ needs to be evaluated by the matching procedure.

In Figs. 6.4 and 6.5 reasonably good agreement is seen between the experimental data and the theoretical results. Because the energy dissipation due to viscous effects is not considered in the theoretical analysis, the theoretical values near resonance are, as expected, higher than the experimental values; more discussion of this will be presented later in this subsection. Four maxima in the range of ka that were investigated can be seen in the curves in Figs. 6.4 and 6.5; the values of ka for these four are: 0.35, 1.988, 3.18, and 3.87. These correspond to four distinct modes of resonant oscillation; the shape of the water surface for these modes of oscillation will be

discussed in detail in Subsection 6.2.4. It can also be seen in Figs. 6.4 and 6.5 that the response in region of ka $\approx$ 3.87 is very peaked, i.e. a large amplification factor and a narrow wave number bandwidth (range of ka); the theoretical amplification factor at the center of the harbor is nearly 10.

As the width of the harbor entrance increases, the difference between the length of the chord and the arc at the entrance increases and the theory for the circular harbor developed in Section 4.1 may no longer be satisfactory. In order to examine the effect of the small entrance approximation of the circular harbor theory on the harbor response when the entrance to the open-sea is relatively large, a circular harbor with a 60° opening was investigated. In this case the length of the chord and the arc at the entrance differ by almost 5%.

Two response curves for the circular harbor with a 60° opening are presented in Figs. 6.6 and 6.7. Fig. 6.6 shows the response curve for the center of the harbor; this position corresponds to that shown in Fig. 6.4 and experimental data from two circular harbors (1.5 and 0.5 ft diameter) are included. This smaller harbor was used to obtain data at smaller values of ka than could be obtained with the 1.5 ft diameter harbor. Fig. 6.7 shows the response curve for the position: r=0.7 ft, $\theta=45^{\circ}$ corresponding in location to the curve shown in Fig. 6.5; experimental data for only the circular harbor of 1.5 ft diameter are included for that location. As before, at both locations theoretical curves obtained from each of the theories are shown.

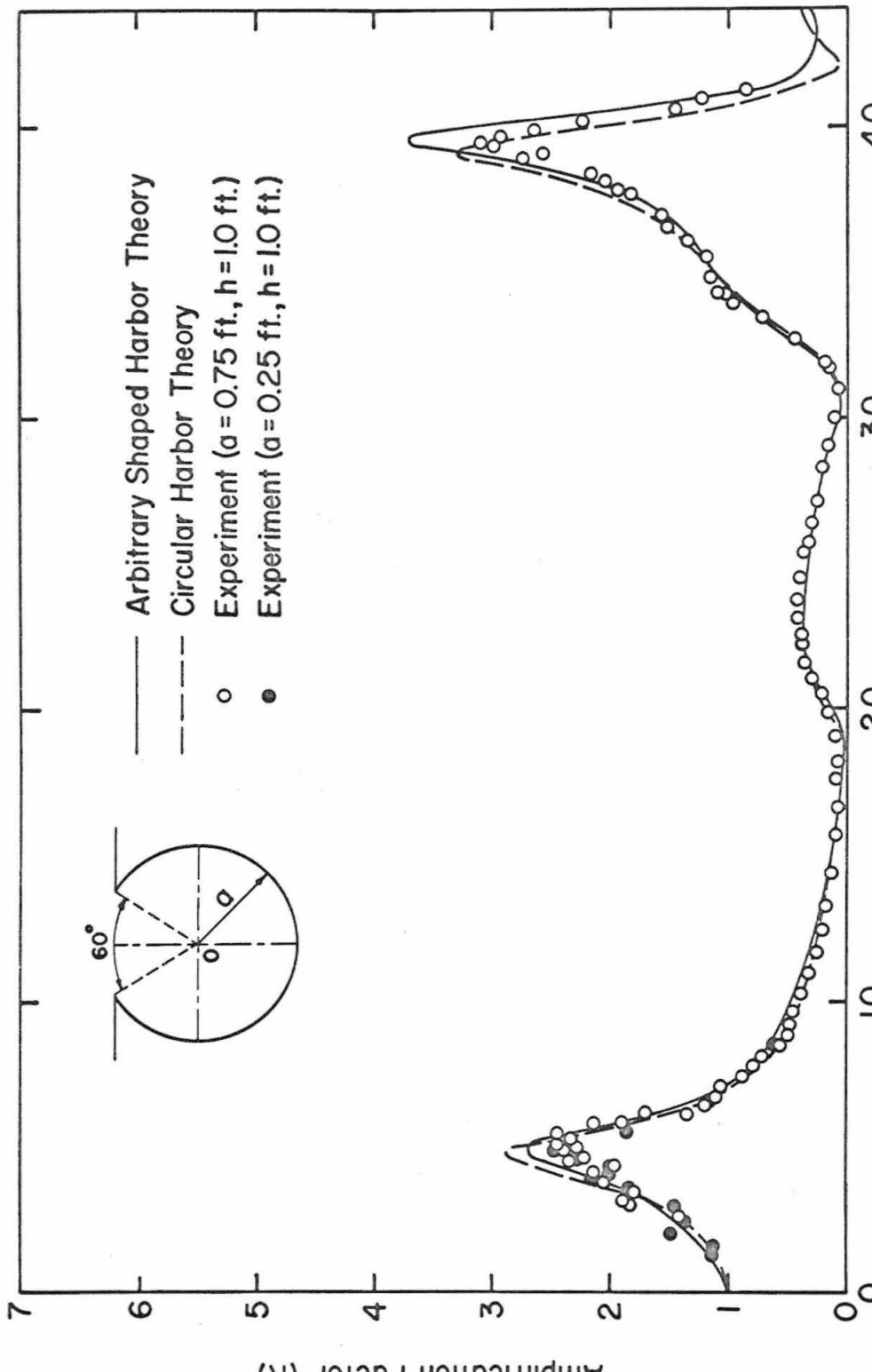

Fig. 6.6 Response curve of the circular harbor with a 60° opening at the center

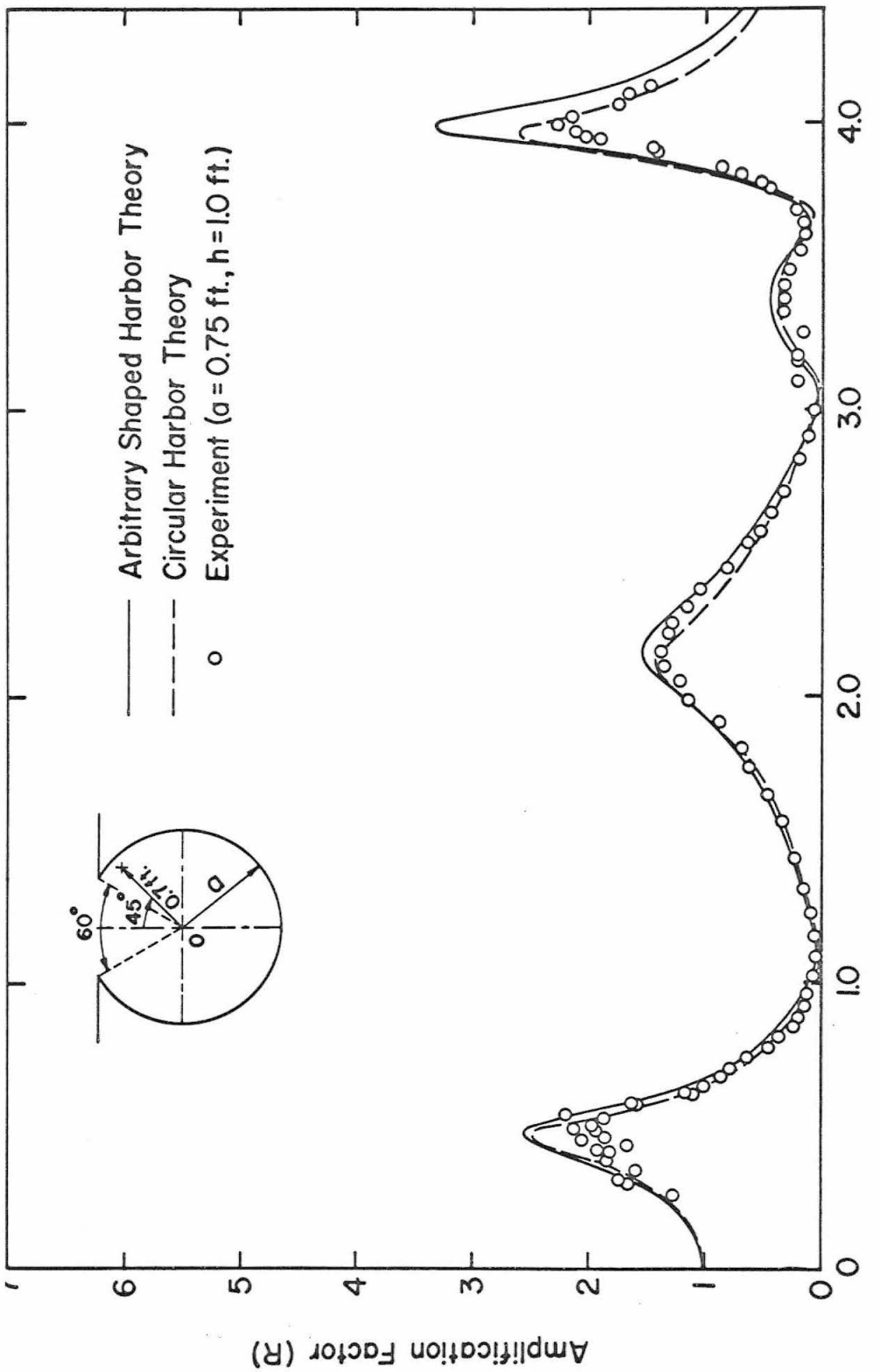

Fig. 6.7 Response curve of the circular harbor with a 60^{o} opening at r=0.7 ft, $\theta=45^{o}$

In using the theory for an arbitrary shaped harbor, the boundary of the harbor (including the harbor entrance) was divided into 36 segments, and for this case the harbor entrance was represented by six of these boundary segments. Therefore, six complex constants of the normal derivative of the wave function $\left(\frac{\partial f_2}{\partial n}\right)$ at the harbor entrance were determined by the matching procedure. However, when applying the circular harbor theory, only one constant was used at the entrance, i.e. the average normal derivative of the wave function across the harbor entrance ($\overline{C}$) obtained by the matching procedure discussed in Section 4.1.

The theoretical results presented in Figs. 6.6 and 6.7 show good agreement with the experimental data. Note that in Fig. 6.6, data obtained from experiments conducted in a circular harbor of 0.5 ft diameter are denoted by solid circles. These data combined with the data obtained in the harbor of larger diameter (1.5 ft) show that the response curve of the harbor at a particular location is only a function of ka.

From the theoretical results presented in Figs. 6.6 and 6.7, it appears that for the two theories there is a small difference in the value of the wave number parameter, ka, which is predicted at resonance. This difference is probably caused by the different treatment at the harbor entrance for the two theories: for the circular harbor theory one segment was used whereas for the arbitrary shaped harbor theory the entrance was divided into six segments. In fact,

it is seen from Figs. 6.6 and 6.7 that in the location of the peaks the experiment agrees better with the arbitrary shaped harbor theory. The values of ka for the four modes of oscillation shown in these figures can be denoted by ka = 0.46, 2.15, 3.38, 3.96 which are the average values from the two theories.

It should be noted that these four maxima are well defined in Fig. 6.7 whereas the third maximum is not obviously shown in the response curve for the center of the harbor (Fig. 6.6). This problem of defining the resonant mode of oscillation solely by a response curve such as this will be discussed more fully in Subsection 6.2.5.4. The amplitude distribution corresponding to these resonant modes will be discussed in Subsections 6.2.3 and 6.2.4.

By comparing Fig. 6.4 with Fig. 6.6 and Fig. 6.5 with Fig. 6.7 one is able to observe the effect of the size of the harbor opening on the amplification of waves inside the harbor. It is obvious from these figures that the maxima which appeared in Figs. 6.4 and 6.5 for the harbor with a 10° opening are replaced by peaks of smaller amplification factors and larger bandwidth for the harbor with a 60° opening (see Figs. 6.6 and 6.7). This effect was called the "harbor paradox" by Miles and Munk (1962). In addition, in comparing these figures it is seen that for the 60° opening, the values of ka of the modes of resonant oscillation are larger than the values of ka for the corresponding modes for the harbor with a 10° opening.

Another characteristic that can be observed from a comparison of Fig. 6.4 with Fig. 6.6 and Fig. 6.5 with Fig. 6.7 is that the theoretical results agree with the experimental results better for the harbor with the larger opening. In order to explain this, some consideration must be given to the effect of energy dissipation at resonance. In the theoretical analysis it was shown that the radiation of energy from the harbor to the open-sea, limits the amplification at resonance. In nature in addition to the radiation effect, viscous dissipation of energy limits the maximum amplification even more. Since the theory only treated the effect of radiation, one expects the theoretical values of the amplification factor in the region of resonance to be larger than the experimental values. Moreover, for the same incident wave characteristics the energy dissipation at the entrance due to viscous effects are relatively more important for the harbor with a smaller entrance. Thus a better agreement between the experimental and theoretical results is apparent for the harbor with a 60° opening. On the other-hand the results in Figs. 6.4 to 6.7 demonstrate that the wave numbers (or periods) at resonance are correctly predicted by the two theories. These effects for the harbor are similar to those for a single-degree-of-freedom oscillator where viscous dissipation affects resonant amplification much more than it affects the natural periods of oscillation.

The agreement between the theories and the experiment is even more encouraging since the experiments conducted for the response curves presented in Figs. 6.4 to 6.7 covered the range of waves

from shallow water waves to deep water waves. The conventional method of classifying waves is: shallow water waves for $h/L < 1/20$, intermediate waves for $1/20 < h/L < 1/2$, and deep water waves for $h/L > 1/2$ (wherein L is the wave length, h is the depth); thus, the experiments conducted for $ka < 0.236$ ($a=0.75$ ft) are shallow water waves, whereas those for $0.236 < ka < 2.36$ are intermediate waves and for $ka > 2.36$ the waves are deep water waves. It should also be mentioned that the experiments were accomplished using a wide-range of stroke settings of the wave machine (see Appendix IV). Since this range of stroke settings results in a wide range of incident wave steepnesses the good agreement between the theories and the experiments also emphasize the applicability of these linear theories even quite close to resonance.

It was mentioned in Chapter 3 that in using the theory for an arbitrary shaped harbor, the boundary of the harbor must be divided into a sufficiently large number of segments. The word "sufficient" implies that the results obtained using the approximate theory must agree with the exact solution within an allowable limit. Obviously, as the number of segments increases, the accuracy of the approximate theory compared to an exact theory will improve; however, with this increase both the required computer storage and computation time may increase significantly. Therefore, these factors may place a practical lower limit on the length of the segments into which the boundary is divided, and therefore, consideration must be given to the relative size of each segment.

The following considerations are necessary in determining the segment length: when the boundary is divided and replaced by straight-line segments these must be a good approximation to the actual boundary, and the length of each straight-line segment, Δs, must be small compared with the wave length, L. To understand this second criterion, it is recalled that in the approximate theory the wave function along each boundary-segment is represented by a constant value located at the mid-point of the segment; thus, the length, Δs, must be small compared to the wave length, L. Therefore, within the distance of one wave length there are a number of these segments along which the wave function is evaluated, thereby assuring the proper representation of the wave form. This criterion can be represented best by the parameter $k\Delta s$. It was shown in Subsection 3.4.1 (Table 3.1) that by using the same number of segments the approximate solution agreed better with the exact solution for a smaller wave number k than for larger wave numbers. Thus, in considering the size of Δs, the case of larger values of k (smaller wave lengths) is more critical than the case of small k. For the circular harbors studied experimentally and simulated theoretically, the length of the segments, Δs, used was 0.13 ft (for N=36) and the largest value of ka for which the experiments were performed was approximately 4.0 (which corresponds to $k=5.3\ ft^{-1}$). Therefore, the critical value of $k\Delta s$ in the present case is 0.69. Judging by the good agreement realized between the approximate theory and the

experimental results, it is concluded that the boundary of the harbor was divided into segments which were sufficiently small; this criterion corresponds to the ratio: $\Delta s/L \approx 1/9$. Therefore, a conservative statement of the criterion for segment length can be stated as: the harbor perimeter should be divided into a number, N, straight-line segments such that the ratio of the length of the largest segment to the smallestwave length to be considered is less than about one-tenth.

6.2.3 Variation of Wave Amplitude Inside the Harbor: Comparison of Experiments and Theory

The results presented in Subsection 6.2.2 on the response of the two circular harbors to incident waves demonstrate that the theoretical results obtained from the arbitrary shaped harbor theory and the circular harbor theory agree well with the experimental data. Both theories will be tested further in this section by comparing the theoretical results with the experimental results for the wave amplitude distribution inside the harbor for various values of the wave number parameter ka.

The wave amplitude distribution within the circular harbor with a 10° opening is presented in Fig. 6.8 for a value of ka = 0.502. In Fig. 6.8 the variation of wave amplitude with angular location is shown along two circular paths: the upper portion of the figure for r = 0.7 ft (r/a = .935) and the lower portion for r = 0.2 ft (r/a = .267). The abscissa in Fig. 6.8 is the angular position, θ, in degrees and the ordinate is the wave amplitude normalized with respect to the

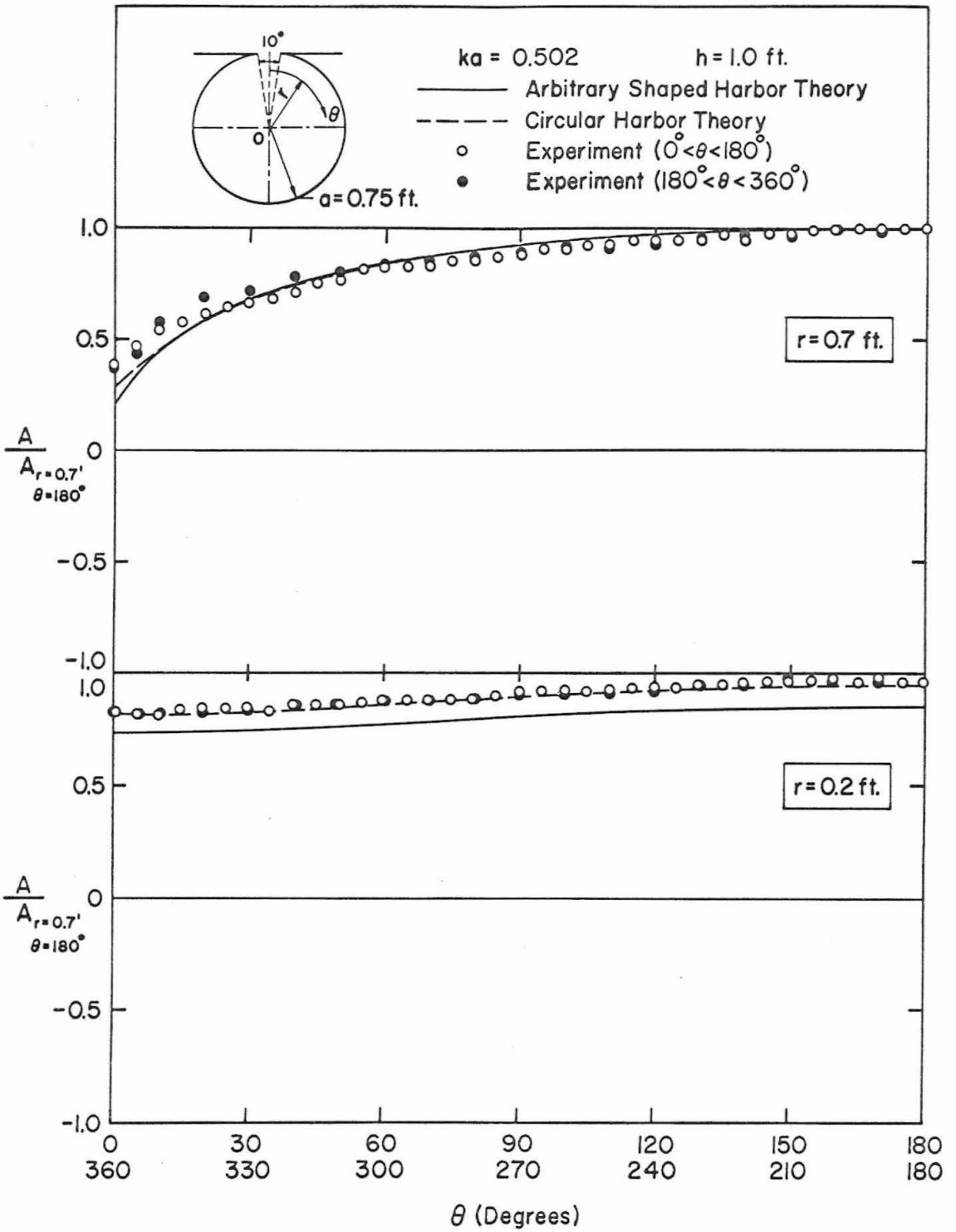

Fig. 6.8 Wave amplitude distribution inside the circular harbor with a 10^{o} opening for ka=0.502

wave amplitude at the position of r = 0.7 ft, $\theta = 180^{\circ}$. (The wave amplitude at r = 0.7 ft, $\theta = 180^{\circ}$ is chosen for normalization as it is the maximum value which was measured along the two circular paths, i.e. r = 0.7 ft and 0.2 ft.) In Fig. 6.8 and in other figures throughout this section, the solid line represents the theoretical amplitude distribution obtained from the theory for an arbitrary shaped harbor (Chapter 3) applied to this special shape; the amplitude distribution obtained from the theory described in Section 4.1 for a circular harbor is shown by a dashed line. Since the theoretical wave function, thus wave amplitude, inside the harbor is symmetrical about a diameter which bisects the entrance ($\theta = 0^{\circ}$), the theoretical results presented only cover the range of θ from 0° to 180°.

Experiments were conducted to measure the wave amplitude for $0^{\circ} < \theta < 360^{\circ}$ along certain radii: in Fig. 6.8 the experimental data for $0^{\circ} \leq \theta \leq 180^{\circ}$ are denoted by an open circle while the data for $180^{\circ} < \theta \leq 360^{\circ}$ are denoted by a solid circle. Reasonably good agreement is seen between the theories and the experimental results; however, for r = 0.2 ft, the theoretical results calculated from the theory for the arbitrary shaped harbor differ by about 10% from the results of circular harbor theory, the experimental results agreeing better with the latter. The experimental data for $0^{\circ} < \theta \leq 180^{\circ}$ agree well with those for $180^{\circ} < \theta \leq 360^{\circ}$ thus demonstrating the symmetry of the wave amplitude inside the harbor with respect to the diameter at $\theta = 0^{\circ}$.

Fig. 6.9 shows the wave amplitude distribution along circular paths with r = 0.7 ft and r = 0.2 ft for ka = 1.988 for the harbor with a 10° opening. As in Fig. 6.8 the wave amplitude at various locations is normalized with respect to the wave amplitude at the position of r = 0.7 ft, $\theta = 180^{\circ}$ which is again the maximum of points measured. This value of ka corresponds to the second maximum in the response curves shown in Figs. 6.4 and 6.5. It is seen that the theoretical results agree well with the experimental data at the locations where the measurements were made. At this value of ka, the wave oscillation inside the harbor is termed the "sloshing mode"; this mode of oscillation will be discussed more fully in Subsection 6.2.4. Fig. 6.9 shows, for r = 0.7 ft a region of negative water surface displacements (negative wave amplitudes) in the region $0^{\circ} < \theta < 97^{\circ}$ with positive displacements in the region $97^{\circ} < \theta < 180^{\circ}$. Similarly, for r = 0.2 ft two regions are seen with opposite phase, i.e. the region $0^{\circ} < \theta < 103^{\circ}$ with negative displacements and the region $103^{\circ} < \theta < 180^{\circ}$ with positive displacements.

Similar results for a value of ka = 3.188 are presented in Fig. 6.10; this value of ka corresponds to that of the third maximum in the response curves shown in Figs. 6.4 and 6.5. The ordinate in Fig. 6.10 is the relative wave amplitude normalized with respect to the wave amplitude at the position r = 0.7 ft, $\theta = 95^{\circ}$, where this amplitude is the maximum which was measured along both circular paths (r = 0.7 ft and r = 0.2 ft). For this mode of oscillation two

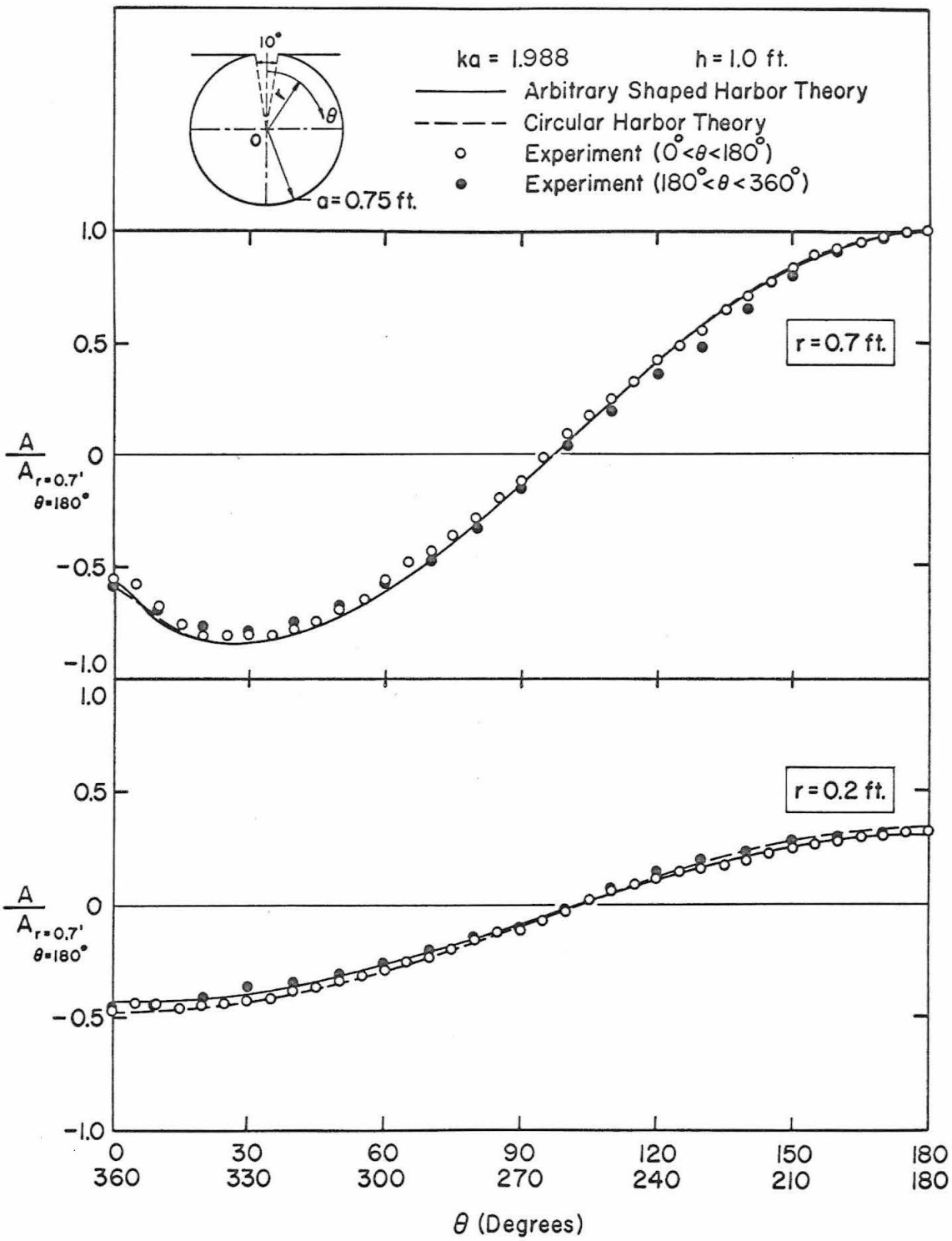

Fig. 6.9 Wave amplitude distribution inside the circular harbor with a 10^{o} opening for ka=1.988

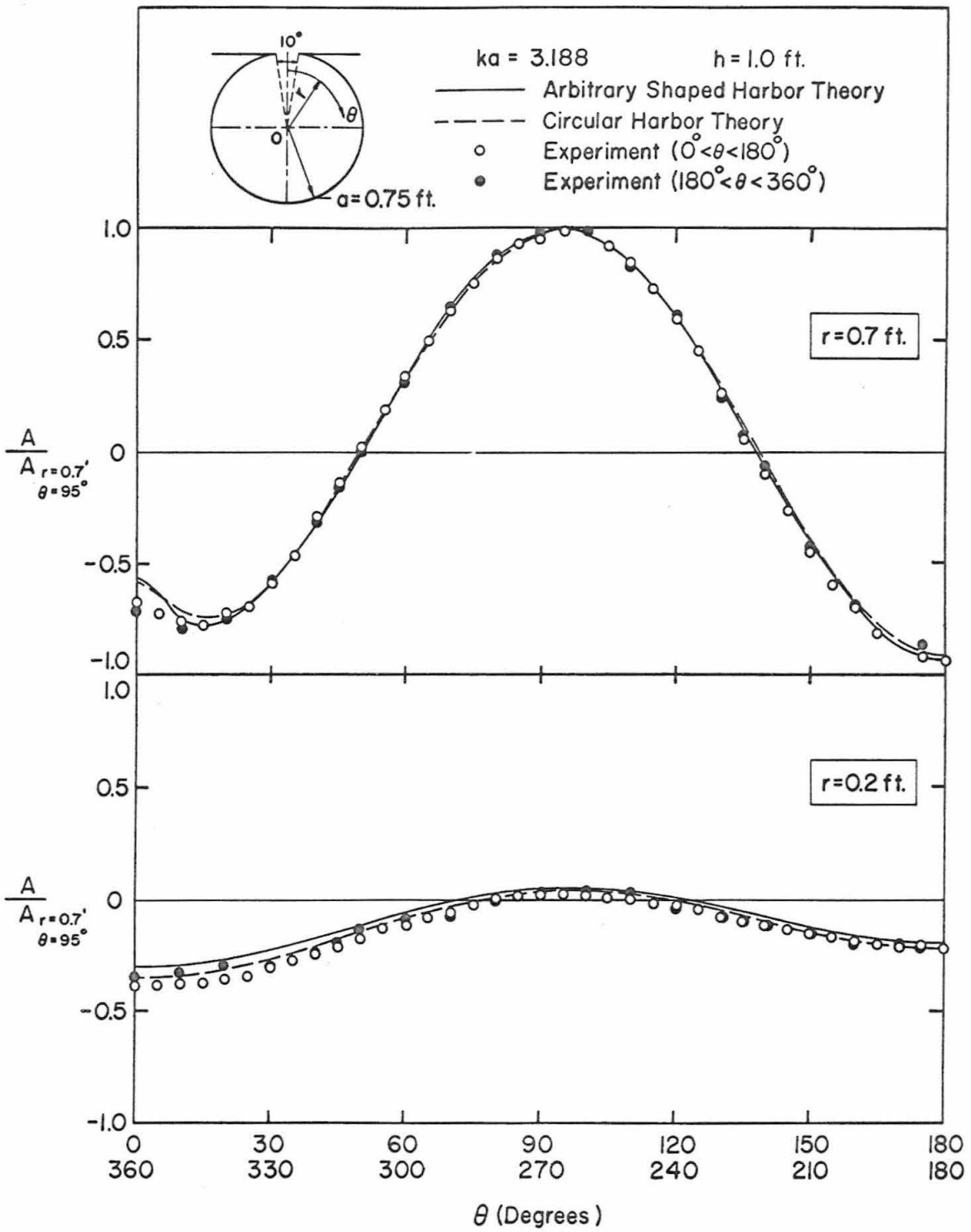

Fig. 6.10 Wave amplitude distribution inside the circular harbor with a 10° opening for ka=3.188

nodal lines exist in the harbor (see Subsection 6.2.4 for a more complete discussion); thus, the nodal lines cross the two circular paths at two locations along each path: $\theta = 50^{\circ}$ and 138° for $r = 0.7$ ft and $\theta = 73^{\circ}$ and 123° for $r = 0.2$ ft. Therefore, in the upper portion of Fig. 6.10 ($r = 0.7$ ft) negative water surface displacements are evident in the regions $0^{\circ} < \theta < 50^{\circ}$ and $138^{\circ} < \theta < 180^{\circ}$ while positive displacements are shown in the region $50^{\circ} < \theta < 138^{\circ}$. Positive and negative water surface displacements can also be seen for $r = 0.2$ ft.

To investigate whether the shape of the water surface is described well by a linear theory experiments were conducted where the wave amplitude distribution inside the harbor at $r = 0.7$ ft was measured for various incident wave amplitudes. These results are presented in Fig. 6.11 for three different incident wave amplitudes: $A_i = 0.0023$ ft, 0.0066 ft, and 0.0105 ft. The value of ka for these experiments was 3.188 which corresponds to the third resonant mode of oscillation (see Figs. 6.4, 6.5, and 6.10). The theoretical curves which are shown in Fig. 6.11 are the same as those presented in the upper portion of Fig. 6.10. The agreement of the experimental data among themselves and with the two linear theories additionally support the linearity assumption made in the theory (for these experiments the incident wave steepnesses are: $0.003 < H_i/L < 0.014$). The major deviation from other data appears to be for the results corresponding to the smallest incident wave amplitude where experimental problems of accurate measurement may arise.

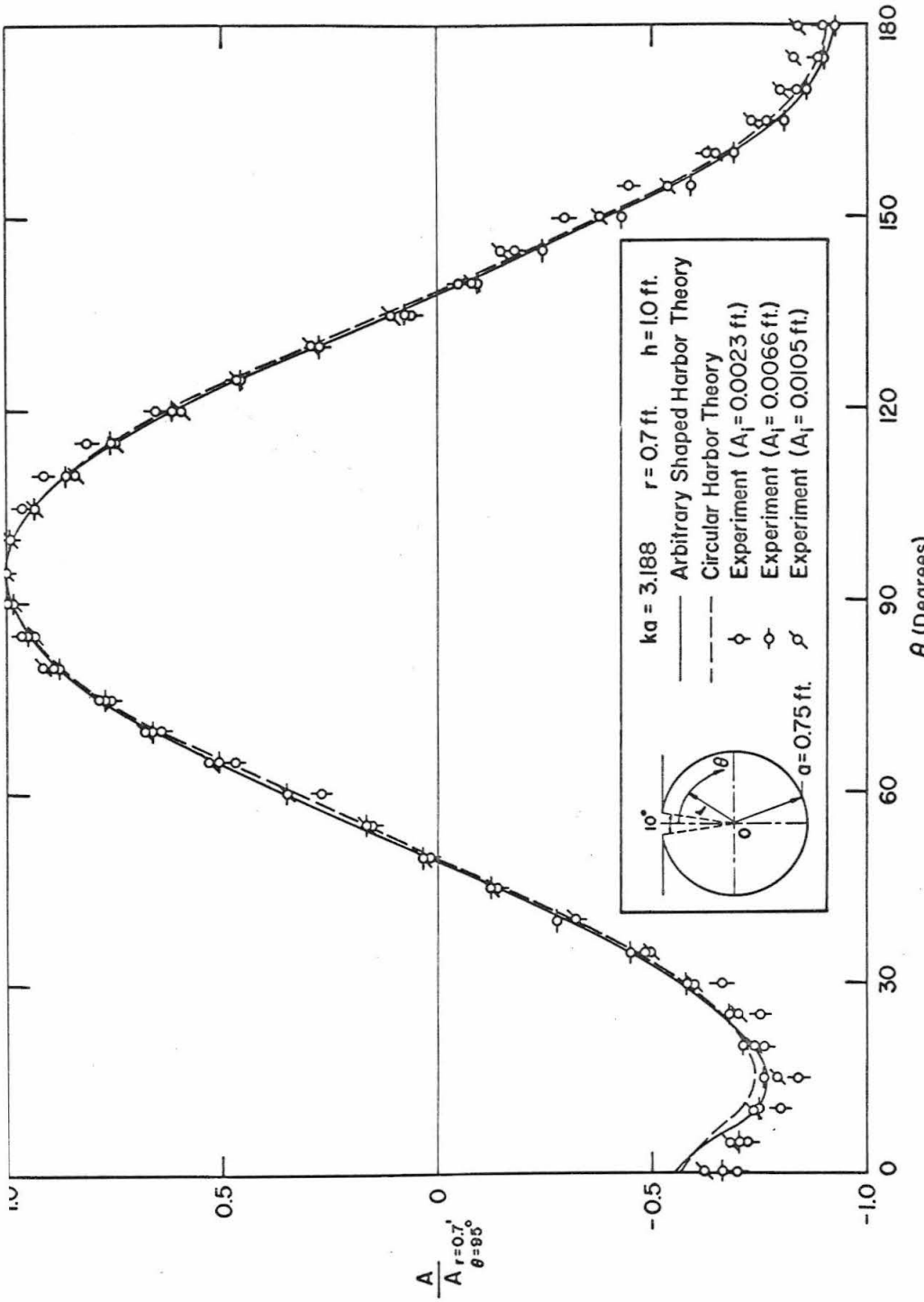

Fig. 6.11 Comparison of wave amplitude distribution along r=0.7 ft for the circular harbor with a 10^{o} opening for three different incident wave amplitudes (ka=3.188)

The variation of the wave amplitude radially at six, fixed, angular positions: $\theta = 0^{\circ}$, 30°, 45°, 90°, 135°, 180° is shown in Fig. 6.12 for ka = 3.891. The abscissa in Fig. 6.12 is the relative radial position, r/a, and the ordinate is the relative wave amplitude normalized with respect to the wave amplitude at the center of the harbor where a maximum occurs. Experimental results are also shown for $\theta = 270^{\circ}$ and are included along with the data and theory for $\theta = 90^{\circ}$ as the oscillation is symmetric about $\theta = 0^{\circ}$. It is seen that the theoretical results agree well with the experimental data for all of the values of θ which were investigated. In Fig. 6.13 these results have been replotted in a manner similar to Figs. 6.8 through 6.11 again showing the amplitude variation along the two circular paths: r = 0.2 ft and r = 0.7 ft.

The previous discussions have shown the applicability of the theories developed in predicting the wave amplitude distribution in a circular harbor with a small opening (10°). In a similar manner experiments were conducted using a harbor with a 60° opening. The theoretical distribution of wave amplitude within the harbor is compared to the results of these experiments in Figs. 6.14 through 6.17.

Fig. 6.14 shows the wave amplitude distribution along r = 0.7 ft and r = 0.2 ft at ka = 0.540 for the harbor with a 60° opening. This value of ka is approximately the same as that which corresponds to the first maximum in the response curves presented in Figs. 6.6 and 6.7.

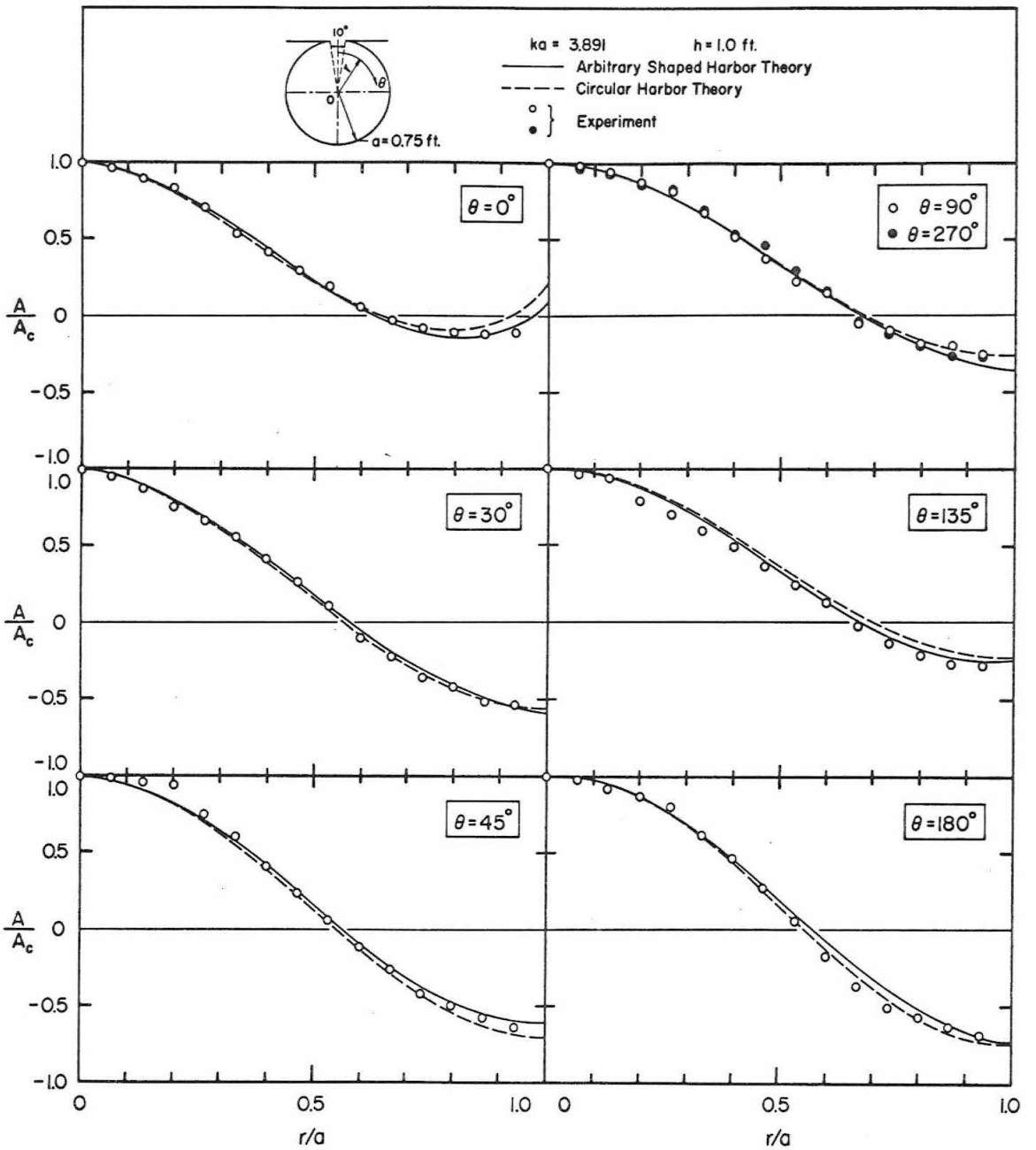

Fig. 6.12 Wave amplitude distribution along six fixed angular positions inside the circular harbor with a 10° opening for ka=3.891

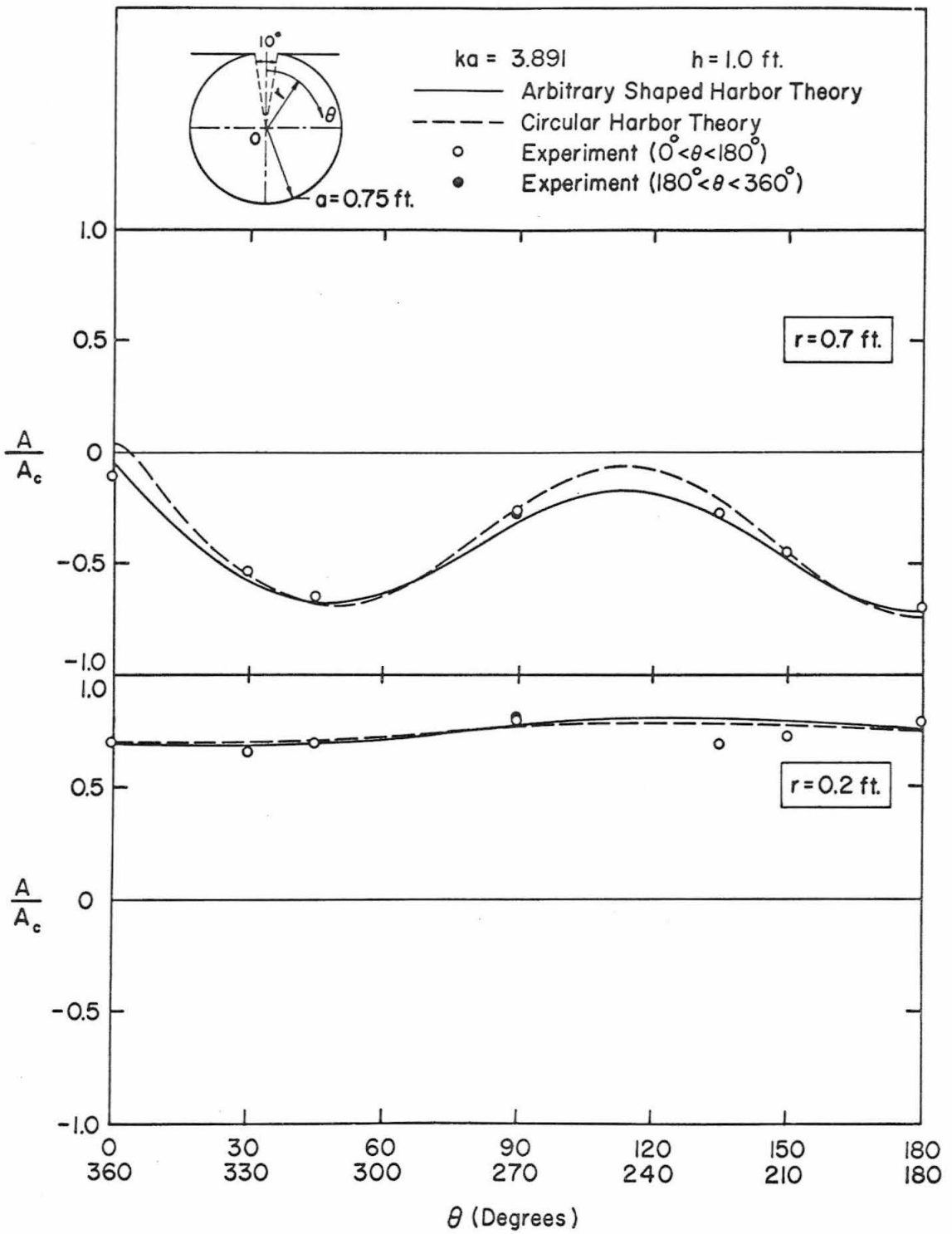

Fig. 6.13 Wave amplitude distribution inside the circular harbor with a 10^{o} opening for ka=3.891

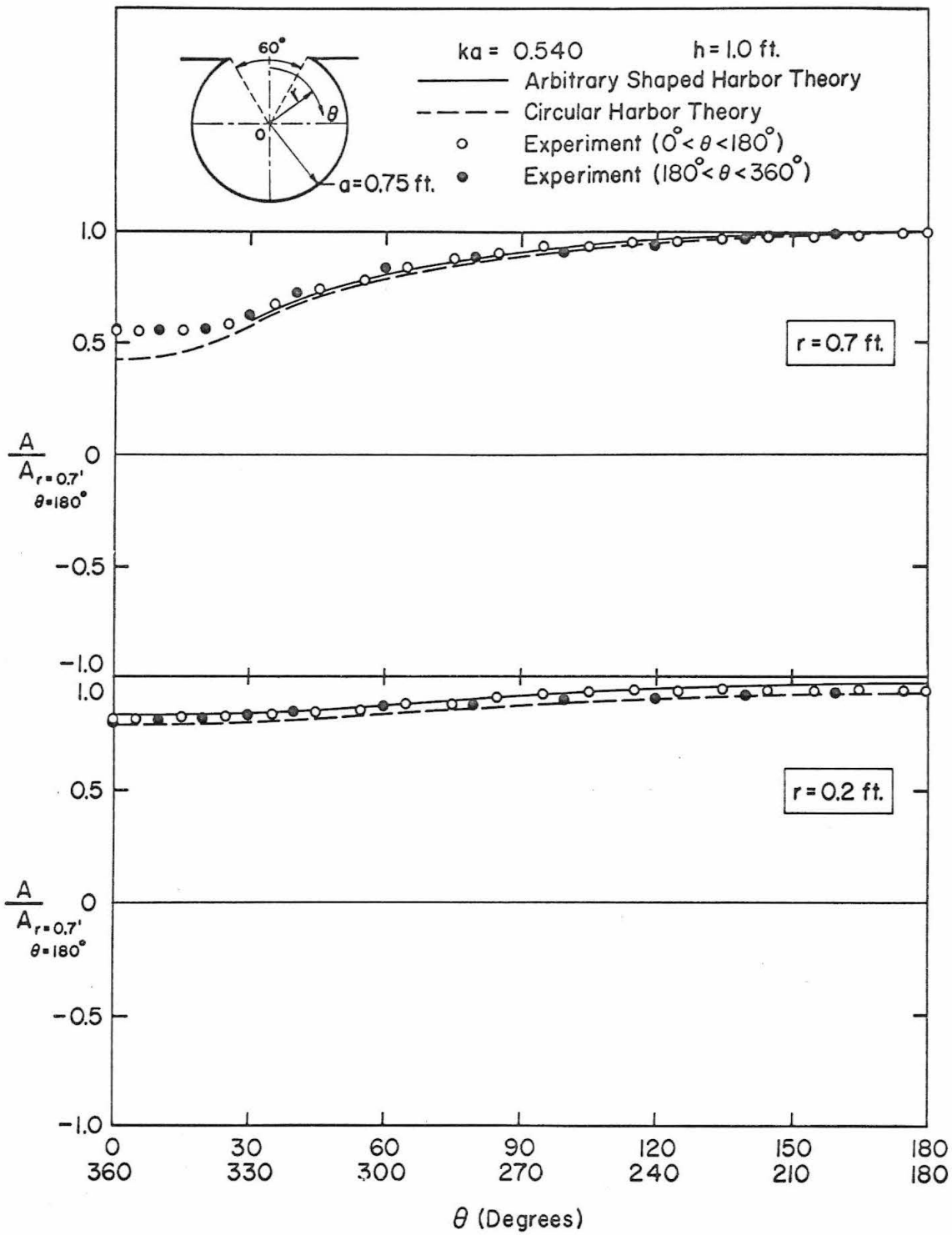

Fig. 6.14 Wave amplitude distribution inside the circular harbor with a 60° opening for ka=0.540

The wave amplitude is normalized with respect to the wave amplitude at the position: $r = 0.7$ ft, $\theta = 180^{\circ}$. Note that the theoretical curve at $r = 0.7$ ft computed using the arbitrary shaped harbor theory covers only the region $30^{\circ} \leq \theta \leq 180^{\circ}$. The experimental data obtained along the circular path $r = 0.7$ ft for the region $\theta < 30^{\circ}$ are in fact outside Region II as defined in the arbitrary shaped harbor theory (see Fig. 3.1). Therefore, it is unrealistic to compare these experiments to this theory for $\theta < 30^{\circ}$ and $r = 0.7$ ft. However, in the theory for the circular harbor it was assumed that the arc was approximately equal to the chord at the harbor entrance, implying that the region along $r = 0.7$ ft for $\theta < 30^{\circ}$ is also contained in Region II. Therefore, only the theoretical curve computed using the circular harbor theory is presented for comparison with the experiments in this region. It can be seen that the wave amplitude is relatively constant along these circular paths except in the region near the harbor entrance and that the theoretical results agree well with the experimental data. As expected, there is some disagreement between the experimental data and the circular harbor theory in the region near entrance ($\theta < 30^{\circ}$ and $r = 0.7$ ft).

Similar results are presented in Fig. 6.15 for a value of ka equal to 2.153. This value of ka is the same as for the second maximum in the response curves presented in Figs. 6.6 and 6.7. It can be seen that the general shape of the water surface (wave amplitude distribution) is similar to the one shown in Fig. 6.9 for the case of a 10° opening.

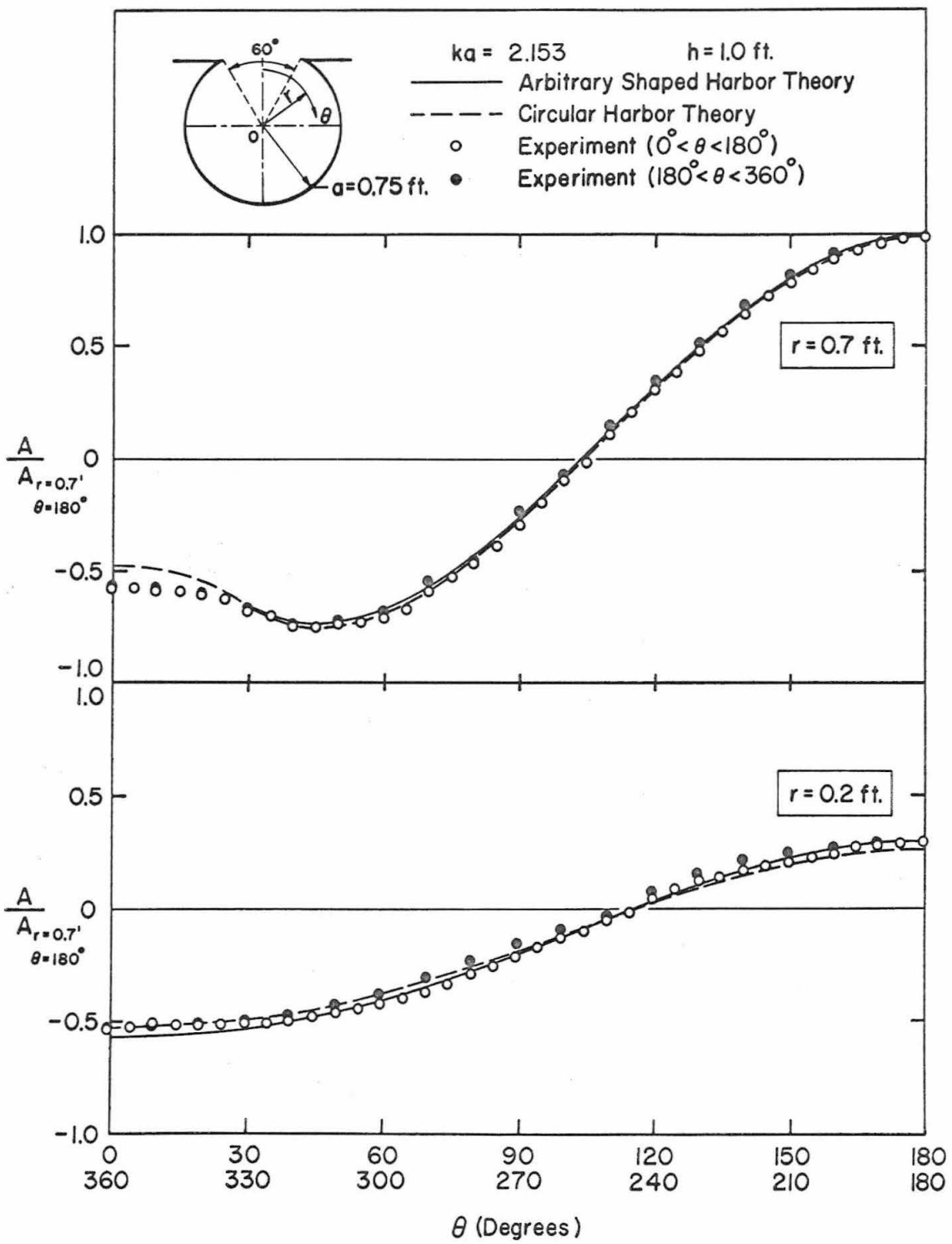

Fig. 6.15 Wave amplitude distribution inside the circular harbor with a 60° opening for ka=2.153

For this case the intersections of the nodal line with the chosen circular paths occur at a larger value of θ: 105° for r = 0.7 ft and 116° for r = 0.2 ft. This indicates that the nodal line for this mode of oscillation is located closer to the back wall region than for the case of a 10° opening.

Theoretical and experimental results are presented in Fig. 6.16 for ka = 3.38, which corresponds to the value of ka at the third maximum in the response curve of Fig. 6.7. The wave amplitude has been normalized with respect to the wave amplitude at the position of r = 0.7 ft, $\theta = 100^{\circ}$, where the amplitude at that location was the maximum of those measured. The shape of the water surface for the harbor with a 10° opening which corresponds to this mode of oscillation has been shown in Fig. 6.10. By comparing Fig. 6.16 with Fig. 6.10 certain similarities and differences between the shape of water surface for the two different openings readily can be seen: the general shape of the wave amplitude distribution is similar. However, the intersections of nodal lines with the circular path r = 0.7 ft occur at a larger value of θ ($\theta = 54^{\circ}$ and 145°) for the harbor with a 60° opening and for this case the nodal line does not intersect the circular path for r = 0.2 ft. It is seen that the theories agree well with the experimental data throughout.

Fig. 6.17 shows the results at a value of ka = 3.953; this corresponds to the value of ka for the fourth maximum in the response curves shown in Fig. 6.7. The wave amplitude shown in

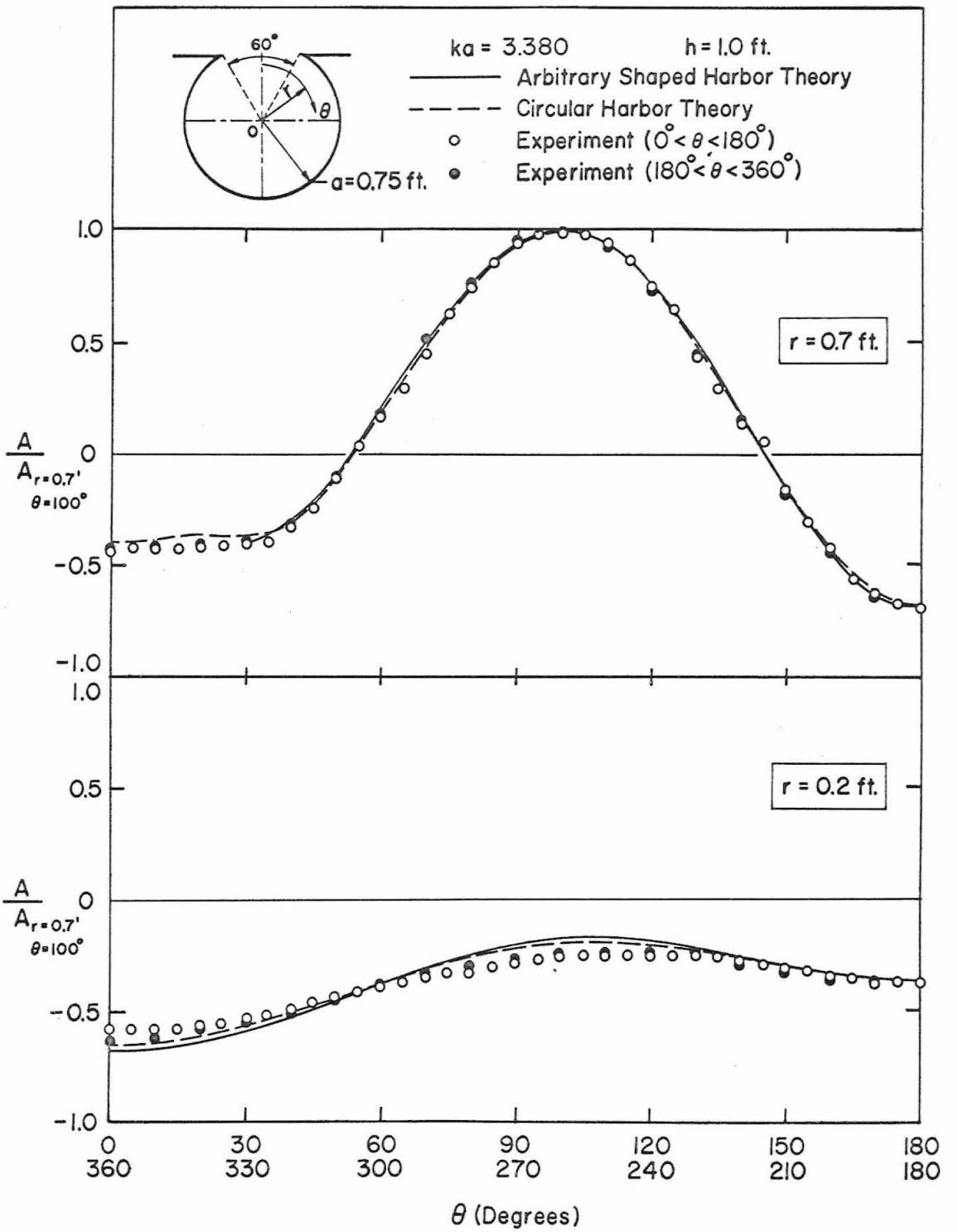

Fig. 6.16 Wave amplitude distribution inside the circular harbor with a 60° opening for ka=3.38

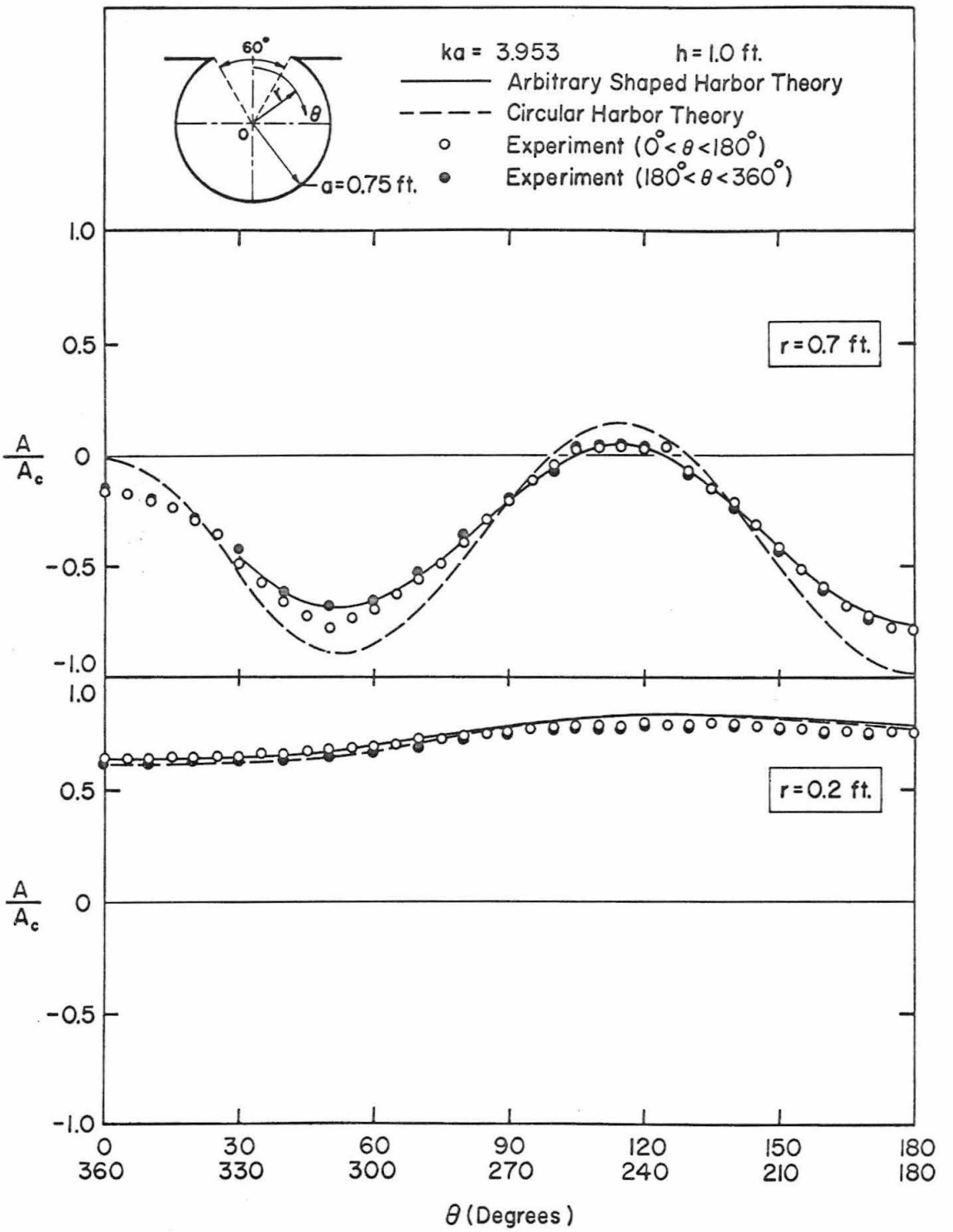

Fig. 6.17 Wave amplitude distribution inside the circular harbor with a 60° opening for ka=3.953

Fig. 6.17 has been normalized with respect to the wave amplitude at the center of the harbor, A_c. It is seen that the agreement is somewhat poorer between the two theories. To understand this, recall that in the fourth peak of the response curve shown in Fig. 6.7, some disagreement is evident between the theories, and the value of ka at resonance predicted by the two theories also differs slightly. Hence one would expect that for the same value of ka the two theories could predict slightly different shapes for the amplitude distribution. By comparing Fig. 6.17 with Fig. 6.13 an obvious difference between the two can be seen: at r = 0.7 ft in Fig. 6.17 there is a limited region, i.e. $100^\circ < \theta < 130^\circ$ in which a different wave phase is seen.

In Subsections 6.2.2 and 6.2.3 the agreement between the theoretical results and the experimental data has been shown. The most questionable element in the circular harbor theory (see Section 4.1) is the small entrance approximation where the arc and chord at the harbor entrance are considered to be identical. It is not surprizing that this approximation should apply well for the case of a 10° opening; however, the results have shown that this approximation still applies well for the case of a 60° opening. Thus, it appears that the small entrance approximation can be applied at least up to a 60° opening. The good agreement between the two theories as well as between the experimental data and these theories shown in these two subsections confirms the applicability of the arbitrary shaped harbor theory to the first extreme case: a curved boundary with a

continuously varying tangent. The application of the arbitrary shaped harbor theory for the second extreme case, a harbor composed of straight-lined boundaries will be presented and discussed in Section 6.3.

6.2.4 Variation of Wave Amplitude Inside the Harbor for the Modes of Resonant Oscillation

As mentioned in Subsection 6.2.2, there are four distinct modes of oscillation shown in the response curves for the circular harbor with a 10^{o} opening as well as 60^{o} opening within the range of ka that has been investigated. In Subsection 6.2.3 wave amplitude distributions along two circular paths inside the harbor for various modes of oscillation have been described in order to compare the theories to the experimental data. However, the complete shape of the water surface inside the harbor for various resonant modes has not been presented yet. In order to understand more fully the shape of the modes of resonant oscillation for circular basins and how they change with changes in the width of the entrance, for each resonant mode described by the response curves of Figs. 6.4 through 6.7, a figure will be presented showing the contour lines of the free surface (lines of constant water surface elevation) along with photographs for these modes.

It is of interest to compare the shape of water surface for each mode of oscillation for the closed circular basin with the corresponding modes for a circular harbor with a 10^{o} opening and with a

60° opening. This comparison will indicate the effect of the size of the harbor opening on the variation of the wave amplitude inside the harbor.

The wave oscillation in a closed basin is usually referred to as the free oscillation in a basin. Suppose the wave function in a closed circular basin of constant depth is $f(r, \theta)$, which satisfies the Helmholtz equation, Eq. 4.1, and also satisfies the condition that fluid does not penetrate the boundary of the harbor, i.e. $\frac{\partial}{\partial r} f(a, \theta) = 0$, where a is the radius of the harbor. As was discussed in Chapter 4, a solution of the wave function $f(r, \theta)$ can be expressed as:

$$f(r, \theta) = J_m(kr) \cos m\theta \quad , \tag{6.3}$$

where m is zero or a positive integer.

The boundary condition and Eq. 6.3 indicate that the following condition must be satisfied:

$$\left[\frac{\partial}{\partial r} \left(J_m(kr) \right) \right]_{r=a} = J_m'(ka) = 0 \quad . \tag{6.4}$$

This condition requires that in order to get a nontrivial solution for the wave function $f(r, \theta)$, the values of ka must be restricted to those which satisfy Eq. 6.4; these roots are often referred to as the eigenvalues. The values of ka which satisfy Eq. 6.4 have been tabulated, e.g. see Morse and Feshback (1953), and several of these eigenvalues are:

$$\begin{aligned} &m=0, \quad ka = 3.83, \ 7.02, \ \ldots . \\ &m=1, \quad ka = 1.84, \ 5.33, \ \ldots . \\ &m=2, \quad ka = 3.05, \ 6.70, \ \ldots . \\ &m=3, \quad ka = 4.20, \ 8.02, \ \ldots . \end{aligned} \tag{6.5}$$

The value of ka for the free modes of oscillation that will be used to compare with the wave induced oscillations in the circular harbors are: ka = 1.84, 3.05, 3.83. Thus, the wave functions which correspond to these values of ka are as follows:

$$f(r,\theta) = J_0(5.11r) \qquad \text{(for m=0, ka = 3.83)}$$

$$f(r,\theta) = J_1(2.45r)\cos\theta \qquad \text{(for m=1, ka = 1.84)} \qquad (6.6)$$

$$f(r,\theta) = J_2(4.065r)\cos 2\theta \qquad \text{(for m=2, ka = 3.05)}$$

In deriving these, the value of "a" is taken as 0.75 ft, the radius of the circular harbor (10° opening and 60° opening) that was investigated experimentally. As shown in Eq. 3.6, the value of the wave function, f, is proportional to the wave amplitude; thus, for the closed basin the relative water surface elevation, $\frac{A}{A_{max}}$, can be obtained by evaluating f from Eq. 6.6 and normalizing with respect to its maximum value.

Contour lines for these three modes of oscillation at the time of maximum water surface displacement are shown in Figs. 6.18 a, b, c. The contour lines result from the intersection of a horizontal plane with the disturbed free surface; the value of each line is the ratio of the water surface displacement at that location normalized with respect to the maximum displacement in the basin. The positive water surface elevations are represented by solid lines, while the negative water surface elevations are described by shown dashed lines.

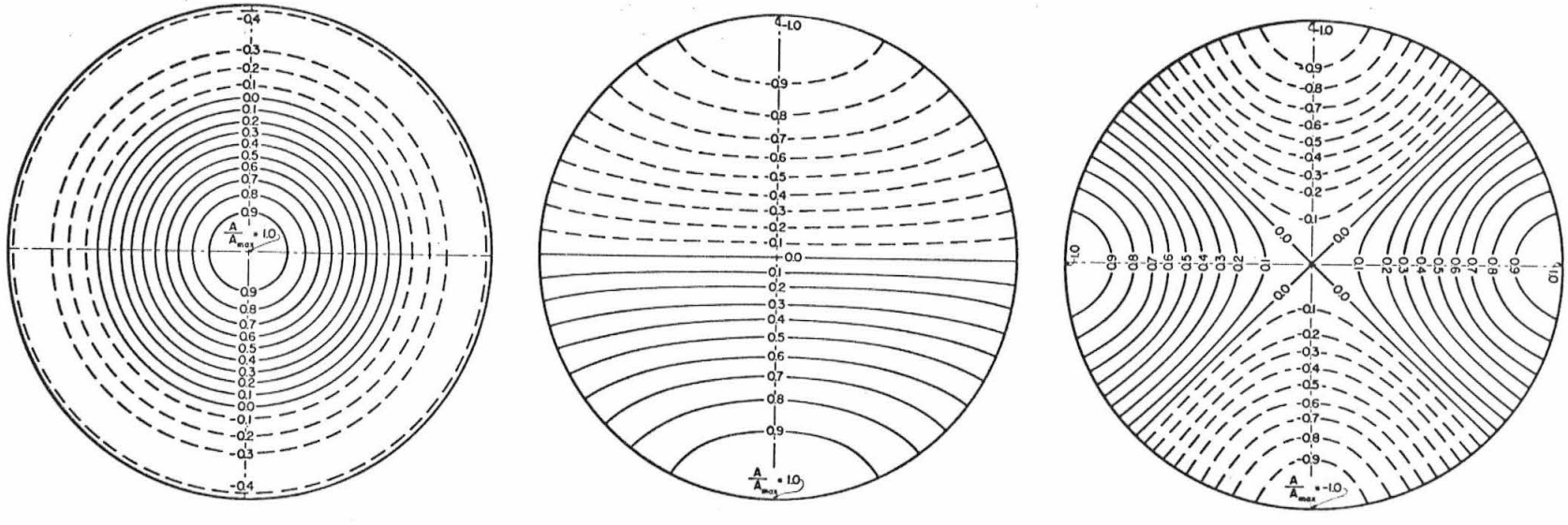

(a) ka=3.83 (b) ka=1.84 (c) ka=3.05

Fig. 6.18 a, b, c Contour drawings of water surface elevation for three modes of free oscillation in a closed circular basin.

The contour drawing of Fig. 6.18 a shows a nodal circle located at the position of $r/a = 0.628$; in this mode of oscillation the contour lines are a series of concentric circles, so that the wave amplitude (or water surface elevation) does not vary with respect to θ. Fig. 6.18 b shows a nodal diameter at the position $\theta = 90^{\circ}$ which divides the basin into two regions of opposite wave phases; this is usually referred to as the "sloshing mode". The contour drawing of Fig. 6.18 c shows two nodal diameters at the positions $\theta = 45^{\circ}$ and 135°; the basin is divided into four regions with each quarter 180° out of phase with its neighbor.

It should be noted that if the basin is no longer completely closed, however small the opening may be, the solution of the wave function $f(r, \theta)$ is no longer limited to the eigenvalues described by Eqs. 6.5. As discussed in Chapter 4, the solution of the wave function $f(r, \theta)$ inside the harbor is continuously dependent upon the wave number k (or the incident wave period). The response curves presented in Subsection 6.2.2 show that resonant oscillations may occur for particular wave numbers producing a large amplification of the wave amplitude inside the harbor. Modes of resonant oscillation will be described in the following discussions with corresponding modes for the case of the 10° opening and the 60° opening discussed together. Therefore, the similarities and differences between the shape of the free surface for the two harbors readily can be seen.

A contour drawing and two photographs showing the water surface for the circular harbor with a 10^{o} opening are presented in Fig. 6.19 for a value of ka = 0.35. This value of ka corresponds to the first maximum in the response curves presented in Figs. 6.4 and 6.5. The value of the wave amplitude within the harbor presented in this contour drawing (or in any other contour drawing that will be presented in this subsection) is calculated from the circular harbor theory developed in Section 4.1. As mentioned earlier, the value of each contour line represents the water surface elevation normalized with respect to the maximum elevation within the harbor; for this mode of oscillation this maximum wave amplitude is located at the boundary of the harbor (r = 0.75 ft) at $\theta = 180^{o}$. It should be noted that all the contour lines are perpendicular to the solid boundary corresponding to the boundary condition that no fluid penetrates a solid boundary. By observing this contour drawing it is obvious that the wave amplitude is fairly uniform throughout the harbor, and that either positive or negative water displacements occur simultaneously within the harbor. Thus, this mode of oscillation can be called the "pumping mode"; there is no "pumping mode" in the case of the free oscillation in a closed circular basin because it is impossible to satisfy conservation of mass. The two photographs provided in Fig. 6.19 show the case of a positive water surface displacement, i.e. above the still water surface. Photographs generally show only displacement along the boundary of the harbor, not the variation of the water surface in the interior of the harbor.

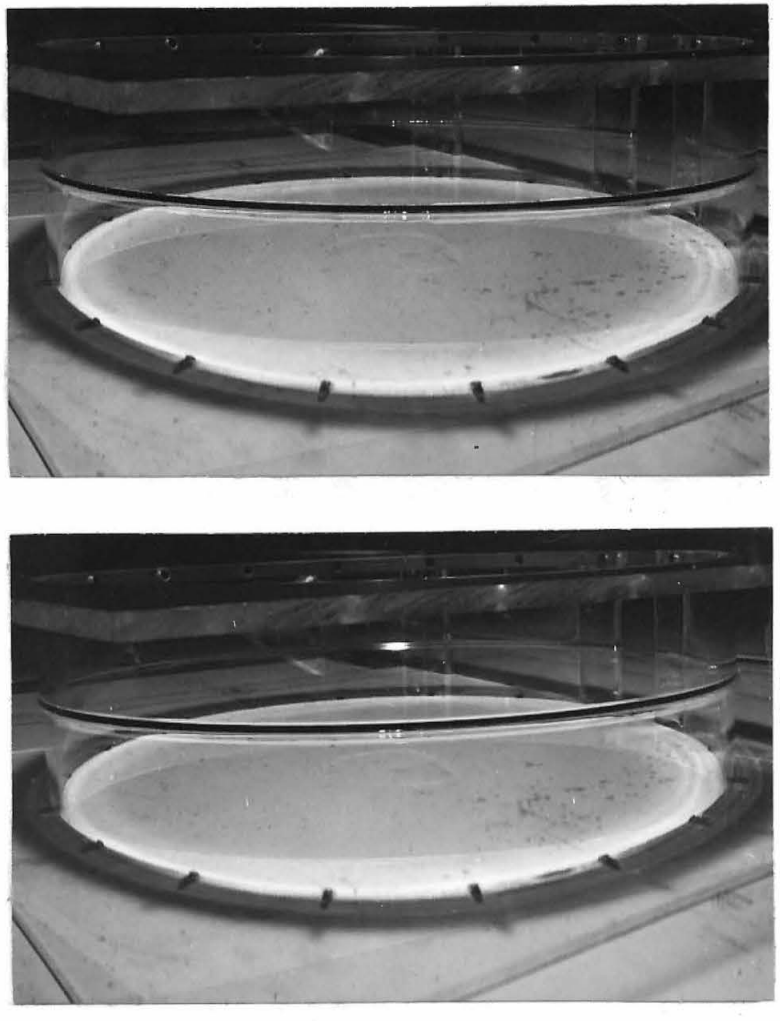

Fig. 6.19 Contour drawing and photographs showing the water surface for the circular harbor with a 10^{o} opening, Mode No. 1, ka=0.35

In the photographs, positive water surface displacement appears as dark stripes along the boundary of the harbor. Some indication of the interior oscillation is provided by shadows on the bottom seen in subsequent photographs; for this mode of oscillation the water surface elevation is evidently so smooth that no such shadow appears in the bottom.

For reasons of convenience, the pumping mode will be named Mode No. 1, and other resonant modes which occur at larger values of ka will then be named Modes No. 2, No. 3, etc. These modes of oscillation will be discussed later in this section.

A similar figure for Mode No. 1 (the "pumping mode") for the harbor with a 60° opening is presented in Fig. 6.20. This mode of oscillation occurs at ka = 0.46, which is the value of ka at the first maximum in the response curves presented in Figs. 6.6 and 6.7. As can be seen from the contour drawing the water surface elevation is fairly constant throughout the harbor and in the phase throughout. The shapes of the water surface shown in Figs. 6.19 and 6.20 are similar; however, for the case of a 60° opening the variation is larger than for the harbor with a 10° opening

The shape of Mode No. 2 ("sloshing mode") for the case of a 10° opening is presented in Fig. 6.21. This mode of oscillation, which corresponds to the second maximum in the response curves of Figs. 6.4 and 6.5 occurs at a value of ka = 1.99. The contour drawing shows a nodal line located near a diameter of the harbor at

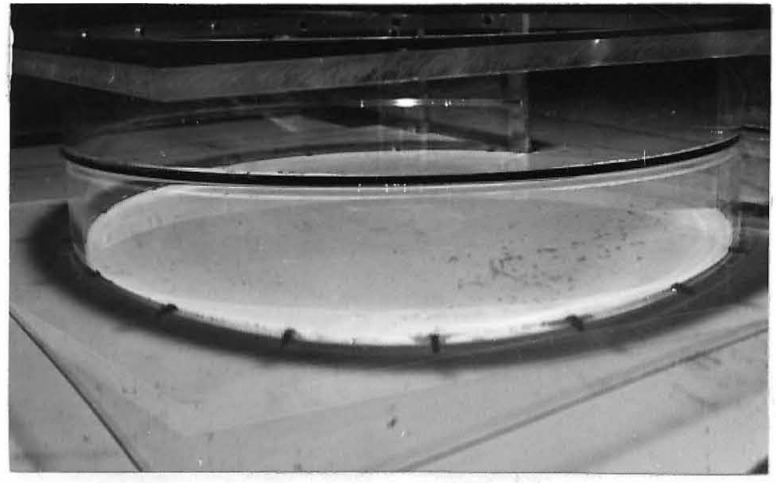

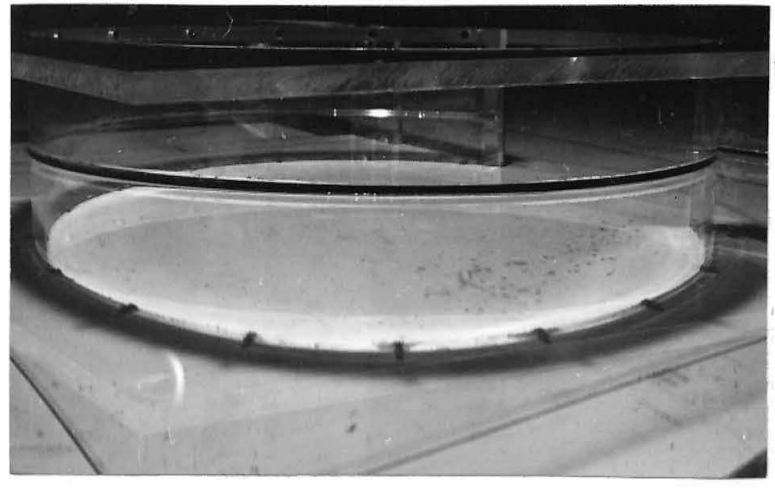

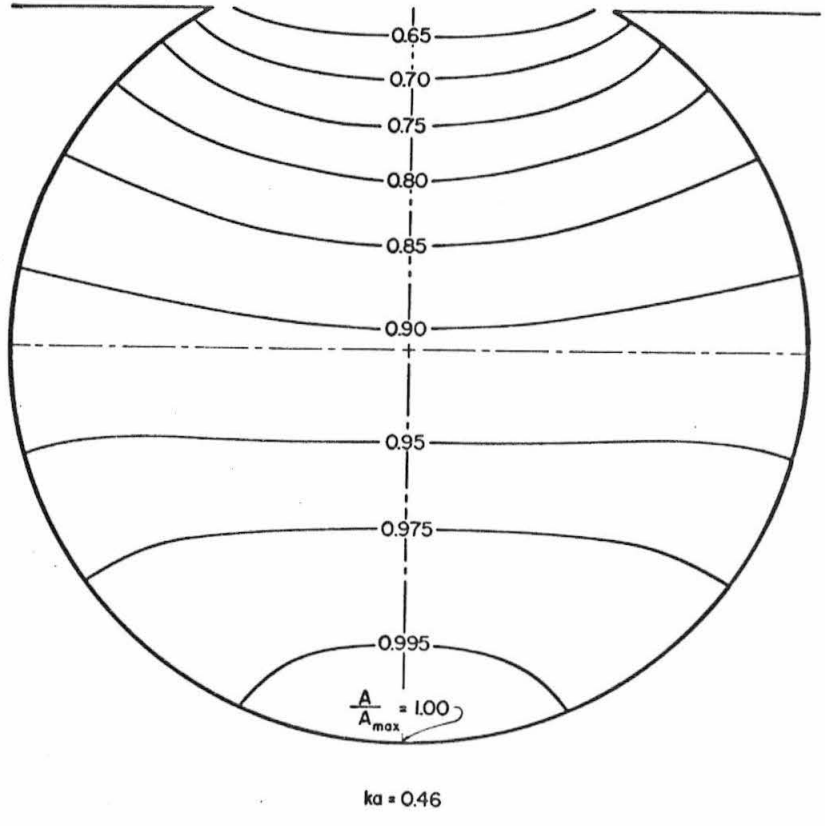

Fig. 6.20 Contour drawing and photographs showing the water surface for the circular harbor with a 60° opening, Mode No. 1, ka=0.46

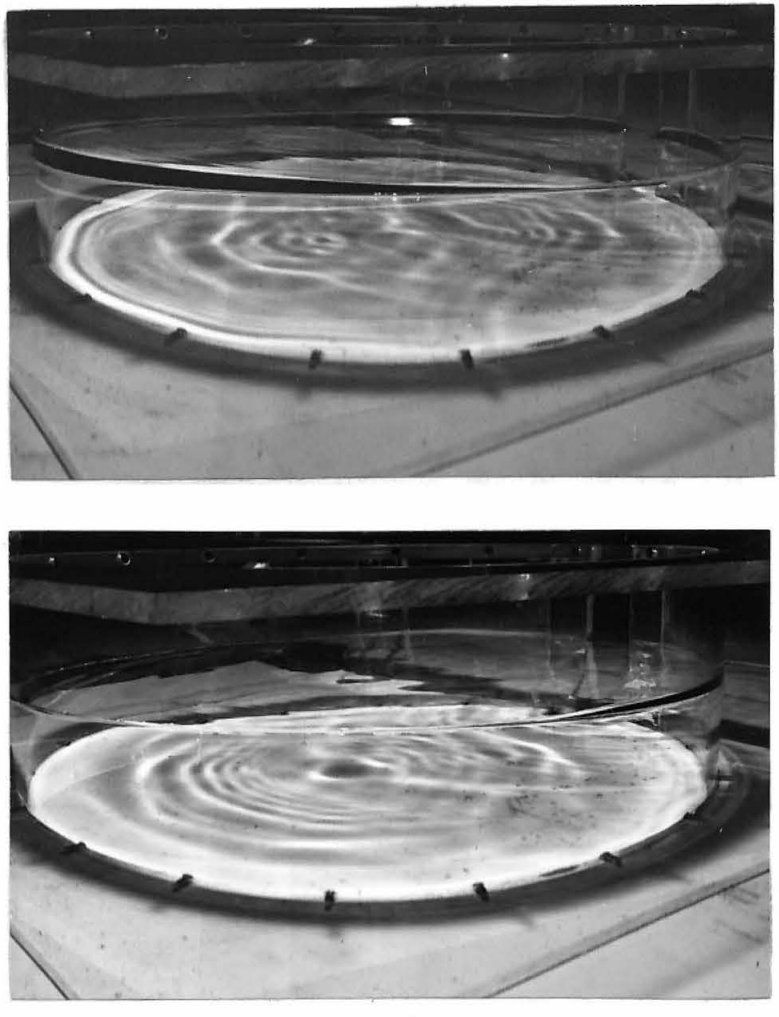

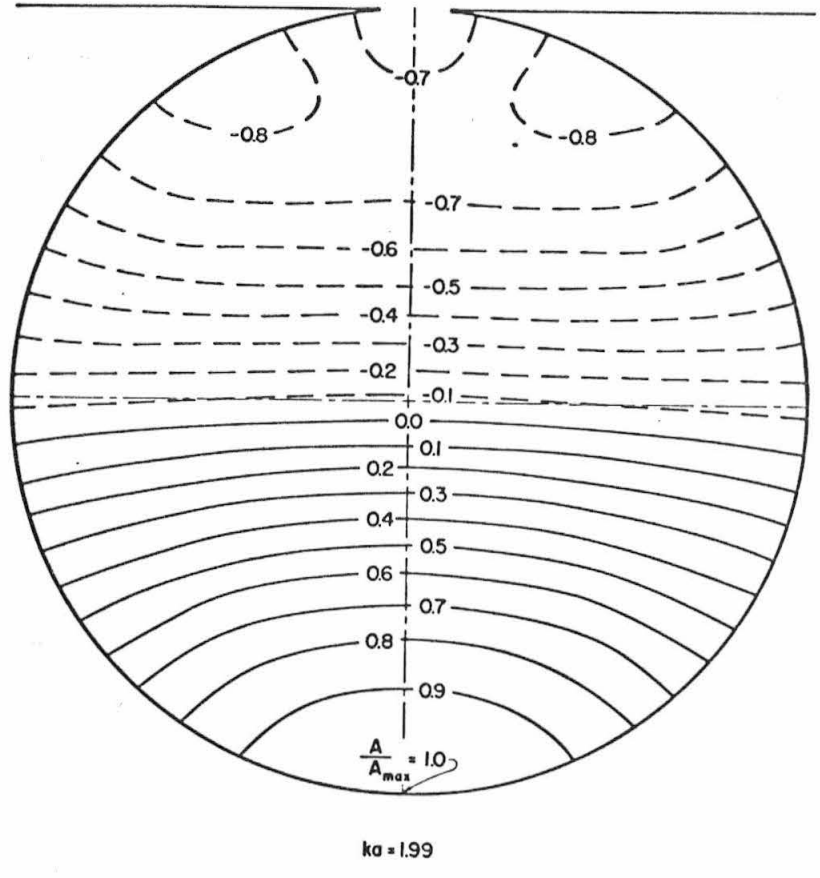

Fig. 6.21 Contour drawing and photographs showing the water surface for the circular harbor with a 10^{o} opening, Mode No. 2, ka=1.99

$\theta = 90^{\circ}$. As before, the lines of constant positive water surface elevation are represented by solid lines, while the surface contours below the still water level are shown dashed. The two photographs provided are for opposite phase: when the water surface displacement is near a maximum or a minimum. The upper photograph in Fig. 6.21 shows a positive water surface displacement approximately in the region $90^{\circ} < \theta < 180^{\circ}$. The lower photograph shows a negative water surface displacement in this same region. In the photographs positive water surface displacements appear as a dark stripe along the boundary of the harbor; however, negative water surface displacements are not easily seen. The shadows which appear on the bottom of the harbor are caused by a series of short wave length ripples on the water surface; however, because their amplitude is small compared with the main water surface displacement, they are not easily detected by measurement except near the nodes. For different modes of oscillation, the pattern of the shadows change; this will be more evident when other modes of oscillation are discussed.

A similar mode of oscillation is presented in Fig. 6.22 for the circular harbor with a 60° opening. For this opening, this mode of oscillation occurs at a value of ka = 2.15 which corresponds to the second peak in the response curve of Figs. 6.6 and 6.7. For the 10° opening this mode occurs at ka = 1.99, and for the completely closed basin it occurs at ka = 1.84. Therefore, the trend is for the wave number at resonance to decrease as the entrance width decreases,

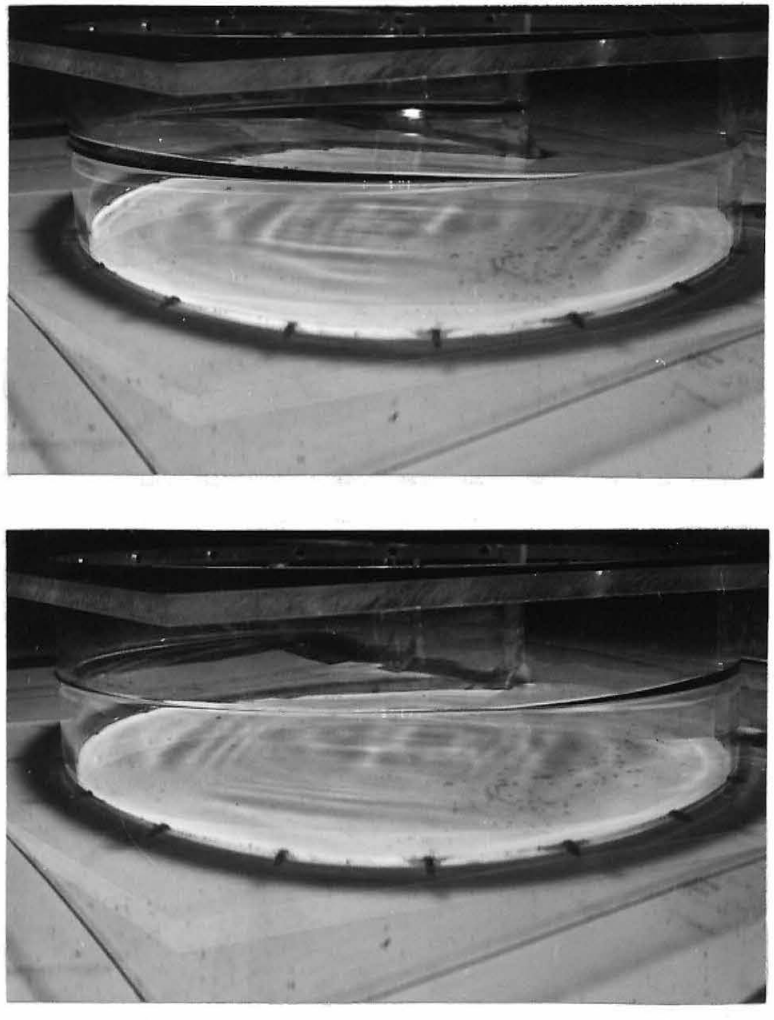

Fig. 6.22 Contour drawing and photographs showing the water surface for the circular harbor with a 60^{o} opening, Mode No. 2, ka=2.15

approaching the value of k for that mode for the closed basin. The upper photograph in Fig. 6.22 shows a positive water surface displacement in the region opposite the harbor entrance (approximately $100^{\circ} < \theta < 180^{\circ}$) and the lower photograph, shows a negative water surface in this region.

It is of interest to compare the contour drawings of Figs. 6.21 and 6.22 with the one shown in Fig. 6.18 b for the case of a closed circular basin where the three figures represent the same mode of oscillation: the "sloshing mode". A direct comparison of Figs. 6.18 b 6.21, and 6.22 reveals changes in the water surface shape as the width of the harbor opening increases. In the case of a closed basin (Fig. 6.18 b) the nodal line is a diameter at $\theta = 90^{\circ}$, for a 10° opening (Fig. 6.21) the nodal line occurs at a position slightly off the center and closer to the region of the back wall; for the case of 60° opening (Fig. 6.22) the nodal line occurs at a position further off the center towards the back wall. Specifically, the relative wave amplitude at the center of the harbor is: $A/A_{max} = -0.08$ for 10° opening, $A/A_{max} = -0.18$ for 60° opening. The wave amplitude at the harbor entrance changes significantly for the three cases: for the closed basin, (Fig. 6.18 b) a maximum amplitude (antinode) occurs at the boundary at $\theta = 0^{\circ}$; however, this antinode does not exist for the case of a 10° opening or a 60° opening. This disappearance of the antinode at the entrance when the harbor is no longer completely closed contradicts the assumption made by McNown (1952) in his

solution of oscillations in circular harbors. (His assumption is that an antinode exists at the harbor entrance for small openings.)

In Fig. 6.23, a contour drawing and two photographs for Mode No. 3 are presented for the case of a 10° opening. This mode of oscillation, which corresponds to the third peak in the response curves shown in Figs. 6.4 and 6.5, occurs at ka = 3.18. In the contour drawing, there are two nodal lines; maximum wave amplitude occurs at the boundary at $\theta = 95^{\circ}$ and its symmetrical counterpart is at $\theta = 265^{\circ}$. (The wave pattern is symmetric with respect to $\theta = 0^{\circ}$.) The two photographs shown differ 180° in phase. The upper photograph of Fig. 6.23 shows an oscillation with the same phase as the contour drawing; thus, a positive water surface displacement is shown in the photograph approximately in the region $50^{\circ} < \theta < 140^{\circ}$. The lower photograph of Fig. 6.23 shows a negative water surface displacement in the same region. It is seen that the shadows on the bottom for this mode of oscillation are quite different from those shown in Figs. 6.21 and 6.22, and hence they must be related to the mode of oscillation.

A similar mode of oscillation for the case of a 60° opening is presented in Fig. 6.24. This mode occurs at ka = 3.38 and corresponds to the third peak in the response curve of Fig. 6.7. Two nodal lines are seen in the contour drawing; the maximum wave amplitude occurs at the boundary at $\theta = 100^{\circ}$ (and 260°). The upper photograph in Fig. 6.24 shows a wave motion in phase with that shown in the

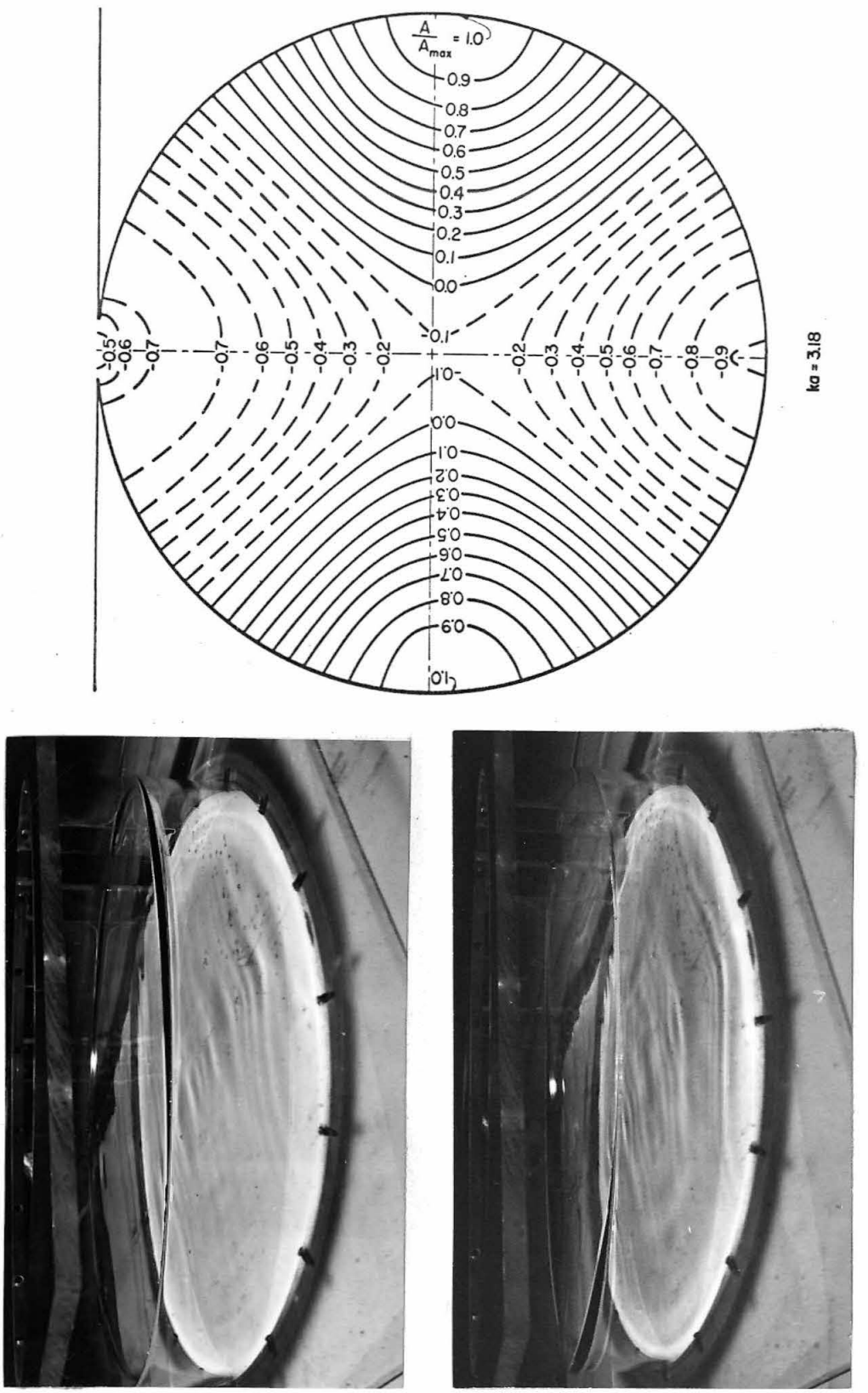

Fig. 6.23 Contour drawing and photographs showing the water surface for the circular harbor with a 10^{o} opening, Mode No. 3, ka=3.18

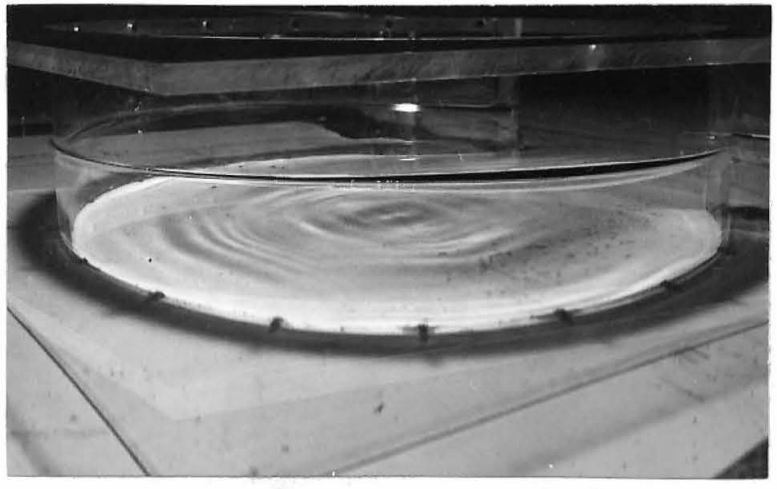

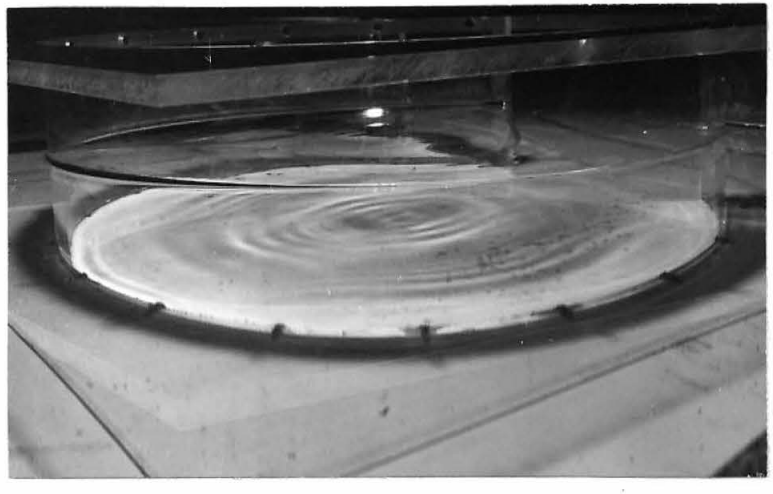

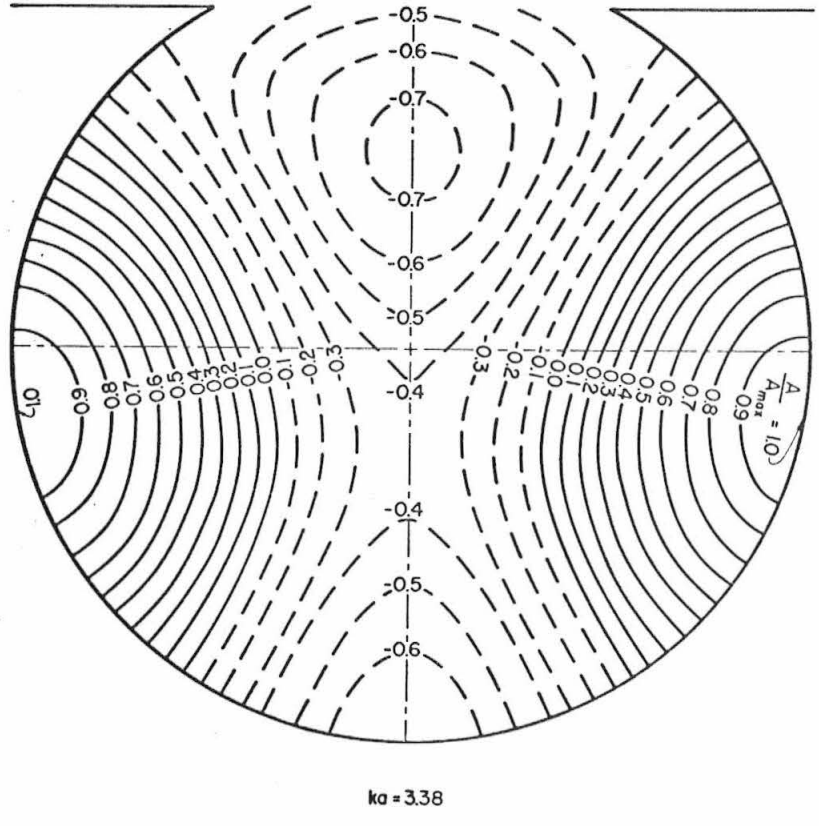

Fig. 6.24 Contour drawing and photographs showing the water surface for the circular harbor with a 60^{o} opening, Mode No. 3, ka=3.38

contour drawing; thus the positive water surface displacement along the boundary is seen in the dark stripe in the region $55^{\circ} < \theta < 145^{\circ}$. The lower photograph shows the motion about 180° out of phase with that on the upper photograph. The shadows on the bottom as seen in the photographs are similar to those shown in Fig. 6.23; however, they are certainly different from those shown in Figs. 6.21 and 6.22 for Mode No. 2.

For the case of a closed basin (Fig. 6.18 c), the position of the maximum amplitude occurs at four points on the boundary of the basin $\theta = 0^{\circ}$, 90°, 180°, and 270°, and the two nodal diameters ($\theta = 45^{\circ}$ and 135°) are perpendicular to each other. For the case of a 10° opening (Fig. 6.23) the two nodal lines are shifted slightly and no longer intersect, whereas for the harbor with a 60° opening (Fig. 6.24) the two nodal lines are shifted even further apart. The wave amplitudes at the center have also changed considerably as the entrance width increases: zero for the case of a closed basin, $A/A_{max} = -0.125$ for the case of a 10° opening, and $A/A_{max} = -0.44$ for the harbor with a 60° opening. As mentioned earlier, the wave amplitudes at the harbor entrance also change with changes in the size of the opening: for the case of a closed basin (Fig. 6.18 c) a maximum wave amplitude (antinode) exists at the boundary at $\theta = 0^{\circ}$; however, for the case of a 10° opening or a 60° opening an antinode does not exist at the entrance. It should be noted that as the wave parameter ka increases, the ratio of the harbor radius to the wave length a/L

also increases; thus, it is expected that the effect of the size of the entrance on the resonant mode of oscillation becomes more significant with increasing ka.

A contour drawing and two photographs are presented in Fig. 6.25 for the harbor with a 10° opening. This mode of oscillation (ka = 3.87) is termed Mode No. 4 and corresponds to the fourth maximum in the response curves shown in Figs. 6.4 and 6.5. From the contour drawing it is seen that the maximum wave amplitude is at the center of the harbor and the nodal line is a closed curve. The water surface displacement shown by the upper photograph of Fig. 6.25 is in opposite phase to what is shown in the contour drawing, however the photograph at the bottom of Fig. 6.25 is approximately in the same phase as the drawing. Although from the photographs it is difficult to see the variation of wave amplitude at the interior of the harbor, the variation around the boundary of the harbor can be seen from the dark stripe in the upper photograph. The variation in the thickness of the dark stripe appears to correspond to the amplitude variation shown in the contour drawing. The shadows on the bottom are nearly circular in the region near the center of the harbor, quite different from the shadows shown for Mode No. 2 (Figs. 6.21 and 6.22) and Mode No. 3 (Figs. 6.23 and 6.24).

A contour drawing with two photographs for a similar mode of oscillation for the case of 60° opening is presented in Fig. 6.26. This mode of oscillation occurs at a value of ka = 3.96 which is corres-

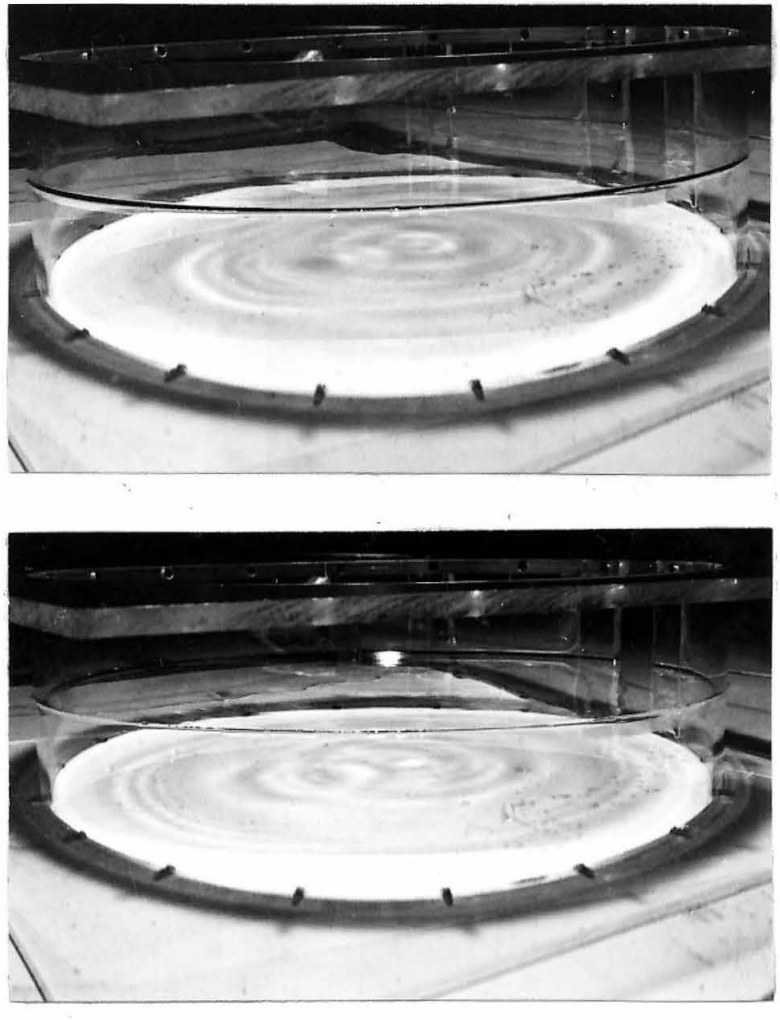

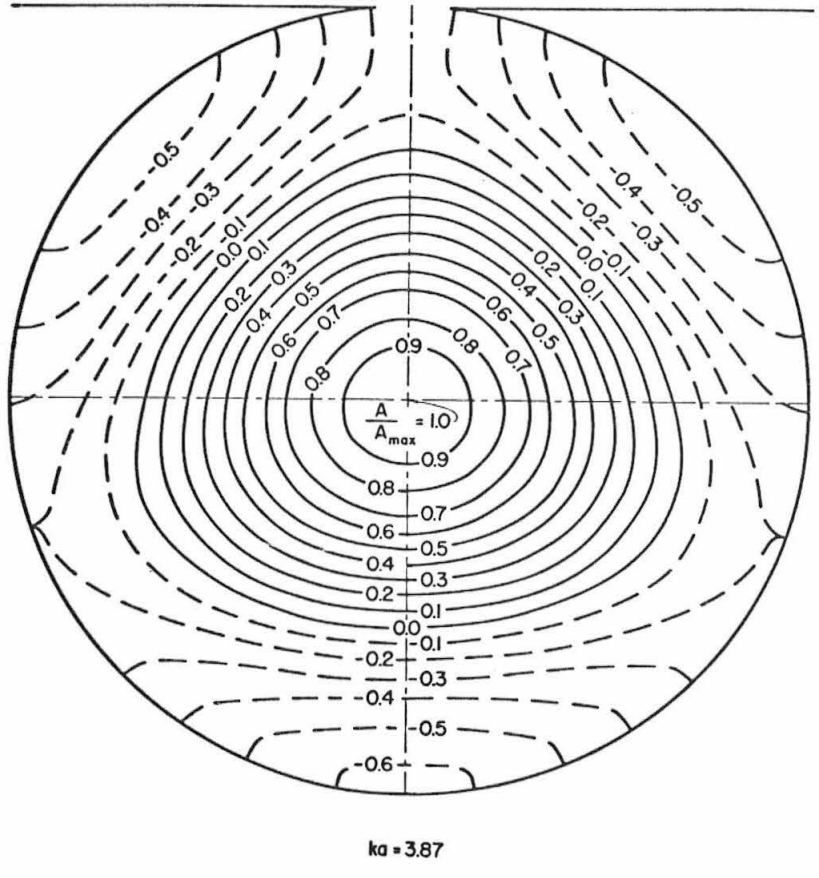

Fig. 6.25 Contour drawing and photographs showing the water surface for the circular harbor with a 10^{o} opening, Mode No. 4, ka=3.87

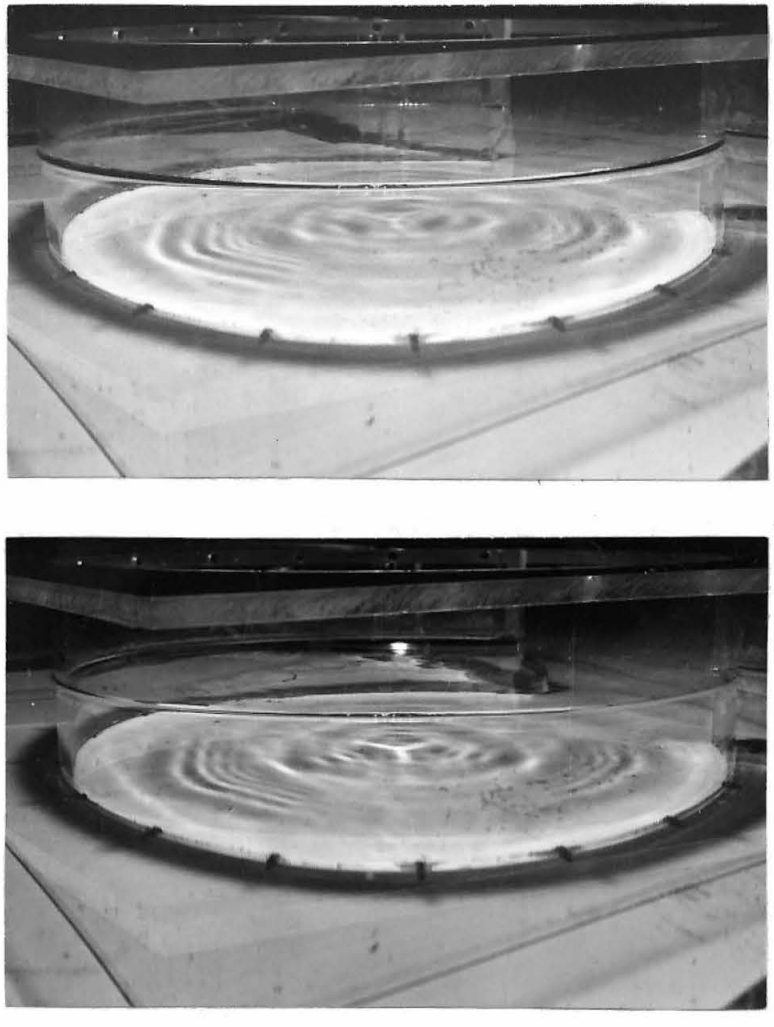

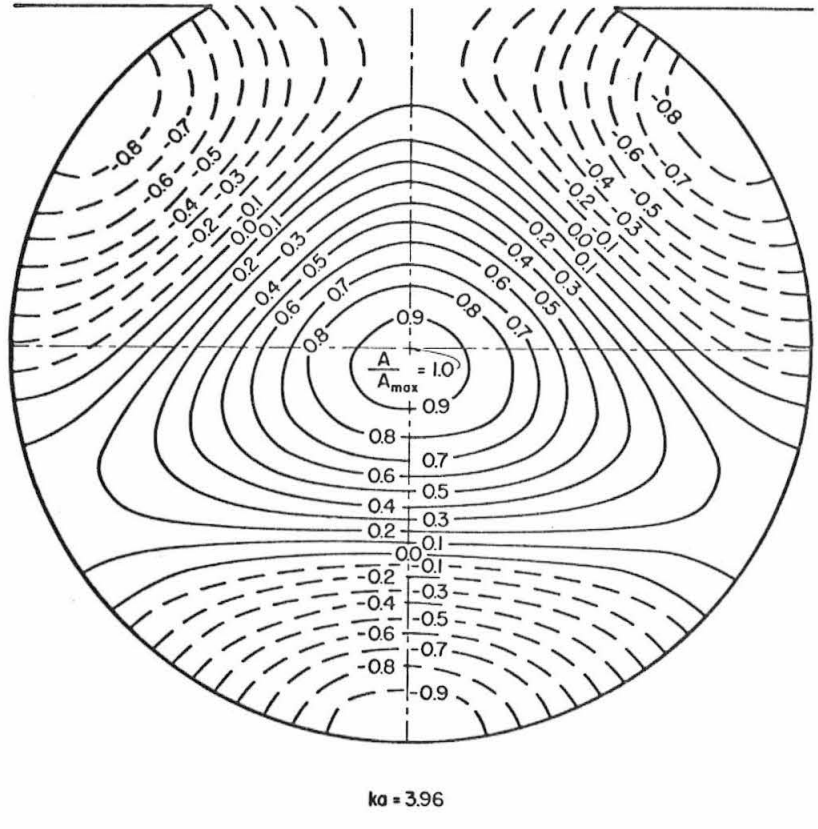

Fig. 6.26 Contour drawing and photographs showing the water surface for the circular harbor with a 60° opening, Mode No. 4, ka=3.96

ponding to the fourth peak in the response curves shown in Fig. 6.7. It is seen from the contour drawing that the maximum wave amplitude is again located at the center of the harbor. The nodal line is no longer a closed curve as for the case of a 10^{o} opening but in this case it interesects the boundary of the harbor. As in Fig. 6.25, the upper and lower photographs in Fig. 6.26 are approximately 180^{o} out of phase. The variation of the water surface elevation around the boundary again can be seen from the dark stripe in the upper photograph; it shows a variation along the boundary similar to that shown in the contour drawing, but with opposite phase.

It is interesting to compare the contour drawings of Figs. 6.25 and 6.26 and 6.18 a: for the case of closed basin the contour lines are a series of concentric circles and the nodal line is represented by a nodal circle (Fig. 6.18 a); however, for the case of a 10^{o} opening (Fig. 6.25) the contour lines are no longer represented by a series of circles, although in the region near the center of the harbor they are in fact close to circular. As the harbor opening increases to 60^{o} (Fig. 6.26) a significant change in the contour lines can be observed: the nodal line is no longer a continuous closed line as in the case of a 10^{o} opening, or a circle as in Fig. 6.18 a; instead it intersects the boundary of the harbor, and even contours near the center of the harbor are no longer circular in form. However, the center of the harbor still remains the position of the maximum wave amplitude.

The results presented in this subsection showed the wave amplitude distribution for four modes of resonant oscillation in the range of ka investigated for both the cases of a 10° and a 60° opening. Except for Mode No. 1 (the "pumping mode") which does not exist in a completely closed circular basin, each mode corresponds to a free mode of oscillation in the closed basin. The results in this subsection can be summarized as:

(1) The corresponding modes of oscillation for the case of a 10° opening and a 60° opening are basically similar, however, the detailed shape of the free surface is different.

(2) The value of ka at which a particular mode of oscillation occurs in the harbor with a 60° opening is larger than the value of ka for the corresponding mode for the case of a 10° opening which itself is larger than the value of ka for the corresponding mode in a closed basin. Hence the tendency is for the wave number parameter (ka) at resonance to approach the value for a closed basin as the entrance width decreases.

(3) No antinode exists at the harbor entrance although an antinode might occur at that position in a closed circular basin.

(4) The effect of the width of harbor entrance on the shape of water surface elevation inside the harbor is more pronounced for those modes of oscillation at higher frequencies, i.e. larger values of ka.

6.2.5 Total Velocity at the Entrance of the Circular Harbor

6.2.5.1 Introduction

In Subsection 3.2.4 the method for analytically evaluating the velocity at the harbor entrance was discussed. The velocity at the harbor entrance is of interest because it is directly related to the kinetic energy transmitted into the harbor. For the present study, the value of the wave function, f_2, its normal derivative, $\frac{\partial f_2}{\partial y}$, as well as the derivative $\frac{\partial f_2}{\partial x}$, evaluated at the harbor entrance are determined during the process of computing the response curves for various values of the wave number parameter, ka. Hence, the theoretical value of the total velocity at the harbor entrance can be obtained readily from Eq. 3.41.

As mentioned in Section 5.5, the velocity was measured at the entrance of the circular harbors (with a 10° opening and a 60° opening) using a hot-film anemometer with a linearizing circuit. In steady flow, either in air or in water, the output from a hot-film anemometer generally has been found to follow King's Law (Eq. 5.2). Thus, after employing the linearization procedure described in Section 5.5 the voltage is directly proportional to the velocity as reported by Townes (1965), Raichlen (1967) and Lee (1967). However, at the time of the present experiments the use of hot-film anemometers in oscillatory flows had not been reported in the literature. Considering the relation of these velocity measurements to the major objectives of the experimental program, a basic assumption was made in reducing these experimental

data: King's Law was assumed to apply equally well for oscillatory flows; thus, after using the linearizer the output signal was assumed to be linearly proportional to the fluid velocity. Therefore, the ratio of two output voltages from the linearizer was considered to be equal to the ratio of the two corresponding velocities.

Recently, Das (1968) used a single hot-film sensor in water to measure turbulence in an oscillatory flow. The results showed that with one of the hot-film sensors which was used, the relation between the voltage output and the fluid velocity was: $E^2 \sim V^{0.25}$ (wherein E is the hot-film anemometer output voltage and V is the resultant fluid velocity in a direction perpendicular to the axis of the hot-film sensor), while another sensor behaved as: $E^2 \sim V^{0.45}$. The latter relation is close to King's Law ($E^2 \sim V^{0.5}$) whereas the former is quite different.

A typical output from the linearizing circuits as recorded on the Sanborn recorder (described in Section 5.4) is presented in Fig. 6.27 (Column C). This velocity measurement was made at the center of the entrance of the harbor with a 10° opening with a wave period of 0.684 sec. The record corresponds to the velocity at three depthwise locations: z = -0.10 ft, -0.15 ft, and -0.25 ft. As expected, the velocity decreases as the distance between the hot-film sensor and the water surface increases. In Fig. 6.27 also the wave amplitude is shown at two positions inside the harbor, i.e. r = 0.2 ft, $\theta = 35^{\circ}$, and r = 0.7 ft, $\theta = 215^{\circ}$. It is seen that the waves in these two

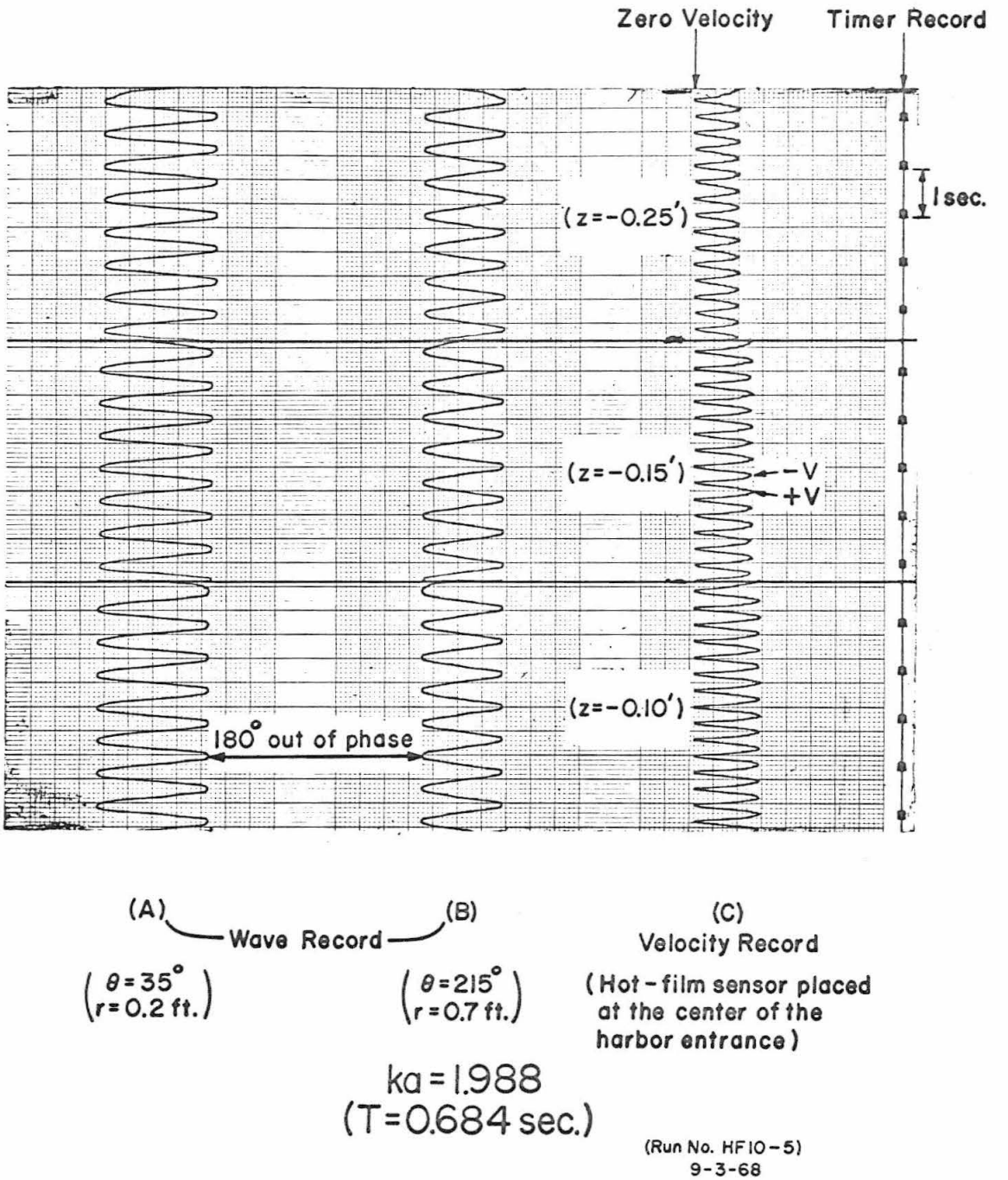

Fig. 6.27 Typical record of the wave amplitude and of the velocity after using the linearizing circuit

positions are 180° out of phase (this was also shown in the contour drawing of Fig. 6.21 evaluated for the same wave number). From Fig. 6.27, it is seen that within one wave period, the velocity reaches its maximum value twice, since in a periodically oscillating flow the hot-film sensor cannot differentiate the direction of the velocity.

In determing the velocity from such records the peak value of the output signal from the linearizing circuit as recorded was averaged. This average value, using the notation of Section 5.5, is denoted as S_2. If this value, S_2, is truly linearly proportional to the fluid velocity, then from Eq. 5.5 it is equal to $\alpha_v V$. Therefore, assuming this proportionality to be true, the relative velocity at any two positions can be obtained from the ratio of the corresponding values of S_2 without prior evaluation of α_v from calibration. (This assumption was used to determine the relative velocities that will be presented in the following subsections even though there is some conflict with the results of Das, 1968.)

6.2.5.2 Velocity distribution in a depthwise direction

The vertical distribution of the velocity at the entrance of the harbor with a 10° opening, averaged across the entrance, is presented in Fig. 6.28 for three different values of the wave number parameter, ka, (three wave periods): ka = 0.482, 1.988, 3.922. The ordinate of Fig. 6.28 is the relative depthwise position, z/h, (where z/h = 0 refers to the still water surface) and the abscissa is the relative velocity normalized with respect to the velocity measured

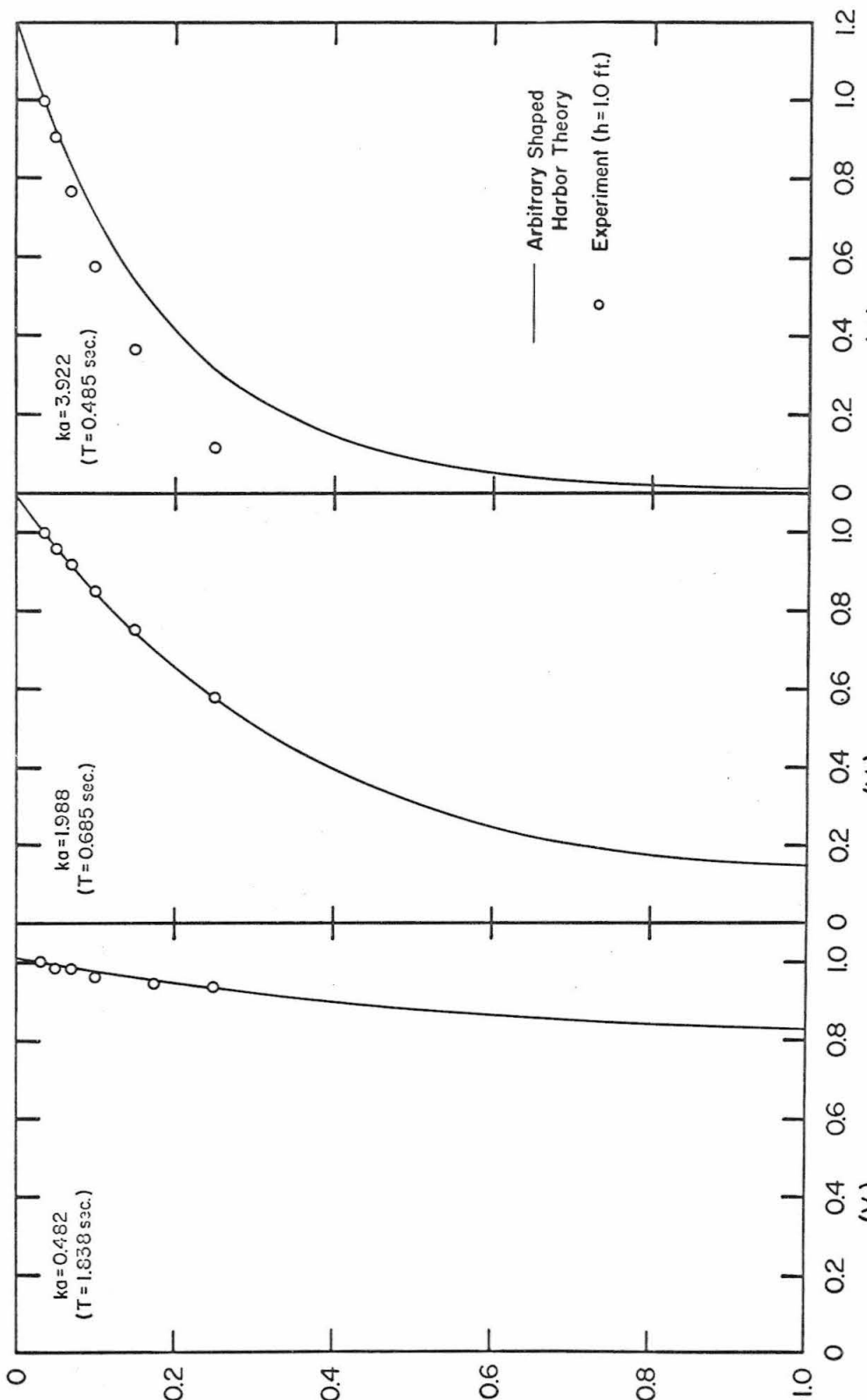

Fig. 6.28 Velocity distribution in a depthwise direction at the entrance of the circular harbor with a 10^{o} opening

nearest the water surface (z/d = -0.03). The theoretical velocity distribution was calculated using Eq. 3.42 (since the hot-film sensor is primarily sensitive to the v and w velocity components); the value of f_2 and $\frac{\partial f_2}{\partial y}$ at the entrance were obtained from the arbitrary shaped harbor theory. In these experiments, measurements of velocity were made at five lateral locations across the harbor entrance for each vertical position (z/h) and each experimental point shown in Fig. 6.28 is therefore the average of the results at these lateral locations. (The locations will be described fully in Subsection 6.2.5.3.)

According to the conventional method of classifying water waves, the distribution curve for ka = 0.482 in Fig. 6.28 is similar to the typical vertical distribution of fluid particle velocities for shallow water waves. (For the present experiments, as mentioned in Subsection 6.2.2, shallow water waves occur in the region $0 < ka < 0.236$, intermediate waves in the region $0.236 < ka < 2.36$, and deep water waves in the region $ka > 2.36$.) The distribution curve for ka = 1.988 belongs to intermediate wave category and the curve for ka = 3.922 corresponds to deep water waves in which the velocity decreases rapidly as the distance from the water surface increases. It is seen that the experimental data for ka = 0.482 (wave period T = 1.838 sec) and ka = 1.988 (T = 0.685 sec) agree well with the theoretical curves; however, the experimental data for ka = 3.922 (T = 0.485 sec) differ considerably from theory. This may indicate that the assumption of linearity between the fluid velocity and the output voltage from the

linearizer is reasonable for ka = 0.482 and 1.988 but not for ka = 3.922, where the wave frequency is larger. In the following, some of the weakness in the experimental procedure and the method of data reduction will be discussed.

From Eq. 3.42, it is seen that the total velocity at the harbor entrance is proportional to the incident wave amplitude A_i, and inversely proportional to the wave frequency σ. In the experiments, for the same stroke of the wave machine, the standing wave amplitude at the harbor entrance (with the entrance closed) for ka = 3.922 was approximately one-half of that for ka = 1.988 because the wave filter is more efficient at higher frequencies; without the filter wavemaker theory implies the reverse. Therefore, experimentally the velocity at the entrance for ka = 3.922 was small compared to the velocity for ka = 1.988. Specifically for the hot-film sensor placed at the center of the entrance at the position z/h = -0.03, for ka = 1.988 (T = 0.685 sec) the output voltage from the linearizer was 28.5 volts; however, for ka = 3.922 (T = 0.485 sec), the output voltage was only 2.66 volts, at this location. As the sensor was moved to the position z/h = -0.25 the recorded output voltage was less than 0.3 volts for ka = 3.922. It is felt that the disagreement between the experimental and theoretical results for ka = 3.922 as shown in Fig. 6.28 could be due to experimental error in measuring the small voltage or velocity.

6.2.5.3 Velocity distribution across the harbor entrance

The velocity distribution across the entrance of the circular harbor with a 10° opening is presented in Fig. 6.29 for ka = 0.482, 1.988, and 3.922. The abscissa is the relative lateral position, $x/\frac{d}{2}$ (where d is the width of the harbor entrance; $x/\frac{d}{2} = 0$ refers to the center of the entrance, and $x/\frac{d}{2} = \pm 1$ refers to the lateral limits of the entrance). The upper portion of Fig. 6.29 shows the velocity distribution normalized with respect to the average velocity across the entrance while in lower portion of the figure the velocities are normalized with respect to the velocity at the center. The theoretical curves shown are obtained from the arbitrary shaped harbor theory (Eq. 3.42), where the entrance was divided into five equal segments with each segment having a central angle of 2° and the boundary was divided into 35 equal segments. The wave function f_2 and its normal derivative $\frac{\partial f_2}{\partial y}$ at the mid-point of each segment at the entrance were obtained by the matching procedure (Subsection 3.2.3). With these values of f_2 and $\frac{\partial f_2}{\partial y}$, the velocity V_o at the mid-point of each entrance segment was calculated from Eq. 3.42 for a particular vertical position z. The average velocity across the entrance, denoted as $(V_o)_{ave}$, was obtained by computing the arithmetic average of the velocities V_o at a particular elevation for the five segments. In Fig. 6.29 the normalized theoretical velocities so computed are denoted by "plus signs" and a solid line fitted through

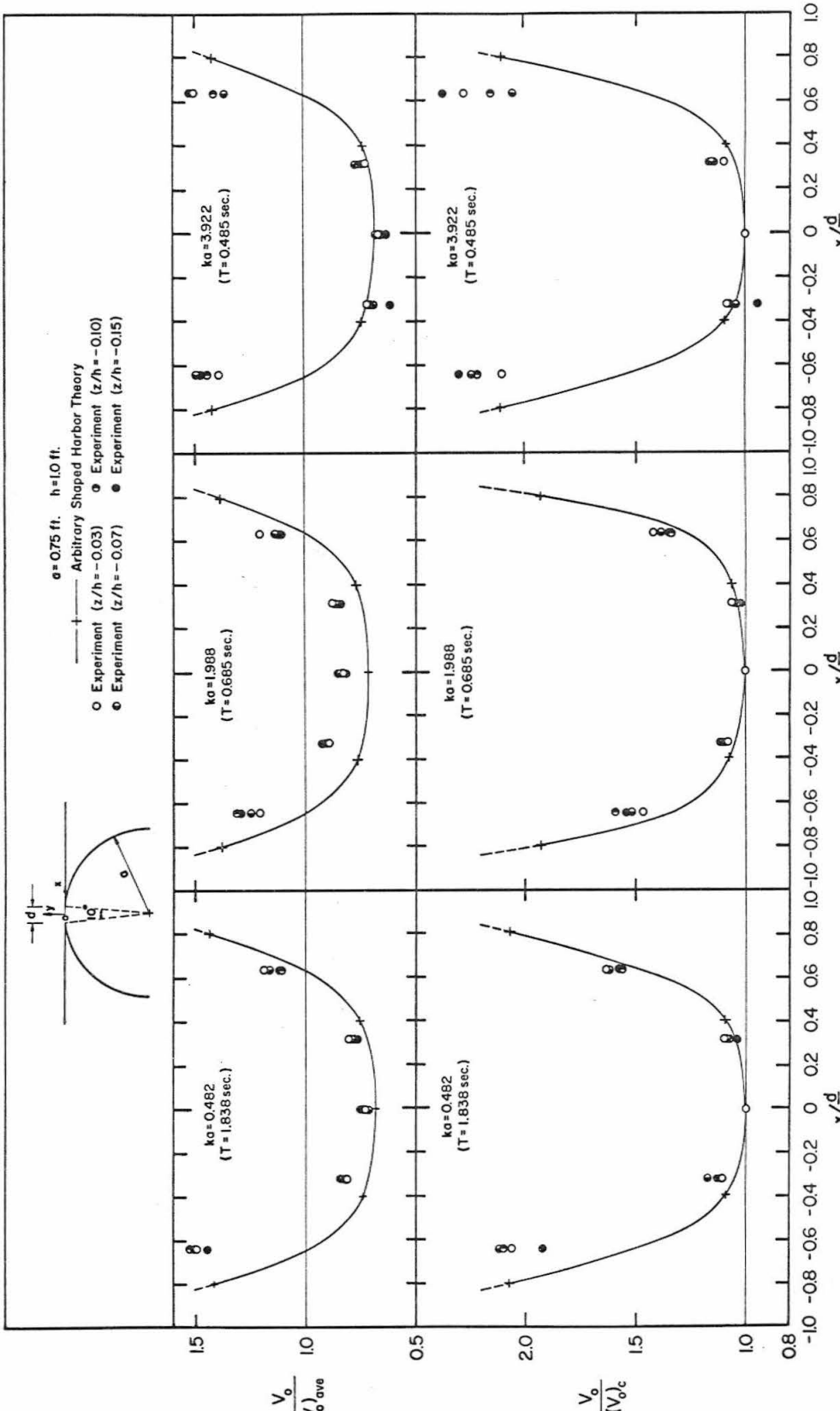

Fig. 6.29 Velocity distribution across the entrance of the circular harbor with a 10° opening

these values is drawn for reference. For a specific value of ka, the velocity V_o is a function of vertical position z (see Eq. 3.42); however, in the range $0 > z/h > -0.15$ corresponding to the experimental data shown, the relative velocity $V_o/(V_o)_{ave}$ at the entrance is essentially independent of z. Therefore, in Fig. 6.29 only one theoretical curve is presented for each value of ka.

Experimental measurements were conducted by placing the hot-film sensor parallel to "the coastline" and the bottom at five lateral positions: $x/\frac{d}{2} = 0, -0.32, -0.64, 0.32, 0.64$. In the upper portion of Fig. 6.29, these experimental data are shown in terms of $V_o/(V_o)_{ave}$ for each lateral position at: $z/h = -0.03, -0.07, -0.10,$ and -0.15. Comparing the theoretical and experimental results, the experimental data are generally larger than the theoretical values, although they qualitatively follow the trend predicted by the theory, i.e. the velocity increases toward the two limits of the entrance. It is felt that in part the reason for the disagreement could be caused by underestimating the experimental value of $(V_o)_{ave}$. Due to the relatively large value of the ratio of the length of the hot-film sensor to the width of the harbor entrance, measurements could not be made close to the edges of the entrance where the velocities were large. Thus, the average value of the data at the five locations is probably smaller than the true average velocity. In order to reduce the influence of the experimentally determined average velocity and to more positively confirm the theoretical velocity distribution across the

entrance, the same data were normalized with respect to the velocity at the center of the harbor entrance, $(V_o)_c$. These results are presented in the lower portion of Fig. 6.29 with the theoretical curves shown for comparison. It is seen that the experimental data qualitatively agree with the theory; the major disagreement again is for the case of ka = 3.922 (T = 0.485 sec) where one possible reason for this has been discussed in Subsection 6.2.5.2. From Fig. 6.29 it is seen that for the case of a 10^o opening the velocity distributions for these three values of ka are similar in that the velocity increases toward the entrance limits.

Similar results for the harbor with a 60^o opening are presented in Fig. 6.30 for four values of ka, i.e. ka = 0.64, 2.22, 3.30, and 4.01. In obtaining the theoretical curves the arbitrary shaped harbor theory and Eq. 3.42 were used again with the harbor entrance divided into six equal segments (each segment having a 10^o central angle) and the boundary divided into 30 equal segments. As before, in Fig. 6.30 for each value of ka presented, a curve is drawn through the theoretically computed values of $V_o/(V_o)_{ave}$ which have been plotted at the mid-point of each segment. The theoretical curve for ka = 0.64 can be considered as representing the velocity distribution corresponding to Mode No. 1 (the "pumping mode"). (For a description of the shape of this resonant mode of oscillation the reader is referred to Subsection 6.2.4.). The velocity distribution for Mode No. 2 (the "sloshing mode") is represented by the curve for ka=2.22, while

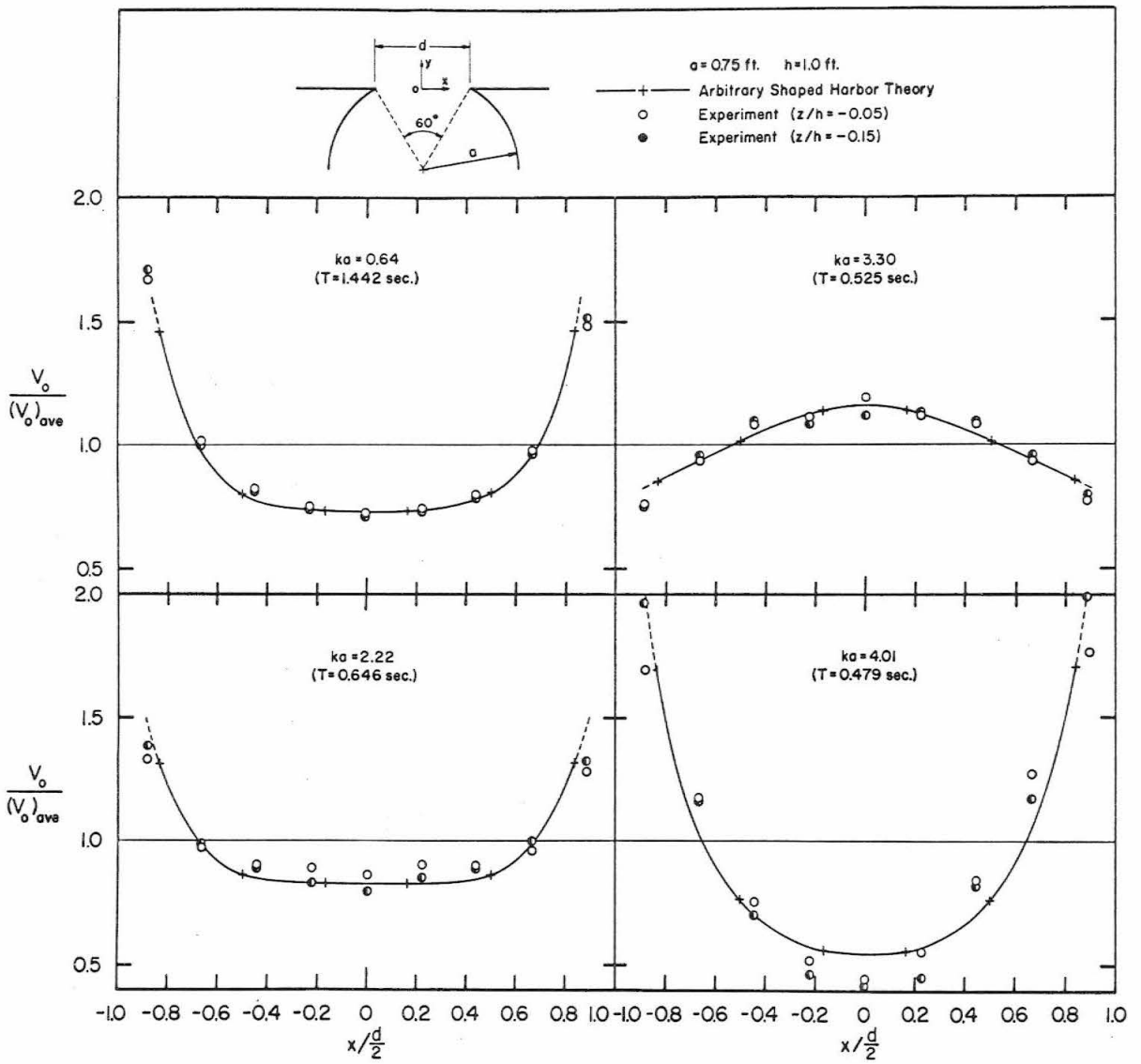

Fig. 6.30 Velocity distribution across the entrance of the circular harbor with a 60° opening

Modes No. 3 and No. 4 correspond to ka = 3.30 and 4.01 respectively. It is interesting to note that the velocity distribution for the third mode (ka = 3.30) is strikingly different in appearance than those of the other three.

For the harbor with a 60^{o} opening, the length of the hot-film sensor is much smaller compared with the width of the entrance than for the 10^{o} case just discussed; hence, measurements could be made relatively closer to the entrance limits. Therefore, it is felt that the experimentally determined average across the entrance, $(V_o)_{ave}$, is reasonably good, and the results are only normalized with respect to the average velocity in comparing experiments to theory. Experimental data at two vertical positions: z/h = -0.05 and -0.15 are shown in Fig. 6.30. Considering the assumptions made in the data reduction procedure it is somewhat surprizing that the experimental data agree as well with the theory as they do. The major disagreement between experiments and theory again is at the largest value of ka, i.e. ka = 4.01.

6.2.5.4 Velocity at the harbor entrance as a function of wave number parameter, ka

It is possible in determining the response curve for a particular harbor that because of the location chosen the amplification factor at that position is small for all incident wave numbers whereas a nearby location has associated with it large amplification factors for particular wave numbers. Therefore, one response curve alone may

not always clearly indicate all resonant conditions. A parameter which may be used as an indicator of resonance, which is independent of location, is the total velocity at the harbor entrance. Since this velocity is associated with the energy input into the harbor, a larger velocity at the entrance at one wave number compared to another would mean a larger kinetic energy input and resultant larger potential energies and hence water surface amplitudes inside the harbor for that wave number. Therefore, a curve showing the variation of the entrance velocity with the incident wave number parameter, ka, may prove to be a useful tool to indicate resonance. In this subsection such curves for the case of a circular harbor with a 10^{o} opening and a 60^{o} opening will be presented and discussed.

As mentioned earlier, Eq. 3.41 can be used to calculate the total velocity at the entrance, V_o^*, and if both sides of Eq. 3.41 are normalized with respect to the maximum horizontal water particle velocity for a shallow water wave, one obtains:

$$\frac{V_o^*}{\sqrt{gh}\,\frac{A_i}{h}} = \frac{\sqrt{gh}}{\sigma}\left[\frac{A_1^2 + A_2^2 + A_3^2}{2} + \frac{1}{2}\left(A_1^4 + A_2^4 + A_3^4 + 2A_1^2A_2^2\cos 2(\alpha_1 - \alpha_2)\right.\right.$$
$$\left.\left. + 2A_2^2A_3^2\cos 2(\alpha_2 - \alpha_3) + 2A_1^2A_3^2\cos 2(\alpha_1 - \alpha_3)\right)^{\frac{1}{2}}\right]^{\frac{1}{2}} \qquad (6.7)$$

wherein A_1, A_2, A_3, α_1, α_2, and α_3 are defined in Eq. 3.41. In using Eq. 6.7 the value of A_2 and A_3 at the harbor entrance are easily obtained since f_2 and $\frac{\partial f_2}{\partial y}$ for each entrance segment are determined from the matching procedure. The value of $\frac{\partial f_2}{\partial x}$ in A_1 is approximated

by $\frac{\Delta f_2}{\Delta x}$, wherein Δf_2 represents the difference in the value of wave function f_2 of two neighboring entrance segments and Δx represents the distance between them.

Fig. 6.31 shows the variation of the total velocity at the entrance of the circular harbor with a 10^o opening as a function of the wave number parameter ka. This curve is calculated from Eq. 6.7 for z=0 (the water surface) and as before, the water depth, h, is 1 ft. The ordinate in Fig. 6.31 is $(V_o^*)_{ave}/\sqrt{gh}\,\frac{A_i}{h}$ (wherein $(V_o^*)_{ave}$ represents the average total velocity, V_o^*, across the harbor entrance); the abscissa is the wave number parameter ka. There are four maxima in the curve shown in Fig. 6.31, the value of ka associated with each maximum is: ka = 0.35, 1.98, 3.18, and 3.87 and these values correspond to those associated with the four modes of resonant oscillation predicted by the arbitrary shaped harbor theory and shown in the response curves, Figs. 6.4 and 6.5.

In an attempt to compare the theory with the velocity measurements using the hot-film anemometer, Eq. 3.42 is used for the theoretical calculations. (Since the hot-film sensor in these experiments was primarily sensitive to the v and w velocity components, it is unrealistic to compare the experiments with Eq. 6.7.) Fig. 6.32 shows the variation of $(V_o)_{ave}/\left[(V_o)_{ave}\right]_{ka = 1.988}$ as a function of ka; the curve shown as a solid line was evaluated from Eq. 3.42 using values of f_2 and $\frac{\partial f_2}{\partial y}$ at the entrance determined by the method discussed in Chapter 3 (arbitrary shaped harbor theory). The velocity ratio

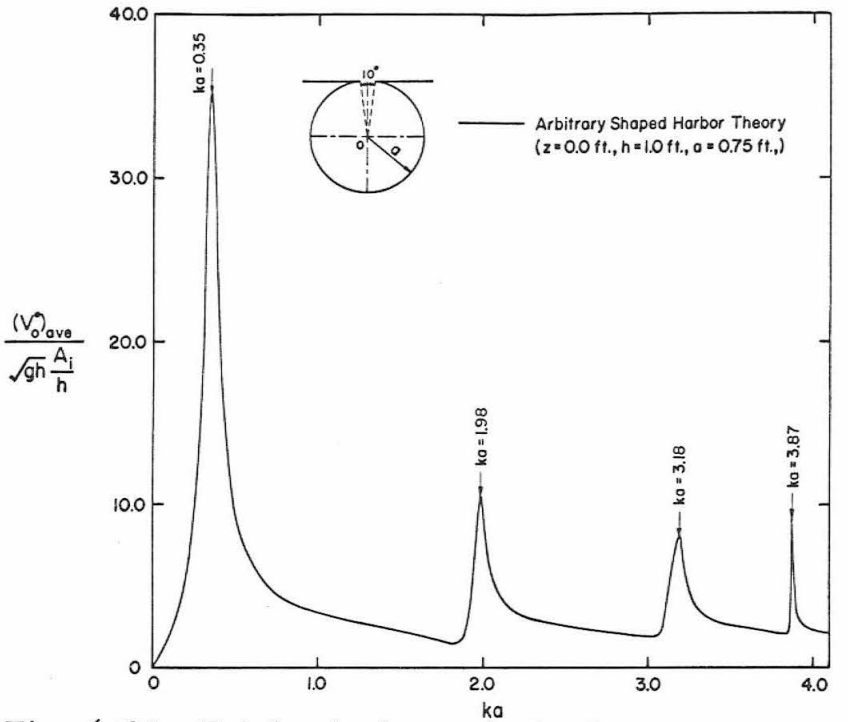

Fig. 6.31 Total velocity at the harbor entrance as a function of ka for the circular harbor with a 10° opening

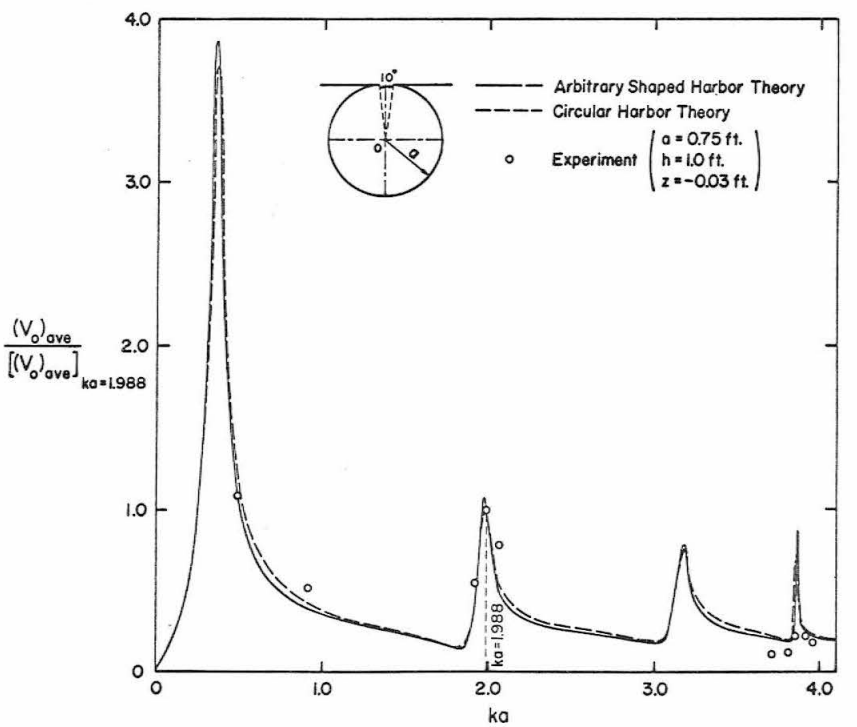

Fig. 6.32 Velocity at the harbor entrance as a function of ka: comparison of theory and experiment (10° opening circular harbor)

computed from Eq. 3.42 using the values of f_2 and $\frac{\partial f_2}{\partial y}$ determined by the method of Section 4.1 (circular harbor theory) is shown in Fig. 6.32 as a dashed curve. In using Eq. 3.42, the value of the incident wave amplitude A_i is taken as a constant for all values of ka.

Experiments were conducted by placing the hot-film sensor at z= -0.03 ft; for each value of ka, measurements were made at five lateral locations across the entrance ($x/\frac{d}{2}$= 0.0, 0.32, 0.64, -0.32, -0.64). The average of the output voltage from the linearizer at these five locations is denoted as S_2. As just mentioned in the theory the incident wave amplitude was considered constant for all wave numbers. However, in the experiment it is impossible to maintain this condition, in fact for the range of ka investigated the wave amplitude varied more than a factor of three. Therefore, to compare the experimental data to the theory, this effect of the varying incident wave amplitude must be eliminated. This was accomplished by dividing the voltage, S_2, by the incident wave amplitude at that wave number. This ratio was then normalized with respect to that at ka=1.988 and the resulting data are shown in Fig. 6.32.

In Fig. 6.32 it is seen that the two theoretical curves agree well and the experimental data agree reasonably well with these theories. However, at large values of ka, again, the data and theories show poorer agreement.

The variation of the velocity at the harbor entrance with ka is presented in Fig. 6.33 for the harbor with a 60° opening. The curve is again obtained from Eq. 6.7 evaluated at the water surface for a total depth of 1.0 ft. It is seen that the values of ka for the four maxima in Fig. 6.33 are: ka=0.50, 2.18, 3.38, 3.97. Again, these values correspond to those predicted by the arbitrary shaped harbor theory. (See the response curves in Figs. 6.6 and 6.7.) It should be noted that the third maximum was not clearly defined in the response curve shown in Fig. 6.6 because of the location chosen (it did appear at the other location, see Fig. 6.7); this clearly emphasizes the importance of the entrance velocity as an indicator of resonance. Comparing Fig. 6.33 with Fig. 6.31, it appears that the average velocity across the entrance at resonance is significantly less for the case of a 60° opening; however, the wave number band-width associated with the maxima is larger for the 60° case compared to the harbor with a 10° opening. This phenomenon is similar to that shown by the response curve presented in Subsection 6.2.2.

For the 60° opening, the velocity at the center of the harbor entrance also was measured using the hot-film anemometer. The sensor was located at a vertical position $z=-0.05$ ft at the center of the entrance (the water depth again was 1.0 ft). The voltages from the linearizer at various values of ka were then normalized with respect to that at ka=2.25 using the same correction procedure as was just described for the harbor with a 10° opening. These data are presented in Fig. 6.34; in contrast to Fig. 6.32 where average velocities

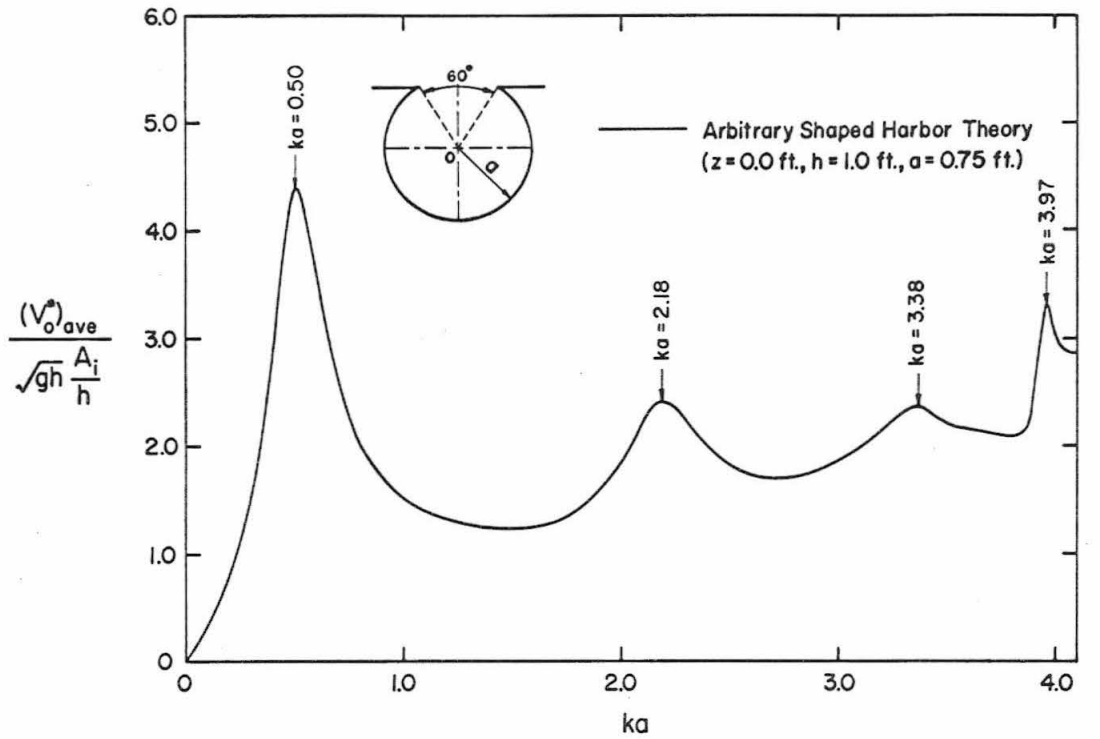

Fig. 6.33 Total velocity at the harbor entrance as a function of ka for the circular harbor with a 60° opening

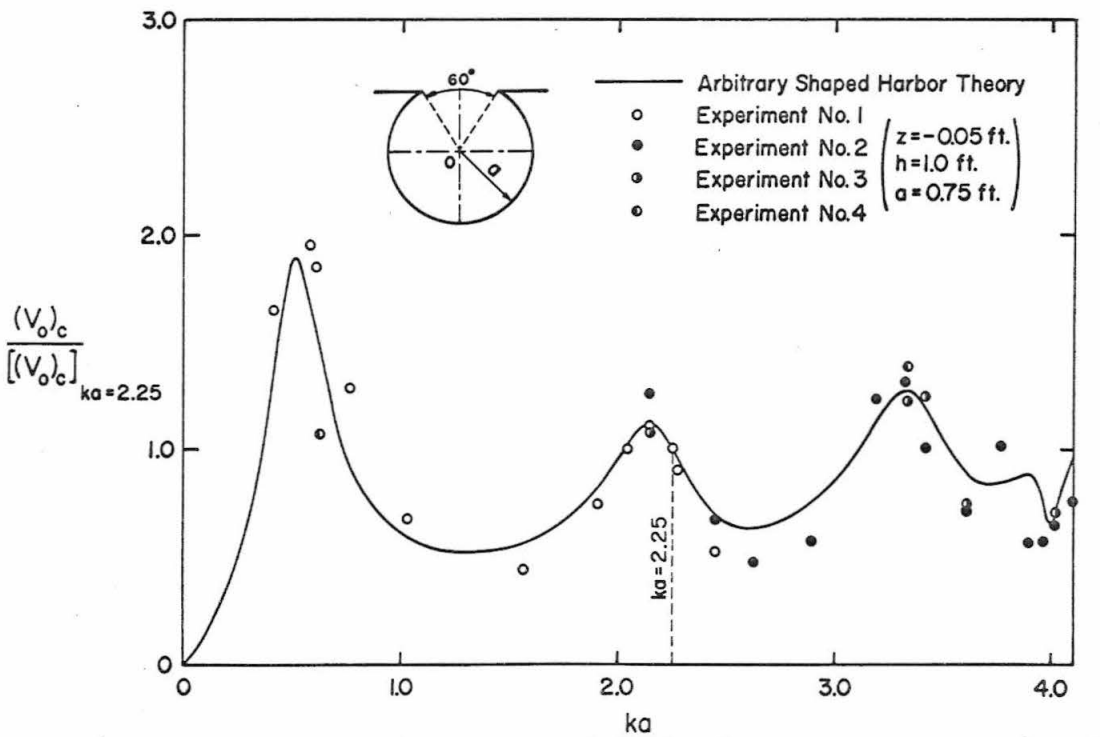

Fig. 6.34 Velocity at the center of the harbor entrance as a function of ka: comparison of theory and experiment (60° opening circular harbor)

across the entrance were used, here the normalized velocity is that obtained at the center of the entrance.

For this case only the theoretical curve obtained from the arbitrary shaped harbor theory is shown, since the circular harbor theory had not been used to determine the values of f_2 and $\frac{\partial f_2}{\partial n}$ at the center of the entrance (it was used only to determine the average values of f_2 and $\frac{\partial f_2}{\partial n}$ across the entrance).

Although the experimental data show considerable scatter, they agree qualitatively with the theory. The results from experiments performed at four different times are shown in Fig. 6.34 providing additional confidence in the experimental procedure. The value of ka associated with the maxima in Fig. 6.34 are different from that of Fig. 6.33 especially the third and fourth peaks. This is because for different values of ka, the shape of the velocity distribution across the harbor entrance is not the same (see Fig. 6.30). Thus, the relative velocity at the center of the entrance, $(V_o)_c / \left[(V_o)_c\right]_{ka=2.25}$, is not necessarily equal to the relative <u>average</u> velocity across the entrance, $(V_o)_{ave} / \left[(V_o)_{ave}\right]_{ka=2.25}$ shown in Fig. 6.33.

The results presented in this subsection have demonstrated that a maximum average total velocity at the harbor entrance corresponds to a resonant mode of oscillation inside the harbor. It is obvious that such velocity considerations will be even more useful for a harbor with a complicated shape; more discussion of this will be given in Subsection 6.4.4.

6.3 RECTANGULAR HARBOR

6.3.1 Introduction

In the initial phases of this investigation a series of experiments was conducted to study the response of a narrow, fully open rectangular harbor to incident waves. As mentioned in Section 6.1, the primary purpose of these experiments was to ensure that the "open-sea" condition was simulated properly in the laboratory basin when using the dissipators described in Section 5.6. This was done by comparing the experimental results to the experiments and the theoretical analysis for a rectangular harbor presented by Ippen and Goda (1963). Their theoretical solution had been confirmed reasonably well by experiments conducted by them using a fully open rectangular harbor (2-3/8 in. wide, 1 ft 1/4 in. long) installed in a basin 11 ft long and 9 ft wide with "satisfactory" wave energy dissipators placed for the simulation of the "open-sea". In this study the harbor dimensions were identical to theirs and the only difference was the basin was larger and the dissipators were more efficient than theirs (see Sections 5.1 and 6.1).

In addition these early experiments also served to provide data to compare to the theory for an arbitrary shaped harbor presented in Chapter 3 as well as the rectangular harbor theory presented in Section 4.2. In the following subsection these theoretical results will be compared to the experimental data of this study as well as to the theory and experimental results obtained by Ippen and Goda (1963).

6.3.2 Response of Harbor to Incident Waves

The response of a fully open rectangular harbor to periodic incident waves is presented in Fig. 6.35. The abscissa is the wave number parameter $k\ell$ (where ℓ is a characteristic dimension of the harbor, in this case the length of the harbor). The ordinate is the amplification factor, R, defined as the wave amplitude at the center of the backwall of the harbor divided by the average standing wave amplitude at the harbor entrance when the entrance is closed (see Section 5.4 for a more complete discussion of the latter). Experimentally it is not possible to measure the wave amplitude exactly at the backwall; in fact the measurements were made at a point 1/4 in. from the backwall and about 3/4 in. off-center. Since the slope of the water surface so near the backwall is essentially zero and the motion of this narrow harbor over the range of $k\ell$ considered is practically two-dimensional, this difference between the location of the experiments and the point of definition of the theoretical value of R is considered unimportant in the comparison of theoretical and experimental results. The depth of the water was constant and equal to 0.844 ft in both the harbor and "open-sea", and the range of the stroke of the wave machine for these experiments is presented in the table in Appendix IV.

In Fig. 6.35, the solid line represents the curve computed from the theory for an arbitrary shaped harbor (Chapter 3); the theory for the rectangular harbor (Section 4.2) is shown with long dashed lines,

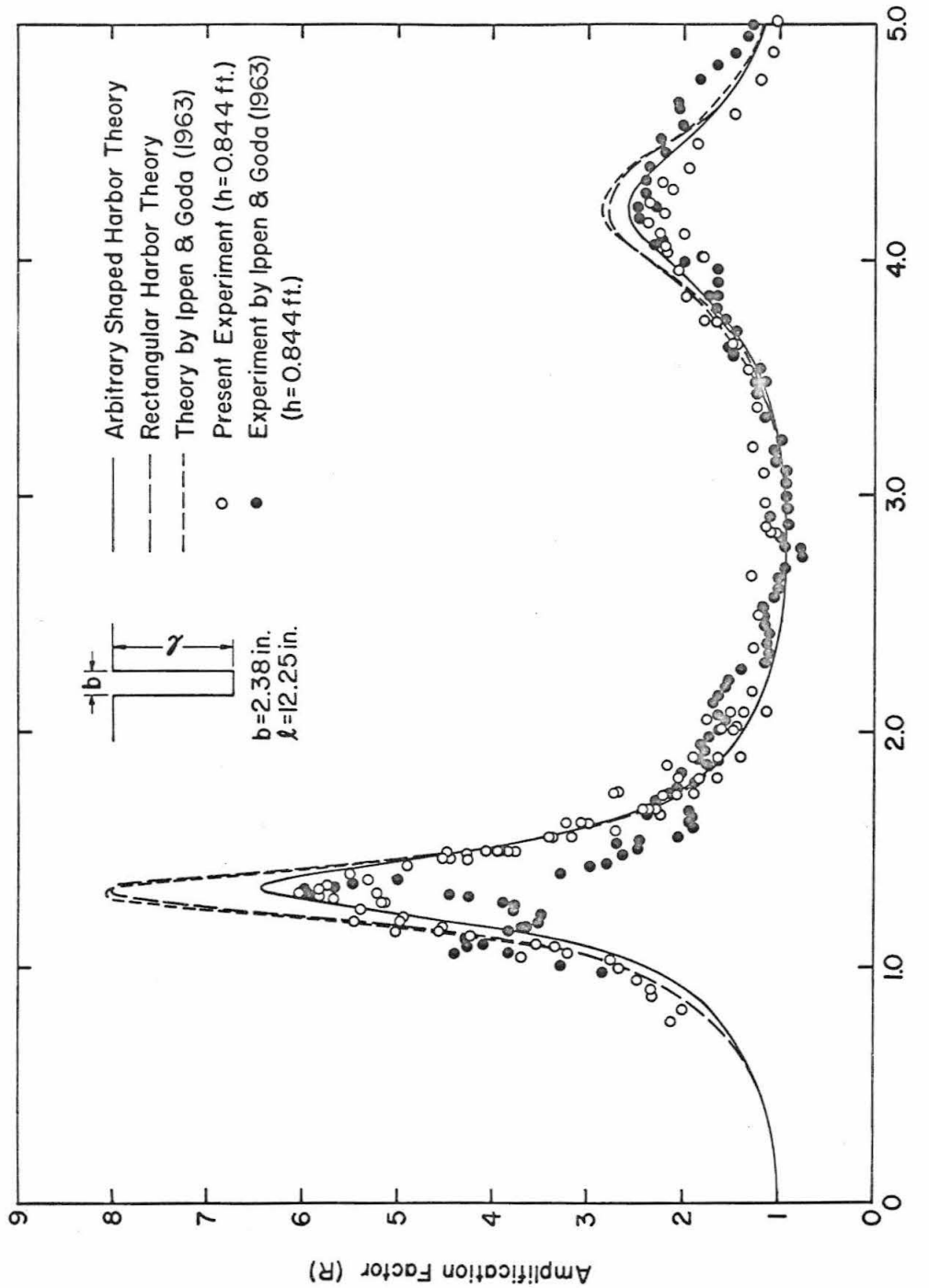

Fig. 6.35 Response curve for a fully open rectangular harbor

while the theory developed by Ippen and Goda (1963) is represented by a line composed of short dashes. The experimental data obtained from the present studies are denoted by open circles while the experimental data of Ippen and Goda (1963) are shown as solid circles.

In using the arbitrary shaped harbor theory the boundary of the harbor is divided into 47 segments (N=47) of unequal length including three segments at the harbor entrance. Since the boundary of the rectangular harbor is composed of straight lines, as discussed in Subsection 3.3.1, the diagonal elements of the matrix G_n are equal to zero, i.e. in Eq. 3.57, $(G_n)_{ii} = 0$ for i=1, 2.....47. After following the procedures described in Chapter 3 the response curve shown is obtained.

In using the rectangular harbor theory the method described in Section 4.2 is used. For a fully open rectangular harbor, Eq. 4.38, which describes the wave function f_2 in the region inside the harbor, can be simplified, since the entrance and the width of the harbor are equal (b=d). Therefore, the term $S_m(x, y)$ defined in Eq. 4.38 is equal to zero and can be simplified to:

$$f_2(x, y) = \overline{C} \cdot S_o(x, y) \quad . \tag{6.8}$$

Thus, the average normal derivative of the wave function at the harbor entrance shown in Eq. 4.41 can be simplified also as:

$$\overline{C} = \frac{1}{\overline{S}_o - B_o} \quad , \tag{6.9}$$

where $\overline{S}_o = -\frac{1}{k}\cot k\ell$ and $B_o = -\frac{i}{2}(J_c + i\frac{2}{\pi}Y_c)\Delta s$ as defined in Eq. 4.27.

The Fourier transformation method used by Ippen and Goda (1963) for the evaluation of the radiation wave function f_3 in the region outside the harbor is different from the present rectangular harbor theory in which Green's identity formula and the Hankel function are used. However, the method used for Region II, i.e. inside the harbor, is the same. Therefore, the difference between the results of the theory of Ippen and Goda (1963) and this theory can be attributed to the difference between the methods used to evaluate the radiation function f_3; from Fig. 6.35 any differences appear to be quite small.

From Fig. 6.35 it is seen that the three theoretical curves agree fairly well with the experimental results, although the theoretical curve obtained from the arbitrary shaped harbor theory agrees better with the experiments near resonance than the other two theoretical curves. This may be because in using the arbitrary shaped harbor theory, the entrance was divided into three segments and the solution was matched at each segment as compared to the other two theories where only the average solution across the entrance was matched. Another feature of Fig. 6.35 is that the present experimental data agree better with the theoretical curves than do the experimental data of Ippen and Goda (1963), especially in the vicinity of resonance. This is probably because the wave basin for the present experiments is both wider and longer than the wave basin used by Ippen and Goda, hence the incident wave is more nearly two dimensional; also the present

energy dissipators are more efficient than those used by Ippen and Goda (1963) and therefore the "open-sea" condition is simulated more satisfactorily. This is supported by the fact that the data of Ippen and Goda (1963) show fluctuations in the region $1.10 < k\ell < 1.70$ indicating that the "open-sea" condition is not properly simulated in this frequency range where the incident wave length is large resulting in small wave steepness. Such fluctuations do not appear in the data corresponding to the present experiments.

As mentioned before, these experimental results led to the conclusion that the open-sea condition was being properly simulated in the laboratory and no additional modification of the wave energy dissipators was necessary. Moreover, the agreement between the theoretical and experimental results as shown in Fig. 6.35 has demonstrated that the arbitrary shaped harbor theory can also be applied successfully to a harbor with straight sides and sharp interior corners.

6.4 A HARBOR WITH COMPLICATED SHAPE: A MODEL OF THE EAST AND WEST BASINS OF LONG BEACH HARBOR

6.4.1 Introduction

As discussed in Sections 6.2 and 6.3, the theoretical solution of the wave induced oscillations in the two specially shaped harbors: circular and rectangular, can be obtained by using the general theory for an arbitrary shaped harbor developed in Chapter 3. The theoretical results for these special harbors obtained from the arbitrary shaped harbor theory have been shown to agree well with

the more exact theories developed in Chapter 4, and with the experimental results.

These two special shaped harbors are of importance because, as mentioned earlier, the circular harbor represents an extreme shape in which the boundary of the harbor is curved and the tangent to the boundary is continuously changing direction whereas the rectangular harbor represents the other extreme where the boundary is composed of straight lines, along each side the tangent to the boundary does not change direction. The boundary of any arbitrary shaped harbor is in fact usually a combination of these two cases.

In order to test the arbitrary shaped harbor theory further, a harbor of complicated shape was studied both theoretically and experimentally. In planform this harbor model is slightly modified from the existing harbor of the East and West Basins of the Long Beach Harbor located in Long Beach, California; the horizontal scale is 1 to 4700. Also it differs only slightly from the hydraulic model studied by Knapp and Vanoni (1945) wherein a distorted hydraulic model was used with attention given to the bathymetry.

A sketch of the model of the East and West Basins of Long Beach Harbor which was used in this investigation is presented in Fig. 6.36 which shows the width of the harbor entrance as 0.2 ft and the characteristic dimension of the harbor, a, equal to 1.44 ft. The depth of the water in the experiments was constant in both the harbor and the "open-sea" and equal to 1 ft.

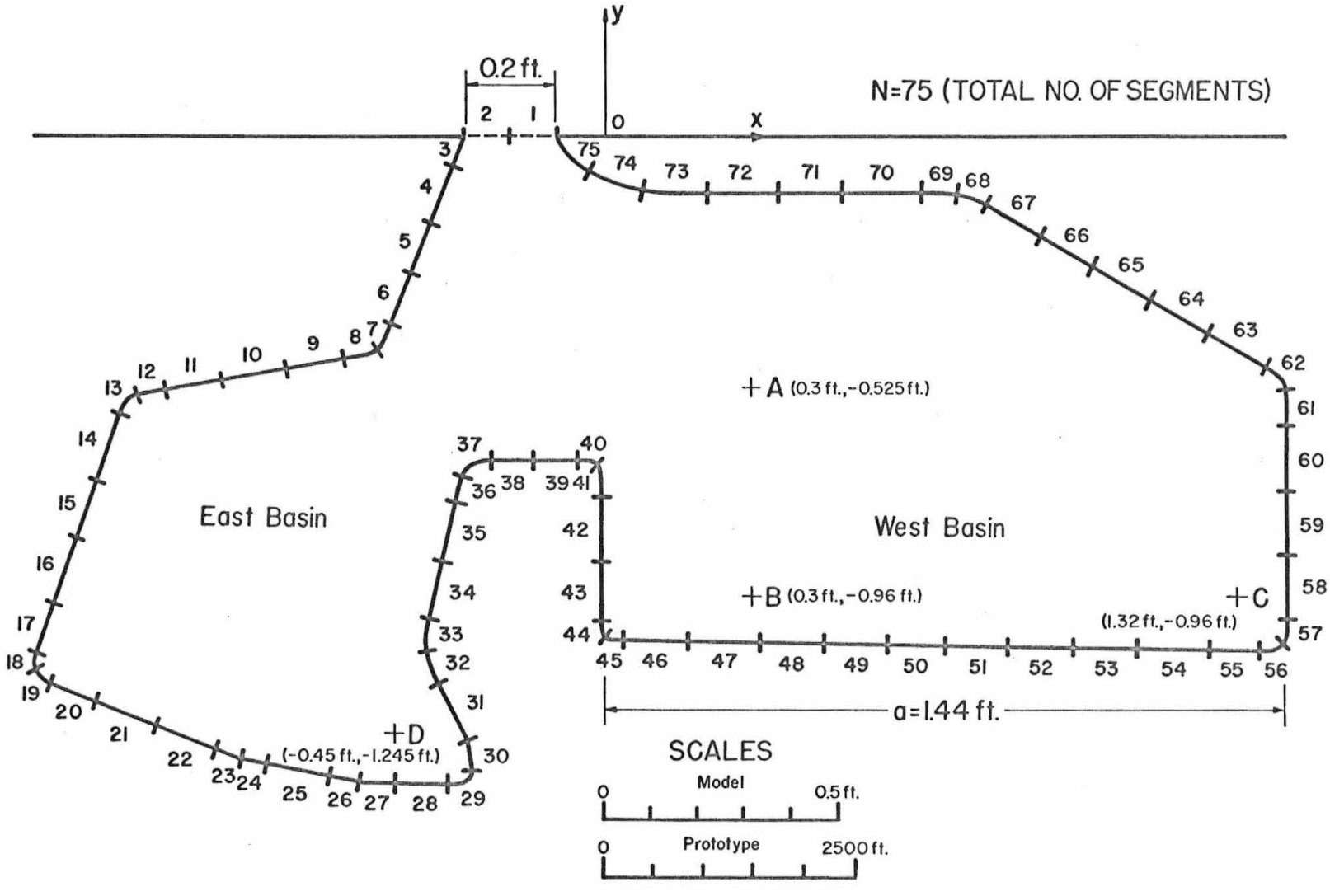

Fig. 6.36 The model of the East and West Basins of Long Beach Harbor, Long Beach, California

The theory for an arbitrary shaped harbor developed in Chapter 3 is used to calculate the response curves, the wave amplitude distribution inside the harbor, and the total velocity at the harbor entrance. In applying the theory, the boundary of the harbor is divided into 75 unequal straight-line segments including two segments for the harbor entrance. The segments are numbered counter-clockwise starting from the right-hand limit of the harbor entrance and this numbering system is shown in Fig. 6.36.

6.4.2 Response of Harbor to Incident Waves

Response curves at four different locations inside the harbor are presented in Figs. 6.37 to 6.40. The four points are designated as point A, B, C, D and, for convenience, they are shown in Fig. 6.36 along with their coordinates in the model: A(0.30 ft, -0.525 ft), B(0.30 ft,-0.96 ft), C(1.32 ft, -0.96 ft) and D(-0.45 ft, -1.245 ft), where the first number inside the bracket is the x-coordinate and the second number is the y-coordinate. For all of the response curves, the abscissa is the wave number parameter, ka (where again k is the wave number, and "a" is a characteristic length equal to 1.44 ft and shown in Fig. 6.36); the ordinate is the amplification factor R, as defined earlier.

It is seen that the theoretical results agree well with the experimental data at all four locations and show that the response of this harbor to periodic waves is much more complicated than the response curves for either a circular or a rectangular harbor. As discussed

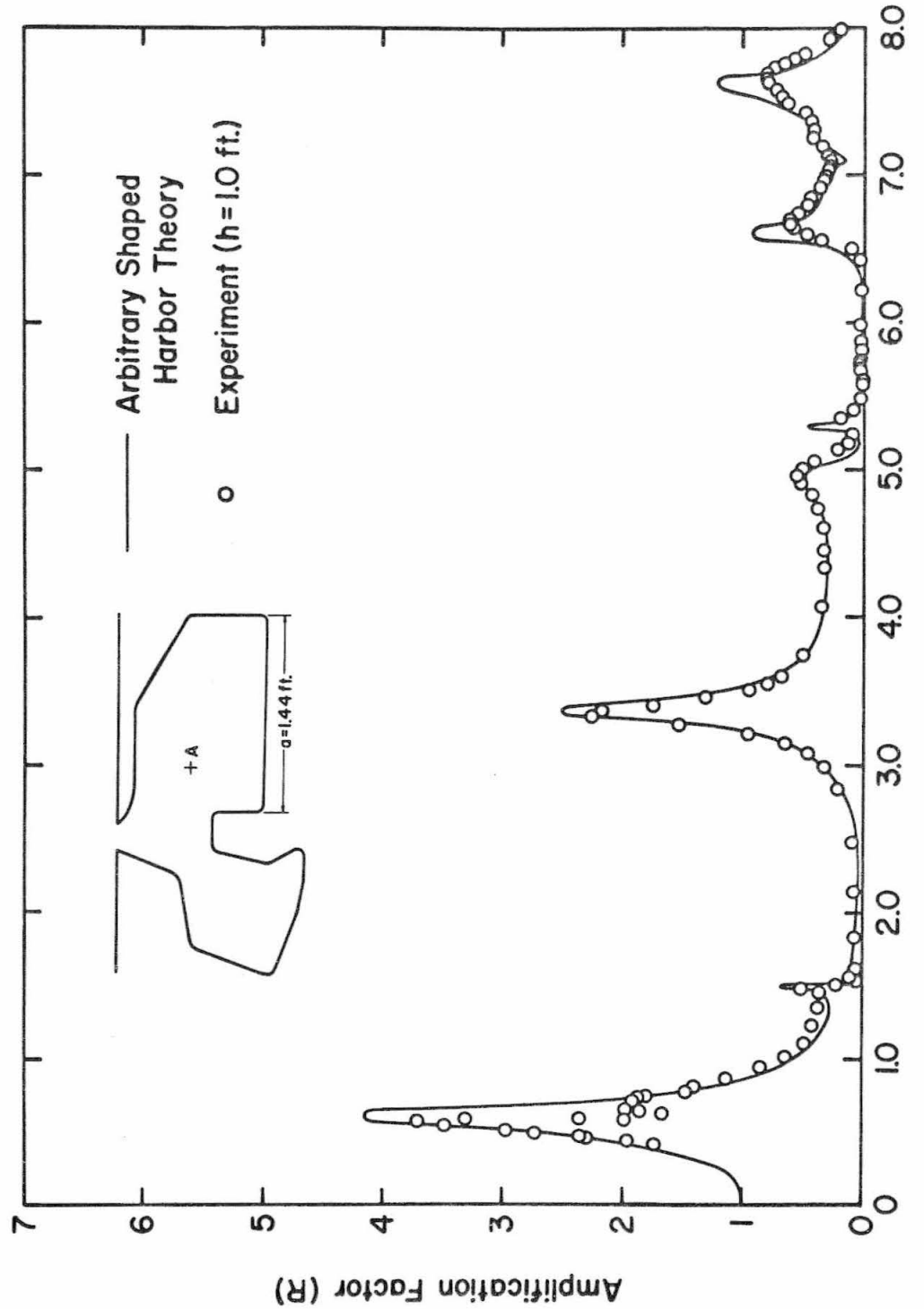

Fig. 6.37 Response curve at point A of the Long Beach Harbor model

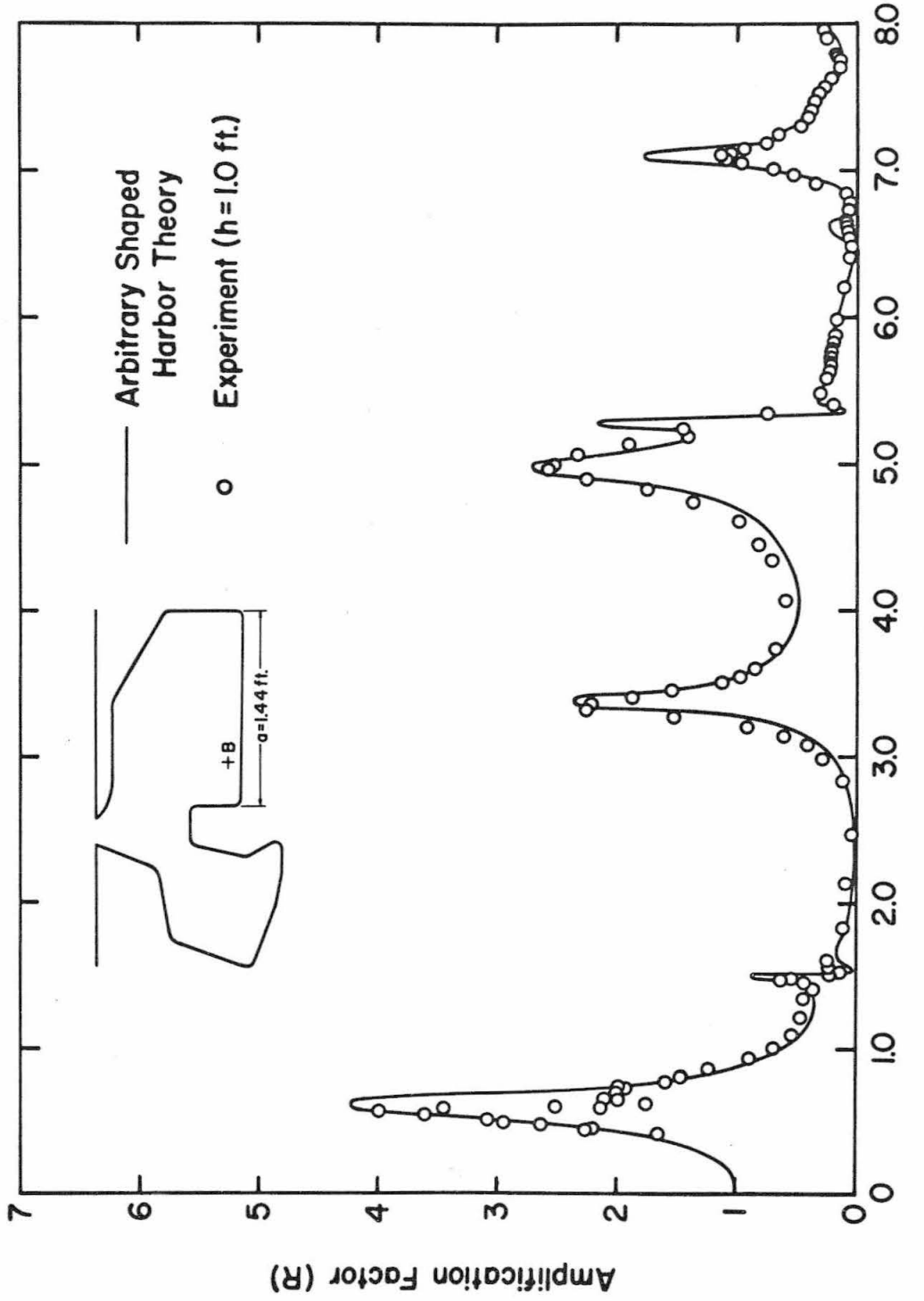

Fig. 6.38 Response curve at point B of the Long Beach Harbor model

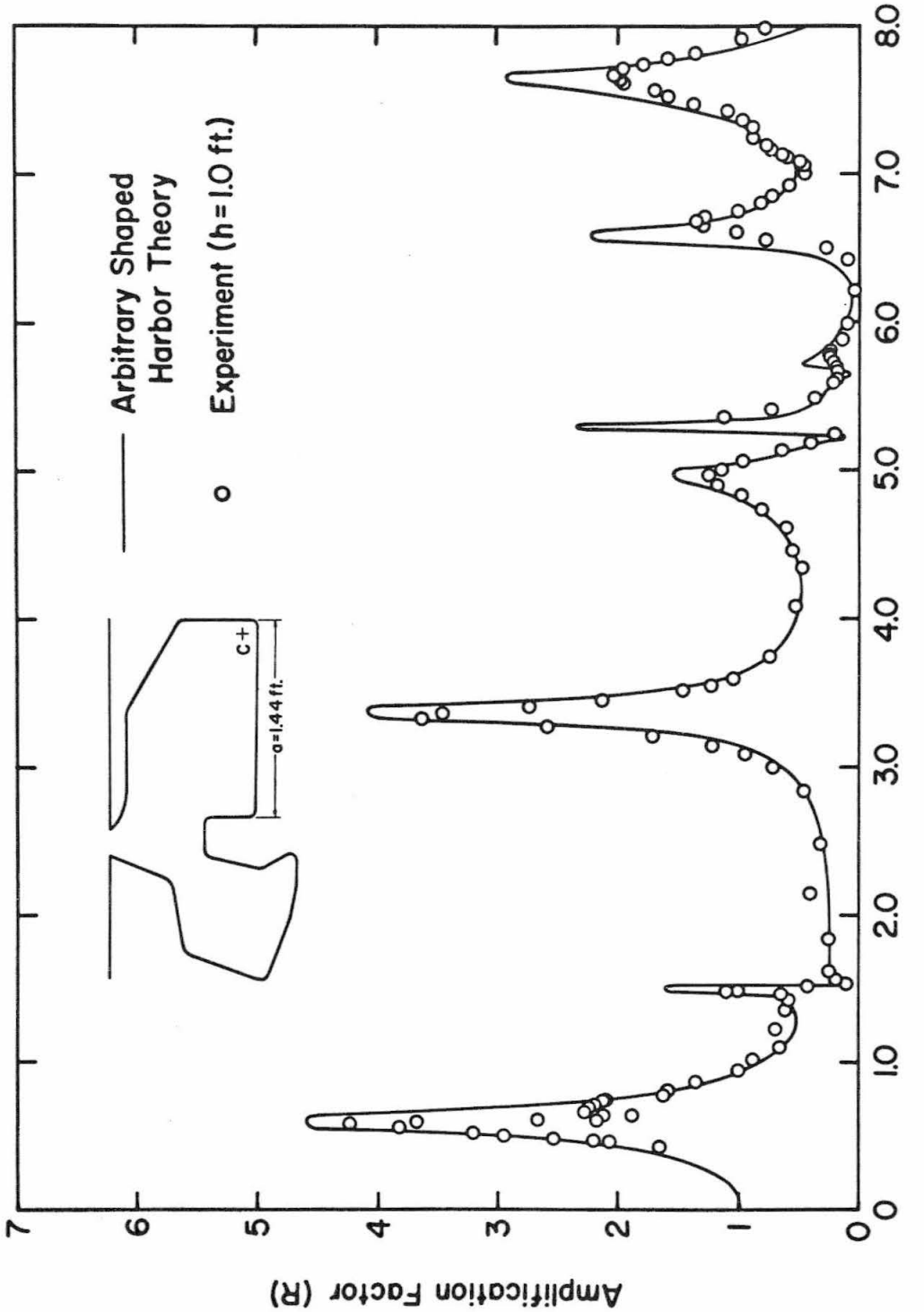

Fig. 6.39 Response curve at point C of the Long Beach Harbor model

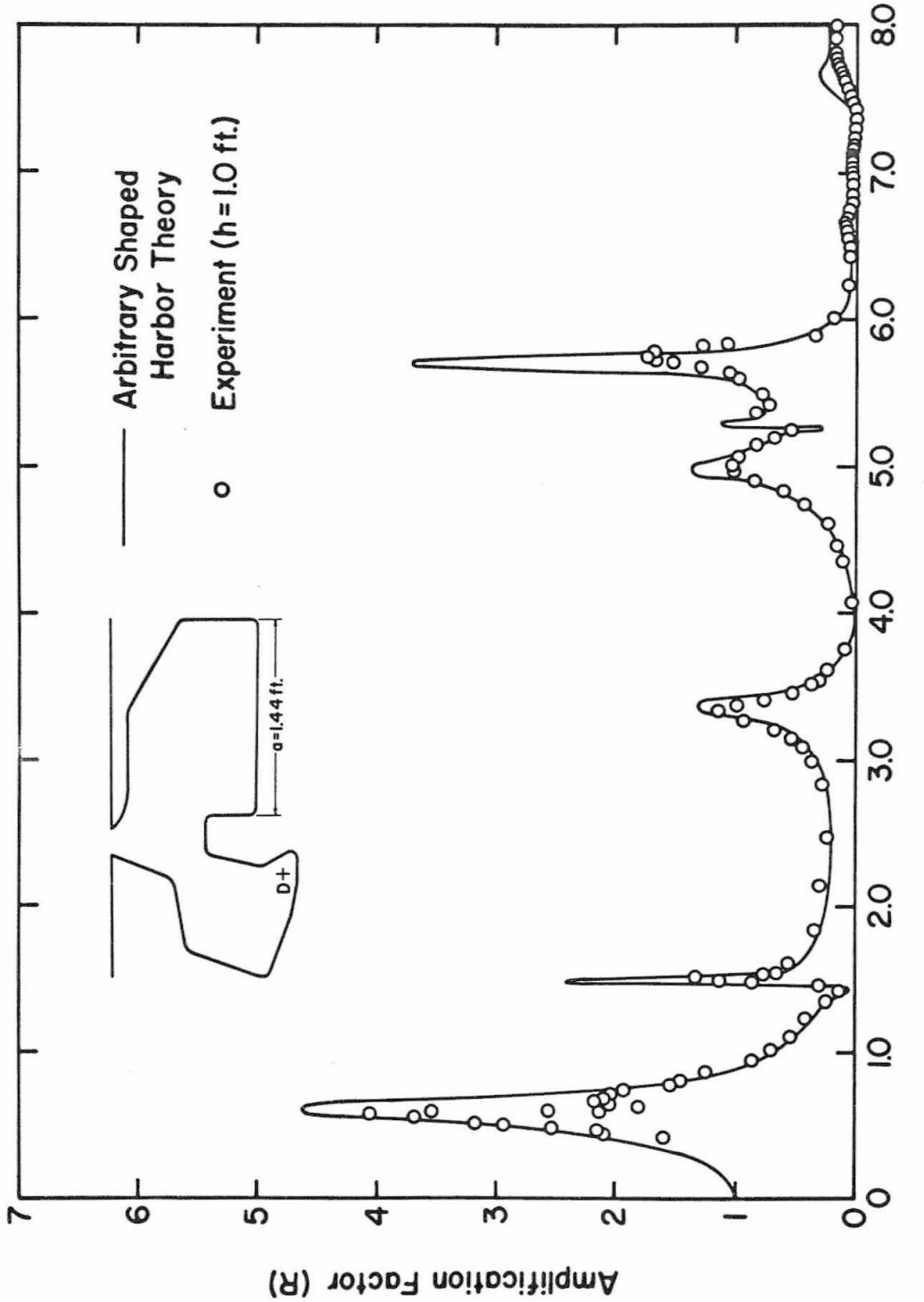

Fig. 6.40 Response curve at point D of the Long Beach Harbor model

in Section 6.2, the shape of the modes of resonant oscillation inside a harbor is simpler for an incident wave of smaller wave frequency, i.e. a smaller value of ka. As the incident wave frequency increases, the shape of mode of oscillation inside the harbor becomes more complex. The results shown in Figs. 6.37 to 6.40 also confirm this. For example, at the first resonant mode (ka = 0.61) the amplification factors at the four different positions (Points A, B, C, and D) differ only slightly. However, for the mode corresponding to ka = 7.62, the amplification factors at the four locations differ considerably; the amplification factors at the points B and D are much smaller than those at the points C and A.

One common feature of the four response curves is that while the theory has predicted the frequency of every resonant mode of oscillation correctly, the theoretical amplification factor at resonance is slightly larger than the experimental data especially for the resonant modes at larger values of ka. This can be attributed to the observation made in Subsection 6.2.2 that in using the same number of segments for the boundary of the harbor at all wave periods, the theoretical results for a smaller value of ka are more accurate than the results which correspond to large ka; therefore, better agreement between the theory and experiments is expected and observed for small values of ka. (This means that the value of $k\Delta s$ is smaller for the former case than the latter case.) In addition the energy dissipation is larger at resonance for large values of ka, thus also tending to decrease the experimental amplification factors compared to those determined theoretically.

It can also be seen from the response curves that the agreement between the theoretical solution and the experimental data is reasonably good at each of the locations; there is no location where better agreement is seen compared to another. This uniformity of the agreement between the theory and experiments suggests that the theory has also accurately predicted the wave amplitude distribution inside the harbor for each mode of resonant oscillation.

In the application of the arbitrary shaped harbor theory (Chapter 3) the singularities are always assumed to be located at the mid-point of each boundary segment. Therefore if an interior point (x, y) is too close to the mid-point of a particular boundary segment, the wave function $f_2(x, y)$ calculated from Eq. 3.37 might be in error because of the excessive influence of that particular singularity (possibly as large as 10 or 20%). To avoid this it was found that the interior point investigated should be more than one-half of the length of the segment ($\frac{1}{2}\Delta s$) away from the harbor boundary. If the wave function desired is at a location very close to the boundary it can be obtained either by: interpolating between the value at the boundary (Eq. 3.22) and the value of $f_2(x, y)$ at a point which is at a distance of approximately $\frac{1}{2}\Delta s$ from the boundary or by reducing the length of the segment to allow the interior point of interest to be closer to the boundary.

As mentioned before, a response curve at a particular location inside the harbor does not necessarily show the maximum amplification within the harbor. The variation of the maximum amplification within the entire basin plotted as a function of the wave number parameter, ka, is presented in the response curve of Fig. 6.41. The ordinate is the ratio of the maximum wave amplitude within the harbor, regardless of location, to the standing wave amplitude with the entrance closed. This curve shows every possible mode of resonant oscillation for the range of ka that has been investigated, as well as the maximum amplification for each mode. It is obvious that the maximum amplification does not always occur at the same location within the harbor for different values of ka. This can be seen by comparing Fig. 6.41 with Figs. 6.37 through 6.40.

The experimental data from a model study conducted by Knapp and Vanoni (1945) are included in Fig. 6.41 for comparison. Data corresponding to the harbor with a 600 ft harbor opening are represented by open circles while the data for a 2000 ft opening are represented by solid circles. The prototype gate opening corresponding to the present model is 940 ft. It should be mentioned that the original data (see Knapp and Vanoni, 1945, p. 89) were plotted as the maximum amplification factor as a function of prototype wave period. In order to compare these data with the present theory the wave period has been converted to the wave parameter, ka. For this conversion, the prototype water depth was taken as an average of 40 ft, and the

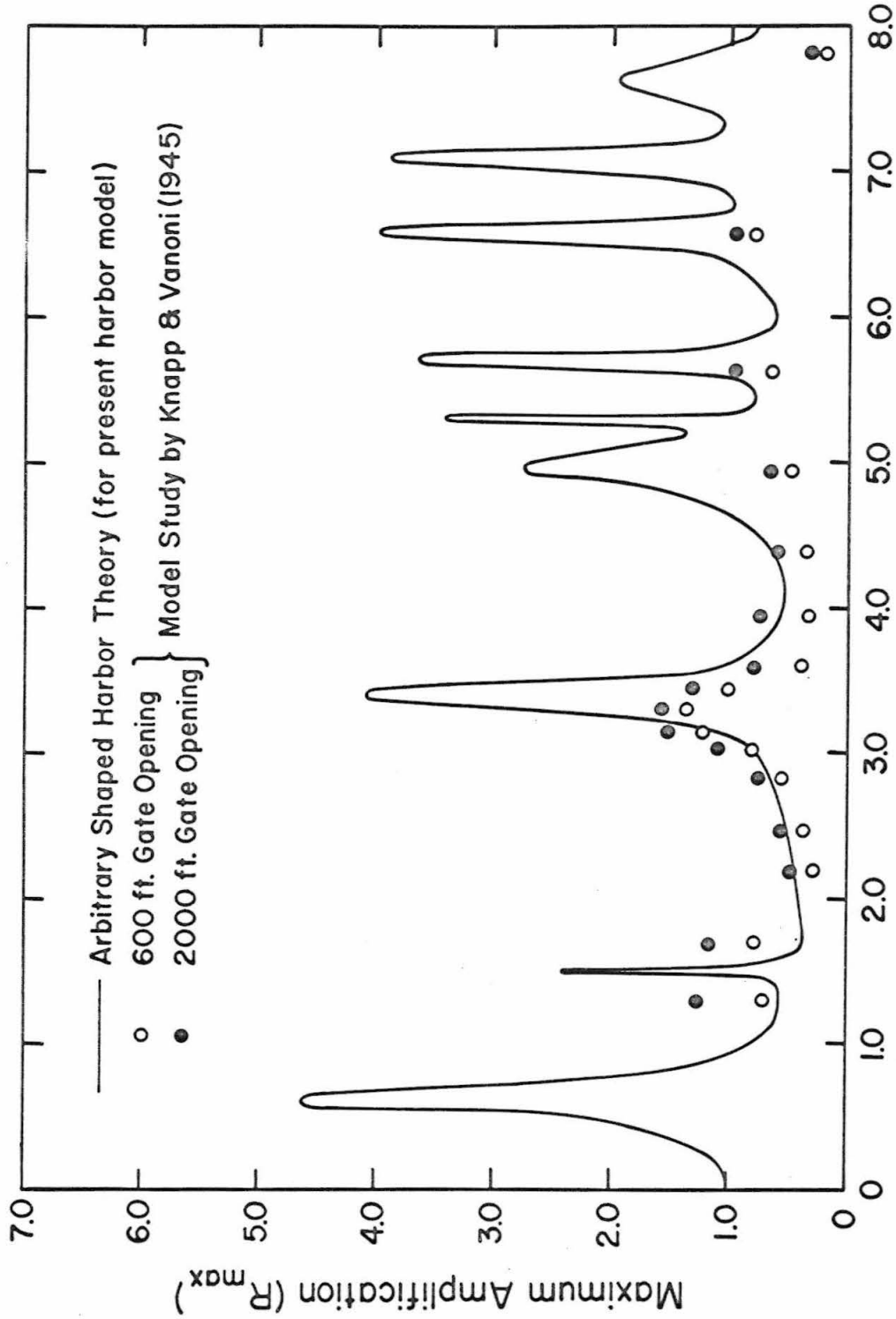

Fig. 6.41 Response curve of the maximum amplification for the model of Long Beach Harbor compared with the data of the model study by Knapp and Vanoni (1945)

prototype characteristic dimension of the harbor a = 6768 ft was used. (The experimental data shown in Fig. 6.41 corresponds to prototype wave periods which range from $2\frac{1}{2}$ min. to 15 min.)

The experimental data from Knapp and Vanoni (1945) show decreasing amplification factors with decreasing harbor opening contradicting one conclusion made in the study of circular harbors (Subsection 6.2.2): decreasing the harbor opening increases the wave amplification in the harbor at resonance. However, if one considers the other conclusion made in Subsection 6.2.2 that the viscous dissipation of energy is more important for a harbor with a smaller opening this contradiction may be resolved. Since it is entirely possible in Long Beach Harbor that energy dissipation for the harbor with a 600 ft opening is so large compared to that for the harbor with a 2000 ft opening that the increase in the resonant amplification due to closing the entrance is more than compensated by energy dissipation. It is possible that if the harbor entrance were much larger than 2000 ft, the amplification factor at resonance would be less, thus, in agreement with the "harbor paradox". This has not been investigated in this study.

Both the data and the theoretical curve presented in Fig. 6.41 more emphatically show an important requirement of harbor resonance studies. That is, in order to insure that certain modes of oscillation are not missed in hydraulic model studies, a sufficient small interval between wave periods must be used in evaluating the response.

6.4.3 Variation of Wave Amplitude Inside the Harbor for One Mode of Resonant Oscillation

Experiments were not conducted specifically to measure the distribution of wave amplitude inside the Long Beach Harbor model at resonance as was done in the investigation of circular harbors. However as mentioned previously, the theoretical amplitude distribution inside the harbor had been reasonably confirmed by the experiments shown in the response curves of Figs. 6.37 through 6.40. The distribution of wave amplitude inside the harbor for one particular mode of resonant oscillation determined from the arbitrary shaped harbor theory is presented in Fig. 6.42 for a value of ka = 3.38. The magnitude of this resonant peak can be seen in any of the response curves (Figs. 6.37 through 6.41); attention is directed to the fact that this is the second largest maximum amplification among the nine resonant modes presented in Fig. 6.41. In the prototype, for this value of ka, using the average depth of 40 ft the wave period is 6.1 minutes.

In Fig. 6.42 the wave amplitude has been normalized with respect to the wave amplitude at point C; the coordinates of this position have been presented in Fig. 6.36. Positive water surface displacements are shown by solid lines and negative displacements by long dash lines. Two nodal lines are seen, one in the East Basin and one in the West Basin with maxima occurring at the ends of each basin and the minimum occurring near the confluence of the two. For

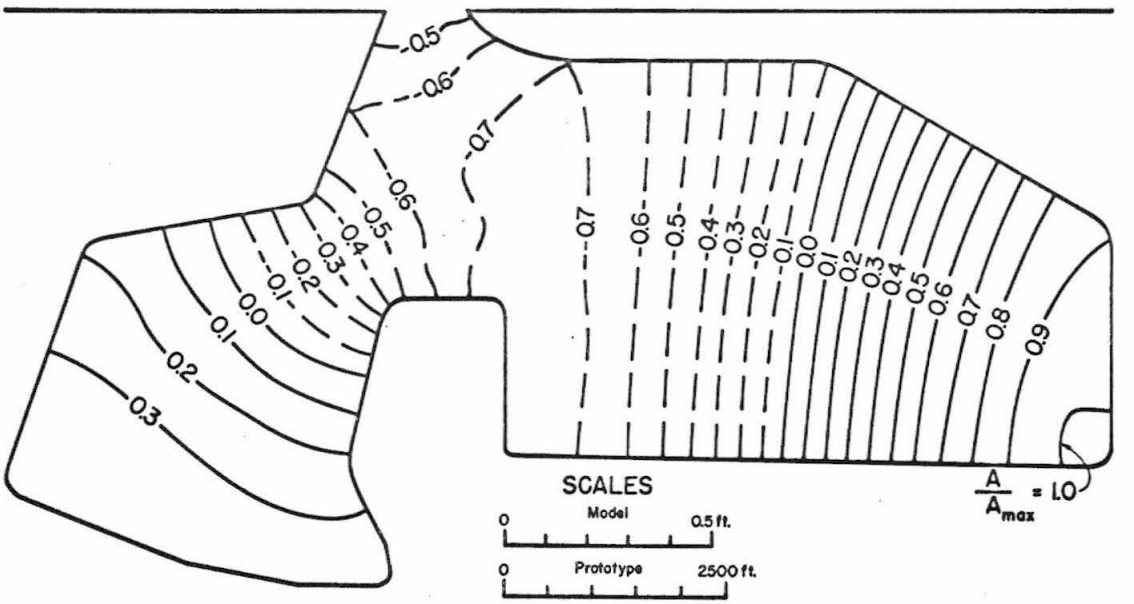

Fig. 6.42 The theoretical wave amplitude distribution in the Long Beach Harbor model (ka=3.38)

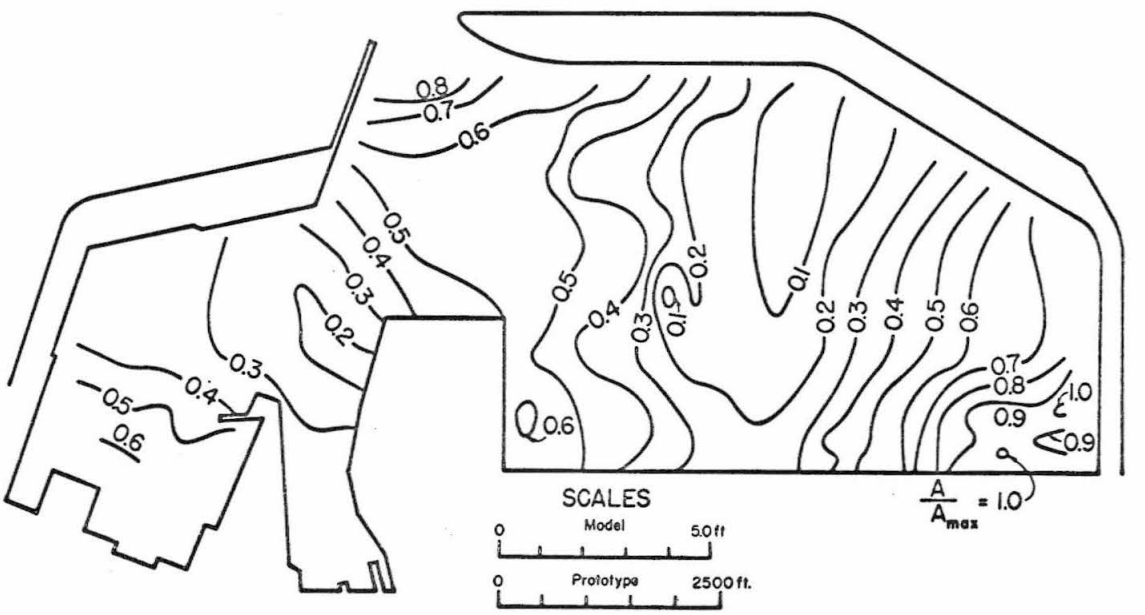

Fig. 6.43 Wave amplitude distribution inside the harbor model of Knapp and Vanoni (1945) for six minute waves (ka=3.30) (see Knapp and Vanoni (1945), p. 133)

this mode of oscillation it can be seen that neither a node nor an antinode exists at the entrance.

In the model study conducted by Knapp and Vanoni (1945) measurements were made of the wave amplitude distribution inside the harbor for various modes of resonant oscillation, and contour drawings similar to Fig. 6.42 were constructed. One such wave amplitude distribution is shown in Fig. 6.43. It is apparent from comparing Figs. 6.42 to 6.43 that in this investigation the boundary of the model has been simplified, especially the East Basin. The contours of constant water surface elevation are shown as all solid lines in Fig. 6.43 since the positive and negative displacements were not differentiated in that study. It is seen that two nodal lines exist, one in each basin, and the maxima exist at the end of each basin as well as near the entrance.

By comparing Figs. 6.43 to 6.42 the similarities in the amplitude distribution are striking. Except for the region near the entrance the location of the two nodes and the maxima are similar for the two models even though the boundary of the model used for present study has been simplified. Difference between the amplitude distribution near the entrance can probably be attributed to the difference of the "coastlines" for the two cases. Another difference between the two models which may contribute to the differences between the amplitude distribution shown in Figs. 6.42 and 6.43 is that all boundaries were vertical and the depth was constant in the model of this investigation compared to the more realistic treatment of the boundaries and bathymetry in the distorted hydraulic model of Knapp and Vanoni (1945).

6.4.4 Velocity at the Harbor Entrance as a Function of Wave Number Parameter, ka

The theoretical curves and the experimental data presented in Subsection 6.2.5.4 established the proposition that the fluid velocity at the harbor entrance reaches a maximum when a resonant oscillation develops inside the harbor. For the model of the East and West Basins of the Long Beach Harbor, no velocity measurements were made at the harbor entrance; however, theoretically this variation was investigated using the arbitrary shaped harbor theory.

The variation of the average velocity at the harbor entrance (normalized with respect to $\sqrt{gh}\ \frac{A_i}{h}$) as a function of the wave number parameter, ka, is presented in Fig. 6.44. Recall that the harbor entrance of the Long Beach Harbor model was divided into two segments (see Fig. 6.36); thus, the ordinate in Fig. 6.44 represents the average value of $V_o^* / \sqrt{gh}\ \frac{A_i}{h}$ at the water surface for the two entrance segments. (As before, the velocity is computed using Eq. 6.7.)

It is seen that there are 9 maxima in the range of ka presented in Fig. 6.44; the values of ka associated with these are: 0.61, 1.50, 3.38, 4.96, 5.30, 5.70, 6.60, 7.10, and 7.64. These values of ka are exactly the same as those associated with the maxima in the response curve of maximum amplification presented in Fig. 6.41.

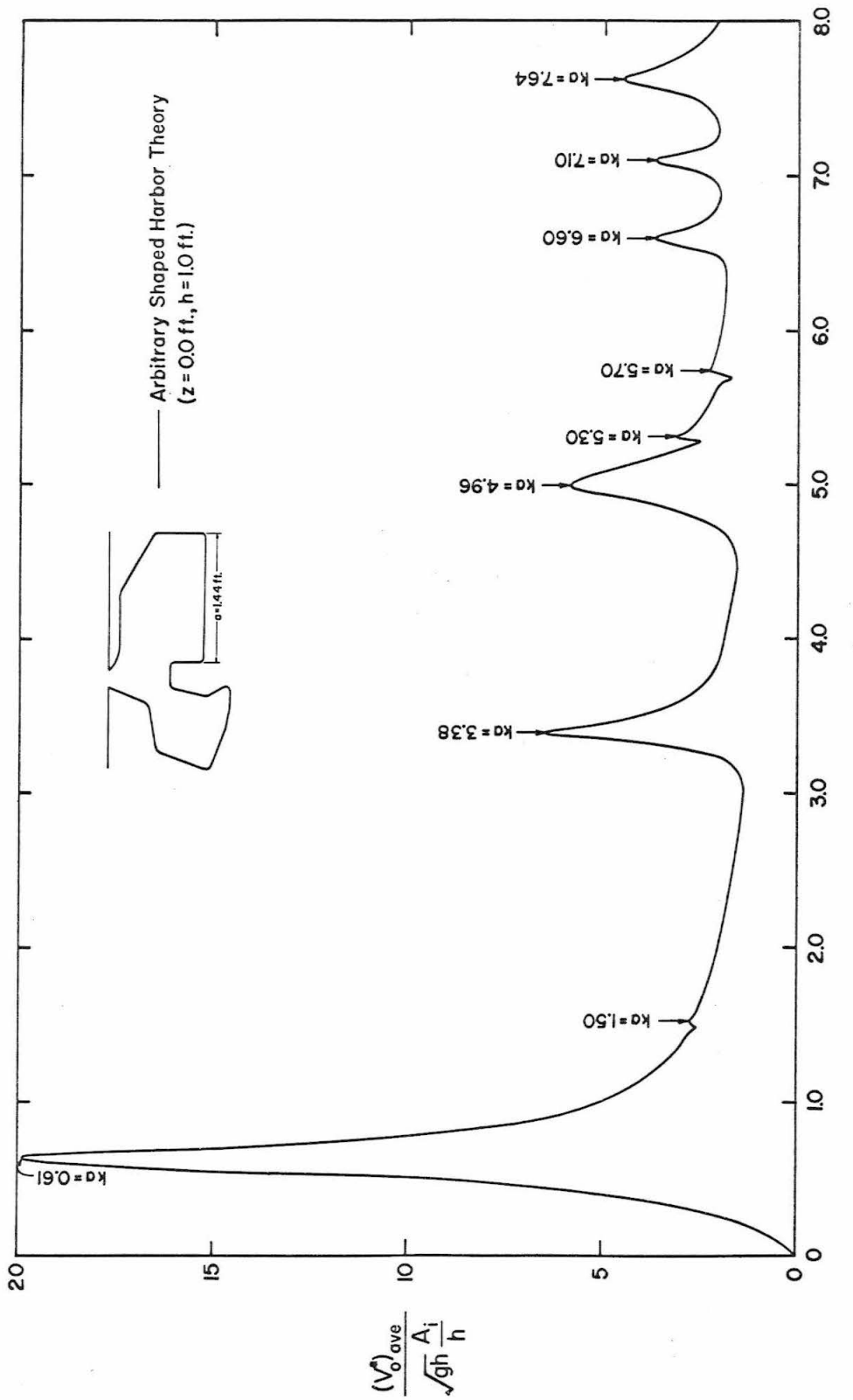

Fig. 6.44 Total velocity at the harbor entrance as a function of ka for the Long Beach Harbor model

This clearly demonstrates that each maximum of the total entrance velocity is associated with a mode of resonant oscillation inside the harbor, no matter how small the value of the peak.

A curve like Fig. 6.41 is not easy to obtain, because in order to obtain a value of the maximum amplification anywhere inside the harbor for a particular wave number the amplification factor at many points inside the harbor must be determined. However, the curve shown in Fig. 6.44 is relatively easy to obtain since one needs only the values of the wave function f_2, the normal derivative $\frac{\partial f_2}{\partial y}$, and the derivative $\frac{\partial f_2}{\partial x}$ at the harbor entrance when evaluating the total velocity from Eq. 6.7.

For a harbor with a complicated shape, it is possible that an interaction of wave motion between interconnected basins inside the harbor may develop and produce a resonant oscillation with only a small velocity at the harbor entrance. For example, the peak associated with ka = 1.50 in Fig. 6.44 is indeed very small; however, at this value of ka, a resonant oscillation does exist inside the harbor as can be seen from the response curves in Figs. 6.40 and 6.41. The same is true for ka = 5.30 and 5.70 at which the peaks in the velocity curve (Fig. 6.44) are also small, but considerable resonant oscillation does develop in the harbor as shown in the response curves in Figs. 6.38, 6.39, and 6.41 (for ka = 5.30) and Figs. 6.40 and 6.41 (for ka = 5.70). Therefore, in using this method of determining the periods of the resonant modes care must be taken that a small interval in wave period is used in the computations.

Fig. 6.44 shows that the velocity at the entrance for the pumping mode (ka = 0.61) is nearly four times that which exist for any other mode of oscillation. Using the prototype dimensions described previously the period of this mode of oscillation is approximately 33 minutes and could possibly be excited by tsunami. If the amplitude of an incident wave were 0.5 ft (using the average depth of 40 ft) Fig. 6.44 indicates that the maximum average entrance velocity for this mode would be about 10 fps and for modes of smaller wave period the velocities are in the order of 2 fps. Such velocities could cause significant damage to structures located near the entrance.

The results presented in Section 6.4 have shown good agreement between the theoretical analysis and the laboratory experiments demonstrating again the applicability of the arbitrary shaped harbor theory to harbors with complicated planforms and constant depth. The variation of the velocity at the harbor entrance as a function of the wave number parameter ka proves to be a good indicator for resonance inside the harbor. It has also been shown that the present theoretical results agree qualitatively with the experimental data obtained from a model study conducted by Knapp and Vanoni (1945), although the planform of the model investigated by them was more complicated and also included depthwise variations.

CHAPTER 7

CONCLUSIONS

The major objective of the present study has been to investigate, both theoretically and experimentally, the response of an arbitrary shaped harbor (with constant depth) to periodic incident waves. In order to ensure that the general theory which was developed (termed the arbitrary shaped harbor theory) could be applied to a harbor with a complicated shape this theory was first applied to two special shaped harbors: a circular harbor and a rectangular harbor. For these two cases different theories termed the circular harbor theory and the rectangular harbor theory were developed and compared to the general theory. Experiments were then conducted for the circular and rectangular harbors to verify the theoretical solutions. The general theory (the arbitrary shaped harbor theory) was also applied to a harbor of more complicated shape: a simplified, constant depth, model of the East and West Basins of the Long Beach Harbor. Experiments were also conducted to confirm the theoretical predictions.

From this study the following major conclusions, applying to the circular harbors, the rectangular harbor, and the Long Beach Harbor model, can be drawn:

1. The present linear-inviscid-theory termed the arbitrary shaped harbor theory predicts the response of an arbitrary shaped harbor (with constant depth) to periodic incident waves quite well even near resonance.

2. The theoretical prediction of the resonant frequencies (or the wave number parameter, ka, at resonance) agree well with the experimental data. The theoretical amplification factor at resonance is generally somewhat larger than the experimental data especially for the resonant modes at larger values of ka.

3. The open-sea condition has been simulated properly in the wave basin used for the experiments; the reflection coefficient for the wave energy dissipators which were used is estimated to be less than 20% for most of the experiments which were conducted.

4. Because of the wave radiation from the harbor entrance to the open-sea region which has been considered in this inviscid theory, the amplification of the wave amplitude inside the harbor at resonance is finite. The effect of viscous dissipation, which has not been considered in this theory, is to decrease the amplification near resonance even more.

5. The average total velocity across the harbor entrance reaches a maximum when a resonant oscillation develops inside the harbor; thus, the variation of the velocity at the

harbor entrance with wave number has been found to be a good indicator for resonance.

Since a relatively more detailed study has been made for circular harbors some of the important conclusions concerning this shape can be stated as follows:

6. The theoretical solution for a circular harbor with a 10° opening obtained using the arbitrary shaped harbor theory agrees well with those obtained from the circular harbor theory and the experiments. These results included the resonant wave numbers, the amplification factors, the shape of water surface inside the harbor for various modes of oscillations, and certain velocities at the harbor entrance.

7. For the circular harbor with a 60° opening both theories only differ slightly in the prediction of the value of the wave number parameter (ka) at resonance; the arbitrary shaped harbor theory agrees better with the experimental results in this respect. The shapes of the modes of oscillation also have been predicted correctly by both theories; thus, the small entrance approximation for the circular harbor theory can be applied at least up to a harbor opening with a 60° central angle.

8. As the width of the harbor entrance increases, the amplification at resonance decreases, but the wave number band-

width at resonance increases; thus, the "harbor paradox" was confirmed both theoretically and experimentally for this shape.

9. Experiments show that the effect of viscous dissipation of energy which is neglected in the present theories is more important for harbors with a smaller opening.

10. There are four modes of resonant oscillations in the range of ka investigated for the harbors with a 10° and a 60° opening. Except for the "pumping mode", which does not exist in a completely closed circular basin, each mode corresponds to a free mode of oscillation in the closed basin. The corresponding modes of oscillation for the two harbors and the closed basin are basically similar; however, the detailed shape of the free surface differs among the three.

11. The wave number parameter (ka) at resonance approaches the value for a closed basin as the entrance width decreases.

12. No antinode, or node, exists at the harbor entrance although an antinode might occur at that position for a closed circular basin.

13. For a larger entrance width the distribution of the velocity across the harbor entrance varies significantly for different modes of oscillation.

14. The experimental data regarding the variation of entrance velocity with the wave number parameter agree reasonably well with the theoretical results.

In addition to the general conclusions the following conclusions can be added for the rectangular harbor:

15. The theoretical results obtained from the present rectangular harbor theory are almost identical to those obtained by the theory of Ippen and Goda (1963); thus, any difference in the two methods for evaluating the radiated waves appear to be quite small.

16. The theoretical results obtained from the arbitrary shaped harbor theory applied to the rectangular harbor agree better with the experiments near resonance than the rectangular harbor theory developed in this study or the theory of Ippen and Goda (1963). Perhaps this is due to the fact that when using the arbitrary shaped harbor theory three segments were used in the matching procedure while in the other two theories only the average solution across the entrance was matched.

17. The present experimental data agree better with the theoretical results than do the experimental data of Ippen and Goda (1963) especially in the vicinity of resonance, probably because the wave basin used for present experiments is both wider and longer and the present wave energy dissipators are more efficient than in that study; thus the

incident wave is more nearly two-dimensional and the "open-sea" condition is simulated more satisfactorily.

The following conclusions may be drawn for the model of the East and West Basins of the Long Beach Harbor in addition to the conclusions stated earlier.

18. The theoretical results agree well with the experimental data for the response at four different positions within the harbor. The uniformity of agreement at the four locations suggests that the theory has also predicted correctly the shape of the various modes of oscillations.

19. The present theoretical results also agree qualitatively with the experimental data obtained from a model study conducted by Knapp and Vanoni (1945) although the planform of the model investigated by Knapp and Vanoni was more complicated and their study included depthwise variations.

20. The results show that the present theory can be applied with confidence to prototype harbors with relatively uniform depth and reflective interior boundaries.

LIST OF REFERENCES

1. Apte, A. S., and Marcou, C. (1954), "Seiche in Ports", Fifth Conference on Coastal Engineering, Grenoble, France, pp. 85-94.

2. Apte, A. S. (1957), "Recherches Theoriques et Experimentales sur Les Mouvements des Liquids Pesants Avec Surface Libre", Publications Scientifiques et Techniques du Ministere de L'Air, No. 333.

3. Baker, B. B., and Copson, E. T. (1950), The Mathematical Theory of Huygen's Principle, Oxford University Press, London.

4. Banaugh, R. P., and Goldsmith, W. (1963), "Diffraction of Steady Acoustic Waves by Surfaces of Arbitrary Shape", The Journal of the Acoustical Society of America, Vol. 35, No. 10, pp. 1590-1601.

5. Banaugh, R. P., and Goldsmith, W. (1963), "Diffraction of Steady Eleastic Waves by Surfaces of Arbitrary Shape", Journal of Applied Mechanics ASME, Vol. 30, Series E, No. 4, pp. 589-597.

6. Biesel, F., and LeMehaute, B. (1955), "Etude Theorique de La Reflexion de La Houle sur Certains Obstacles", LaHouille Blanche, March-April, pp. 130-140.

LIST OF REFERENCES (Cont'd)

7. Biesel, F., and LeMehaute, B. (1956), "Mouvements de Resonance a Deux Dimensions dans une Enceinte Sous L'Action d'Ondes Incidentes", LaHouille Blanche, July-August, pp. 348-374.

8. Carr, J.H. (1953), "Long-Period Waves or Surges in Harbors", Transactions, ASCE, Vo. 118, pp. 588-616.

9. Chen, L.H., and Schweikert, D.G. (1963), "Sound Radiation from an Arbitrary Body", The Journal of the Acoustical Society of America, Vol. 35, No. 10, pp. 1626-1632.

10. Chertock, G. (1964), "Sound Radiation from Vibrating Surfaces", The Journal of the Acoustical Society of America, Vol. 36, No. 7, pp. 1305-1313.

11. Copley, L.G. (1967), "Integral Equation Method for Radiation from Vibrating Bodies", The Journal of the Acoustical Society of America, Vol. 41, No. 4, pp. 807-816.

12. Courant, R. and Hilbert, D. (1953, 1962), Method of Mathematical Physics, Vol. I and II, Interscience Publishers Inc., New York.

13. Das, M.M. (1968), "Extended Application of a Single Hot-film Probe for the Measurement of Turbulence in a Flow Without Mean Velocity", HEL 2-20, Hydraulic Engineering Laboratory, University of California, Berkeley, California.

LIST OF REFERENCES (Cont'd)

14. Dettman, J. W. (1965), Applied Complex Variables, The Macmillan Company, New York.

15. Friedman, M. B., and Shaw, R. (1962), "Diffraction of Pulses by Cylindrical Obstacles of Arbitrary Cross Section", Journal of Applied Mechanics ASME, Vol. 29, Series E, No. 1, pp. 40-46.

16. Goda, Y., and Ippen, A. T. (1963), "Theoretical and Experimental Investigation of Wave Energy Dissipators Composed of Wire Mesh Screens", Report No. 60, Hydrodynamics Laboratory, M. I. T.

17. Hildebrand, F. B. (1962), Advanced Calculus for Applications, Prentice-Hall, Inc., Englewood Cliffs, New Jersey.

18. Hino, M., and Hino, K. (1965), "Response Characteristics of Tokyo Bay to Incident Long Waves", Coastal Engineering in Japan, Vol. 8, pp. 57-69.

19. Hinze, J. O. (1959), Turbulence, McGraw-Hill Book Company, New York.

20. Hwang, L. S., and Tuck, E. O. (1969), "On the Oscillations of Harbors of Arbitrary Shape", Submitted to Journal of Fluid Mechanics (publication pending).

21. Ippen, A. T., Editor (1966), Estuary and Coastline Hydrodynamics, McGraw-hill Book Company, New York.

LIST OF REFERENCES (Cont'd)

22. Ippen, A. T., and Goda, Y. (1963), "Wave Induced Oscillations in Harbors: The Solution for a Rectangular Harbor Connected to the Open-Sea", Report No. 59, Hydrodynamics Laboratory, M. I. T.

23. Ippen, A. T., and Raichlen, F. (1962), "Wave Induced Oscillations in Harbors: The Problem of Coupling of Highly Reflective Basins", Report No. 49, Hydrodynamics Laboratory, M. I. T.

24. Ippen, A. T., Raichlen, F., and Sullivan, R. K. (1962), "Wave Induced Oscillations in Harbors: Effect of Energy Dissipators in Coupled Basin Systems", Report No. 52, Hydrodynamics Laboratory, M. I. T.

25. Kellog, O. D. (1953), Foundations of Potential Theory, Dover Publications, Inc., New York.

26. Keulegan, G. H. (1968), "Wave Damping Effects of Screens", Research Report No. 2-12, U. S. Army Engineer Waterways Experimental Station.

27. Knapp, R. T., and Vanoni, V. A. (1945), "Wave and Surge Study for the Naval Operating Base, Terminal Island, California", Hydraulic Structure Laboratory of the California Institute of Technology.

28. Kravtchenko, J., and McNown, J. S. (1955), "Seiche in Rectangular Ports", Quarterly of Applied Mathematics, Vol 13, pp. 19-26.

LIST OF REFERENCES (Cont'd)

29. Kuo, E. Y. T. (1968), "Acoustic Field Generated by a Vibrating Boundary: I. General Formulation and Sonar-Dome Noise Loading", The Journal of the Acoustical Society of America, Vol. 43, No. 1, pp. 25-31.

30. Lamb, H. (1945), Hydrodynamics, Sixth Edition, Dover Publications, New York.

31. Lee, J. J. (1967), Discussion of paper "Some Turbulence Measurements in Water" by F. Raichlen, Journal of the Engineering Mechanics Division, ASCE, Vol. 93, No. EM 6, pp. 287-293.

32. Leendertse, J. J. (1967), "Aspects of a Computational Model for Long-Period Water Wave Propagation" Memorandum, RM-5294-PR, The Rand Corporation.

33. LeMehaute, B. (1960), "Periodical Gravity Wave on a Discontinuity", Journal of the Hydraulics Division, ASCE, Vol. 86, No. HY 9, pp. 11-41.

34. LeMehaute, B. (1961), "Theory of Wave Agitation in a Harbor", Journal of the Hydraulics Division, ASCE, Vol. 87, No. HY 2, pp. 31-50.

35. LeMehaute, B. (1962), Discussion of the paper "Harbor Paradox" by J. Miles and W. Munk, Journal of the Waterways and Harbors Division, ASCE, Vol. 88, No. WW 2, pp. 173-185.

LIST OF REFERENCES (Cont'd)

36. McNown, J. S. (1952), "Waves and Seiche in Idealized Ports", Gravity Wave Symposium, National Bureau of Standards Circular 521.

37. Mikhlin, S. G., and Smolitskiy, K. L. (1967), Approximate Methods for Solution of Differential and Integral Equations, American Elsevier Publishing Company, New York.

38. Miles, J., and Munk W. (1961), "Harbor Paradox", Journal of the Waterways and Harbors Division, ASCE, Vol. 87, No. WW 3, pp. 111-130.

39. Morse, P. M., and Feshback, H. (1953), Method of Theoretical Physics, Vol. I and II, McGraw-Hill Book Company, New York.

40. Mullin, C. R., Sandburg, R., and Velline, C. O. (1965), "A Numerical Technique for the Determination of Scattering Cross Sections of Infinite Cylinders of Arbitrary Geometrical Cross Section", Transactions of Antennas and Propagation, IEEE, Vol. AP-13, pp. 141-149.

41. Muskhelishvili, N. I. (1946), Singular Integral Equations, P. Noordhoff Ltd., Groningen, Holland.

42. Raichlen, F. (1965), "Wave-Induced Oscillations of Small Moored Vessels", Report KH-R-10, W. M. Keck Laboratory of Hydraulics and Water Resources, California Institute of Technology.

LIST OF REFERENCES (Cont'd)

43. Raichlen, F., and Ippen, A. T. (1965a), "Wave Induced Oscillations in Harbors", Journal of the Hydraulics Division, ASCE, Vol. 91, No. HY 2, pp. 1-26.

44. Raichlen, F. (1965b), "Long Period Oscillations in Basins of Arbitrary Shapes", Chapter 7, Coastal Engineering, Santa Barbara Speciality Conference, pp. 115-145.

45. Raichlen, F. (1967), "Some Turbulence Measurements in Water", Journal of the Engineering Mechanics Division, ASCE, Vol. 93, No. EM 2, pp. 73-97.

46. Richmond, J. H. (1965), "Scattering by a Dielectric Cylinder of Arbitrary Cross Section Shape", Transactions of Antennas and Propagation,IEEE, Vol. AP-13, pp. 334-341.

47. Shaw, R. P. (1967), "Diffraction of Acoustic Pulses by Obstacles of Arbitrary Shape with a Robin Boundary Condition", The Journal of the Acoustical Society of America, Vol. 41, No. 4, pp. 855-859.

48. Stoker, J. J. (1957), Water Waves, Interscience Publishers Inc., New York.

49. Townes, H. W. (1965), "Flow Over a Rough Boundary", Thesis presented to the California Institute of Technology, at Pasadena, California, in partial fulfillment of the requirements for the degree of Doctor of Philosophy.

LIST OF REFERENCES (Cont'd)

50. Watson, G. N. (1945), A Treatise on the Theory of Bessel Functions, The Macmillan Comapny, New York.

51. Wilson, B. W. (1959), "Research and Model Studies on Wave Action in Table Bay Harbor, Cape Town", Transaction of the South African Institution of Civil Engineers, Vol. I, No. 6 and 7 (June, July 1959); Vol. II, No. 5 (May 1960).

52. Wilson, B. W., Hendrickson, J. A., and Kilmer, R. C. (1965), "Feasibility Study for a Surge-Action Model of Monterey Harbor, California", Report 2-136, Science Engineering Associates, San Marino, California.

LIST OF SYMBOLS

A	Wave amplitude.
A_i	Incident wave amplitude.
A_{max}	Maximum wave amplitude within the harbor.
A_1, A_2, A_3	Functions representing the magnitude of the velocity components (defined in Eq. 3.41).
a	Characteristic dimension of a harbor, the radius of a circular harbor.
B_o	A function representing the average radiation effect at the harbor entrance (defined in Eq. 4.27).
b_o	A constant equal to $-\frac{i}{2}$.
b	Width of a rectangular harbor.
C	Normal derivative of the wave function at the harbor entrance.
$\overline{C}$	Average of the normal derivative of the wave function across the harbor entrance.
$\underline{C}$	A vector representing the normal derivative of the wave function at the mid-point of each entrance segment.
c_1, c_2, c_3, c_a, c_b	Constants associated with the hot-film sensor and the linearization procedure.
D	Diameter of the screen wires of the wave energy dissipator.
D, D_1, D_2	Used in Appendix I and Appendix II representing various domains of interest.
d	Width of the harbor entrance.
d_o	Distance from left-hand boundary of the rectangular harbor to the left-hand limit of the harbor entrance.
E	Output voltage of the hot-film anemometer.
e	Base of the Naperian logarithm.

LIST OF SYMBOLS (Cont'd)

f	Wave function which describes the variation of the velocity potential in the x and y directions.
f_1	Wave function in Region I (in the open-sea).
f_2	Wave function in Region II (inside the harbor).
f_3	Radiated wave function.
f_i	Incident wave function.
f_r	Reflected wave function.
f_{jo}	An infinite series defined in Eq. 4.23 and Eq. A.3.3.
f_{yo}	An infinite series defined in Eq. 4.23 and Eq. A.3.6.
G	An N x N matrix defined in Eq. 3.17d (elements of the matrix are defined in Eqs. 3.59 and 3.60).
G_n	An N x N matrix defined in Eq. 3.17b (elements of the matrix are defined in Eqs. 3.43 and 3.57).
$g(\vec{x}, \vec{\xi})$	Green's function.
g	Acceleration due to gravity.
H_{ij}	Radiation matrix (a p x p matrix, see Eq. 3.33), the elements of the matrix are defined in Eqs. 3.62 and 3.63.
H	Wave height.
H_i	Incident wave height.
H_r	Reflected wave height.
H_t	Transmitted wave height.
$H_o^{(1)}, H_1^{(1)}$	Zero and first orders of the Hankel function of first kind.
h	Water depth.
I	Indentity matrix.
I_a	Electrical currents to the hot-film sensor.
λ	$\sqrt{-1}$.

LIST OF SYMBOLS (Cont'd)

$\vec{i}, \vec{j}, \vec{k}$	Unit vectors in the directions x, y, x respectively.
J_m	Bessel function of the first kind and order m.
J_c	An infinite series defined in Eq. 4.26a and Eq. A.3.7.
K_r	Reflection coefficient.
K_t	Transmission coefficient.
k	Wave number.
L	Wave length.
ℓ	Length of a rectangular harbor.
log	Logarithm to the Naperian base (e=2.7128).
M	A N x p matrix defined in Eq. 3.21.
M_c	An infinite series defined in Eqs. 4.18 and 4.19.
M_p	A p x p matrix defined in Eq. 3.35, (a matrix formed by the p rows and p columns of the matrix M).
m	Number of layers of screens.
N	Total number of segments into which the boundary of the harbor (including entrance) is divided.
n	Outward normal to the boundary of the domain.
o	Order of magnitude.
$\underline{P}$	A N-dimensional vector representing the normal derivative of the wave function at the mid-point of the straight-line segments of the harbor boundary.
p	Total number of segments into which the harbor entrance is divided.
Q	A function used in Appendix II representing the contribution to the value of wave function as the field point approaching a boundary point.
$q(\vec{x}_o)$	Source strength along the reflecting boundary (see Eq. 2.3).

LIST OF SYMBOLS (Cont'd)

R	Amplification factor.
R_o	Radius of a large circle.
R_w	Operating resistance of the hot-film sensor.
r	Distance between points or radial position in a polar coordinates.
S	Center to center distance between the screen wires.
S_1	Output voltage of the first squaring circuit of the linearizer of the hot-film anemometer.
S_2	Output voltage of the linearizer of the hot-film anemometer.
S_b	Output voltage of the bias control, after using the first squaring circuit of the linearizer of the hot-film anemometer.
S_o, S_m	Special functions defined in Eq. 4.38.
$\overline{S}_o$, $\overline{S}_m$	Average of S_o, S_m across the harbor entrance (defined in Eq. 4.39).
s	Tangent to the boundary of the domain in a counter-clockwise direction.
Δs	Length of the boundary segments.
T	Wave period.
t	Time.
U_m	A N x p matrix with the diagonal of the first p rows equal to unity, all other elements equal to zero (Eq. 3.19).
u, v, w	Velocity components in x, y, z directions.
$\vec{u}$	Velocity vector with components u, v, w.
V	Resultant fluid velocity in the direction perpendicular to the longitudinal axis of the hot-film sensor.
V^*	Total velocity defined as $(u^2 + v^2 + w^2)^{\frac{1}{2}}$.

LIST OF SYMBOLS (Cont'd)

V_o^*	Maximum total velocity with respect to time at a location.
$(V_o^*)_{ave}$	Average of V_o^* across the harbor entrance.
V_o	Maximum resultant velocity of the components v and w with respect to time at a location.
$(V_o)_{ave}$	Average of V_o across the harbor entrance.
$(V_o)_c$	Value of V_o at the center of the harbor entrance.
$\underline{X}$	A N-dimensional vector defined in Eq. 3.17a representing the wave function at the boundary of the harbor.
x	Coordinate axis in horizontal direction parallel to the coastline.
$\vec{x}$	Position vector for the point (x, y).
Y_m	Bessel function of the second kind of order m.
Y_c	An infinite series defined in Eq. 4.26b and Eq. A.3.9.
y	Coordinate axis in horizontal direction perpendicular to the coastline.
Z	Function which describes the variation of the velocity potential in depthwise direction z.
z	Coordinate axis in vertical direction.
$(\ )_j$	Quantities at the j^{th} segment of the boundary.
$(\ )_s, (\ )_{ss}$	First, second partial derivatives with respect to the tangent of the boundary.
$\bar{(\ )}$	Spatial average value.
$\underline{1}$	A p-dimensional vector with each element equal to unity.
α	Interior angle of a boundary point (see Fig. A.2.2).
$\alpha_1, \alpha_2, \alpha_3$	Phase angles defined in Eq. 3.41.
α_v	Calibration constant of the hot-film sensor.

LIST OF SYMBOLS (Cont'd)

β_m	A constant defined in Eq. 4.33.
Γ	A large circle.
γ	Euler's constant (γ=0.577216.....).
Δ	Difference operator.
δ	Kronecker delta.
ϵ	Radius of a circle.
η	Displacement of water surface elevation from the mean water level.
θ	Angular position.
ν	Kinematic viscosity of the fluid.
π	3.14159..... .
$\rho(n)$	Sum of an infinite series, $\rho(n) = \sum_{n=1}^{\infty} \frac{1}{n}$.
ρ_o	A small circle or a half circle with a radius ϵ.
σ	Circular wave frequency ($2\pi/T$).
Φ	Velocity potential.
$\varphi(h/L)$	Depth effect factor (Eq. 6.1).
φ_o	Potential function for standing wave system (Eq. 2.3).
φ_t	Total potential function (defined in Eq. 2.3).
∇	Gradient operator.
∇^2	Laplacian operator.
∂D	Boundary of a domain.
$\lvert\ \rvert$	Absolute value.

APPENDIX I

WEBER'S SOLUTION OF THE HELMHOLTZ EQUATION

The derivation of Weber's solution of the two dimensional Helmholtz equation in a bounded domain (as used in Eq. 3.11) and an unbounded domain (as used in Eq. 3.29) will be presented in this appendix. This subject has been discussed by Baker and Copson (1950); the interested reader is referred to that book for other related topics as well.

I.1 Weber's Solution in a Bounded Domain

Let ∂D be a closed curve bounding a domain D in the x-y plane, if f and g are two functions whose first- and second-order partial derivatives are continuous within the domain D and on the boundary ∂D, then Green's identity formula gives (see Kellog (1953)):

$$\int_{\partial D} \left(f \frac{\partial g}{\partial n} - g \frac{\partial f}{\partial n}\right) ds = \int\int_{D} (f\nabla^2 g - g\nabla^2 f)\, dxdy \quad , \tag{A.1.1}$$

where $\partial/\partial n$ means differentiation along the outward normal to the boundary of the domain.

If the functions f and g are both solutions of the two-dimensional Helmholtz equation,

$$\nabla^2 f + k^2 f = 0 \tag{A.1.2}$$

then the right-hand-side of Eq. A. 1. 1 equals to zero, thus, Eq. A. 1. 1 reduces to:

$$\int_{\partial D} \left(f\frac{\partial g}{\partial n} - g\frac{\partial f}{\partial n}\right) ds = 0 \quad . \tag{A. 1. 3}$$

In particular, if $g = H_o^{(1)}(kr)$, where r denotes the distance from a point $\vec{x}(x, y)$ and if the point $\vec{x}(x, y)$ lies outside the domain D, one obtains

$$\int_{\partial D} \left[f\frac{\partial}{\partial n}\left(H_o^{(1)}(kr)\right) - H_o^{(1)}(kr)\frac{\partial f}{\partial n}\right]ds = 0 \tag{A. 1. 4}$$

However, if $\vec{x}(x, y)$ lies inside the domain D, Eq. A. 1. 4 no longer holds since $H_o^{(1)}(kr)$ has a logarithmic singularity at the point $\vec{x}(x, y)$ $\left(H_o^{(1)}(kr) \sim \lambda\frac{2}{\pi}\log kr, \text{ as } r \to 0\right)$. To avoid this singularity, Green's identity formula will be applied to the region D_1, bounded externally by ∂D and internally by a circle ρ_o with its center at $\vec{x}$ and with radius ϵ (see Fig. A. 1. 1). Thus, Green's identity formula, Eq. A. 1. 1, becomes:

$$\int_{\partial D}\left(f\frac{\partial g}{\partial n} - g\frac{\partial f}{\partial n}\right)ds + \int_{\rho_o}\left(f\frac{\partial g}{\partial n} - g\frac{\partial f}{\partial n}\right)ds = \int\int_{D_1}\left(f\nabla^2 g - g\nabla^2 f\right)dxdy \quad . \tag{A. 1. 5}$$

Since the singularity is now outside the domain D_1, by taking $g=H_o^{(1)}(kr)$, the right-hand-side of Eq. A. 1. 5 is equal to zero. Thus, one obtains:

$$\int_{\partial D}\left[f\frac{\partial}{\partial n}\left(H_o^{(1)}(kr)\right) - H_o^{(1)}(kr)\frac{\partial f}{\partial n}\right]ds = -\int_{\rho_o}\left[f\frac{\partial}{\partial n}\left(H_o^{(1)}(kr)\right) - H_o^{(1)}(kr)\frac{\partial f}{\partial n}\right]ds \tag{A. 1. 6}$$

Note that the direction of n on the boundary ρ_o as shown in the right-hand-side of Eq. A. 1. 6 is inward toward the center $\vec{x}(x, y)$, i. e. out-

ward from the boundary of the domain D_1 (see Fig. A. 1. 1); for convenience this differentiation is changed to the r direction (negative n direction). Thus, one obtains:

$$\int_{\partial D}\left[f\frac{\partial}{\partial n}\left(H_o^{(1)}(kr)\right) - H_o^{(1)}(kr)\frac{\partial f}{\partial n}\right]ds = \int_{\rho_o}\left[f\frac{\partial}{\partial r}\left(H_o^{(1)}(kr) - H_o^{(1)}(kr)\frac{\partial f}{\partial r}\right]ds \qquad (A.\,1.\,7)$$

Since the integral around the boundary ∂D does not depend upon the radius ϵ of the circle ρ_o, the right-hand-side of Eq. A. 1. 7 can be evaluated at a radius ϵ as small as desired. Thus the right-hand-side of Eq. A. 1. 7 can be written as:

$$\lim_{\epsilon\to 0}\int_{\rho_o}\left[f\frac{\partial}{\partial r}\left(H_o^{(1)}(kr)\right) - H_o^{(1)}(kr)\frac{\partial f}{\partial r}\right]ds \quad . \qquad (A.\,1.\,8)$$

By using the asymptotic behavior of the Hankel function for $r\to 0$:

$$H_o^{(1)}(kr) \sim 1 + i\frac{2}{\pi}\log(kr) \quad ,$$

$$\frac{\partial}{\partial r}\left(H_o^{(1)}(kr)\right) \sim i\frac{2}{\pi}\frac{1}{r} \quad ,$$

the limit of Eq. A. 1. 8 can be evaluated. Since the functions f and $\frac{\partial f}{\partial r}$ are continuous at $\vec{x}(x, y)$, the second term and the first term of Eq. A. 1. 8 can be evaluated as follows:

$$\lim_{\epsilon\to 0}\int_{\rho_o} H_o^{(1)}(kr)\frac{\partial f}{\partial r}\,ds = \lim_{\epsilon\to 0}\int_0^{2\pi}\left(1+i\frac{2}{\pi}\log(k\epsilon)\right)\epsilon\,d\theta\left(\frac{\partial f}{\partial r}(\vec{x})+o(\epsilon)\right) = 0 \qquad (A.\,1.\,9a)$$

$$\lim_{\epsilon\to 0}\int_{\rho_o} f\frac{\partial}{\partial r}\left(H_o^{(1)}(kr)\right)ds = \lim_{\epsilon\to 0}\int_0^{2\pi} i\frac{2}{\pi}\frac{\epsilon}{\epsilon}\,d\theta\left(f(\vec{x})+o(\epsilon)\right) = 4if(\vec{x}) \qquad (A.\,1.\,9b)$$

Substituting Eqs. A. 1. 9 a and b into Eq. A. 1. 7, one obtains:

$$f(\vec{x}) = -\frac{\lambda}{4}\int_{\partial D}\left[f\frac{\partial}{\partial n}\left(H_o^{(1)}(kr)\right) - H_o^{(1)}(kr)\frac{\partial f}{\partial n}\right]ds \qquad \text{(A. 1. 10)}$$

This completes the proof of the following theorem due to Weber:

Let f be a solution of the Helmholtz equation

$$\frac{\partial^2 f}{\partial x^2} + \frac{\partial^2 f}{\partial y^2} + k^2 f = 0$$

in a closed domain D, whose first- and second-order partial derivatives are continuous within and on the closed boundary ∂D. Then the function of f at any interior point $\vec{x}$ can be expressed as:

$$f(\vec{x}) = -\frac{\lambda}{4}\int_{\partial D}\left[f\frac{\partial}{\partial n}\left(H_o^{(1)}(kr)\right) - H_o^{(1)}(kr)\frac{\partial f}{\partial n}\right]ds$$

where r is the distance from the interior point $\vec{x}$ to the boundary, and $\partial/\partial n$ means differentiation along the outward normal to the boundary ∂D.

I. 2 Weber's Solution in an Unbounded Domain

Suppose the function f is a solution of the Helmholtz equation, $\nabla^2 f + k^2 f = 0$, outside the domain D, i. e. in the unbounded domain, whose first- and second-order partial derivatives are continuous on/and outside the closed curve ∂D. Then the Green's identity formula can be applied to a region D_2 bounded internally by the closed curve ∂D and externally by a circle Γ with radius R_o which is so chosen that the circle Γ encloses the closed curve ∂D (see Fig. A. 1. 2).

Thus, from the theorem presented in Section I. 1 one obtains:

$$f(\vec{x}) = -\frac{\lambda}{4}\left[\left(\int_{\partial D} + \int_{\Gamma}\right)\left[f\frac{\partial}{\partial n}\left(H_o^{(1)}(kr)\right) - H_o^{(1)}(kr)\frac{\partial f}{\partial n}\right]ds\right] \quad , \qquad (A.1.11)$$

if $\vec{x}$ is in the domain D_2, wherein n denotes the outward normal to the bounding curves, ∂D and Γ (see Fig. A.1.2).

The outward normal to the circle Γ is in r direction, thus Eq. A.1.11 can be rewritten as:

$$f(\vec{x}) = -\frac{\lambda}{4}\int_{\partial D}\left[f\frac{\partial}{\partial n}\left(H_o^{(1)}(kr)\right) - H_o^{(1)}(kr)\frac{\partial f}{\partial n}\right]ds$$

$$-\frac{\lambda}{4}\int_{\Gamma}\left[f\frac{\partial}{\partial r}\left(H_o^{(1)}(kr)\right) - H_o^{(1)}(kr)\frac{\partial f}{\partial r}\right]ds \quad . \qquad (A.1.12)$$

For simplicity, the second integral in the right-hand-side of Eq. A.1.12 is denoted as $J(\vec{x})$. The radius of the circle Γ, R_o, can be made as large as desired to cover the entire unbounded domain, i.e. $R_o \to \infty$. Thus the function $J(\vec{x})$ can be rewritten as:

$$J(\vec{x}) = -\frac{\lambda}{4}\lim_{r\to\infty}\int_0^{2\pi}\left[f\frac{\partial}{\partial r}\left(H_o^{(1)}(kr)\right) - H_o^{(1)}(kr)\frac{\partial f}{\partial r}\right]rd\theta \quad . \qquad (A.1.13)$$

The asymptotic behavior of $H_o^{(1)}(kr)$ and $\frac{\partial}{\partial r}\left(H_o^{(1)}(kr)\right)$ for $r\to\infty$ are:

$$H_o^{(1)}(kr) \sim \sqrt{\frac{2}{\pi(kr)}}\, e^{\lambda(kr - \frac{\pi}{4})} \quad ,$$

$$\frac{\partial}{\partial r}\left(H_o^{(1)}(kr)\right) = -kH_1^{(1)}(kr) \sim -k\sqrt{\frac{2}{\pi(kr)}}\, e^{\lambda(kr - \frac{\pi}{4} - \frac{\pi}{2})} \quad . \qquad (A.1.14)$$

Substituting Eq. A.1.14 into Eq. A.1.13, one obtains:

$$J(\vec{x}) = -\frac{\lambda}{4}\lim_{r\to\infty}\int_0^{2\pi}\sqrt{\frac{2}{\pi(kr)}}\; e^{\lambda(kr - \frac{\pi}{4})}\left[-kfe^{-\lambda\frac{\pi}{2}} - \frac{\partial f}{\partial r}\right]rd\theta$$

$$= \frac{\lambda}{4}\sqrt{\frac{2}{\pi k}}\lim_{r\to\infty}\int_0^{2\pi} e^{\lambda(kr - \frac{\pi}{4})}\sqrt{r}\left[\frac{\partial f}{\partial r} - \lambda kf\right]d\theta \quad . \qquad (A.1.15)$$

Thus the function $J(\vec{x})$ tends to zero, if the function:

$$\sqrt{r}\left(\frac{\partial f}{\partial r} - \imath k f\right) \rightarrow 0 \qquad \text{(A. 1. 16)}$$

uniformly with respect to θ as $r \rightarrow \infty$. This condition, Eq. A. 1. 16 , is referred to as the "Sommerfeld radiation condition". A sufficient condition for this is that the function f should behave like $H_o^{(1)}(kr)$ for large values of r . Since for $f = H_o^{(1)}(kr)$, and $\frac{\partial f}{\partial r} = -kH_1^{(1)}(kr)$, the Sommerfeld radiation condition is satisfied as $r \rightarrow \infty$:

$$\sqrt{r}\left[\frac{\partial f}{\partial r} - \imath k f\right] = -k\sqrt{r}\left[H_1^{(1)}(kr) + \imath H_o^{(1)}(kr)\right]$$

$$\sim -k\sqrt{\frac{2}{\pi k}}\, e^{\imath\left(kr - \frac{\pi}{4}\right)}\left[e^{-\imath\frac{\pi}{2}} + \imath\right]$$

$$= -k\sqrt{\frac{2}{\pi k}}\, e^{\imath\left(kr - \frac{\pi}{4}\right)}\left[-\imath + \imath\right] = 0 \quad .$$

This completes the proof for the following Weber's theorem in an unbounded domain:

Let f be a solution of $\frac{\partial^2 f}{\partial x^2} + \frac{\partial^2 f}{\partial y^2} + k^2 f = 0$, whose first- and second-order partial derivatives are continuous outside and on a closed curve ∂D and let

$$\sqrt{r}\left(\frac{\partial f}{\partial r} - \imath k f\right) \rightarrow 0$$

uniformly with respect to θ, as $r \rightarrow \infty$, then the function $f(\vec{x})$ at a fixed point $\vec{x}$ located outside the domain bounded by ∂D, i. e. inside the unbounded domain,can be expressed as:

$$f(\vec{x}) = -\frac{i}{4}\int_{\partial D}\left[f\frac{\partial}{\partial n}\left(H_o^{(1)}(kr)\right) - H_o^{(1)}(kr)\frac{\partial f}{\partial n}\right]ds \quad ,$$

where r is the distance between the fixed point $\vec{x}$ and the boundary and n denotes the outward normal to the boundary ∂D (in the direction out of the unbounded domain).

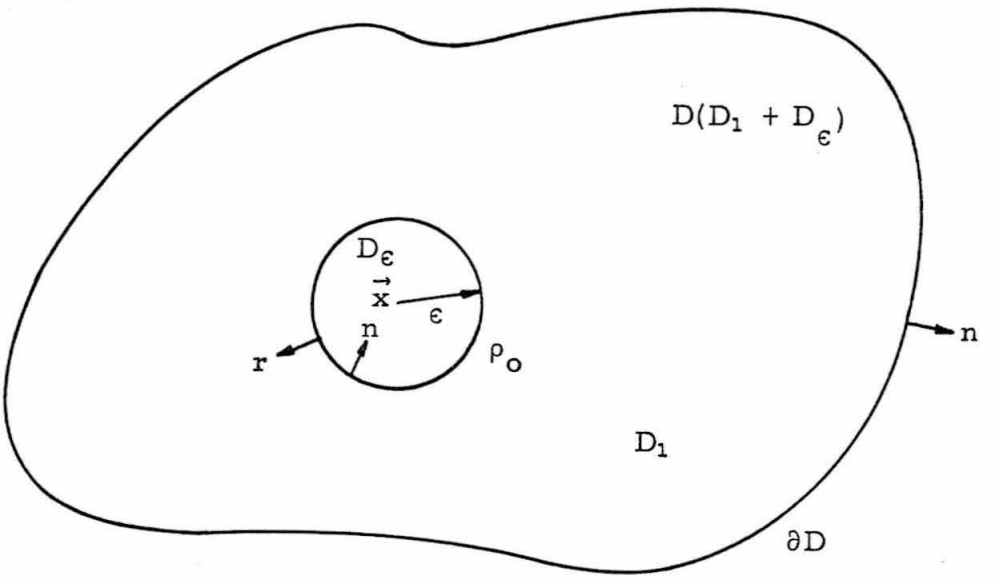

Fig. A. 1. 1 Definition sketch for a bounded domain

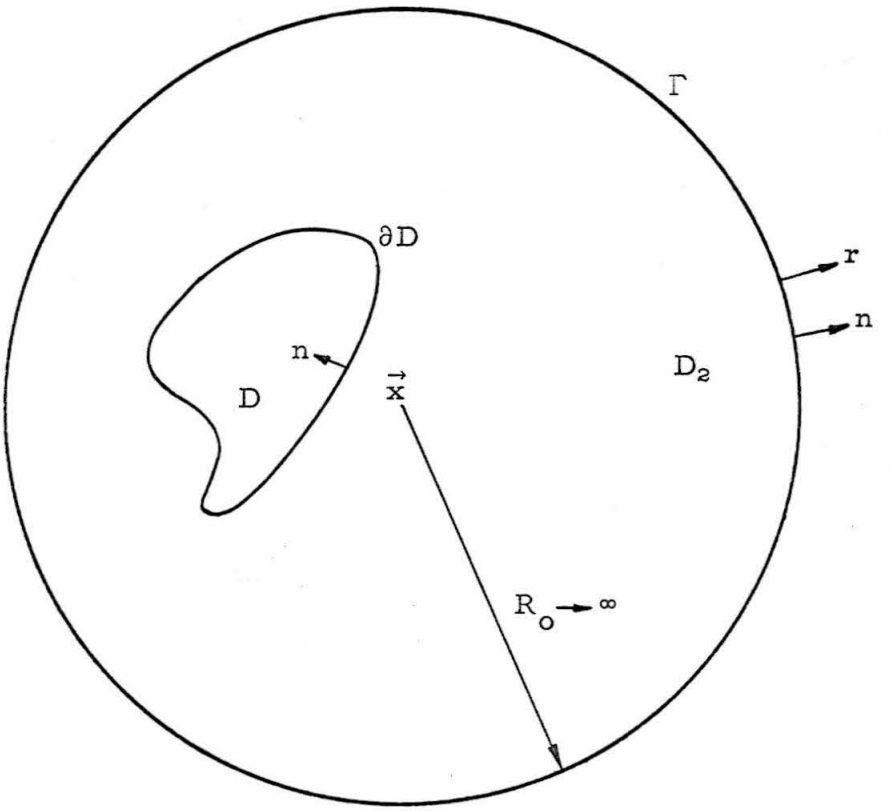

Fig. A. 1. 2 Definition sketch for an unbounded domain

APPENDIX II

DERIVATION OF EQ. 3.12

The Weber's solution of the two-dimensional Helmholtz equation expressed the wave function f at an interior point $\vec{x}$ as a function of the wave function and its normal derivative at the boundary as follows (see also Eq. 3.11):

$$f(\vec{x}) = -\frac{i}{4}\int_s \left[f(\vec{x}_o)\frac{\partial}{\partial n}\left(H_o^{(1)}(kr)\right) - H_o^{(1)}(kr)\frac{\partial}{\partial n}\left(f(\vec{x}_o)\right)\right]ds(\vec{x}_o) \quad (A.2.1)$$

In order to determine the wave function $f(\vec{x}_o)$ along the boundary, the field point $\vec{x}$ is allowed to approach the boundary at a point $\vec{x}_i$; the path of integration is deformed around a small half circle, ρ_o, with radius ϵ (see Fig. A.2.1). Then Eq. A.2.1 can be written as:

$$f(\vec{x}_i) = -\frac{i}{4}\int_{s-\rho_o} \left[f(\vec{x}_o)\frac{\partial}{\partial n}\left(H_o^{(1)}(kr)\right) - H_o^{(1)}(kr)\frac{\partial}{\partial n}\left(f(\vec{x}_o)\right)\right]ds(\vec{x}_o)$$

$$-\frac{i}{4}\int_{\rho_o} \left[f(\vec{x}_o)\frac{\partial}{\partial n}\left(H_o^{(1)}(kr)\right) - H_o^{(1)}(kr)\frac{\partial}{\partial n}\left(f(\vec{x}_o)\right)\right]ds(\vec{x}_o) \quad . (A.2.2)$$

The radius of the half circle ρ_o, ϵ, can be made to approach zero, i.e. $\epsilon \to 0$; using the definition of Cauchy principal value Eq. A.2.2 can thus be rewritten as:

$$f(\vec{x}_i) = -\frac{\lambda}{4}\int_S \left[f(\vec{x}_o)\frac{\partial}{\partial n}\left(H_o^{(1)}(kr)\right) - H_o^{(1)}(kr)\frac{\partial}{\partial n} f(\vec{x}_o)\right] ds(\vec{x}_o) + Q(\vec{x}_i) \qquad (A.2.3)$$

where the first integral represents the Cauchy principal value and the second term , $Q(\vec{x}_i)$, represents the limit of the integration along the small half circle ρ_o as $\varepsilon \to 0$. This limit value, $Q(\vec{x}_i)$, can be evaluated by the procedures which will be discussed in the following.

Since along the small half circle ρ_o, the direction of n is in the direction of r, the function $Q(\vec{x}_i)$ can be rewritten as:

$$Q(\vec{x}_i) = -\frac{\lambda}{4}\lim_{\varepsilon\to 0}\int_{\rho_o}\left[f(\vec{x}_o)\frac{\partial}{\partial r}\left(H_o^{(1)}(kr)\right) - H_o^{(1)}(kr)\frac{\partial}{\partial r}\left(f(\vec{x}_o)\right)\right] ds(\vec{x}_o) \quad . \qquad (A.2.4)$$

The asymptotic formulas of the Hankel functions for very small argument ($r \to 0$) are:

$$\begin{aligned} H_o^{(1)}(kr) &\sim 1 + \lambda\frac{2}{\pi}\log(kr) \quad ; \\ -\frac{\partial}{\partial r} H_o^{(1)}(kr) &= -kH_1^{(1)}(kr) \sim \lambda\frac{2}{\pi}\frac{1}{r} \quad . \end{aligned} \qquad (A.2.5)$$

Substituting Eq. A.2.5 into Eq. A.2.4 one obtains:

$$\begin{aligned} Q(\vec{x}_i) &= -\frac{\lambda}{4}\lim_{\varepsilon\to 0}\int_{\rho_o}\left[f(\vec{x}_o)\left(\lambda\frac{2}{\pi}\frac{1}{r}\right) - \left(1+\lambda\frac{2}{\pi}\log(kr)\right)\frac{\partial}{\partial r}(f(\vec{x}_o))\right] ds(\vec{x}_o) \\ &= -\frac{\lambda}{4}\lim_{\varepsilon\to 0}\int_0^{\pi}\lambda\frac{2}{\pi}\frac{\varepsilon}{\varepsilon}d\theta\left(f(\vec{x}_i) + o(\varepsilon)\right) \\ &\quad + \frac{\lambda}{4}\lim_{\varepsilon\to 0}\int_0^{\pi}\left(1+\lambda\frac{2}{\pi}\log(k\varepsilon)\right)\varepsilon d\theta\left(\frac{\partial}{\partial r}f(\vec{x}_i) + o(\varepsilon)\right) \\ &= \tfrac{1}{2}f(\vec{x}_i) \quad , \end{aligned} \qquad (A.2.6)$$

since as $\varepsilon\to 0$ the limit of the second integral in Eq. A.2.6 is zero.

Substituting Eq. A.2.6 into Eq. A.2.3, it becomes:

$$f(\vec{x}_i) = -\frac{\lambda}{4}\int_s \left[f(\vec{x}_o)\frac{\partial}{\partial n}\left(H_o^{(1)}(kr)\right) - H_o^{(1)}(kr)\frac{\partial}{\partial n}\left(f(\vec{x}_o)\right)\right] ds(\vec{x}_o) + \tfrac{1}{2} f(\vec{x}_i), \quad \text{(A.2.7)}$$

where $r = \left|\vec{x}_o - \vec{x}_i\right|$.

If the point $\vec{x}_i$ is a corner point on the boundary (see Fig. A.2.2), the result of Eq. A.2.1 as $\vec{x}$ approaching $\vec{x}_i$ can be expressed as:

$$f(\vec{x}_i) = -\frac{\lambda}{4}\int_s \left[f(\vec{x}_o)\frac{\partial}{\partial n}\left(H_o^{(1)}(kr)\right) - H_o^{(1)}(kr)\frac{\partial}{\partial n}\left(f(\vec{x}_o)\right)\right] ds(\vec{x}_o) + \left(1 - \frac{\alpha}{2\pi}\right) f(\vec{x}_i) \quad \text{(A.2.8)}$$

where the interior angle α is defined in Fig. A.2.2. For a smooth curve α is equal to π, thus Eq. A.2.8 is identical to Eq. A.2.7.

(The approach used for these derivations can also be found in a number of books; for example, see Muskhelishvili (1946) and Dettman (1965).)

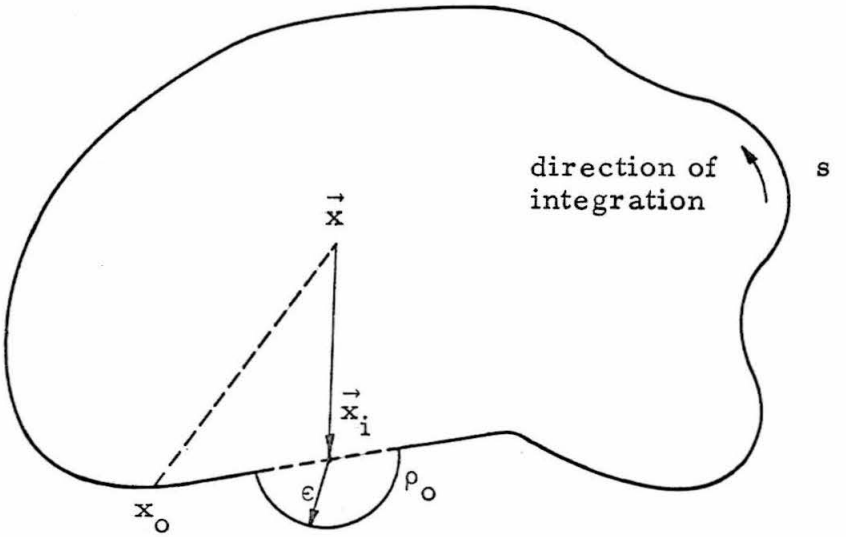

Fig. A.2.1 Definition sketch for an interior point approaching a boundary point on a smooth curve.

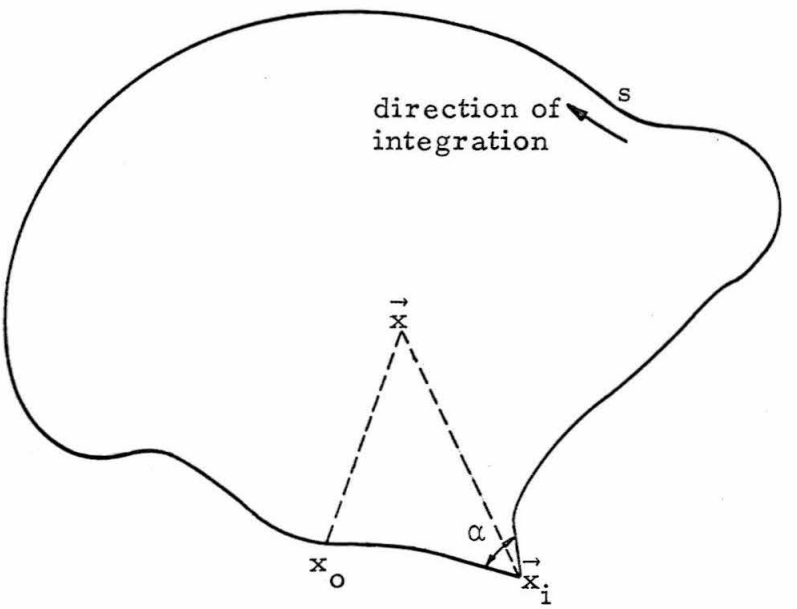

Fig. A.2.2 Definition sketch for an interior point approaching a corner point at the boundary

APPENDIX III

EVALUATION OF THE FUNCTIONS f_{jo}, f_{yo}, J_c, AND Y_c

III. 1 The Evaluation of the Function f_{jo}

The function f_{jo} in Eq. 4.23 is defined as:

$$f_{jo}(x,0) = \left[\int_0^x + \int_0^{\Delta s - x}\right] J_o(kr)\,dr \quad , \qquad (A.3.1)$$

where Δs is the width of the harbor entrance. The Bessel function $J_o(kr)$ in Eq. A.3.1 can be represented in an infinite series as:

$$J_o(kr) = \sum_{n=0}^{\infty} \frac{(-1)^n \left(\frac{kr}{2}\right)^{2n}}{n!\ n!} \quad . \qquad (A.3.2)$$

Substituting Eq. A.3.2 into Eq. A.3.1 and interchanging the order of integration and summation one obtains:

$$f_{jo}(x,0) = \sum_{n=0}^{\infty} \frac{(-1)^n}{(n!)^2}\left[\int_0^x \left(\frac{kr}{2}\right)^{2n} dr + \int_0^{\Delta s - x} \left(\frac{kr}{2}\right)^{2n} dr\right]$$

$$= \sum_{n=0}^{\infty} \frac{(-1)^n}{(n!)^2} \left(\frac{k}{2}\right)^{2n} \left[\frac{x^{2n+1}}{2n+1} + \frac{(\Delta s - x)^{2n+1}}{2n+1}\right] \quad . \qquad (A.3.3)$$

III. 2 The Evaluation of the Function f_{yo}

The function f_{yo} in Eq. 4.23 is defined as:

$$f_{yo}(x,0) = \left[\int_0^x + \int_0^{\Delta s - x}\right] \frac{\pi}{2} Y_o(kr)\,dr \quad . \qquad (A.3.4)$$

The Bessel function $Y_o(kr)$ can be represented in an infinite series as:

$$Y_o(kr) = \frac{2}{\pi}\left[(\log \frac{kr}{2} + \gamma) J_o(kr) + \sum_{n=1}^{\infty} (-1)^{n+1} \rho(n) \frac{\left(\frac{kr}{2}\right)^{2n}}{(n!)^2} \right], \quad \text{(A. 3. 5)}$$

where: $\gamma = 0.5772157.....$ is the Euler's constant,

$\rho(n) = 1 + \frac{1}{2} + \frac{1}{3} + ... + \frac{1}{n}$,

and $J_o(kr)$ is defined in Eq. A. 3. 2 .

Thus, substituting Eq. A. 3. 5 into Eq. A. 3. 4 and interchanging the order of integration and summation one obtains:

$$f_{yo}(x, 0) = \sum_{n=0}^{\infty} \frac{(-1)^n \left(\frac{k}{2}\right)^{2n}}{(n!)^2} \left[\left(\int_0^x + \int_0^{\Delta s - x} \right) \left(\log \frac{kr}{2} + \gamma \right) r^{2n} dr \right]$$

$$+ \sum_{n=1}^{\infty} \frac{(-1)^{n+1} \rho(n) \left(\frac{k}{2}\right)^{2n}}{(n!)^2} \left[\left(\int_0^x + \int_0^{\Delta s - x} \right) r^{2n} dr \right]$$

$$= \sum_{n=0}^{\infty} \frac{(-1)^n \cdot x}{(n!)^2 (2n+1)} \left[\left(\frac{kx}{2}\right)^{2n} \left(\log \left(\frac{kx}{2}\right) + \gamma \right) - \frac{\left(\frac{kx}{2}\right)^{2n}}{2n+1} \right]$$

$$+ \sum_{n=1}^{\infty} \frac{(-1)^{n+1} \rho(n) \cdot x}{(n!)^2 (2n+1)} \left(\frac{kx}{2}\right)^{2n} + \sum_{n=1}^{\infty} \frac{(-1)^{n+1} \rho(n) (\Delta s - x)}{(n!)^2 (2n+1)} \left(\frac{k(\Delta s - x)}{2}\right)^{2n}$$

$$+ \sum_{n=0}^{\infty} \frac{(-1)^n \cdot (\Delta s - x)}{(n!)^2 (2n+1)} \left[\left(\frac{k(\Delta s - x)}{2}\right)^{2n} \left(\log \left(\frac{k(\Delta s - x)}{2}\right) + \gamma \right) - \frac{\left(\frac{k(\Delta s - x)}{2}\right)^{2n}}{2n+1} \right] .$$

(A. 3. 6)

III. 3 The Evaluation of the Function J_c

According to Eqs. 4.24 and 4.25, the function $J_c \Delta s$ is equal to the average of $f_{yo}(x, 0)$ across the harbor entrance. Thus, the function J_c can be evaluated as follows:

$$J_c = \frac{1}{(\Delta s)^2}\int_0^{\Delta s} f_{jo}(x, 0)dx$$

$$= \frac{1}{(\Delta s)^2}\sum_{n=0}^{\infty} \frac{(-1)^n}{(n!)^2}\left(\frac{k}{2}\right)^{2n}\int_0^{\Delta s}\left[\frac{x^{2n+1}}{2n+1} + \frac{(\Delta s - x)^{2n+1}}{2n+1}\right]dx$$

$$= \sum_{n=0}^{\infty} \frac{(-1)^n\left(\frac{k\Delta s}{2}\right)^{2n}}{(n!)^2(n+1)(2n+1)}$$

$$= 1 - \frac{\left(\frac{k\Delta s}{2}\right)^2}{6} + \frac{\left(\frac{k\Delta s}{2}\right)^4}{60} - \frac{\left(\frac{k\Delta s}{2}\right)^6}{1008} + \frac{\left(\frac{k\Delta s}{2}\right)^8}{25920} + \cdots\cdots \qquad \text{(A. 3. 7)}$$

III. 4 The Evaluation of the Function Y_c

The function $Y_c \Delta s$ is equal to the average of $f_{yo}(x, 0)$ across the harbor entrance; therefore, the function Y_c can be evaluated as follows:

$$Y_c = \frac{1}{(\Delta s)^2}\int_0^{\Delta s} f_{yo}(x, 0)\, dx \qquad . \qquad \text{(A. 3. 8)}$$

Substituting Eq. A. 3. 6 into Eq. A. 3. 8 and interchanging the order of integration and summation, after performing the integration the function Y_c can be expressed as:

$$Y_c = \sum_{n=0}^{\infty} \frac{(-1)^n \left(\frac{k\Delta s}{2}\right)^{2n}}{(n!)^2 (2n+1)(n+1)} \left[\log\left(\frac{k\Delta s}{2}\right) + \gamma - \frac{1}{2(n+1)} - \frac{1}{2n+1}\right]$$

$$+ \sum_{n=1}^{\infty} \frac{(-1)^{n+1} \rho(n) \left(\frac{k\Delta s}{2}\right)^{2n}}{(n!)^2 (2n+1)(n+1)}$$

$$= \left[\log\left(\frac{k\Delta s}{2}\right) + \gamma - \frac{3}{2}\right] - \frac{\left(\frac{k\Delta s}{2}\right)^2}{6}\left[\log\left(\frac{k\Delta s}{2}\right) + \gamma - \frac{19}{12}\right]$$

$$+ \frac{\left(\frac{k\Delta s}{2}\right)^4}{60}\left[\log\left(\frac{k\Delta s}{2}\right) + \gamma - \frac{55}{30}\right] - \frac{\left(\frac{k\Delta s}{2}\right)^6}{1008}\left[\log\left(\frac{k\Delta s}{2}\right) + \gamma - \frac{353}{168}\right]$$

$$+ \frac{\left(\frac{k\Delta s}{2}\right)^8}{25920}\left[\log\left(\frac{k\Delta s}{2}\right) + \gamma - \frac{826}{360}\right] + \ldots\ldots \qquad \text{(A.3.9)}$$

APPENDIX IV

SUMMARY OF THE STROKES OF THE WAVE GENERATOR USED IN EXPERIMENTAL STUDIES

Harbor Model	Stroke of Wave Generator (inches)	Range of ka Covered in Experiments
Circular Harbor (10^{o} Opening)	0.128	3.180 ~ 3.190
	0.295	3.767 ~ 3.959
	0.424	3.188
	0.673	0.976 ~ 3.293
	0.758	0.231 ~ 0.522
	0.792	0.337 ~ 1.991
	0.842	0.337 ~ 3.940
Circular Harbor (60^{o} Opening)	0.425	0.365 ~ 4.123
	0.758	0.129 ~ 0.852
Rectangular Harbor	0.294	1.735 ~ 5.010
	0.675	1.49 ~ 2.08
	0.835	0.765 ~ 1.648
Long Beach Harbor	0.423	3.746 ~ 7.985
	0.758	0.420 ~ 3.600